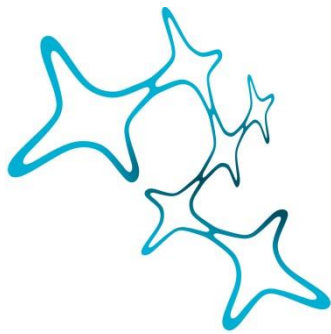

PROTEOMIC HETEROGENEITY OF GLIAL CELLS OF THE CENTRAL NERVOUS SYSTEM

Lew Kaplan



Graduate School of
Systemic Neurosciences

LMU Munich



Dissertation at the
Graduate School of Systemic Neurosciences
Ludwig-Maximilians-Universität München

December 2022

Supervisor
Prof. Dr. Antje Grosche
Physiological Genomics
Ludwig-Maximilians-Universität München

First Reviewer: Prof. Dr. Antje Grosche
Second Reviewer: Prof. Dr. Susanne Koch
External Reviewer Prof. Dr. Marius Ader

Date of Submission: 12.12.2022
Date of Defense: 08.05.2023

„Sage, was du weißt, tue, was du musst,
komme, was kommen mag.“

- *Sofja Kowalewskaja*

SUMMARY	1
I. INTRODUCTION	3
GLIAL CELLS – ASTROCYTES AND MÜLLER CELLS	3
REGIONAL HETEROGENEITY OF MACROGLIA	5
OMICS – GENE AND PROTEIN LEVEL QUANTIFICATION	8
BIOINFORMATICS – FROM USER-FRIENDLY TO SOPHISTICATED SOFTWARE	9
AIM OF THE THESIS	10
II. MANUSCRIPTS	12
HETEROGENEITY OF GLIAL CELLS OF THE CENTRAL NERVOUS SYSTEM – A PROTEOMIC STUDY	12
RETINAL REGIONS SHAPE HUMAN AND MURINE MÜLLER CELL PROTEOME PROFILE AND FUNCTIONALITY	51
RELEASE OF VAMP5-POSITIVE EXTRACELLULAR VESICLES BY RETINAL MÜLLER GLIA IN VIVO	76
III. DISCUSSION	105
WITH GREAT DATA COMES GREAT COMPUTATION	105
COMMON PROTEOMIC PATTERNS SHAPE GLOBAL AND LOCAL GLIAL IDENTITY	108
DISTINCT PROTEOMIC PATTERNS BETWEEN REGIONS OF THE CNS CONVERGE ON YAP1 SIGNALING	110
IV. MAIN CONCLUSIONS & OUTLOOK	115
V. REFERENCES	117
VI. APPENDIX	124
ACKNOWLEDGMENTS	124
LIST OF PUBLICATIONS	126
VII. EIDESSTATTLICHE VERSICHERUNG/AFFIDAVIT	127
VIII. DECLARATION OF AUTHOR CONTRIBUTIONS	128

SUMMARY

Mammalian brain and retina, both part of the central nervous system (CNS), contain a multitude of distinct glial cell populations. On a rough scale they can be categorized for example as oligodendrocytes, microglia and astroglia. While oligodendroglia are mostly absent from the eye, astrocytes line the inner surface of the retina and microglia reside between its nuclear layers. Most importantly, the retina has its own kind of specialized glial cells: Müller glia. These long cells are evenly distributed, span the whole thickness of the retina and fulfil similar homeostatic functions as astrocytes in the brain. As the CNS is divided in functional and anatomical subunits that additionally differ by species, the respective glia are also thought to vary in their duties. In this work I addressed the question which cellular functions are shared between, and which are specific for astroglial cells from different brain regions and retina. Additionally, Müller cell heterogeneity was under special scrutiny focusing on cells from the macular and peripheral human retina.

As glial cells constitute only a subpopulation of all CNS cells, it was necessary to enrich our cells of interest to make the following analysis as precise as possible. We achieved this by magnetic bead associated cell sorting. These cell fractions were then subjected to tandem mass spectrometry and served as the basis of the subsequent work. To extract the information hidden in such complex datasets, I used various bioinformatics tools to break them down into smaller protein lists that allowed conclusions on their role in glial biology. Furthermore, I selected individual proteins for in-depth validation and functional examination.

I identified transcription factors of the nuclear factor 1 family to be expressed across glial cells of all contemplated regions and species, which corroborated their reported role in gliogenesis of brain and retina. Several of the pathways with interregional differential expression, including candidate proteins SLMAP and ZEB1, converged onto Hippo pathway signaling and alternative splicing. Furthermore, Müller cells of the human macula displayed an increased expression of proteins of the extracellular matrix, cell adhesion and exosomal pathways hinting towards a shift in

the extracellular milieu. In this context, I showed how EPPK1 might play a role in establishing the intricate Müller cell morphology, their biomechanical properties and the secretion of extracellular vesicles.

Finally, the proteomic datasets generated as part of my thesis have expanded our understanding of the biology of glia in different regions of the CNS and the retina specifically. The present findings will help to better understand the regional adaptations of astrocytes and Müller cells allowing the development of better tools or treatments targeting the desired subpopulations and translate insights between them.

I. INTRODUCTION

GLIAL CELLS – ASTROCYTES AND MÜLLER CELLS

Central nervous tissues like brain and retina are populated not only by neurons but also amongst others by a variety of glial cells including microglia originating from the hematopoietic lineage, myelinating oligodendrocytes, and importantly, astrocytes. While there are no myelinating glia in the human or murine retina, astrocytes reside at the border between vitreous and retina and microglia can be found throughout the plexiform layers under healthy conditions [1]. The main macroglia in the retina, Müller cells, have a unique, elongated morphology spanning the whole thickness of the retina from the inner limiting membrane at the vitreous to the outer limiting membrane and beyond, reaching out into the space between the inner segments of photoreceptors with their microvilli. They are distributed in an even pattern in the retina and thus come into contact with every other retinal cell type [2], [3]. Regarding their association with photoreceptors it is worthwhile to mention that a single Müller cell associates with only a single cone, but depending on the species and the retinal region with 10 or more rod photoreceptors [4]–[6].

Developmentally, brain and retina are closely related as they both emerge from the neuroectoderm and the subsequently formed anterior neural tube. Later, different brain vesicles give rise to specific brain regions but also the retina: While the telencephalon for example develops into the cerebrum with its various cortices, the diencephalon generates the thalamic areas as well as the retina, which is why this ocular tissue is regarded as part of the central nervous system (Figure 1) [7].

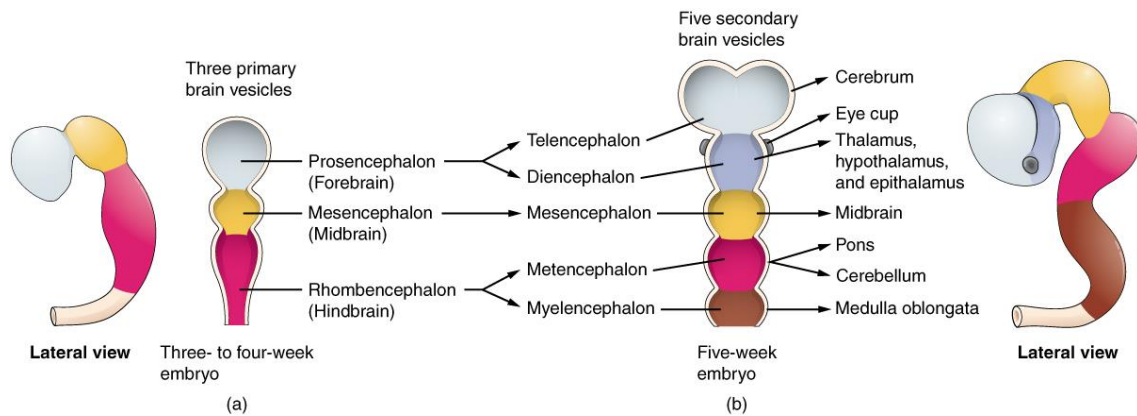


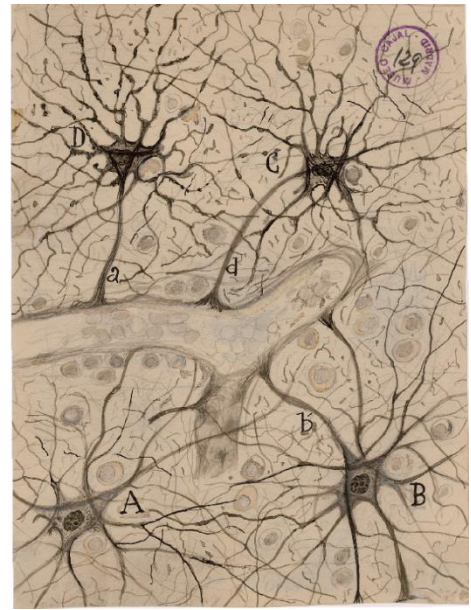
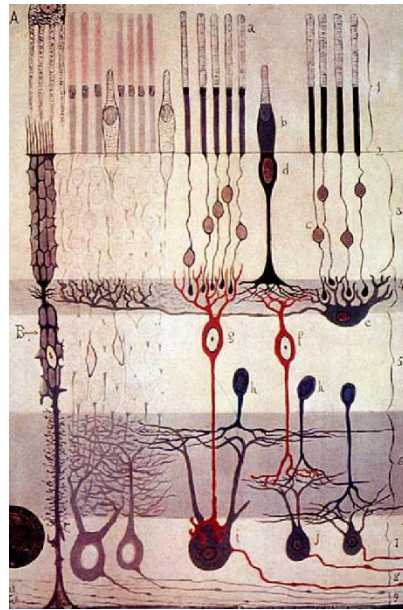
Figure 1: Development of brain vesicles. While astrocytes from grey and white matter develop from the telencephalon, Müller cells and thalamic astrocytes both originate from the diencephalon. (Source: Download for free at <http://cnx.org/contents/14fb4ad7-39a1-4eee-ab6e-3ef2482e3e22@11.1.>)

Consequently, astrocytes in the brain and retinal Müller glia fulfil similar functions and thus express many of the same genetic markers. Through their fine perisynaptic processes and the expression of excitatory amino acid transporter 1 (GLAST) and glutamine synthetase (GLUL) these glial cells are involved in neurotransmitter uptake and recycling thereby modulating the signal-to-noise ratio at synapses and influencing neuronal information processing [8], [9]. Furthermore, studies have proposed a metabolic coupling that involves intense exchange of glucose, pyruvate, lactate and lipids between neurons and glia [10]–[12]. Both, Müller cells and astrocytes were shown to have stem-cell potential depending on the species investigated. Müller cells can fully regenerate damaged retina in zebrafish, while astrocytes can proliferate upon tissue injury and generate subsets of neurons [13], [14].

There are however, specific features setting these related cell types apart. Ramon y Cajal captured their intricate morphology in his famous drawings: Müller cells have an elongated and bipolarized morphology (Figure 2) and are evenly spread across the retina, while astrocytes have more isotropic arborization (Figure 2) and show varied distribution depending on the brain region [15]. The above mentioned regenerative potential of Müller cells is not reproduced in adult mammals, while astrocytes do retain some proliferative tendencies in murine brains [16]. The retina with its light sensing capabilities poses special challenges that are not present in brain. For example, Müller cells are involved in the cone-specific visual cycle in which retinoids are regenerated to be used in the light-sensitive opsins of photoreceptors [17], [18]. Furthermore, it has been suggested that these glia contribute to the biomechanical stability of the retina and can act as biological light guides [19], [20]. How astrocytes contribute to brain tissue stiffness is poorly understood, but there is some evidence that these cells can sense and react to mechanical cues [21]–[25].

Figure 2: Drawings from Ramon y Cajal.

Left: Drawing of a retina with several neuronal cell types and a Müller cell (marked with B in the picture) (source: from Wikimedia, public domain). Right: Drawing of astrocytes close to a blood vessel and interspersed with neuronal somata. (Source: adapted from [26], creative commons CC BY 4.0)



REGIONAL HETEROGENEITY OF MACROGLIA

The section above described general parallels and differences between brain and retina and their respective macroglia. Zooming in on the level of the individual organ it becomes clear, that there is also intraregional heterogeneity between glial cells of the same nominal type. Such variation may have developmental origins and is exhibited on several levels: Müller cells developmentally all originate from the same secondary brain vesicle, the diencephalon. The origin of astrocytes on the other hand can already bifurcate at this level; cells from the telencephalon, for example, generate astrocytes in the cortex, while diencephalic progenitors might produce astrocytes in the thalamus [27]. There is evidence, that both grey and white matter astrocytes develop from radial glia of the subventricular zone albeit from different lineages [28], [29]. Furthermore, the microenvironment and the cellular composition of the embryonic and adult nerve tissue potentially promotes the specialization into distinct macroglial subtypes [15]. One can imagine that astrocytes resident in grey matter, rich in neuronal somata, may have different duties than for example cells surrounded by axonal fibers in white matter.

Another source of locally well-defined heterogeneity for Müller cells is the presence of the macula in the human retina. In this region, the cone-to-rod ratio continuously increases from periphery through the central region of the macula and peaks in the centermost part of the fovea, the foveola, where only cones and Müller cells reside (Figure 3). Here, the retina shows a characteristic indentation and laterally displaced inner nuclear layers allowing light to hit photoreceptors unhindered [30], leading to a higher light intensity and metabolite turnover. The latter is exacerbated by

the fact that cone photoreceptors, which are dominant in the outer nuclear layer of the macula, have a higher energy consumption [31]. Both factors, direct light exposure and increased metabolism are thought to be sources of reactive oxygen species that may cause oxidative stress [32]. Additionally, the fovea lacks the stratified vasculature present in multiple layers of the periphery, but instead relies mostly on the subretinal choroid for the supply of oxygen and other metabolites. Lastly, the indented shape of this tissue region is associated with a morphological change of Müller cells from columns that are parallel to the light path in the periphery to a z-shaped formation in the macula [30], [33], [34] (Figure 3B). Consequently, it can be speculated that there might be at least two Müller cell subtypes in the human retina, one residing in the peripheral retina and one or more inside the perimeter of the macula. This view is supported by the observation of macula-specific Müller cell degeneration in macular telangiectasia type 2 disease [35], [36].

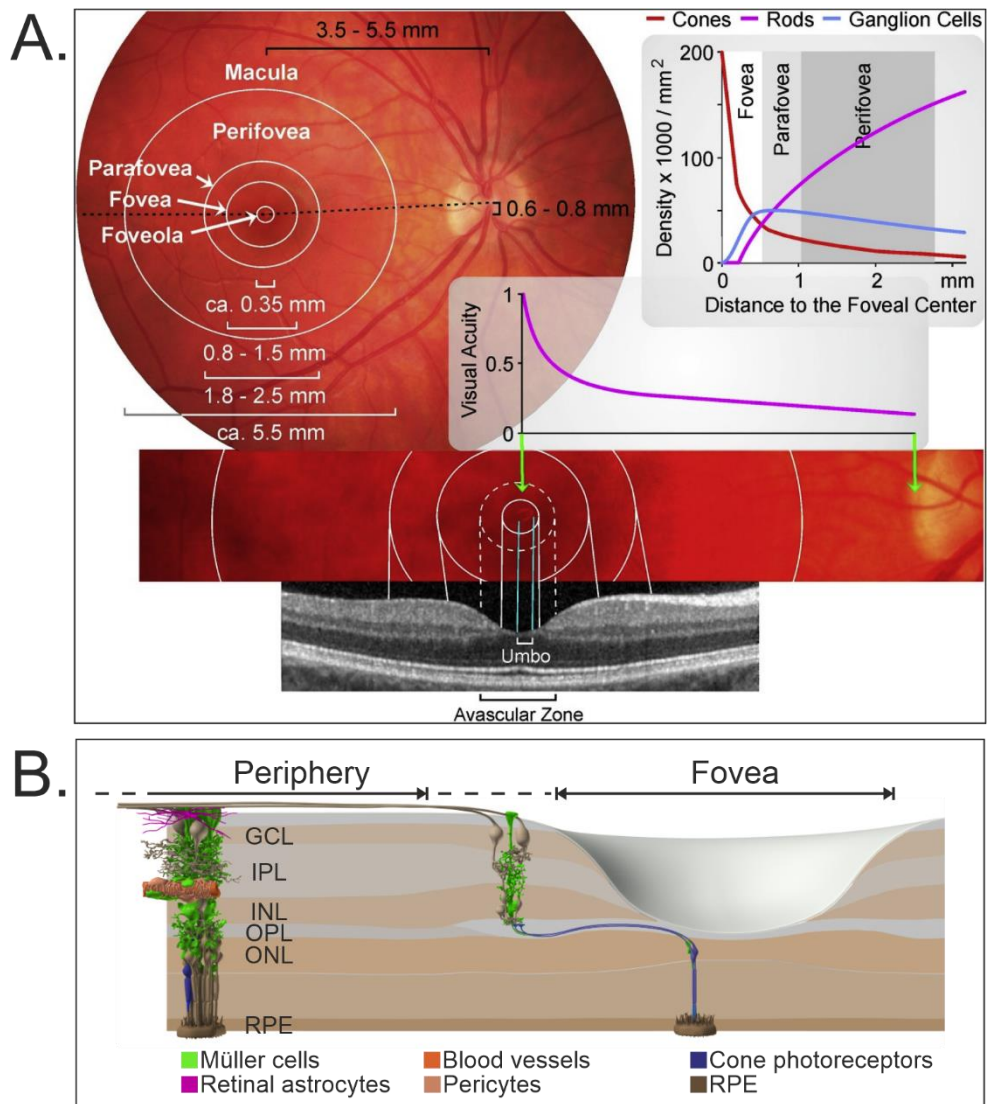


Figure 3: The anatomy of the human macula. A: The macula is a circular, central area in the human retina in which the cone density increases towards its center. Through the course from the outer edge across the perifovea to the parafovea the retina thickens, but in the centermost part, the fovea, a pit is formed through the lateral displacement of the nuclei of the inner retinal layers. In the foveal center cones reach their highest density and are accompanied solely by Müller cells. This is the area of highest visual acuity and free from intraretinal vessels. In fundus images the so called umbo is a visible light reflex at the bottom of the foveal pit. Reprinted from Bringman et al. [30] with permission from Elsevier. **B:** The cross-section of the human retina is structured in different layers. In the periphery the ganglion-cell layer (GCL), closest to the vitreous contains nuclei of ganglion cells and retinal astrocytes. Ganglion cells' dendrites are connected to interneurons in the inner plexiform layer (IPL). The inner nuclear layer (INL) contains cell somata of interneurons and Müller cells. Photoreceptor to interneuron synapses are located in the outer plexiform layer (OPL) while the outer nuclear layer (ONL) contains the somata of cone and rod photoreceptor cells. The outer segments of photoreceptor outer segments reach the retinal pigment epithelium (RPE). In the periphery, Müller cells exhibit a columnar morphology parallel to the light path and interact with all other cell types. In the fovea their morphology changes to a z-shape and subsequently they contact mostly cones in the ONL. Human Eye Explorer © Effigos

In summary, it can be stated that although astrocytes in the brain and Müller cells in the retina seem to fulfil analogous basic functions, there is inter- and intraregional heterogeneity that becomes evident on morphological and functional level. It depends

on the interplay with the local microenvironment and is reflected in cell-biological processes that are characteristic for the individual subtypes.

OMICS – GENE AND PROTEIN LEVEL QUANTIFICATION

There are many ways to uncover and define subpopulations of cells be it purely morphologically or by developmental origin. Depending on the cells in question, these characteristics might not be easily distinguishable but still lead to functionally distinct subtypes. In such cases, one can attempt to describe a population on an expression-wide level, for example through transcriptomic, proteomic or metabolomics means. Today many nucleic acid-based methods are available to analyze the genome, transcriptome, or epigenome.

All these techniques allow deep insights into certain aspects of the regulation of gene expression. The outcome of such gene expression tuning is the precisely controlled translation of amino acid chains that can then be further folded, modified, transported across the cell and finally degraded. This also means that the final action in the cell is mainly performed by mature proteins at the right time at the right place. Consequently, to fully understand how a cell's function is shaped by gene expression changes it is necessary to not only consider transcript levels, but to carefully assess its proteomic landscape as well.

Tandem mass spectrometry allows the quantification of thousands of proteins from biological samples needing minimal sample input amount and is comprehensively reviewed in [37]. The general pipeline begins with tissue/cell lysis and protein isolation before performing a peptidase digest at defined amino acids to receive short peptides. These samples are fed into a chromatography machine where the individual peptides are separated according to their biochemical properties like size, charge or most-commonly polarity. The spectra of these peptides, so called precursor ions, or MS1 spectra, allow the quantification, while their fragments' spectra (MS2) are used for the identification of the amino acid sequence. Intensities of peptides with sequences that are not shared between different proteins, so called unique peptides, are then used as a proxy to calculate the final protein abundance [38]–[40]. Depending on the acquisition mode, the identification and quantification of a protein may rely on its abundance in the sample and on appropriate spectra database entries.

BIOINFORMATICS – FROM USER-FRIENDLY TO SOPHISTICATED SOFTWARE

Classical technologies in molecular biology developed in the later part of the last century, like immunofluorescence or histochemical staining, Western blot, ELISA, PCR or qPCR aimed to investigate various aspects of gene expression from cellular localization to quantification. All these techniques are still used today in one form or another and although there have been technological advances, these methods are limited to the analysis of a rather small number of samples and/or targets. Recent developments in omics and high throughput techniques on the other hand produce vast datasets allowing detailed insights into thousands of measurements at a time. Such complex datasets are impossible to interpret without the help of specialized software and may require sophisticated bioinformatic pipelines, making the latter a pivotal tool in many modern experiments.

In the context of microscopy and imaging, using applications like ImageJ [41] or CellProfiler [42], [43] it is now for example possible to easily quantify dozens of cell parameters across hundreds of images reproducibly, objectively and with minimal manual labor. Such and similar tools allow the tracking of individual cells in time-lapse live-cell imaging or even the scanning of whole animals via tissue clearing and the subsequent reconstruction of cell morphology with artificial intelligence [44].

Proteomics and RNAseq use dedicated software for gene identification and expression quantification like MaxQuant [45] and Progenesis (Nonlinear Dynamics, Waters) or RSEM [46] and Kallisto [47], respectively. Some very recent methods escalate the level of detail by offering single cell resolution and thus requiring even more specialized software usually implemented in packages for general purpose programming languages like Scanpy [48] for Python or Seurat for R [49], [50]. Omic technologies additionally rely on curated databases with gene/protein annotation for identification and ultimately produce sample/cell x feature matrices with tens or hundreds of thousands or even millions of expression values.

These expression matrices can then be used to reduce dimensionality or distill information about distance metrics, differential feature expression, and gene enrichment. Moving one step up from individual genes, one can identify groups of highly interconnected genes for example using weighted gene co-expression network analysis (WGCNA) [51]. While WGCNA yields correlated feature groups based on the measured expression values, it might be helpful to look for possible functional relationships between the members within one gene/protein group in a next step. Such gene networks incorporating dozens or hundreds of functionally linked proteins can be

found through pathway enrichment analyses or categorization through databases like PANTHER [52], Gene Ontology [53], [54] or KEGG [55]–[57]. These can further be combined with other connectivity metrics via the meta database STRING [58], [59] to extract meaningful gene/protein networks fundamentally based on your quantified data, enriched with database results and assignable to specific pathways.

Although many of the tools described so far offer user friendly graphical interfaces or browser-based applications that need minimal bioinformatic knowledge, it is important to stress that where possible a coding approach is advisable to guarantee proper documentation and maximal reproducibility as well as speed. Reproducibility is highly desirable and might be achieved more easily in informatics than in other fields of science, but it has specific limitations that hinder scientists to run code written by another, on a different machine even with the same nominal software. Differences in software version, operating system, hardware and respective drivers, missing documentation or software that is proprietary or unavailable due to obsolescence can be high obstacles to pass before rerunning published code. There are however efforts to alleviate most of these problems via the open source movement, software repositories like Bioconductor [60], [61] and package and version control utilities like Conda [62] and Docker [63].

AIM OF THE THESIS

On the one hand, I aimed to generate a broad understanding of proteins and pathways that define a general macroglial identity and thus translate our knowledge of one glial subtype to another in a systemic view. On the other hand, it was my goal to capture the specific adaptations of glial subpopulations to their own niche and further our understanding of region-specific mechanisms of glia-neuron interaction, cell adhesion, cell-matrix interaction, and signal/metabolite transduction. I based my research on multiomic and bioinformatic analyses of isolated cell populations across multiple tissues of the central nervous system originating from human and mouse with a prime focus on the retina, a structurally rather simple and comparably easily accessible part of the CNS. Therefore, the following specific aims were pursued in my thesis:

1. Define molecular pathways related to macroglial heterogeneity (astrocytes/Müller glia) in the retina and brain.
2. Determine the molecular signature of Müller glial subpopulations in the human retina and defined mouse models to mimic aspects of the human fovea.
3. Functionally validate candidate genes identified as potential drivers of glial heterogeneity.

These novel insights will help to improve our understanding of processes related to glial biology relevant for the establishment of distinct functional subdomains of the CNS and might point to pathways potentially relevant also in pathologies affecting retina and brain.

II. MANUSCRIPTS

HETEROGENEITY OF GLIAL CELLS OF THE CENTRAL NERVOUS SYSTEM – A PROTEOMIC STUDY

Authors:

Kaplan L, Natarajan P, Ohlig S, Rossner, M, Kannayian N, Lauerer, M, Neueder A, Smialowski P, Fischer-Sternjak J, Hauck SM, Götz M, Grosche A

Author contributions:

LK: designed experiments, sorted retinal fractions, performed bioinformatic analyses and immunofluorescence stainings with corresponding microscopy and image analysis. Prepared figures, conceptualized and wrote the manuscript. **PN**: performed immunofluorescence stainings with corresponding microscopy and image analysis. Generated ZEB1 KO and validated the used primary antibody. **SO, MR, KN, LM**: sorted brain fractions for RNAseq and performed RNAseq data acquisition and preprocessing. **AN**: Helped with the establishment of WGCNA analysis and edited the manuscript. **SP**: Primary bioinformatic analysis of brain RNAseq data. **JF**: sorted cells from brain regions for proteomic analysis, edited the manuscript. **SMH**: designed experiments, performed tandem mass spectrometry of retinal and brain samples and the primary analysis of the resulting data. Edited the manuscript. **MG**: designed experiments, conceptualized and edited the manuscript. **AG**: designed experiments, analyzed data, prepared figures, conceptualized and edited the manuscript.

Heterogeneity of glial cells of the central nervous system – a proteomic study

Lew Kaplan¹, Poornemaa Natarajan^{1,2}, Stefanie Ohlig^{1,2}, Moritz Rossner³, Nirmal Kannayian³, Markus Lauerer^{1,2}, Andreas Neueder⁴, Pawel Smialowski^{1,2}, Judith Fischer-Sternjak^{1,2}, Stefanie Hauck⁵, Magdalena Götz^{1,2}, Antje Grosche¹

1: Department of Physiological Genomics, Ludwig-Maximilians-Universität München, Munich, Germany

2: Institute for Stem Cell Research, Helmholtz Center Munich, Neuherberg/Munich, Germany

3: Molecular Neurobiology, Department of Psychiatry, Ludwig-Maximilians-Universität München, Munich, Germany

4: Department of Neurology, Ulm University, Ulm, Germany

5: Research Unit Protein Science and Metabolomics and Proteomics Core, Helmholtz Center Munich, Neuherberg/Munich, Germany

Abstract

As the central nervous system of adult mice is subdivided in anatomical and functional compartments, the local astroglia also need to adapt to the characteristics of their native environment. Nevertheless, such glial subpopulations oftentimes fulfil similar basic functions in tissue homeostasis or even neuronal signal modulation. Previously, studies reported various subpopulations in brain and retinal regions but direct comparison between retinal Müller glia and brain astrocytes is still missing. Here we used magnetic bead associated cell sorting to enrich Müller cells from the retina and astrocytes from diencephalon, grey and white matter and subjected these cell fractions to tandem mass spectrometry. We found transcription factors of the nuclear factor 1 family and known astrocytic markers to be uniformly expressed across glial samples. Müller cells and diencephalic glia exhibited a close relationship on proteomic level indicating their common developmental origin. Furthermore, we identified SLMAP and ZEB1 to be specifically expressed in Müller cells or cortical astrocytes, respectively. Pathways that showed interregional differential regulation seemed to converge onto Hippo signalling and thereby the regulation of YAP/TAZ. Together our findings suggest that a region-specific modulation of this pathway might contribute to the variance in proliferative and stem cell characteristics of glia between retina, diencephalon, grey matter and white matter.

Introduction

The central nervous system exhibits a degree of heterogeneity on cellular as well as developmental level which leads to interregional differences even between the same nominal cell type. In this work we focused on the non-myelinating macroglia of the murine central nervous system: astrocytes from three different brain regions, namely diencephalon, grey and white matter and retinal Müller cells. The relationship between diencephalic astrocytes and Müller cells was of special interest, since these developmentally both originate from the same secondary brain vesicle, while grey and white matter astrocytes stem from the telencephalon [1]–[3]. Although astrocytes and Müller cells serve comparable purposes across their respective tissues e.g. in clearing the tripartite synapse off neurotransmitters [4], [5], potassium siphoning [6]–[9] as well as metabolic coupling with neurons and blood vessels [10]–[12], there are also obvious morphological as well as functional differences. Most apparently, Müller cells are very elongated and bipolar in shape extending their processes across the entire thickness of the retina maintaining the morphology of a radial glia cell. Astrocytes on the other hand exhibit a rather equally arborized, but less polarized appearance. Other obvious differences of retinal Müller glia compared to brain astrocytes include their involvement in retinoid recycling in the visual cycle [13] and the increased presence of oxidative stress due to light exposure and as a result of the extremely high metabolic rate of photoreceptors [14], [15]. Additionally, Müller cells have been shown to contribute to the biomechanical stability of the retina providing the necessary traction forces [16], while comparably little is known in this regard about astrocytes. Both astrocytes and Müller glia exhibit stem cell potential of varying propensity depending on species, pathological state and tissue localization. In zebra fish, Müller cells can fully regenerate injured retina [17], while brain damage is resolved in the absence of classical astrocytes but rather through ependymal cells [18]. Although no such regeneration is found in mammalian retina, the limited capability of brain astrocytes to generate neurons after injury implies some degree of stem cell potential [19], [20]. This potential seems to vary not only between retina and brain, but also between astrocytes of different brain regions [21] indicating a broad heterogeneity of astroglia that can be further elaborated if one contemplates the diverse microenvironments these cells are integrated in. A better understanding of the variation or conservation of the astroglial proteomic landscape between regions of the central nervous system may allow not only the targeting of all or just specific subpopulations as necessary, but also the transfer of knowledge about one to the others. This should help advance the growing field in which the retina and retinal degeneration are used as "windows to the brain" in many neurological disorders, including neuromyelitis optica spectrum disorders (NMOSD), as well as Alzheimer's disease, multiple sclerosis, Parkinson's disease, or hyperkinetic disorders [22]–[26].

Single cell transcriptomic profiling is a powerful tool to uncover cellular heterogeneity but suffers from shallow sequencing depth as compared to its bulk counterpart. Furthermore, studying transcript expression alone does not allow reliable conclusions on resulting protein levels due to posttranscriptional factors like differences in the translation rate or ribosome usage of distinct mRNAs, variance in protein stability or translational delay during a shift in cell state [27], [28]. Additionally, apart from some noncoding RNA species, it is typically the protein that drives the cell's function. There have been efforts to untangle these levels of heterogeneity assessing differences between regions and cell-types in the retina [29]–[34] as well as the brain [21], [35]–[38] using transcriptomic and proteomic techniques. However, direct comparison between retinal and brain glia are missing. Consequently, to better understand glial functional heterogeneity, but also to identify commonalities, we used magnetic bead activated cell sorting to isolate Müller cells from the retina as well as astrocytes from cortical grey matter, diencephalon and white matter to generate cell type-specific proteome profiles.

Results

Magnetic activated cell sorting (MACS) allows the retrieval of enriched glial fractions for proteomic analysis.

Müller cells from the retina and astrocytes from diencephalon, grey and white matter, respectively, were purified in a multistep procedure termed magnetic activated cell sorting (MACS) [33], [39], [40]. To validate efficient enrichment, we compared the glial fractions to their respective flow-through, which consists mostly of photoreceptors in the retina [33], and neuronal, but also other cell types including microglia in the brain.

Immunostaining for the Müller cell marker glutamine synthetase (GLUL) confirmed a high purity of Müller cells (~70 %) in the retinal glial fraction (CD29⁺) and their almost complete absence from the respective flow-through (~2%, CD29⁻) (Fig. 1A). Importantly, the gentle MACS protocol allowed the cells to retain their characteristic polar morphology, in which the long inner and outer stem processes are still clearly discernible. This observation translated well to the respective protein expression data, where a highly specific expression of GLUL (Fig. 1C) was found in the Müller cell fraction, while neuronal markers like cone arrestin (ARR3) or rod specific phosphodiesterase (PDE6B) were enriched in the flow-through fraction (Fig. S1).

Similarly, the ACSA2⁺ brain astrocytic fractions showed specific expression of astroglial marker S100B in comparison to the respective flow-through fractions (Fig. 1C), while microglial and blood as well as innate immunity markers were enriched in the flow-through (Fig. S1).

We also noticed a possible contamination with oligodendrocytes in the ACSA2⁺ fraction indicated by OLIG1 expression (Fig. S1). A previous study, where a similar MACS-based approach was used to isolate astrocytes from diencephalon, found a contamination with ependymal cells in the ACSA2⁺ fraction [21]. However, the ependymal-specific marker genes

defined by the authors were not present at significant levels in our diencephalic glia fractions (Fig. S1). Keeping these caveats in mind, we focused our deeper analysis of region-specific proteins on retina and grey matter.

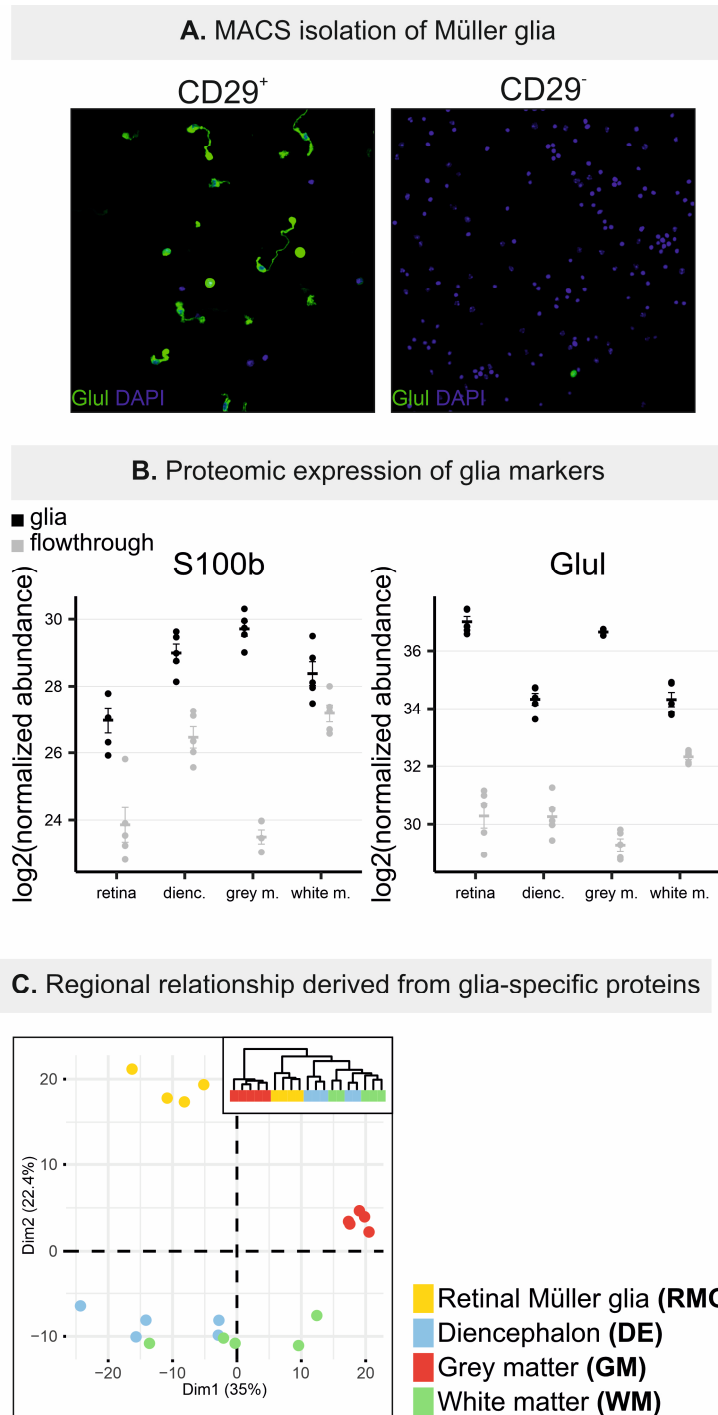


Figure 1: Protein signatures suggests closer relationship of Müller glia to subcortical astrocytes. From each individual mouse ($n=5$) Müller glia from retina and astrocytes from grey matter, white matter or diencephalon, respectively, were isolated via MACS protocol followed by tandem mass spectrometry to generate a combined proteomic data set. **A:** Müller cells were isolated targeting the surface marker CD29 after sequential depletion of CD11B⁺ microglia and CD31⁺ vascular cells. Immunostaining for Müller cell marker glutamine synthetase (GLUL) confirms the enrichment of Müller cells in the CD29⁺ fraction. A complete absence of GLUL was found in the respective flow-through. **B:** Proteomic profiling corroborated the glial character of the CD29⁻ or ACSA2-positive fractions with an increased expression of glial markers S100B and GLUL in comparison to their respective glia-depleted flow-through. **C:** Left: Principal component and distance (inset) analysis show distinct clusters for grey

matter astrocytes and retinal Müller glia (RMG), while astrocytes from diencephalon and white matter seem to intermingle.

Tandem mass spectrometry uncovers close relationship of Müller glia with subcortical astrocytes.

Proteomic analysis of the glial and flow-through fractions delivered a dataset with overall almost five thousand identified proteins. To further investigate the glia-intrinsic players responsible for heterogeneity, as well as the factors that define a shared macroglial identity, we based our analysis on proteins enriched in glial fractions relative to their neuron-rich counterparts. 3749 proteins met our requirements of being significantly enriched in a glial fraction of at least one CNS region (glia/flow-through expression ratio > 1, p-value < 0.05). We identified 78 proteins that did not show a significantly different expression between regions (ANOVA p-value > 0.05) but were glia-specific in every region (glia/flow-through expression p-value < 0.05) (Tab. 2). One of these was glial fibrillary acidic protein (GFAP), which is known to be a marker for subcortical astrocytes [37], as well as reactive Müller cells [41]. NFIX and NFIA, transcription factors that were shown to play a role in Müller cell-driven retinal regeneration [42] were consistently and specifically expressed in all glial populations tested (Tab. 2).

Principal component analysis (PCA), a common dimensionality reduction technique, showed distinct clusters for retinal Müller cells and grey matter astrocytes, respectively, while diencephalic and white matter astrocytic samples seemed to intermingle in a common, more diffuse cluster (Fig. 1C). A dendrogram based on Manhattan distance revealed a closer proteomic relationship between retinal Müller cells and subcortical astrocytes from the white matter and diencephalon, while grey matter samples clustered more distantly (Fig. 1C).

The fact that diencephalon contains nerve fibre tracts and therefore inevitably also astrocytes of white matter origin, is recapitulated in the aforementioned close relationship of DE and WM through a substantial amount of similarly expressed proteins: Indeed, we found 1817 proteins, which showed a global difference in variance (ANOVA p-value < 0.05) between all glial fractions but no significant difference between WM and DE (paired t-test p-value > 0.05). Since we were interested in the major differences between the regions, especially the relationship between retinal Müller glia and the ontologically related diencephalic cells, we sought to separate WM and DE by excluding these proteins. This led to a clear separation of clusters in the PCA, as well as distance analysis, now revealing a closer connection between Müller cells and diencephalic than with white or grey matter astrocytes. (Fig. 2A)

Next, we looked specifically for proteins that represented a diencephalic character by being expressed at comparable levels between retinal Müller cells and diencephalic astrocytes but showing significant difference with grey and white matter, respectively. Thus, we not only

excluded the aforementioned 1817 white matter/diencephalon proteins but those proteins with a significant difference between RMG and GM. The resulting 341 proteins (Fig. 2B) were analyzed using the Search Tool for the Retrieval of Interacting Genes/Proteins (STRING) database, which features direct and indirect protein/protein interactions based on experimental and bioinformatic metrics [43], [44]. In addition, we implemented Cytoscape [45], a powerful software allowing the visualization and analysis of networks, that can be fitted with the *stringApp* [46] for *in situ* STRING queries. Subclustering of the complete network via the Markov Cluster Algorithm (MCL) available through Cytoscape's *clusterMaker* plugin [47] preceded pathway enrichment analysis. Proteins in the five largest STRING clusters were associated with synaptic vesicular signalling pathways as well as the Ras pathway, among others (Fig. 2C). The latter included proteins such as the GTPases HRAS, KRAS, NRAS, and RHOA, but also the proto-oncogenic tyrosine protein kinase SRC and the serine/threonine protein kinase MTOR, all of which are involved in a variety of cell biological functions such as growth and proliferation regulation and are considered proto-oncogenes [48], [49].

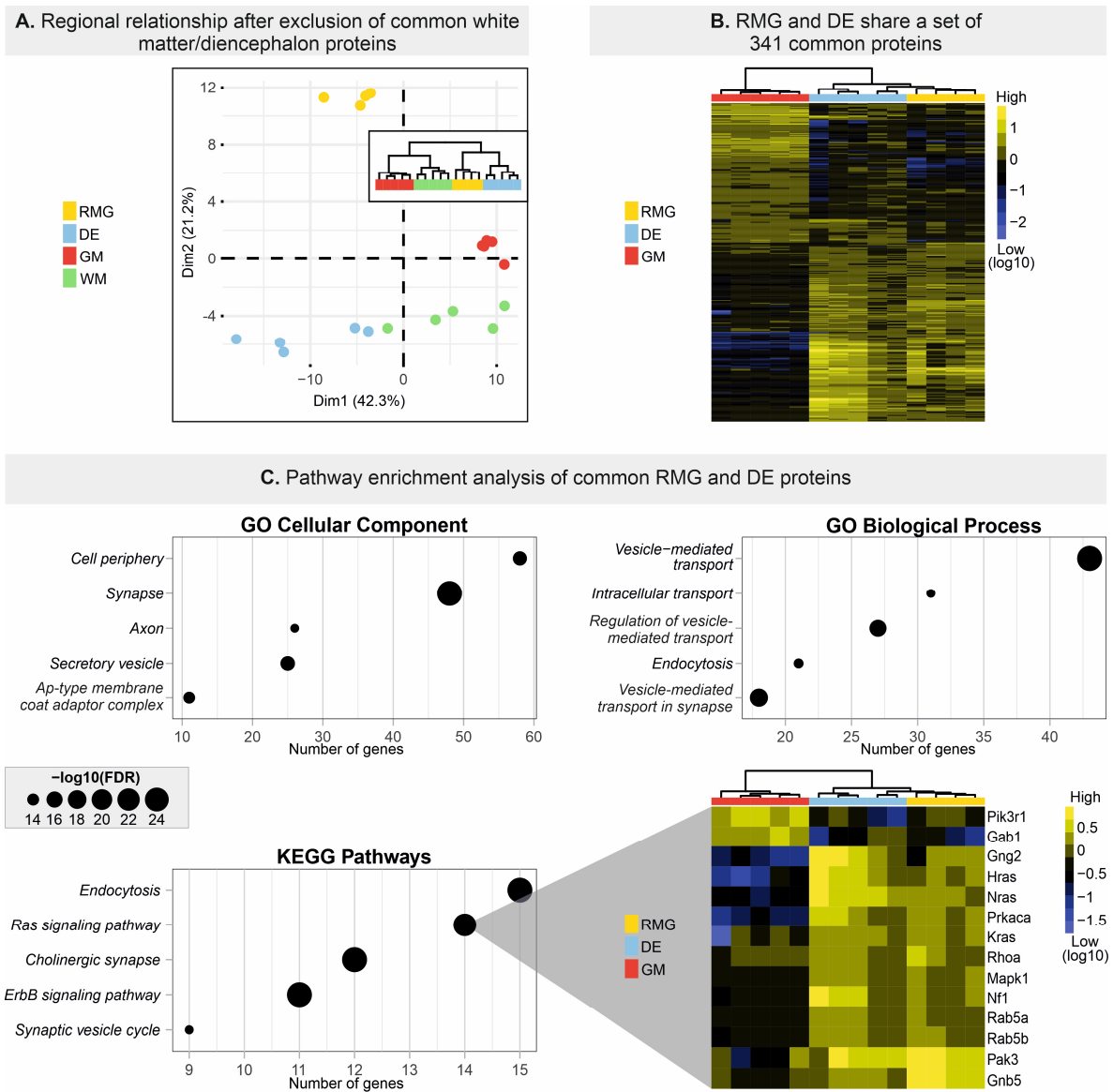


Figure 2: Subregional glial proteomic profiles suggest closest relationship of retinal Müller cells to diencephalic astrocytes. **A:** PCA analysis on basis of glial proteomes after exclusion of proteins that were not found to have differential expression between diencephalic and white matter astrocytes (DE vs. WM $p > 0.05$). **B:** Further excluding proteins that show a difference between RMG and grey matter ($p < 0.05$) and focusing on proteins with no expression difference between Müller cells and DE, resulted in 341 common proteins. **C:** Search and subclustering via STRING/Cytoscape resulted in several interconnected protein subclusters, of which the biggest 5 were subjected to pathway enrichment analysis. Significant pathways were sorted by number of genes and only the top 5 are presented here. 14 proteins were assigned to the Ras signaling pathway and showed distinct expression pattern between glial cells from retina/diencephalon and grey matter.

Identification and validation of region-specific glia proteins.

Finally, to determine proteins specific for astrocytes of the individual regions, we performed differential protein expression analysis via ANOVA. For each group we found a set of glia-specific proteins that were at least two-fold enriched compared to all glial populations investigated (Fig. S2A, Tab. S1). Amongst others, we found known Müller cell-specific markers like RDH10 or RLBP1 to be highly enriched in the retinal glia fraction, while ALDH1L1, often regarded a pan-astrocytic marker [37], showed highest expression in grey matter astrocytes (Tab. S1). Furthermore, this list includes a number of differentially expressed transcription

factors and potential novel marker proteins. For instance, Transcriptional coactivator YAP1 (YAP1) (Fig. S2B) and Zinc Finger E-Box Binding Homeobox 1 (ZEB1) were enriched in grey matter astrocytes, while N-myc-interactor (NMI) was specific for retinal Müller glia (Tab. 3).

Sarcolemmal Membrane-Associated Protein (SLMAP) showed on average an ~80-fold higher expression in Müller cells than in astrocytes of the different brain regions (Fig. 3A). Immunostaining confirmed this Müller cell specificity. In retinal sections, SLMAP exclusively localized to the Müller cell endfeet, their stem processes stretching towards the inner nuclear layer and to their cell somata (Fig. 3A). In contrast, SLMAP-positive cells were neither detected in grey or white matter nor in diencephalon (Fig. 3A, B), thereby establishing it as a novel Müller cell marker in mice to discriminate them from brain astrocytes.

ZEB1 exhibited grey matter-specific expression (~17-fold vs. RMG and WM, ~3-fold vs. DE) in our proteomic analysis (Fig. 3C). Performing ZEB1 immunofluorescence staining using an antibody we validated to be highly specific for ZEB1 (Fig. S3), we found nuclear ZEB1 in S100B/SOX9-positive astrocytes (Fig. 3C). In grey matter most analysed cells (71.4 %) showed triple staining, validating the astrocyte-specific expression of this transcription factor in this region. In the white matter, about half of the cells (54.9%) showed SOX9/S100B staining, indicating their glial identity without being ZEB1-positive at the same time (Fig. 3D). Like in white matter, less than 50% of diencephalic astrocytes were ZEB1-positive (Fig. 3D). In support of the proteome profiles, ZEB1 could not be detected in Müller cells or any other cell type of the retina (Fig. 3D).

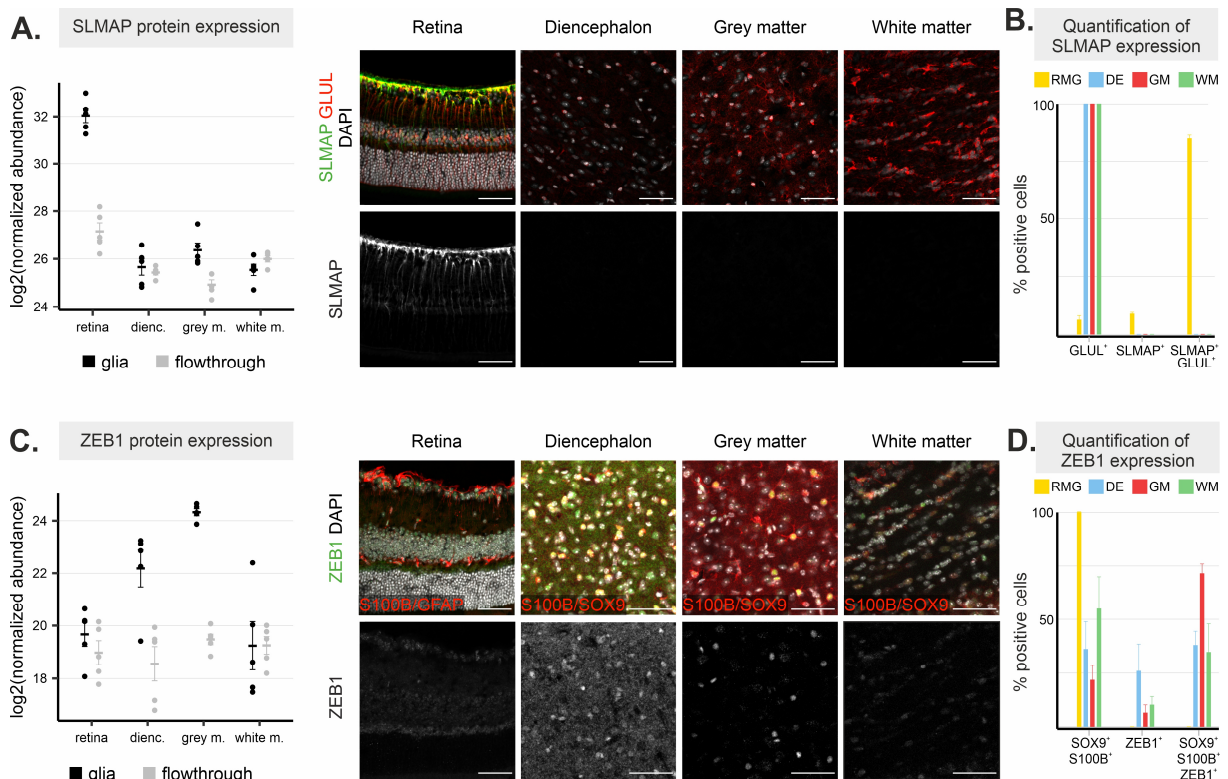


Figure 3: Expression of the region-specific glial proteins SLMAP and ZEB1. **A:** The SLMAP protein was enriched in Müller cells and was found exclusively in this cell type in immunostaining colocalized with the Müller cell marker glutamine synthetase (GLUL), whereas it was absent in astrocytes in the brain. **B:** Quantification of SLMAP in brain and retina shows Müller cell-specific localization. **C:** ZEB1 was found to be enriched in grey matter astrocytes on proteomic level and in immunofluorescence staining, while being absent from Müller cells. Blood vessels show typical unspecific staining due to the secondary anti-mouse antibody. **D:** Quantification of ZEB1 in the brain and retina shows that the number of ZEB1-positive astrocytes is highest in the gray matter, whereas in the white matter and diencephalon, a larger proportion of SOX9/S100B-positive astrocytes does not express ZEB1. We did not find any ZEB1-positive cells in the retina. B: n=3, D: n = 4. RMG, retinal Müller glia; DE, diencephalic astrocytes; GM, gray matter astrocytes; WM, white matter astrocytes.

As a transcription factor ZEB1 potentially has strong impact on the cell's functional phenotype. For instance, it was shown that ZEB1 exhibits transcriptional repressor as well as activator activity, depending on the cellular and developmental context [50], [51]. This prompted us to investigate ZEB1 predicted target genes in our proteome data set. We used the oPOSSUM-3 webtool [52] to search for putative ZEB1 binding sites in the regulatory sequences of genes coding for the glia-specific proteins we have identified and found 1043 of those with a relative matrix score of > 96%, allowing only stricter matches of putative binding site and position weight matrix. Together with a set of known ZEB1 target genes directly validated in functional studies [51], [53], we found 251 proteins in our glia-specific proteomes (Tab. S2) to be significantly correlated in their expression with that of respective ZEB1 protein levels in the respective CNS regions. For 180 out of those 251 proteins we found a positive strong (absolute values 0.4 – 0.69; 207 proteins) to very strong (absolute values >0.7; 41 proteins) Spearman correlation. Medium-chain acyl-CoA ligase (ACSF2) and Alpha-amino adipic semialdehyde dehydrogenase (ALDH7A1) showed highest Spearman correlation coefficients (>0.9), while from the 71 negatively correlated proteins Peptidyl-tRNA hydrolase 2 (PTRH2) and Contactin-2 (CNTN2) stood out with values around -0.7 (Fig. 4). In particular, YAP1, a master regulator that plays a role in a variety of cellular functions including proliferation, regeneration, and mechanotransduction [54], [55] and is thought to interact with ZEB1 in a tumor-promoting manner [51], [53], was strongly correlated with ZEB1 at the level of protein expression (Fig. 4). Overall, we found enrichment of proteins associated with metabolic/mitochondrial processes, as well as proteins involved in mRNA splicing and nucleoside biosynthetic pathways, which are putatively under the control of ZEB1 especially in grey matter astrocytes.

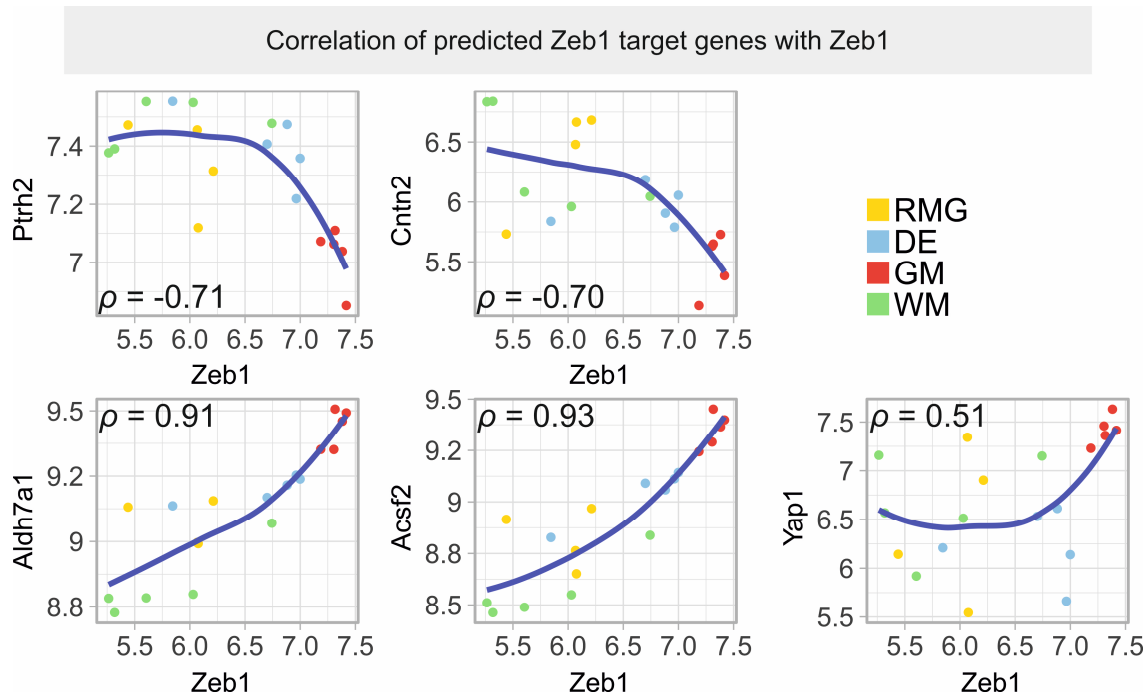


Figure 4: Correlation of putatively ZEB1 regulated proteins with ZEB1 expression levels. We used the oPOSSUM-3 webtool to identify 251 proteins with predicted ZEB1 binding sites in their regulatory regions and a significant Spearman correlation in their protein expression with ZEB1. While YAP1, ALDH7A1 and ACSF2 showed strongest positive correlation, PTRH2 and CNTN2 were strongest negatively correlated with ZEB1. Log₂ transformed protein expression across samples are plotted for respective proteins as indicated on the x- and y-axis. RMG, retinal Müller glia; DE, diencephalic astrocytes; GM, gray matter astrocytes; WM, white matter astrocytes.

Functional region-specific glia hallmarks

We employed weighted gene correlation network analysis (WGCNA), an unsupervised method to uncover clusters of highly intercorrelated glial proteins, so called modules. Proteins belonging to one module are expressed in a similar pattern across all investigated samples, which then can be condensed into the so-called *module eigengene*. Similar to the first principal component, it is based on and summarizes the expression of the individual module proteins in one shared value, which in turn makes it possible to correlate whole modules with external traits, like age, sex, weight, disease phenotype or other experimental groups [56], [57]. Similarly, *gene significance* can be defined as the correlation of a single protein to an external trait, which might be of interest since all proteins of one module do not necessarily exhibit the same correlation. The fact that this method yields clusters of proteins that are not only differentially expressed between experimental groups but are also interconnected is advantageous for the subsequent discovery of underlying pathways.

We were able to find distinct modules with highly interconnected proteins that showed a positive correlation with specific CNS macroglia populations. Of note, the modules differed regarding the number of proteins they are comprised of as well as in the strength of the correlation of their *eigengene* to the respective groups. Modules *RMG_1* and *RMG_2*, totalling to 323 proteins, both had high positive correlation with retinal Müller glia (RMG), but no

significant correlation to any other group, showing its specificity (Fig. 5). The diencephalic (DE) module, comprising 489 candidate proteins, correlated positively with the diencephalic astrocyte fraction but also showed a negative correlation with grey matter, suggesting opposing regulation. The grey matter (GM) modules *GM_1* and *GM_2*, containing 782 proteins in total, had a high positive correlation with cortical grey matter astrocytes with *GM_2* being also negatively correlated with the white matter trait (Fig. 5). Lastly, the modules related to white matter (WM), *WM_1* and *WM_2*, showed the smallest positive correlation values compared to the other groups' modules, at the same time being highly negatively correlated to Müller cells or grey matter, respectively. This and the highest total number of proteins of all group-specific modules (974 proteins) indicate a comparatively lower specificity (Fig. 5).

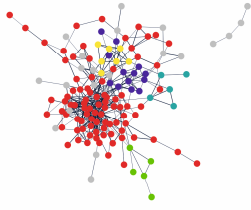
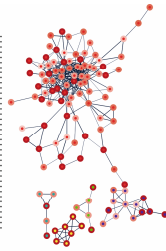


Figure 5: Expression data was subjected to weighted gene correlation network analysis (WGCNA) resulting in modules each comprised of hundreds of putatively co-regulated and interconnected proteins. In a next step the module eigengenes (ME) were correlated to external traits (respective CNS regions). Groups of proteins were identified that are not only highly correlated with specific glial subpopulations but are also interconnected in their expression. Positive correlation of MEs with respective external traits is represented by red color scales, while blue hues indicate negative correlation. Only modules with a significant, highly positive correlation with one of the regions are shown. The numbers to the left of the modules represent how many proteins in total they contain.

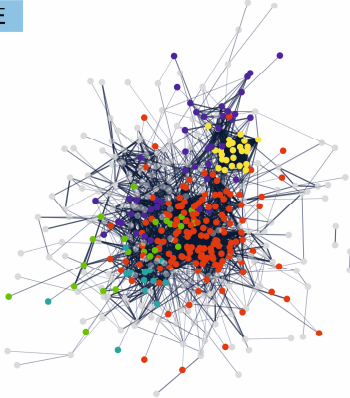
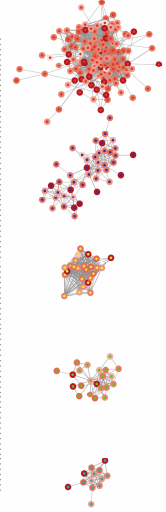
After we subdivided the majority of the proteins in this way into groups related to the different putative glial populations, we set out to identify the major functional pathways potentially controlled by these protein sets. Our STRING/Cytoscape based pipeline with the region-related modules (filtered for being glia-specific in the respective region), as input yielded complex networks of hundreds of nodes (Fig. 6 A-D). We assumed that due to the character of the networks stemming from WGCNA and thus being putatively co-regulated in our system, functional enrichment analysis would be more informative in assigning interesting pathways to the modules. However, with these networks it produced unsatisfactory results, since the most significant terms, were very general (data not shown), meaning higher up in the respective

hierarchical gene ontology trees. This was possibly due to the high number of input proteins. Since nodes aggregated in dense sub-networks, we used the MCL clustering algorithm and obtained, depending on module size, up to 92 subclusters ranging in size from two to 169 nodes. The five biggest clusters per glia population were chosen for separate functional enrichment analysis which identified major pathways accounting for most of the included proteins (Fig. 6A'-D').

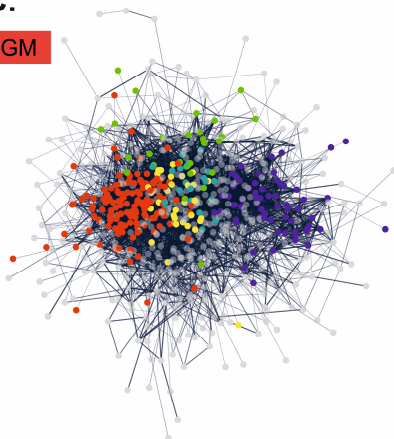
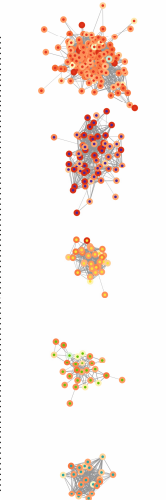
The modules *RMG_1* and *RMG_2*, correlating with retinal Müller glia, yielded one big cluster related to focal adhesion (KEGG pathways, FDR = 5.78×10^{-13} , 15/87 cluster proteins) and cell junction (GO-CC, FDR = 2.9×10^{-19} , 33/87 cluster proteins) (Fig. 6A, A'). In contrast, the biggest cluster of grey matter modules *GM_1* and *GM_2* could almost entirely be explained with terms related to mRNA splicing and RNA processing with over one hundred (118) out of 142 proteins falling within this category (Fig. 6C, C').

A.**RMG****A`.**

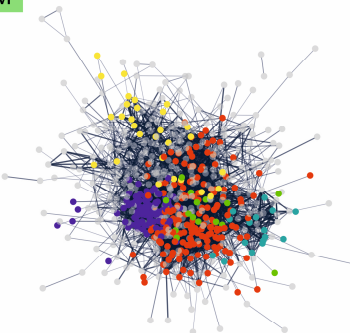
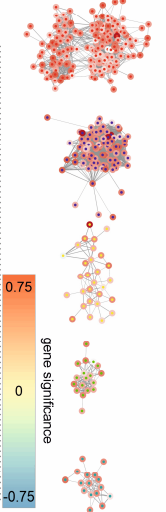
- **GO Component:** Cell junction, cytoplasmic vesicle
- **GO Function:** Protein binding, cytoskeletal protein binding
- **GO Process:** Actin cytoskeleton organization, anatomical structure morphogenesis
- **KEGG Pathways:** Focal adhesion, Tight junction, Rap1 signaling pathway
- **GO Component:** Plasma membrane
- **GO Function:** Transporter activity, oxidoreductase activity
- **GO Process:** Organic anion transport, retinol metabolic process, response to stimulus
- **KEGG Pathways:** Retinol metabolism

B.**DE****B`.**

- **GO Component:** Vesicle, synapse
- **GO Function:** SNARE binding, ribonucleoside triphosphatase activity
- **GO Process:** Vesicle mediated transport, intracellular transport
- **KEGG Pathways:** Synaptic vesicle cycle, Lysosome
- **GO Component:** Mitochondrion, mitochondrial part
- **GO Process:** Protein targeting to mitochondrion, regulation of apoptotic process
- **KEGG Pathways:** Sphingolipid signaling pathway
- **GO Component:** Mitochondrial respirasome, respiratory chain complex
- **GO Function:** Oxidoreductase activity
- **GO Process:** Electron transport chain, oxidation reduction process
- **KEGG Pathways:** Oxidative phosphorylation
- **GO Component:** Microtubule cytoskeleton, centrosome
- **GO Function:** Microtubule motor activity
- **GO Process:** Microtubule-based movement, protein transport
- **KEGG Pathways:** Phagosome, endocytosis
- **GO Component:** heterotrimeric G-protein complex, neuron part
- **GO Function:** GTPase activity, signaling receptor binding
- **GO Process:** G protein-coupled receptor signaling pathway
- **KEGG Pathways:** Glutamatergic/GABAergic synapse

C.**GM****C`.**

- **GO Component:** Nucleus, nuclear part
- **GO Function:** Nucleic acid binding, mRNA binding
- **GO Process:** mRNA processing, RNA splicing
- **KEGG Pathways:** Spliceosome, mRNA transport
- **GO Component:** Mitochondrion, mitochondrial part
- **GO Function:** Oxidoreductase activity, electron transfer activity
- **GO Process:** Oxidation-reduction process, electron transport chain
- **KEGG Pathways:** Metabolic pathways, oxidative phosphorylation
- **GO Component:** Ribonucleoprotein complex, cytosolic ribosome
- **GO Function:** Translation factor activity, RNA binding
- **GO Process:** Translation, translational initiation
- **KEGG Pathways:** Ribosome, RNA transport
- **GO Component:** Microtubule cytoskeleton, centrosome
- **GO Function:** Cytoskeletal protein binding, motor activity
- **GO Process:** Establishment of localization in cell
- **KEGG Pathways:** /
- **GO Component:** Proteasome complex
- **GO Function:** Hydrolase activity, transcription factor binding
- **GO Process:** Ubiquitin-dependent protein catabolic process
- **KEGG Pathways:** Proteasome

D.**WM****D`.**

- **GO Component:** Nucleus, chromosome; Golgi apparatus part, cytoplasmic vesicle
- **GO Function:** Nucleic acid binding, chromatin binding, transcription regulatory activity, unfolded protein binding
- **GO Process:** mRNA splicing, chromatin organization; protein folding, golgi vesicle transport
- **KEGG Pathways:** Spliceosome; protein processing in ER
- **GO Component:** Cytosolic ribosome
- **GO Function:** RNA binding, translation regulatory activity
- **GO Process:** Translation, ribosome biogenesis
- **KEGG Pathways:** Ribosome, RNA transport
- **GO Component:** Mitochondrion, Peroxisome
- **GO Function:** Catalytic activity, oxidoreductase activity
- **GO Process:** lipid metabolic process
- **KEGG Pathways:** metabolic pathways, ubiquitin mediated proteolysis
- **GO Component:** Nuclear pore, chromosomal part
- **GO Function:** structural constituent of nuclear pore, chromatin binding
- **GO Process:** chromosome segregation, RNA transport
- **KEGG Pathways:** RNA transport, cell cycle
- **GO Component:** Cilium, dynein complex
- **GO Function:** motor activity
- **GO Process:** microtubule bundle formation, axoneme assembly
- **KEGG Pathways:** /

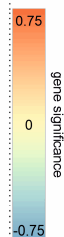


Figure 6: STRING Analysis of significant WGCNA modules. Modules determined to be highly correlated with glial subgroups by WGCNA contained proteins that were not enriched in the glia fraction of the respective region as compared to its flow-through. These were excluded before pathway analysis via the Search Tool for the Retrieval of Interacting Genes/Proteins (STRING) was performed, which resulted in highly complex network representations of the modules. Proteins are depicted as nodes while edges show their connections based on a score calculated from several experimental, text mining and database metrics with thicker edges indicating a higher score. Pathway enrichment analysis yielded no clear results due to the size and heterogeneity of these whole module networks. To leverage the full potential of the STRING data, further dissection was performed via subclustering of the main networks through the Cytoscape software and the MCL algorithm allowing more detailed insights into the pathways which together might explain the characters of the modules. A, B, C, D show main networks from Müller cells, diencephalon, grey matter and white matter, respectively, with the five major subclusters colored in red, blue, yellow, green, petrol. A', B', C', D' depict the corresponding subclusters derived by MCL and some noteworthy, enriched pathways (right). Rims of the nodes indicate gene significance. RMG, retinal Müller glia; DE, diencephalic astrocytes; GM, gray matter astrocytes; WM, white matter astrocytes.

Interestingly, some subclusters originating from different modules were enriched in proteins of similar pathways. We contemplated proteins isolated from such clusters and examined their expression between the regions (Fig. 7). Comparing modules of white and grey matter, we found proteins related to ribosomes and translation to be prominent in individual subclusters of both regions (Fig. 7A). In direct comparison, we identified 46 proteins with at least twofold significant difference, of which most showed enhanced expression not only in white matter but also in diencephalon (Fig. 7A).

Clusters originating from GM and DE-related modules contained a high number of proteins involved in mitochondrial pathways (Fig. 7B). While proteins of these subclusters have intermediate expression in RMG and WM, they show a clear differential expression between white and grey matter astrocytes (Fig. 7B), including 93 proteins with a minimum of twofold expression difference. Finally, through WGCNA coupled with STRING analysis we were able to find and correctly assign known Müller cell-specific proteins involved in the retinoic acid metabolism necessary for phototransduction to a specific RMG-related subcluster (Fig. 7C).

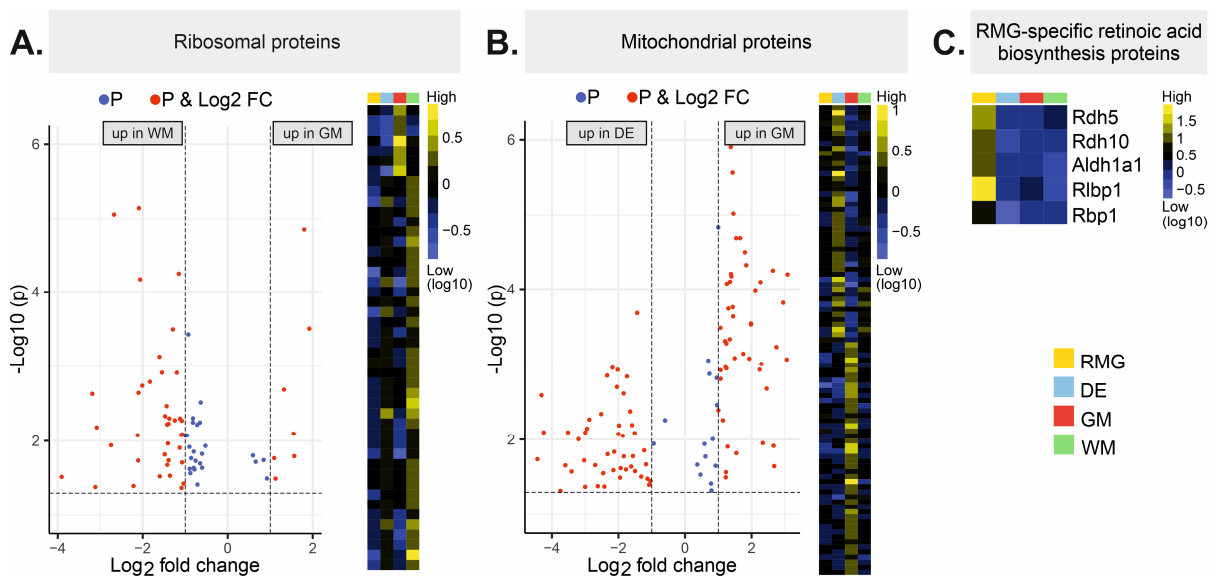


Figure 7: Comparison of glia- and region-specific protein subclusters derived from STRING networks. STRING based network analysis delivered protein clusters with defined pathway association. Proteins of similar/identical pathways could be found in distinct subclusters of region-specific modules hinting to separate

regions using different proteins for a similar purpose. **A:** Volcano plot showing proteins originating from ribosome associated subclusters that are differentially expressed between grey matter (Fig 6C', yellow) and white matter (Fig 6D', blue) astrocytes. Heat map represents proteins that are at least twofold different between WM and GM. While grey matter proteins are specific to that region, white matter proteins are also abundant in diencephalon. **B:** Differential expression of proteins of the mitochondrion pathway specifically enriched in either diencephalon (Fig 6B', blue) or grey matter (Fig 6C', blue) with generally lower abundance in retinal Müller glia and white matter astrocytes. Heat map represents proteins that are at least twofold different between DE and GM. **C:** Proteins involved in the retinoic acid biosynthesis are characteristic for Müller cells and represent their unique involvement in opsin recycling in the retina. **A, B:** P: proteins showing significant difference at $p < 0.05$; P & Log2 FC: proteins significantly differing by at least twofold. RMG, retinal Müller glia; DE, diencephalic astrocytes; GM, gray matter astrocytes; WM, white matter astrocytes.

Brain region-dependent complementary picture of transcriptional and translational regulation of glial genes

High sequencing depth in bulk RNAseq and detailed separation of cell populations in single cell RNAseq allow first insights into cell biology. However, it is well known that protein synthesis rates do not necessarily follow transcriptional changes and vice versa, leading to the challenge in molecular and cell biology that one cannot simply extrapolate from mRNA amount to the resulting protein level and thus to the function of a cell [27], [58], [59]. To investigate the extent to which this discrepancy is reflected in our system, we checked comparable RNAseq datasets against the respective glial proteomes generated in the current study. Comparing the glia-specific proteins with the transcriptional expression matrix of nearly 15000 genes, we found 3534 to be matching in both datasets. For each gene, we calculated a mean expression value per region relative to the median across all samples of the respective dataset. This allowed us to compare the extent to which interregional regulation between datasets was maintained regardless of the underlying assay used to generate the datasets.

Correlation values of 0.4 to 0.7 between transcript and protein have been reported in tightly controlled experiments [27], [28], [60], [61]. We found a rather weak correlation between our transcript and protein datasets (Fig 8A) with Spearman correlation values ranging between 0.12 for grey matter and 0.34 for white matter astrocytes. We then asked whether the proteins for which we detected at least two-fold regional enrichment showed a comparable pattern at the transcriptional level and whether we could identify additional candidates using this combinatorial approach. Analogous to the analysis of proteomes, we first identified 1564 transcripts with two-fold and significant enrichment in a region in at least one data set (proteome or transcriptome) (Fig. 8B, Tab. S3) that in addition needed to be present in both data sets. From these 1564 transcripts/proteins, 50.8 % and 30.4 %, respectively, showed such enrichment pattern exclusively in either transcripts or protein, encompassing for example ZEB1, which was only significant on protein level (Fig. 8B). 9.3% of genes were concordantly regulated between transcriptome and proteome - SLMAP was a member of this group (Fig. 8B). The proportion of genes for which transcript levels correlated with the amount of the respective protein varied between regions. For example, RMG had the most RNA-exclusive genes, but also the highest proportion of concordant transcript/proteins (pie charts in Fig. 8B).

Interestingly, some genes were above the fold change threshold (>2-fold against other regions) on the transcriptome and protein level but reached significance in only one of the two datasets (Fig. 8B).

After individual transcript-protein correlation, we used 2D-annotation enrichment [62] to determine pathways represented in up- or down-regulated genes/proteins per region with respect to their transcript-protein regulatory pattern (Fig. 8C). For example, we found that pathways related to mRNA processing are less represented at the transcriptome level in RMG, DE, and GM. However, consistently low expression of the corresponding proteins was detected only in RMG and DE, whereas GM astrocytes appeared to produce comparatively higher amounts of protein, than would have been inferred from the transcript levels. Together with the finding that ribosomal protein signatures differ significantly between GM astrocytes and their counterparts in other brain regions (Fig. 7A), this might indicate that even though transcripts for mRNA processing genes are expressed comparably low in these three regions, grey matter seems to maintain high protein levels hinting towards a region-specific predominantly posttranscriptional regulation for this gene group.

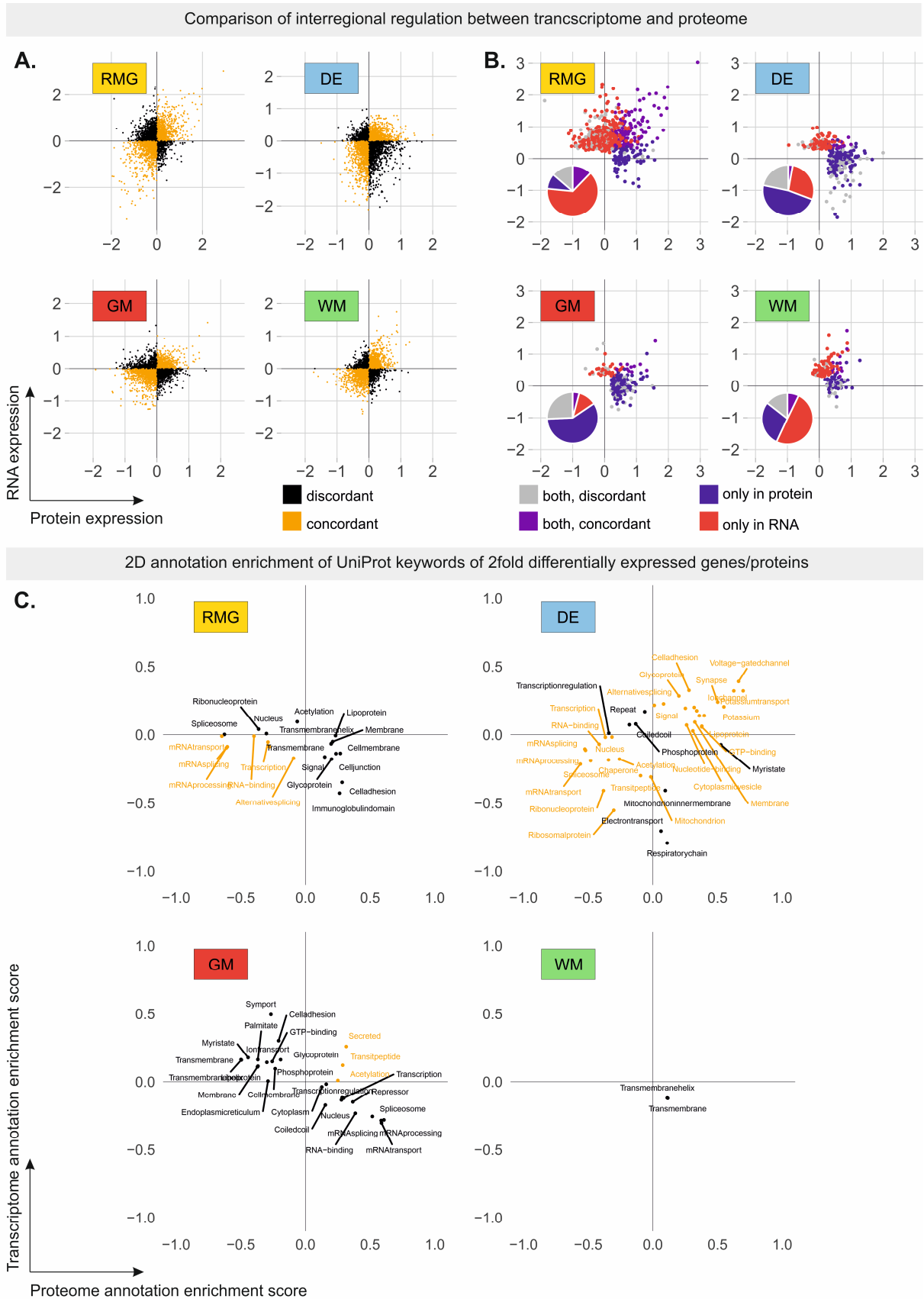


Figure 8. Correlation of region-specific glial proteomes and transcriptomes. *A, B:* Scatterplots show the interregional differences of proteins (x-axis) and transcript (y-axis). Each point represents the regional mean log₁₀ expression of an individual gene/protein above the median. *A:* Interregional regulation of all genes/proteins that were detected in both datasets is weakly correlated between transcriptome and proteome. *B:* Comparison of only significantly differentially expressed genes/proteins, that were at least twofold enriched in proteome or transcriptome in one region compared to all others. Only genes that were detected in both datasets are presented here. Pie charts indicate percentage of genes identified as differentially expressed in either RNA (red), proteome

(blue), or in both (purple or grey). **C:** 2D annotation enrichment analysis of differentially expressed genes reveals how pathways are regulated on transcriptome and proteome level. Orange: enriched UniProt keywords with concordant interregional regulation, black: enriched UniProt keywords with discordant interregional regulation. Positive enrichment score values indicate keywords with upregulated genes, while negative values represent downregulated genes.

Discussion

The glia of the central nervous system fulfil many similar functions but also exhibit region-specific adaptations. In this study, we employed magnetic bead activated cell sorting in combination with proteomic profiling of enriched populations of mouse retinal Müller cells as well as astrocytes from murine diencephalon, grey matter and white matter to gain a deeper understanding of their common or differential functional kinship. We first checked for the global relationship between the glial subpopulations and found a close relationship between Müller cells and subcortical astrocytes with especially tight clustering of the latter. We identified 78 proteins enriched in the glial fractions of all regions examined, but with no differences between the respective glial populations and thus can be considered a pan-astroglial core proteome. Of note, we found transcription factors of the nuclear factor 1 (NFI) family to be expressed uniformly in the three brain regions as well as in retinal Müller cells. These factors have been implicated in gliogenesis [63], [64] and, in line with our findings, were reported to be expressed across most brain regions [65]. In the retina, these factors seem to drive Müller cell maturation and retinal regeneration [42], [66], [67]. Accordingly, our data showing that NFI factors are ubiquitously expressed at protein level in mature glial cells of the central nervous system support the concept that this transcription factor family is important for the establishment and potential maintenance of a glial character.

In line with the idea that from a developmental point of view retinal Müller cells should be closest related to DE astrocytes, we found that indeed Müller cell proteome matches best with that of diencephalic astrocytes and significantly less with that of grey or white matter counterparts. This may indicate that genetic programs that are maintained from developmental stages into adulthood persist in spatially separated cell types. The close relationship between Müller cells and DE astrocytes is based on a set of 341 shared proteins in our data set. These include proteins involved in various synaptic and vesicular transport pathways. Müller cells have been shown to be a major source of extracellular vesicles secreting various subtypes with partially distinct cargo [68], while comparatively little is known about secretory function of DE astrocytes. Furthermore, we observed a consistently higher expression of SRC- and RAS-related proteins in glia of these CNS regions as compared to GM and WM astrocytes. These signal transduction proteins have been documented to be involved in a variety of cell biological processes and their mutant variants promote the development of various cancers by inducing continuous cell growth and division [48]. Their enhanced expression could contribute to the proliferative potential of Müller cells and DE astrocytes. However, since the latter have been

shown to exhibit some degree of proliferation in the adult, uninjured mouse brain [21], but Müller cells lack this ability [69]–[71], an additional molecular switch must be present to exploit the regenerative potential of Müller cells. In this context, a complex relationship between RAS and SRC signalling and YAP1 activation has previously been discussed [72], [73] (Fig. 9). However, because these are signalling cascades that can start from different cellular cues, it remains unclear which exact processes occur in Müller cells or DE astrocytes.

Next, we focussed on the identification of proteins specific to the respective glial populations. We identified SLMAP as a Müller cell-specific protein that did not show expression in any other retinal or brain cell type. This gene or its regulatory regions could be used to drive the expression of molecular tools such as reporter genes, Cre recombinases, or Cas9-based constructs to answer research questions where differentiation between Müller cells and brain astrocytes is desired. This could be particularly useful since currently available glial transgenic lines are usually based on marker genes such as GLAST (Slc1a3) [74], [75] or Aldh111 [76], which cannot distinguish astrocytes from Müller cells. However, an expression in retinal astrocytes could not be ruled out definitively as our sorting protocol does not allow to separate them from Müller cells due to the aforementioned reasons. Consequently, such a model would require thorough validation. In addition, it has to be taken into account that considerable SLMAP expression has been detected in tissues outside the central nervous system, especially in muscle [77], [78]. Functionally, SLMAP was reported to confer the binding of the striatin-interacting phosphatase and kinase (STRIPAK) complex to mammalian serine/threonine-protein kinase 3 and 4 (STK3/4 alias MST1/2), which are then dephosphorylated [79] (Fig. 9). This in turn leads to the inactivation of the Hippo signalling pathway and subsequent translocation of YAP1 into the nucleus [80]. This is followed by the activation of its downstream targets which are associated amongst others with increased proliferation and cell cycle entry [55]. In contrast to this finding, two studies independently reported that inhibition of YAP1 signalling via the Hippo pathway prevents Müller cell proliferation upon injury in mammals whereas proliferation is induced via enhanced YAP1 activation [70], [71], [81]. Thus, a SLMAP/STRIPAK independent cascade might contribute to Müller cell quiescence in mammals – a regulatory pathway that might not be active in the otherwise closely related DE astrocytes with higher proliferative activity than Müller cells.

In contrast, grey matter astrocytes seem to have a higher propensity for proliferation after injury [82], [83] and we found them to express highest ZEB1 protein levels as compared to all other investigated glial populations. ZEB1, a transcriptional regulator, is not only a major agent of epithelial to mesenchymal transition [50], [84], [85] but is also able to physically cooperate with YAP1 and induce a subset of its targets [51], [53] (Fig. 9). In adult hippocampus, ZEB1 seems to play a pivotal role in self-renewal, as it drives asymmetric cell division of radial glia and inhibits their premature acquisition of a neuronal cell fate [86]. Accordingly, elevated

expression of ZEB1 and YAP1 levels would indicate an increased proliferative capacity of grey matter astrocytes.

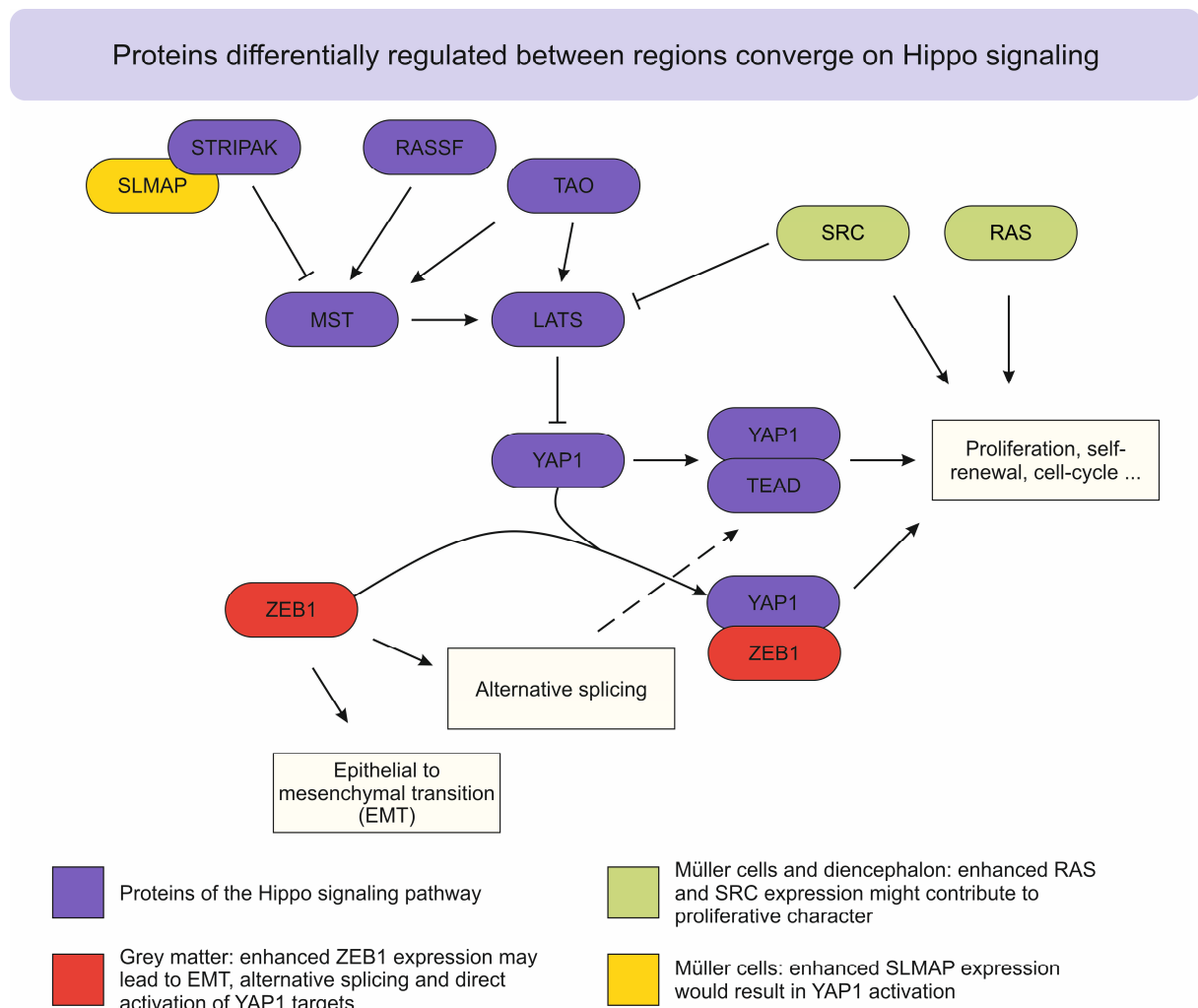


Figure 9: Proteins with interregional difference in expression pattern between retinal and brain glia seem to belong to a network of pathways converging on Hippo signaling (purple). In Müller cells (yellow), a high expression of SLMAP might confer dephosphorylation of MST1/2 and the subsequent activation of YAP1. Grey matter's (red) increased ZEB1 expression might not only be able to induce EMT, it can also coregulate YAP1 target genes by physical interaction. Furthermore, alternative splicing of TEAD1 (dashed arrow) was also implicated in the modulation of YAP1 dependent transcriptional regulation. Diencephalic and retinal glia (green) exhibit elevated levels of SRC and RAS. While SRC was reported to directly influence Hippo signaling by LATS1/2 inhibition, RAS and YAP1 were shown to fulfil complementary functions in cancer.

In contrast to that, a recent study provided evidence for injury-independent proliferative astrocytes in diencephalon [21], a region showing intermediate ZEB1 and low YAP1 expression in our proteomic data (Fig. S2B). One possible explanation for this discrepancy could be alternative splicing, an additional function of ZEB1 that has been demonstrated *in vitro* in the context of EMT [87]. Some evidence supporting this hypothesis can be deduced from our proteome data as well. We saw proteins of alternative splicing pathways being specifically upregulated in GM astrocytes. Moreover, the genes that had a predicted ZEB1-binding site in their regulatory region and were co-expressed with ZEB1 at high levels in GM

astrocytes largely belonged to protein families involved in mRNA processing and alternative splicing. The significance of this finding is corroborated by the notion that alternative splicing seems to play a role in cortical fate determination between neuronal progenitor cells and neurons via RNA binding protein fox-1 homolog (RBFOX) proteins [88]. RBFOX2 was recently shown to lead to the alternative splicing of Transcriptional enhancer factor TEF-1 (TEAD1), a co-effector of YAP1, with a concomitant modulation in transcriptional activation and oncogenic potential in human cell lines [89]. Lastly, when comparing our complementary RNAseq with proteome data, we found transcripts of splicing related genes to be downregulated in grey matter hinting towards a posttranscriptional regulation. In this scenario ZEB1 would act as a transcriptional switch, whereas final protein abundance would be tuned on higher regulatory levels such as mRNA or protein stability/degradation, alternative splicing or posttranslational modification. A similar hypothesis regarding this kind of mechanism was recently developed and promoted by Vogel and Marcotte [28].

Conclusion

In this study, we used a multi-omic approach in combination with a toolbox of different bioinformatics instruments to uniquely decipher the relationship between brain astroglia and retinal Müller cells. The complexity of the resulting data forced us to focus on few cell biological pathways. However, our analysis does not exhaust the information content of the dataset and sets the stage for further investigation into additional region-specific or common glial protein networks in the future. Many of the pathways with interregional differential expression described here appear to converge onto the YAP1 pathway and ZEB1-mediated alternative splicing between glial subpopulations of central nervous system including the retina. A deeper understanding of these mechanisms may help to uncover not only the origin of differences in injury-induced reactive gliosis and resulting proliferation, but also to translate findings from one type of glia to another.

Acknowledgments

We thank Tatiana Simon-Ebert and Gabriele Jäger for excellent technical assistance.

Materials and Methods

Magnetic activated cell sorting (MACS)

Müller cells were isolated from retina following an established protocol [33]. Briefly, murine retinæ were dissected (C57BL/6J, 3 months of age, 3 animals per sample, same individuals

as for brain) and digested with papain to receive a cell suspension. Microglia, endothelial cells and Müller cells were extracted in a sequential manner using cell-type-specific magnetic microbeads: First, CD11b MicroBeads (130-049-601, Miltenyi Biotec) were used to deplete microglia from the cell suspension, following by depletion of endothelial cells with CD31 MicroBeads (130-097-418, Miltenyi Biotec). Finally, we captured the Müller cell fraction by selection with biotinylated anti-CD29 antibody (130-101-943, Miltenyi Biotec) in combination with anti-biotin MicroBeads (130-090-485, Miltenyi Biotec). 100 µl of Müller cell and flow-through fraction, respectively, were fixed in 400 µl 4% paraformaldehyde for 15 minutes at room temperature. After centrifugation at 600 g for 10 minutes, we discarded the supernatant and resuspended the cells in 50 µl phosphate buffered saline (PBS), before transferring the suspension on a microscope slide. The rest of the CD29⁺ and the flow through (CD11b⁻CD31⁻CD29⁻) fractions were centrifuged at 13 000g, 15 min. Supernatants were removed and cell pellets stored at -80 °C until processing for tandem mass spectrometry.

Astrocytes were enriched from three different brain regions in a similar manner. Briefly, brains were dissected from adult mice (C57BL/6J, 3 months of age, 3 animals per sample, same individuals as for retina) and divided into cortical grey matter, white matter and diencephalon. Additionally, meninges were manually removed during dissection to avoid contamination with vascular cells. The brain regions were mechanically dissociated with the gentleMACS Octo Dissociator (Adult Brain Dissociation Kit, 130-107-677, Miltenyi Biotec) to receive a single cell solution. Cells were passed through a 70-µm strainer and labeled with astrocyte-specific magnetic beads (Anti-ACSA-2 MicroBead Kit, 130-097-678, Miltenyi Biotec) for 15 min. after which they were loaded on MS columns for separation by an OctoMACS magnet. The debris removal step was prolonged by 10 minutes during phase formation which lead to an increase in cell number yield. ACSA2⁺ and flow through fractions were centrifuged at 13 000 g, 15 min. Supernatants were removed and cell pellets stored at -80 °C until processing for tandem mass spectrometry.

Tandem mass spectrometry

MACS sorted cells were proteolysed by a modified FASP protocol [33], [90]. Briefly, proteins were reduced and alkylated in solution using dithiothreitol and iodoacetamide. After dilution to 4 M urea the denatured protein samples were centrifuged on a 30 kDa filter device (PALL). After several washing steps using 8 M urea and 50 mM ammoniumbicarbonate, proteins were digested on the filter by Lys-C and trypsin overnight. Generated peptides were eluted by centrifugation, acidified with TFA and stored at -20 °C.

Samples were measured on a QExactive HF mass spectrometer (Thermo scientific) online coupled to an Ultimate 3000 nano-RSLC (Dionex). Tryptic peptides were automatically loaded on a trap column (300 µm inner diameter (ID) × 5 mm, Acclaim PepMap100 C18, 5 µm, 100

Å, LC Packings) prior to C18 reversed phase chromatography on the analytical column (nanoEase MZ HSS T3 Column, 100 Å, 1.8 µm, 75 µm x 250 mm, Waters) at 250 nl/min flow rate in a 95 minutes non-linear acetonitrile gradient from 3 to 40% in 0.1% formic acid. Profile precursor spectra from 300 to 1500 m/z were recorded at 60000 resolution with an automatic gain control (AGC) target of 3e6 and a maximum injection time of 50 ms. Subsequently TOP10 fragment spectra of charges 2 to 7 were recorded at 15000 resolution with an AGC target of 1e5, a maximum injection time of 50 ms, an isolation window of 1.6 m/z, a normalized collision energy of 28 and a dynamic exclusion of 30 seconds.

Acquired raw data was analyzed in the Proteome Discoverer 2.2 SP1 software (Thermo Fisher Scientific; version 2.2.0.388) for peptide and protein identification via a database search (Sequest HT search engine) against the SwissProt Mouse database (SwissProt Mouse release 2017_02, 16872 sequences), considering full tryptic specificity, allowing for up to one missed tryptic cleavage site, precursor mass tolerance 10 ppm, fragment mass tolerance 0.02 Da. Carbamidomethylation of cysteine was set as a static modification. Dynamic modifications included deamidation of asparagine and glutamine, oxidation of methionine, and a combination of methionine loss with acetylation on protein N-terminus. The Percolator algorithm [91] was used for validating peptide spectrum matches and peptides. Only top-scoring identifications for each spectrum were accepted, additionally satisfying a false discovery rate < 1% (high confidence). The final list of proteins satisfying the strict parsimony principle included only protein groups passing an additional protein confidence false discovery rate < 5% (target/decoy concatenated search validation).

Quantification of proteins, after precursor recalibration, was based on intensity values (at RT apex) for all unique peptides per protein. Peptide abundance values were normalized on total peptide amount. Missing values were replaced with random values between the minimum and the lower 5 percent of all detected values. The protein abundances were calculated summing the abundance values for admissible peptides. The final protein ratio was calculated using median abundance values of five biological replicates each. The statistical significance of the ratio change was ascertained with ANOVA and the respect P values are adjusted for multiple testing by Benjamini-Hochberg correction. To define the glia-specific subset, proteins were filtered per region as follows: 1) ratio between glia and flowthrough fraction > 1, p-value < 0.05; 2) exclude proteins with no “high” ratings in glial fraction’s “Found in Sample” columns; 3) exclude proteins that show more than 1 “not found” rating in glial fraction’s “Found in Sample” columns.

Immunofluorescent labelling

For the assessment of the of Müller glia enrichment, we stained the dried samples on slide with an antibody against the Müller cell marker glutamine synthetase.

Paraformaldehyde fixed retinal cryosections were washed in PBS and primary antibodies were diluted in PBS containing 0.5 % Triton X-100 and 2 % bovine serum albumin (BSA). Sections were incubated in primary antibody solution at 4 °C over night followed by several washing steps with PBS. Finally, we applied the secondary antibody solution (secondary antibody 1:500, nuclear stain DAPI) for 1.5 to 2 h at room temperature. Confocal images were taken with a custom-made VisiScope CSU-X1 confocal system (Visitron Systems, Puchheim, Germany) equipped with high-resolution sCMOS camera (PCO AG, Kehlheim, Germany).

Table 1: Primary and secondary antibodies used for immunofluorescence staining.

Primary antibodies	host	Company	Catalogue number / Reference	Dilution
GLUL	mouse	Merck	MAB302	1:500
ZEB1	rabbit	Sigma-Aldrich	HPA027524	1:1500
GFAP	mouse	Sigma-Aldrich	G3893	1:500
S100B	mouse	Sigma-Aldrich	S2532	1:300
SLMAP	mouse	Santa Cruz	sc-393336	1:200
SOX9	goat	R&D Systems	AF3075	1:500
Secondary antibodies				
Anti-rabbit-Cy3	goat	Dianova	111-165-144	1:500
Anti-mouse-AF488	goat	LifeTech	A-1109	1:500
Anti-mouse-AF488	donkey	LifeTech	A21202	1:500
Anti-rat-cy3	goat	Dianova	112-165-167	1:500
Anti-goat-cy3	donkey	Dianova	705-165-147	1:500
Anti-rabbit-cy3	goat	Dianova	111-605-144	1:500

For verification of ZEB1 expression in cortical GM, WM and diencephalon astrocytes, immunostainings were performed in adult (3 or 4 month old) mice. Mice were anaesthetized by intraperitoneal injection of ketamine (100 mg/kgbw) and xylazine (10 mg/kgbw) and after transcardial perfusions with 4% paraformaldehyde (PFA, vol/vol; Roth) in PBS for 20 min, brains were postfixed overnight. For immunohistology, 40 µm sections were pre-incubated for 1 h in blocking solution (3% Bovine Serum Albumin (Sigma-Aldrich, A2153), 0.5% Triton X-100 (Sigma) in PBS). The following primary antibodies (against ZEB1, SOX9 and S100β) were diluted in blocking solution and incubated with the sections for 24 h at 4°C. After washing in PBS, secondary antibodies were diluted in blocking solution and incubated at room temperature for 2 h using fluorophore-coupled antibody to mouse IgG AF488, antibody to goat IgG Cy3 and antibody to rabbit AF647. Confocal images were taken using Zeiss LSM710 microscope at 25X magnification, with a z-stack step size of 1 µm. Quantification of

immunostaining was performed on the multi-channel, maximum intensity projection images using Fiji/ImageJ software.

The specificity of anti-ZEB1 antibodies was determined by checking the expression level of ZEB1 after CRISPR mediated knock-out using transgenic wt-Cas9 R26-Cas9 Fezh (Jax: 024858, [92]) mice. Zeb1 targeting gRNAs (CATTATCCTGAGGCGCCCG & TGTCATATGACGTTCAAGCT or GTACCGCCATGAGAAGAACG & CCCGCAGGGTTACTCTTGTG) were cloned into STAgR constructs containing a fluorophore (tdTomato) as previously described [93]. In brief, postnatal astrocyte cultures were made from P5 as previously described [94]. Subsequently, the astrocytes were transfected with DNA-liposome complexes prepared in OptiMem (Thermo Fisher Scientific, 31985070) medium using the STAgR plasmids and Lipofectamine 2000 (Thermo Fisher Scientific, 11668030). The efficiency of knockdown and specificity of the ZEB1 antibody was checked by immunostaining 7 days post transfection.

RNAseq

Isolation of RNA from brain samples was performed using RNeasy Micro Kit (Qiagen) before reverse transcription with Ovation RNA-seq System v2 (NuGEN). cDNA fragmentation and library preparation with sample specific indices was done using Xpress Plus gDNA and Amplicon Library Preparation kit (Thermo Fisher Scientific). Pooled libraries were sequenced on an Ion Proton Sequencer. Raw reads were demultiplexed and barcodes and adapters were trimmed, before quality control via FASTQC (Babraham Bioinformatics) and alignment to mouse genome with STAR software (version 2.4.2a [95])

Bioinformatic analyses

Differential protein expression and other statistical analyses were performed using R programming language in RStudio unless stated otherwise. For heatmap visualization [96], normalized protein abundance values of individual samples are expressed relative to their median across all samples and log₁₀ transformed. Volcano plots were drawn using the *EnhancedVolcano* package [97], PCA and dendrograms were plotted with *factoextra* [98]. Distances were calculated using Manhattan distance as it is thought more suitable for high dimensional data than Euclidean distance [99], including but not limited to the fact, that in Euclidean distance high variation in few variables or outliers might exaggerate the metric. Clustering was done via the Ward algorithm implemented in the *hclust* function using *ward.D2* method suggested for proteomics data [100]–[102].

For WGCNA, filtered, glia-specific protein values for all regions were log₂ transformed and used as input for a workflow in general concordance to the guidelines of Horvath et al. [56] as

well as Neueder and Bates [103]. First, the *bicor* function was used to calculate pairwise correlation between all proteins. To construct a signed adjacency matrix and achieve approximate scale-free topology ($R^2 > 0.8$), the correlation matrix was raised to the soft-thresholding power of 26. This matrix, describing the direct pairwise relationships between individual proteins, was the basis to calculate the topological overlap matrix (TOM) which additionally takes the respective connections to all other proteins into account [104]. Distance and clustering analysis on the TOM allowed us to cluster similar proteins into modules, which were merged if the eigengene correlation was bigger than 0.2 resulting in 14 distinct modules. Using the eigengenes, we were able to correlate the modules with CNS region membership defined as external trait. To select modules of interest we further calculated gene significance, which is a measure of protein-trait correlation as well as module membership (k_{ME}) describing how well a protein fits into its associated module. Modules of interest had to fulfil following criteria: I) eigengene-region correlation > 0.5 , p-value < 0.05 , II) no significant positive correlation with other regions, III) correlation between k_{ME} and gene significance > 0.5 , p-value < 0.05 . The last criterion ensured that not only the module as a whole was correlated with the trait, but also the individual proteins and that these proteins were indeed highly interconnected. While these criteria were perfectly met by modules related to RMG and GM, we excluded one module connected to diencephalon, since it also showed weak positive correlation with white matter. There were no modules adhering to these standards for white matter, which is why we decided to take the closest possible modules.

Modules derived from WGCNA represent networks of genes that show similar expression pattern across the analysed samples. To uncover and visualize the underlying pathways we used the module genes as input for STRING analysis inside the Cytoscape (version 3.8.0) plugin *stringApp* (version 1.5.0) with default settings. We excluded nodes without connections before subclustering with the MCL algorithm of the *ClusterMaker* (version 1.3.1) plugin using the combined STRING score as array source and setting the inflation value to 2.2. The nodes of the five biggest subclusters were coloured in red, blue, yellow, green, and petrol from biggest to smallest. Furthermore, the border paint of the subclusters was mapped to the gene significance, with blue hues representing negative and red hues positive correlation of the gene to the respective trait. Functional enrichment was performed separately for individual subclusters against the whole genome as background.

For oPOSSUM transcription factor binding site analysis we used glia-specific proteins and searched their putative regulatory regions (default values: 5000 bp up/downstream) for predicted ZEB1 binding sites based on binding motifs from the JASPAR database [105] with otherwise default settings.

2D annotation enrichment was performed using the Perseus software [62] with the means of the median transformed values of genes/proteins that that were at least twofold

enriched in one region against all others. For annotation we used UniProt keywords at a FDR of 0.05 and plotted the enrichment scores for terms with more than 10 members.

General image analysis was performed using Fiji [106].

Table 2. Proteins with no significant difference between regions (ANOVA p -value ≥ 0.05), but glia-specific in every region (p -value < 0.05).

Protein Name	UniProt ID	Description
Acadsb	Q9DBL1	Short/branched chain specific acyl-CoA dehydrogenase, mitochondrial
Acadvl	P50544	Very long-chain specific acyl-CoA dehydrogenase, mitochondrial
Actbl2	Q8BFZ3	Beta-actin-like protein 2
Acy3	Q91XE4	N-acyl-aromatic-L-amino acid amidohydrolase (carboxylate-forming)
Aldh9a1	Q9JLJ2	4-trimethylaminobutyraldehyde dehydrogenase
Anapc4	Q91W96	Anaphase-promoting complex subunit 4
Arhgdia	Q99PT1	Rho GDP-dissociation inhibitor 1
Atic	Q9CWJ9	Bifunctional purine biosynthesis protein PURH
Bag5	Q8CI32	BAG family molecular chaperone regulator 5
Bzw1	Q9CQC6	Basic leucine zipper and W2 domain-containing protein 1
Cad	B2RQC6	CAD protein
Cap1	P40124	Adenylyl cyclase-associated protein 1
Capns1	O88456	Calpain small subunit 1
Cc2d1b	Q8BRN9	Coiled-coil and C2 domain-containing protein 1B
Cd81	P35762	CD81 antigen
Cope	O89079	Coatomer subunit epsilon
Coro1c	Q9WUM4	Coronin-1C
Cpt2	P52825	Carnitine
Cryz11	Q921W4	Quinone oxidoreductase-like protein 1
Dhrs4	Q99LB2	Dehydrogenase/reductase SDR family member 4
Dnaja1	P63037	DnaJ homolog subfamily A member 1
Eif4a2	P10630	Eukaryotic initiation factor 4A-II
Fam98b	Q80VD1	Protein FAM98B
Fmr1	P35922	Synaptic functional regulator FMR1
Fscn1	Q61553	Fascin
Gart	Q64737	Trifunctional purine biosynthetic protein adenosine-3
Gca	Q8VC88	Grancalcin
Gfap	P03995	Glial fibrillary acidic protein
Gga1	Q8R0H9	ADP-ribosylation factor-binding protein GGA1
Gyg1	Q9R062	Glycogenin-1
Hsd17b8	P50171	Estradiol 17-beta-dehydrogenase 8
Hsp90b1	P08113	Endoplasmic
Idh2	P54071	Isocitrate dehydrogenase [NADP], mitochondrial
Itm2b	O89051	Integral membrane protein 2B
Ldah	Q8BVA5	Lipid droplet-associated hydrolase
Lrrc57	Q9D1G5	Leucine-rich repeat-containing protein 57
Macf1	Q9QXZ0	Microtubule-actin cross-linking factor 1
Mapre1	Q61166	Microtubule-associated protein RP/EB family member 1
Mink1	Q9JM52	Misshapen-like kinase 1
Mthfd1	Q922D8	C-1-tetrahydrofolate synthase, cytoplasmic

Naga	Q9QWR8	Alpha-N-acetylgalactosaminidase
Naxd	Q9CZ42	ATP-dependent (S)-NAD(P)H-hydrate dehydratase
Ndufb1	P0DN34	NADH dehydrogenase [ubiquinone] 1 beta subcomplex subunit 1
Nfix	P70257	Nuclear factor 1 X-type
Npepps	Q11011	Puromycin-sensitive aminopeptidase
Nt5c3b	Q3UFY7	7-methylguanosine phosphate-specific 5'-nucleotidase
Nudt4	Q8R2U6	Diphosphoinositol polyphosphate phosphohydrolase 2
Pdia4	P08003	Protein disulfide-isomerase A4
Plec	Q9QXS1	Plectin
Pls3	Q99K51	Plastin-3
Ppp2r5a	Q6PD03	Serine/threonine-protein phosphatase 2A 56 kDa regulatory subunit alpha isoform
Prdx3	P20108	Thioredoxin-dependent peroxide reductase, mitochondrial
Psm2	P49722	Proteasome subunit alpha type-2
Psm6	Q60692	Proteasome subunit beta type-6
Rabggtb	P53612	Geranylgeranyl transferase type-2 subunit beta
Rac1	P63001	Ras-related C3 botulinum toxin substrate 1
Rcctb1	Q6NXM2	RCC1 and BTB domain-containing protein 1
Rdx	P26043	Radixin
Rnpep	Q8VCT3	Aminopeptidase B
Rock1	P70335	Rho-associated protein kinase 1
Selenbp1	P17563	Selenium-binding protein 1
Slc12a9	Q99MR3	Solute carrier family 12 member 9
Slc25a23	Q6GQS1	Calcium-binding mitochondrial carrier protein SCaMC-3
Snx1	Q9WV80	Sorting nexin-1
Snx27	Q3UHD6	Sorting nexin-27
Snx6	Q6P8X1	Sorting nexin-6
Tbrg4	Q91YM4	Protein TBRG4
Tmem47	Q9JJG6	Transmembrane protein 47
Tollip	Q9QZ06	Toll-interacting protein
Trap1	Q9CQN1	Heat shock protein 75 kDa, mitochondrial
Trim9	Q8C7M3	E3 ubiquitin-protein ligase TRIM9
Ttc38	A3KMP2	Tetratricopeptide repeat protein 38
Twf1	Q91YR1	Twinfilin-1
Vamp4	O70480	Vesicle-associated membrane protein 4
Wars	P32921	Tryptophan--tRNA ligase, cytoplasmic
Wdyhv1	Q80WB5	Protein N-terminal glutamine amidohydrolase
Ywhaq	P68254	14-3-3 protein theta
Zw10	O54692	Centromere/kinetochore protein zw10 homolog

Table 3. Glia-specific, differentially expressed transcriptional regulators. Proteins having an entry in the “enriched in” column are at least twofold enriched in the stated region. Proteins were classified to have transcriptional regulation by Genomatix software (<http://www.genomatix.de>), furthermore proteins of the type “TF” are transcription factors or cofactors according to Panther database (protein class ids PC00218 or PC00217).

Protein name	Enriched in	type	UniProt ID	Description
Dpf3	GM	TF	P58269	Zinc finger protein DPF3
Morf4l1	GM	TF	P60762	Mortality factor 4-like protein 1
Phf10	GM	TF	Q9D8M7	PHD finger protein 10
Pqbp1	GM	TF	Q91VJ5	Polyglutamine-binding protein 1
Taf10	GM	TF	Q8K0H5	Transcription initiation factor TFIID subunit 10

Yap1	GM	TF	P46938	Transcriptional coactivator YAP1
Zeb1	GM	TF	Q64318	Zinc finger E-box-binding homeobox 1
Zhx1	GM	TF	P70121	Zinc fingers and homeoboxes protein 1
Zhx2	GM	TF	Q8C0C0	Zinc fingers and homeoboxes protein 2
Nmi	RMG	TF	O35309	N-myc-interactor
Arnt2		TF	Q61324	Aryl hydrocarbon receptor nuclear translocator 2
Cnot1		TF	Q6ZQ08	CCR4-NOT transcription complex subunit 1
Cnot3		TF	Q8K0V4	CCR4-NOT transcription complex subunit 3
Cnot7		TF	Q60809	CCR4-NOT transcription complex subunit 7
Ctbp1		TF	O88712	C-terminal-binding protein 1
Ctbp2		TF	P56546	C-terminal-binding protein 2
Dpf2		TF	Q61103	Zinc finger protein ubi-d4
Ewsr1		TF	Q61545	RNA-binding protein EWS
Fus		TF	P56959	RNA-binding protein FUS
Gtf2a2		TF	Q80ZM7	Transcription initiation factor IIA subunit 2
Gtf2b		TF	P62915	Transcription initiation factor IIB
Gtf2f1		TF	Q3THK3	General transcription factor IIF subunit 1
Hdgf		TF	P51859	Hepatoma-derived growth factor
Hmgb1		TF	P63158	High mobility group protein B1
Kat7		TF	Q5SVQ0	Histone acetyltransferase KAT7
Khdrbs1		TF	Q60749	KH domain-containing, RNA-binding, signal transduction-associated protein 1
Mettl14		TF	Q3UIK4	N6-adenosine-methyltransferase subunit METTL14
Morf4l2		TF	Q9R0Q4	Mortality factor 4-like protein 2
Mybbp1a		TF	Q7TPV4	Myb-binding protein 1A
Ncor2		TF	Q9WU42	Nuclear receptor corepressor 2
Nfia		TF	Q02780	Nuclear factor 1 A-type
Nfyc		TF	P70353	Nuclear transcription factor Y subunit gamma
Nr2f1		TF	Q60632	COUP transcription factor 1
Olig1		TF	Q9JKN5	Oligodendrocyte transcription factor 1
Olig2		TF	Q9EQW6	Oligodendrocyte transcription factor 2
Phc2		TF	Q9QWH1	Polyhomeotic-like protein 2
Psip1		TF	Q99JF8	PC4 and SFRS1-interacting protein
Purb		TF	O35295	Transcriptional activator protein Pur-beta
Rxrb		TF	P28704	Retinoic acid receptor RXR-beta
Sap30bp		TF	Q02614	SAP30-binding protein
Smad4		TF	P97471	Mothers against decapentaplegic homolog 4
Smarcc1		TF	P97496	SWI/SNF complex subunit SMARCC1
Smarcc2		TF	Q6PDG5	SWI/SNF complex subunit SMARCC2
Snw1		TF	Q9CSN1	SNW domain-containing protein 1
Sox1		TF	P53783	Transcription factor SOX-1
Sp1		TF	O89090	Transcription factor Sp1
Sp3		TF	O70494	Transcription factor Sp3
Stat3		TF	P42227	Signal transducer and activator of transcription 3
Stat5a		TF	P42230	Signal transducer and activator of transcription 5A
Taf9		TF	Q8VI33	Transcription initiation factor TFIID subunit 9
Tcea1		TF	P10711	Transcription elongation factor A protein 1
Tcerg1		TF	Q8CGF7	Transcription elongation regulator 1
Tcf12		TF	Q61286	Transcription factor 12
Thrap3		TF	Q569Z6	Thyroid hormone receptor-associated protein 3
Yy1		TF	Q00899	Transcriptional repressor protein YY1

Ccnk	DE	O88874	Cyclin-K Structural maintenance of chromosomes flexible hinge domain-containing protein 1
Smchd1	DE	Q6P5D8	Sin3 histone deacetylase corepressor complex component
Suds3	DE	Q8BR65	SDS3
Zmynd11	DE	Q8R5C8	Zinc finger MYND domain-containing protein 11
Brd8	GM	Q8R3B7	Bromodomain-containing protein 8
Brms1l	GM	Q3U1T3	Breast cancer metastasis-suppressor 1-like protein
Gatad2b	GM	Q8VHR5	Transcriptional repressor p66-beta
Hnrnpa2b1	GM	O88569	Heterogeneous nuclear ribonucleoproteins A2/B1
Nono	GM	Q99K48	Non-POU domain-containing octamer-binding protein
Npm1	GM	Q61937	Nucleophosmin
Actn4	RMG	P57780	Alpha-actinin-4
Ctnnb1	RMG	Q02248	Catenin beta-1
Maged1	RMG	Q9QYH6	Melanoma-associated antigen D1
Myo6	RMG	Q64331	Unconventional myosin-VI
Dnmt3a	WM	O88508	DNA (cytosine-5)-methyltransferase 3A
Toe1	WM	Q9D2E2	Target of EGR1 protein 1
Add1		Q9QYC0	Alpha-adducin
Aip		O08915	AH receptor-interacting protein
Alyref		O08583	THO complex subunit 4
Apex1		P28352	DNA-(apurinic or apyrimidinic site) lyase
Arid1a		A2BH40	AT-rich interactive domain-containing protein 1A
Arrb1		Q8BWG8	Beta-arrestin-1
Asah1		Q9WV54	Acid ceramidase
Atrx		Q61687	Transcriptional regulator ATRX
Basp1		Q91XV3	Brain acid soluble protein 1
Brd2		Q7JJ13	Bromodomain-containing protein 2
Brd3		Q8K2F0	Bromodomain-containing protein 3
Brd4		Q9ESU6	Bromodomain-containing protein 4
Btf3		Q64152	Transcription factor BTF3
Cbx1		P83917	Chromobox protein homolog 1
Cbx3		P23198	Chromobox protein homolog 3
Cbx5		Q61686	Chromobox protein homolog 5
Chd4		Q6PDQ2	Chromodomain-helicase-DNA-binding protein 4
Chd8		Q09XV5	Chromodomain-helicase-DNA-binding protein 8
Chmp1a		Q921W0	Charged multivesicular body protein 1a
Cops2		P61202	COP9 signalosome complex subunit 2
Creb1		Q01147	Cyclic AMP-responsive element-binding protein 1
Csnk2a1		Q60737	Casein kinase II subunit alpha
Csnk2b		P67871	Casein kinase II subunit beta
Ctcf		Q61164	Transcriptional repressor CTCF
Ddx21		Q9JIK5	Nucleolar RNA helicase 2
Ddx3x		Q62167	ATP-dependent RNA helicase DDX3X
Dhx9		O70133	ATP-dependent RNA helicase A
Dr1		Q91WV0	Protein Dr1
Edf1		Q9JMG1	Endothelial differentiation-related factor 1
Elp3		Q9CZX0	Elongator complex protein 3
Eny2		Q9JIX0	Transcription and mRNA export factor ENY2
Gtf3c5		Q8R2T8	General transcription factor 3C polypeptide 5
H2afy		Q9QZQ8	Core histone macro-H2A.1

H2afy2	Q8CCK0	Core histone macro-H2A.2
Hdac11	Q91WA3	Histone deacetylase 11
Hdac3	O88895	Histone deacetylase 3
Hdac6	Q9Z2V5	Histone deacetylase 6
Hmg20a	Q9DC33	High mobility group protein 20A
Hmga1	P17095	High mobility group protein HMG-I/HMG-Y High mobility group nucleosome-binding domain-containing protein 3
Hmgn3	Q9DCB1	
Htatsf1	Q8BGC0	HIV Tat-specific factor 1 homolog
Ilf2	Q9CXY6	Interleukin enhancer-binding factor 2
Kdm1a	Q6ZQ88	Lysine-specific histone demethylase 1A
Maz	P56671	Myc-associated zinc finger protein
Mbd2	Q9Z2E1	Methyl-CpG-binding domain protein 2
Mecp2	Q9Z2D6	Methyl-CpG-binding protein 2
Mettl3	Q8C3P7	N6-adenosine-methyltransferase subunit METTL3
Mta2	Q9R190	Metastasis-associated protein MTA2
Mta3	Q924K8	Metastasis-associated protein MTA3
Mtdh	Q80WJ7	Protein LYRIC
Myef2	Q8C854	Myelin expression factor 2
Naa15	Q80UM3	N-alpha-acetyltransferase 15, NatA auxiliary subunit
Ncoa5	Q91W39	Nuclear receptor coactivator 5 NADH dehydrogenase [ubiquinone] 1 alpha subcomplex subunit 13
Ndufa13	Q9ERS2	
Nelfb	Q8C4Y3	Negative elongation factor B
Nif3l1	Q9EQ80	NIF3-like protein 1
Nme2	Q01768	Nucleoside diphosphate kinase B
Nr3c1	P06537	Glucocorticoid receptor
Pa2g4	P50580	Proliferation-associated protein 2G4
Padi2	Q08642	Protein-arginine deiminase type-2
Pbrm1	Q8BSQ9	Protein polybromo-1
Pfdn5	Q9WU28	Prefoldin subunit 5
Phb	P67778	Prohibitin
Phb2	O35129	Prohibitin-2
Phf2	Q9WTU0	Lysine-specific demethylase PHF2
Preb	Q9WUQ2	Prolactin regulatory element-binding protein
Prmt5	Q8CIG8	Protein arginine N-methyltransferase 5
Prpf6	Q91YR7	Pre-mRNA-processing factor 6
Psmc5	P62196	26S protease regulatory subunit 8
Pspc1	Q8R326	Paraspeckle component 1
Ptma	P26350	Prothymosin alpha
Rad21	Q61550	Double-strand-break repair protein rad21 homolog
Ran	P62827	GTP-binding nuclear protein Ran
Rbbp5	Q8BX09	Retinoblastoma-binding protein 5
Rbbp7	Q60973	Histone-binding protein RBBP7
Rbm14	Q8C2Q3	RNA-binding protein 14
Ring1	O35730	E3 ubiquitin-protein ligase RING1
Rps3	P62908	40S ribosomal protein S3
Safb	D3YXK2	Scaffold attachment factor B1
Sall2	Q9QX96	Sal-like protein 2
Sap18	O55128	Histone deacetylase complex subunit SAP18
Setd7	Q8VHL1	Histone-lysine N-methyltransferase SETD7

Sfpq	Q8VIJ6	Splicing factor, proline- and glutamine-rich
Slc30a9	Q5IRJ6	Zinc transporter 9
Smarca2	Q6DIC0	Probable global transcription activator SNF2L2
Smarca4	Q3TKT4	Transcription activator BRG1
Smarca5	Q91ZW3	SWI/SNF-related matrix-associated actin-dependent regulator of chromatin subfamily A member 5
Smarcb1	Q9Z0H3	SWI/SNF-related matrix-associated actin-dependent regulator of chromatin subfamily B member 1
Smarcd1	Q61466	SWI/SNF-related matrix-associated actin-dependent regulator of chromatin subfamily D member 1
Smarce1	O54941	SWI/SNF-related matrix-associated actin-dependent regulator of chromatin subfamily E member 1
Snf8	Q9CZ28	Vacuolar-sorting protein SNF8
Sox10	Q04888	Transcription factor SOX-10
Sox9	Q04887	Transcription factor SOX-9
Ssbp1	Q9CYR0	Single-stranded DNA-binding protein, mitochondrial
Ssbp3	Q9D032	Single-stranded DNA-binding protein 3
Ssrp1	Q08943	FACT complex subunit SSRP1
Strap	Q9Z1Z2	Serine-threonine kinase receptor-associated protein
Sub1	P11031	Activated RNA polymerase II transcriptional coactivator p15
Tardbp	Q921F2	TAR DNA-binding protein 43
Terf2ip	Q91VL8	Telomeric repeat-binding factor 2-interacting protein 1
Tgfb1i1	Q62219	Transforming growth factor beta-1-induced transcript 1 protein
Ube2l3	P68037	Ubiquitin-conjugating enzyme E2 L3
Ube2n	P61089	Ubiquitin-conjugating enzyme E2 N
Ube3a	O08759	Ubiquitin-protein ligase E3A
Ubtf	P25976	Nucleolar transcription factor 1
Vbp1	P61759	Prefoldin subunit 3
Wdr5	P61965	WD repeat-containing protein 5
Ybx1	P62960	Nuclease-sensitive element-binding protein 1
Ybx3	Q9JKB3	Y-box-binding protein 3

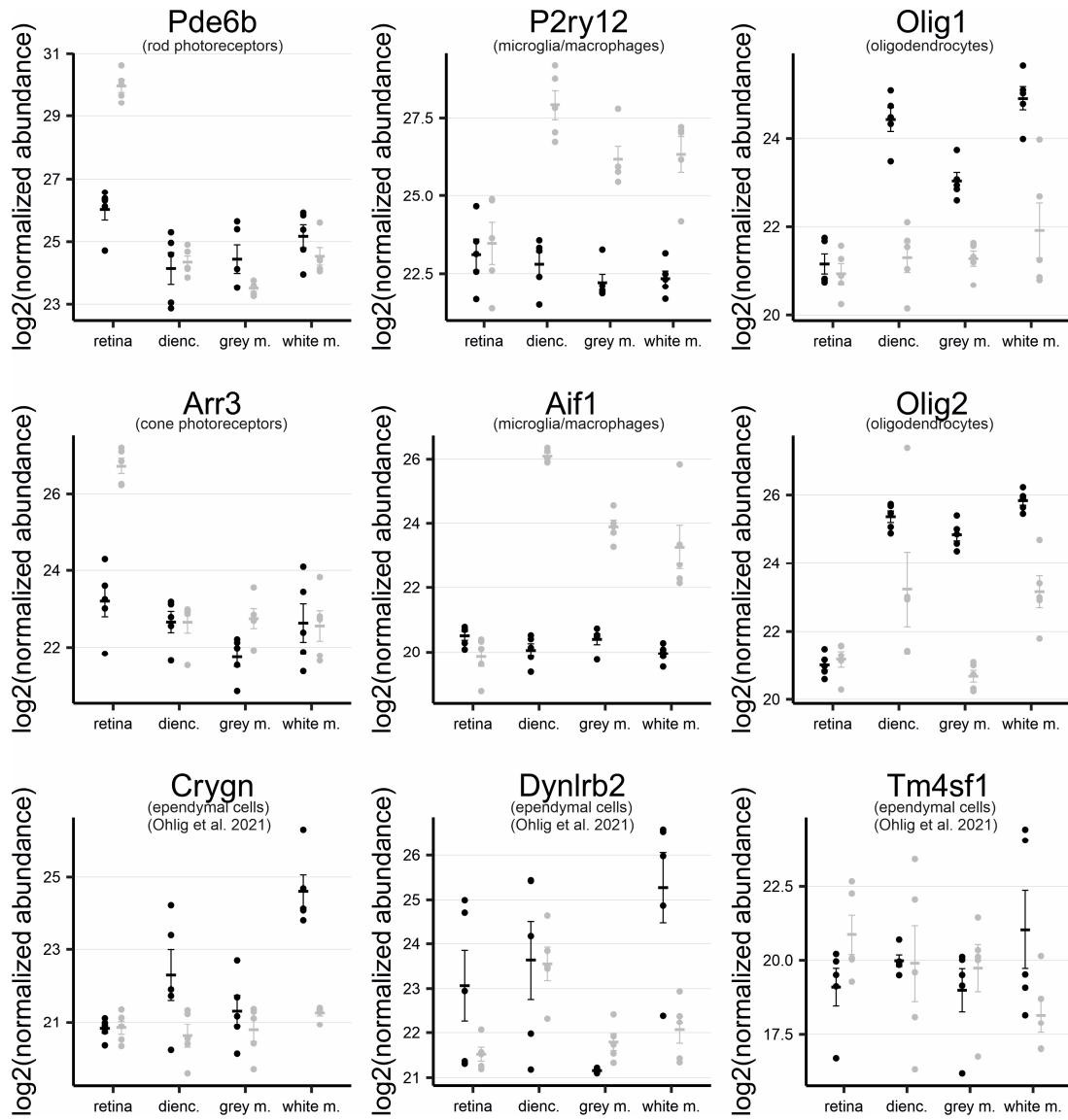
References:

- [1] P. D. J. Gordon Betts, Kelly A. Young, James A. Wise, Eddie Johnson, Brandon Poe, Dean H. Kruse, Oksana Korol, Jody E. Johnson, Mark Womble, "13.1 The Embryologic Perspective – Anatomy and Physiology - Secondary Vesicles," 2013. <https://openstax.org/books/anatomy-and-physiology/pages/13-1-the-embryologic-perspective> (accessed Jun. 15, 2022).
- [2] J. García-Marqués and L. López-Mascaraque, "Clonal identity determines astrocyte cortical heterogeneity," *Cereb. Cortex*, vol. 23, no. 6, pp. 1463–1472, Jun. 2013, doi: 10.1093/cercor/bhs134.
- [3] M. Bugiani, B. C. Plug, J. H. K. Man, M. Breur, and M. S. van der Knaap, "Heterogeneity of white matter astrocytes in the human brain," *Acta Neuropathol.*, vol. 143, no. 2, pp. 159–177, Feb. 2022, doi: 10.1007/s00401-021-02391-3.
- [4] A. Bringmann, A. Grosche, T. Pannicke, and A. Reichenbach, "GABA and Glutamate Uptake and Metabolism in Retinal Glial (Müller) Cells," *Front. Endocrinol. (Lausanne)*, vol. 4, p. 48, 2013, doi: 10.3389/fendo.2013.00048.
- [5] I. Farhy-Tselnicker and N. J. Allen, "Astrocytes, neurons, synapses: a tripartite view on cortical circuit development," *Neural Dev.*, vol. 13, no. 1, p. 7, 2018, doi: 10.1186/s13064-018-0104-y.
- [6] F. Wang, X. Qi, J. Zhang, and J. Huang, "Astrocytic modulation of potassium under seizures," *Neural Regen. Res.*, vol. 15, no. 6, p. 980, Jun. 2020, doi: 10.4103/1673-5374.270295.
- [7] P. Kofuji and E. A. Newman, "Potassium buffering in the central nervous system," *Neuroscience*, vol. 129, no. 4, pp. 1043–1054, Jan. 2004, doi: 10.1016/j.neuroscience.2004.06.008.
- [8] C. J. Karwoski, H.-K. Lu, and E. A. Newman, "Spatial Buffering of Light-Evoked Potassium Increases by Retinal Müller (Glial) Cells," *Science (80-.)*, vol. 244, no. 4904, pp. 578–580, May 1989, doi: 10.1126/science.2785716.
- [9] E. A. Newman, D. A. Frambach, and L. L. Odette, "Control of Extracellular Potassium Levels by Retinal Glial Cell K + Siphoning," *Science (80-.)*, vol. 225, no. 4667, pp. 1174–1175, Sep. 1984, doi: 10.1126/science.6474173.
- [10] L. Liu, K. R. MacKenzie, N. Putluri, M. Maletić-Savatić, and H. J. Bellen, "The Glia-Neuron Lactate Shuttle and Elevated ROS Promote Lipid Synthesis in Neurons and Lipid Droplet Accumulation in Glia via APOE/D," *Cell Metab.*, vol. 26, no. 5, pp. 719–737.e6, 2017, doi: 10.1016/j.cmet.2017.08.024.
- [11] J. B. Hurley, K. J. Lindsay, and J. Du, "Glucose, lactate, and shuttling of metabolites in vertebrate retinas," *J. Neurosci. Res.*, vol. 93, no. 7, pp. 1079–1092, Jul. 2015, doi: 10.1002/jnr.23583.
- [12] A. K. Toft-Kehler, D. M. Skytt, and M. Kolko, "A Perspective on the Müller Cell-Neuron Metabolic Partnership in the Inner Retina," *Mol. Neurobiol.*, vol. 55, no. 6, pp. 5353–5361, Jun. 2018, doi: 10.1007/s12035-017-0760-7.
- [13] J.-S. Wang and V. J. Kefalov, "The Cone-specific visual cycle," *Prog. Retin. Eye Res.*, vol. 30, no. 2, pp. 115–128, Mar. 2011, doi: 10.1016/j.preteyeres.2010.11.001.
- [14] A. Rübsam, S. Parikh, and P. E. Fort, "Role of Inflammation in Diabetic Retinopathy," *Int. J. Mol. Sci.*, vol. 19, no. 4, Apr. 2018, doi: 10.3390/IJMS19040942.
- [15] Y. Du, A. Veenstra, K. Palczewski, and T. S. Kern, "Photoreceptor cells are major contributors to diabetes-induced oxidative stress and local inflammation in the retina," *Proc. Natl. Acad. Sci. U. S. A.*, vol. 110, no. 41, p. 16586, Oct. 2013, doi: 10.1073/PNAS.1314575110.
- [16] R. B. MacDonald, O. Randlett, J. Oswald, T. Yoshimatsu, K. Franze, and W. A. Harris, "Müller glia provide essential tensile strength to the developing retina," *J. Cell Biol.*, vol. 210, no. 7, pp. 1075–1083, 2015, doi: 10.1083/jcb.201503115.
- [17] J. Wan and D. Goldman, "Retina regeneration in zebrafish," *Curr. Opin. Genet. Dev.*, vol. 40, pp. 41–47, Oct. 2016, doi: 10.1016/J.GDE.2016.05.009.
- [18] A. Zambusi and J. Ninkovic, "Regeneration of the central nervous system-principles from brain regeneration in adult zebrafish," *World J. Stem Cells*, vol. 12, no. 1, p. 8, Jan. 2020, doi: 10.4252/WJSC.V12.I1.8.
- [19] M. Götz, S. Sirko, J. Beckers, and M. Irmeler, "Reactive astrocytes as neural stem or progenitor cells: In vivo lineage, In vitro potential, and Genome-wide expression analysis," *Glia*, vol. 63, no. 8, p. 1452, Aug. 2015, doi: 10.1002/GLIA.22850.
- [20] N. Mattugini *et al.*, "Inducing Different Neuronal Subtypes from Astrocytes in the Injured Mouse Cerebral Cortex," *Neuron*, vol. 103, no. 6, p. 1086, Sep. 2019, doi: 10.1016/J.NEURON.2019.08.009.
- [21] S. Ohlig *et al.*, "Molecular diversity of diencephalic astrocytes reveals adult astrogenesis regulated by Smad4," *EMBO J.*, vol. 40, no. 21, Nov. 2021, doi: 10.15252/embj.2020107532.
- [22] J. Kuchling and F. Paul, "Visualizing the Central Nervous System: Imaging Tools for Multiple Sclerosis and Neuromyelitis Optica Spectrum Disorders," *Front. Neurol.*, vol. 11, p. 450, Jun. 2020, doi: 10.3389/fneur.2020.00450.
- [23] F. C. Oertel *et al.*, "Retinal ganglion cell loss in neuromyelitis optica: a longitudinal study," *J. Neurol. Neurosurg. Psychiatry*, vol. 89, no. 12, pp. 1259–1265, Dec. 2018, doi: 10.1136/jnnp-2018-318382.
- [24] R. Mancino *et al.*, "Neurodegenerative Process Linking the Eye and the Brain," *Curr. Med. Chem.*, vol. 26, no. 20, pp. 3754–3763, 2019, doi: 10.2174/0929867325666180307114332.
- [25] S. Chiquita *et al.*, "The Retina as a Window or Mirror of the Brain Changes Detected in Alzheimer's Disease: Critical Aspects to Unravel," *Mol. Neurobiol.*, vol. 56, no. 8, pp. 5416–5435, Aug. 2019, doi: 10.1007/s12035-018-1461-6.
- [26] K. J. Lizarraga, N. Chunga, N. A. Yannuzzi, H. W. Flynn, C. Singer, and A. E. Lang, "The retina as a window to the basal ganglia: Systematic review of the potential link between retinopathy and hyperkinetic disorders in diabetes," *Parkinsonism Relat. Disord.*, vol. 80, pp. 194–198, Nov. 2020, doi:

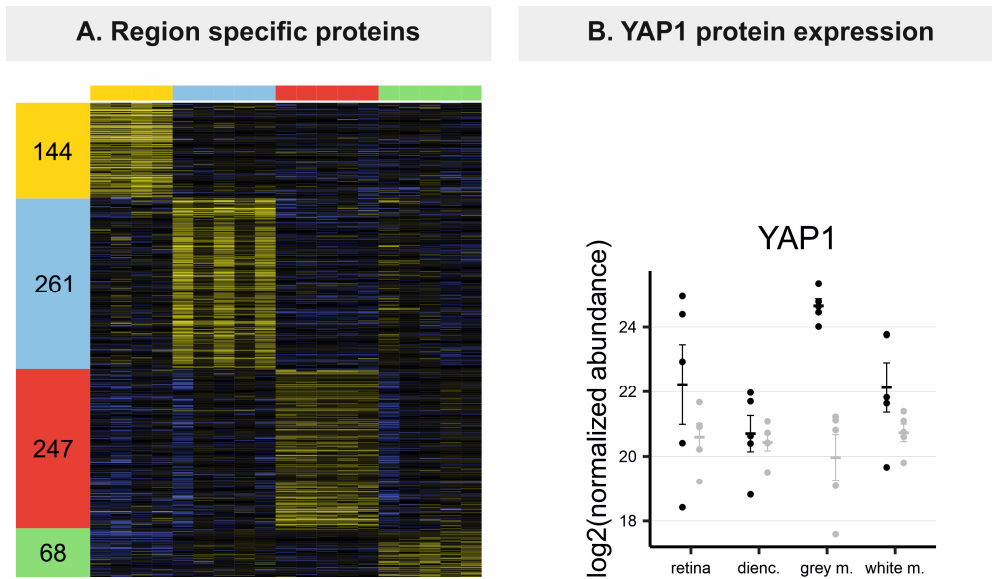
- 10.1016/j.parkreldis.2020.10.025.
- [27] Y. Liu, A. Beyer, and R. Aebersold, "On the Dependency of Cellular Protein Levels on mRNA Abundance," *Cell*, vol. 165, no. 3, pp. 535–550, Apr. 2016, doi: 10.1016/j.cell.2016.03.014.
- [28] C. Vogel and E. M. Marcotte, "Insights into the regulation of protein abundance from proteomic and transcriptomic analyses," *Nat. Rev. Genet.*, vol. 13, no. 4, pp. 227–232, Apr. 2012, doi: 10.1038/nrg3185.
- [29] A. P. Voigt *et al.*, "Molecular characterization of foveal versus peripheral human retina by single-cell RNA sequencing," *Exp. Eye Res.*, vol. 184, no. May, pp. 234–242, Jul. 2019, doi: 10.1016/j.exer.2019.05.001.
- [30] W. Yan *et al.*, "Cell Atlas of The Human Fovea and Peripheral Retina," *Sci. Rep.*, vol. 10, no. 1, pp. 1–17, 2020, doi: 10.1038/s41598-020-66092-9.
- [31] E. Z. Macosko *et al.*, "Highly Parallel Genome-wide Expression Profiling of Individual Cells Using Nanoliter Droplets," *Cell*, vol. 161, no. 5, pp. 1202–1214, May 2015, doi: 10.1016/j.cell.2015.05.002.
- [32] K. Roesch *et al.*, "The transcriptome of retinal Müller glial cells," *J. Comp. Neurol.*, vol. 509, no. 2, pp. 225–238, 2008, doi: 10.1002/cne.21730.
- [33] A. Grosche *et al.*, "The Proteome of Native Adult Müller Glial Cells From Murine Retina.," *Mol. Cell. Proteomics*, vol. 15, no. 2, pp. 462–80, Feb. 2016, doi: 10.1074/mcp.M115.052183.
- [34] L. Kaplan *et al.*, "Retinal regions shape human and murine Müller cell proteome profile and functionality," *Glia*, Nov. 2022, doi: 10.1002/glia.24283.
- [35] K. Sharma *et al.*, "Cell type- and brain region-resolved mouse brain proteome.," *Nat. Neurosci.*, vol. 18, no. 12, pp. 1819–31, Dec. 2015, doi: 10.1038/nn.4160.
- [36] A. Zeisel *et al.*, "Molecular Architecture of the Mouse Nervous System," *Cell*, vol. 174, no. 4, pp. 999–1014.e22, Aug. 2018, [Online]. Available: <https://linkinghub.elsevier.com/retrieve/pii/S009286741830789X>.
- [37] J. D. Cahoy *et al.*, "A Transcriptome Database for Astrocytes, Neurons, and Oligodendrocytes: A New Resource for Understanding Brain Development and Function," *J. Neurosci.*, vol. 28, no. 1, pp. 264–278, Jan. 2008, doi: 10.1523/JNEUROSCI.4178-07.2008.
- [38] L. Morel *et al.*, "Molecular and Functional Properties of Regional Astrocytes in the Adult Brain.," *J. Neurosci.*, vol. 37, no. 36, pp. 8706–8717, Sep. 2017, doi: 10.1523/JNEUROSCI.3956-16.2017.
- [39] M. Y. Batiuk *et al.*, "An immunoaffinity-based method for isolating ultrapure adult astrocytes based on ATP1B2 targeting by the ACSA-2 antibody," *J. Biol. Chem.*, vol. 292, no. 21, pp. 8874–8891, 2017, doi: 10.1074/jbc.M116.765313.
- [40] L. M. Holt and M. L. Olsen, "Novel applications of magnetic cell sorting to analyze cell-type specific gene and protein expression in the central nervous system," *PLoS One*, vol. 11, no. 2, p. e0150290, Feb. 2016, doi: 10.1371/journal.pone.0150290.
- [41] A. Bringmann *et al.*, "Müller cells in the healthy and diseased retina.," *Prog. Retin. Eye Res.*, vol. 25, no. 4, pp. 397–424, Jul. 2006, doi: 10.1016/j.preteyeres.2006.05.003.
- [42] T. Hoang *et al.*, "Gene regulatory networks controlling vertebrate retinal regeneration," *Science (80-.)*, vol. 370, no. 6519, p. eabb8598, Nov. 2020, doi: 10.1126/science.abb8598.
- [43] B. Snel, G. Lehmann, P. Bork, and M. A. Huynen, "String: A web-server to retrieve and display the repeatedly occurring neighbourhood of a gene," *Nucleic Acids Res.*, vol. 28, no. 18, pp. 3442–3444, Sep. 2000, doi: 10.1093/nar/28.18.3442.
- [44] D. Szklarczyk *et al.*, "STRING v11: protein-protein association networks with increased coverage, supporting functional discovery in genome-wide experimental datasets.," *Nucleic Acids Res.*, vol. 47, no. D1, pp. D607–D613, Jan. 2019, doi: 10.1093/nar/gky1131.
- [45] P. Shannon *et al.*, "Cytoscape: a software environment for integrated models of biomolecular interaction networks.," *Genome Res.*, vol. 13, no. 11, pp. 2498–2504, Nov. 2003, doi: 10.1101/gr.1239303.
- [46] N. T. Doncheva, J. H. Morris, J. Gorodkin, and L. J. Jensen, "Cytoscape StringApp: Network Analysis and Visualization of Proteomics Data.," *J. Proteome Res.*, vol. 18, no. 2, pp. 623–632, Feb. 2019, doi: 10.1021/acs.jproteome.8b00702.
- [47] S. Brohé and J. van Helden, "Evaluation of clustering algorithms for protein-protein interaction networks," *BMC Bioinformatics*, vol. 7, no. 1, p. 488, Dec. 2006, doi: 10.1186/1471-2105-7-488.
- [48] H. Lavoie, J. Gagnon, and M. Therrien, "ERK signalling: a master regulator of cell behaviour, life and fate," *Nat. Rev. Mol. Cell Biol.*, vol. 21, no. 10, pp. 607–632, Oct. 2020, doi: 10.1038/s41580-020-0255-7.
- [49] D. Mossmann, S. Park, and M. N. Hall, "mTOR signalling and cellular metabolism are mutual determinants in cancer," *Nat. Rev. Cancer*, vol. 18, no. 12, pp. 744–757, Dec. 2018, doi: 10.1038/s41568-018-0074-8.
- [50] S. Singh *et al.*, "Zeb1 controls neuron differentiation and germinal zone exit by a mesenchymal-epithelial-like transition," *Elife*, vol. 5, no. MAY2016, pp. 1–31, May 2016, doi: 10.7554/eLife.12717.
- [51] W. Lehmann *et al.*, "ZEB1 turns into a transcriptional activator by interacting with YAP1 in aggressive cancer types," *Nat. Commun.*, vol. 7, no. 1, p. 10498, Apr. 2016, doi: 10.1038/ncomms10498.
- [52] A. T. Kwon, D. J. Arenillas, R. Worsley Hunt, and W. W. Wasserman, "oPOSSUM-3: advanced analysis of regulatory motif over-representation across genes or ChIP-Seq datasets.," *G3 (Bethesda)*, vol. 2, no. 9, pp. 987–1002, Sep. 2012, doi: 10.1534/g3.112.003202.
- [53] N. Feldker *et al.*, "Genome-wide cooperation of EMT transcription factor ZEB 1 with YAP and AP -1 in breast cancer," *EMBO J.*, vol. 39, no. 17, p. e103209, Sep. 2020, doi: 10.15252/embj.2019103209.
- [54] T. Panciera, L. Azzolin, M. Cordenonsi, and S. Piccolo, "Mechanobiology of YAP and TAZ in physiology and disease," *Nat. Rev. Mol. Cell Biol.*, vol. 18, no. 12, pp. 758–770, 2017, doi: 10.1038/nrm.2017.87.
- [55] A. Totaro, T. Panciera, and S. Piccolo, "YAP/TAZ upstream signals and downstream responses," *Nat. Cell Biol.*, vol. 20, no. 8, pp. 888–899, Aug. 2018, doi: 10.1038/s41556-018-0142-z.
- [56] P. Langfelder and S. Horvath, "WGCNA: an R package for weighted correlation network analysis.," *BMC Bioinformatics*, vol. 9, p. 559, Dec. 2008, doi: 10.1186/1471-2105-9-559.
- [57] M. Keck *et al.*, "A systems level analysis of epileptogenesis-associated proteome alterations," *Neurobiol.*

- Dis.*, vol. 105, pp. 164–178, Sep. 2017, doi: 10.1016/j.nbd.2017.05.017.
- [58] S. B. Noya *et al.*, “The forebrain synaptic transcriptome is organized by clocks but its proteome is driven by sleep,” *Science (80-.)*, vol. 366, no. 6462, p. eaav2642, Oct. 2019, doi: 10.1126/science.aav2642.
- [59] J. Kjell *et al.*, “Defining the Adult Neural Stem Cell Niche Proteome Identifies Key Regulators of Adult Neurogenesis,” *Cell Stem Cell*, vol. 26, no. 2, pp. 277–293.e8, 2020, doi: 10.1016/j.stem.2020.01.002.
- [60] E. Lundberg *et al.*, “Defining the transcriptome and proteome in three functionally different human cell lines,” *Mol. Syst. Biol.*, vol. 6, no. 1, p. 450, Jan. 2010, doi: 10.1038/msb.2010.106.
- [61] T. Maier, M. Güell, and L. Serrano, “Correlation of mRNA and protein in complex biological samples,” *FEBS Lett.*, vol. 583, no. 24, pp. 3966–3973, Dec. 2009, doi: 10.1016/j.febslet.2009.10.036.
- [62] J. Cox and M. Mann, “1D and 2D annotation enrichment: a statistical method integrating quantitative proteomics with complementary high-throughput data,” *BMC Bioinformatics*, vol. 13, no. S16, p. S12, Nov. 2012, doi: 10.1186/1471-2105-13-S16-S12.
- [63] P. Kang *et al.*, “Sox9 and NFIA Coordinate a Transcriptional Regulatory Cascade during the Initiation of Gliogenesis,” *Neuron*, vol. 74, no. 1, pp. 79–94, Apr. 2012, doi: 10.1016/j.neuron.2012.01.024.
- [64] B. Deneen, R. Ho, A. Lukaszewicz, C. J. Hochstim, R. M. Gronostajski, and D. J. Anderson, “The Transcription Factor NFIA Controls the Onset of Gliogenesis in the Developing Spinal Cord,” *Neuron*, vol. 52, no. 6, pp. 953–968, Dec. 2006, doi: 10.1016/j.neuron.2006.11.019.
- [65] B. Lozzi, T.-W. Huang, D. Sardar, A. Y.-S. Huang, and B. Deneen, “Regionally Distinct Astrocytes Display Unique Transcription Factor Profiles in the Adult Brain,” *Front. Neurosci.*, vol. 14, p. 61, Feb. 2020, doi: 10.3389/fnins.2020.00061.
- [66] B. R. Nelson *et al.*, “Genome-Wide Analysis of Müller Glial Differentiation Reveals a Requirement for Notch Signaling in Postmitotic Cells to Maintain the Glial Fate,” *PLoS One*, vol. 6, no. 8, p. e22817, Aug. 2011, doi: 10.1371/journal.pone.0022817.
- [67] B. S. Clark *et al.*, “Single-Cell RNA-Seq Analysis of Retinal Development Identifies NFI Factors as Regulating Mitotic Exit and Late-Born Cell Specification,” *Neuron*, vol. 102, no. 6, pp. 1111–1126.e5, Jun. 2019, doi: 10.1016/j.neuron.2019.04.010.
- [68] V. Demais *et al.*, “Release of VAMP5-positive extracellular vesicles by retinal Müller glia in vivo,” *J. Extracell. Vesicles*, vol. 11, no. 9, p. e12254, Sep. 2022, doi: 10.1002/jev2.12254.
- [69] D. Goldman, “Müller glial cell reprogramming and retina regeneration,” *Nat. Rev. Neurosci.*, vol. 15, no. 7, pp. 431–442, Jul. 2014, doi: 10.1038/nrn3723.
- [70] A. Hamon *et al.*, “Linking YAP to Müller Glia Quiescence Exit in the Degenerative Retina,” *Cell Rep.*, vol. 27, no. 6, pp. 1712–1725.e6, May 2019, doi: 10.1016/j.celrep.2019.04.045.
- [71] E. M. Rueda *et al.*, “The Hippo Pathway Blocks Mammalian Retinal Müller Glial Cell Reprogramming,” *Cell Rep.*, vol. 27, no. 6, pp. 1637–1649.e6, May 2019, doi: 10.1016/j.celrep.2019.04.047.
- [72] Y. Si *et al.*, “Src Inhibits the Hippo Tumor Suppressor Pathway through Tyrosine Phosphorylation of Lats1,” *Cancer Res.*, vol. 77, no. 18, pp. 4868–4880, Sep. 2017, doi: 10.1158/0008-5472.CAN-17-0391.
- [73] D. D. Shao *et al.*, “KRAS and YAP1 Converge to Regulate EMT and Tumor Survival,” *Cell*, vol. 158, no. 1, pp. 171–184, Jul. 2014, doi: 10.1016/j.cell.2014.06.004.
- [74] J. Wang, M. L. O’Sullivan, D. Mukherjee, V. M. Puñal, S. Farsiu, and J. N. Kay, “Anatomy and spatial organization of Müller glia in mouse retina,” *J. Comp. Neurol.*, vol. 525, no. 8, pp. 1759–1777, Jun. 2017, doi: 10.1002/cne.24153.
- [75] T. Mori, K. Tanaka, A. Buffo, W. Wurst, R. Kühn, and M. Götz, “Inducible gene deletion in astroglia and radial glia—A valuable tool for functional and lineage analysis,” *Glia*, vol. 54, no. 1, pp. 21–34, Jul. 2006, doi: 10.1002/glia.20350.
- [76] Y. Yang *et al.*, “Molecular comparison of GLT1+ and ALDH1L1+ astrocytes in vivo in astroglial reporter mice,” *Glia*, vol. 59, no. 2, pp. 200–207, Feb. 2011, doi: 10.1002/glia.21089.
- [77] R. M. Guzzo, J. Wigle, M. Salih, E. D. Moore, and B. S. Tuana, “Regulated expression and temporal induction of the tail-anchored sarcolemmal-membrane-associated protein is critical for myoblast fusion,” *Biochem. J.*, vol. 381, no. 3, pp. 599–608, Aug. 2004, doi: 10.1042/BJ20031723.
- [78] M. Uhlén *et al.*, “Tissue-based map of the human proteome,” *Science (80-.)*, vol. 347, no. 6220, Jan. 2015, doi: 10.1126/science.1260419.
- [79] Y. Zheng, B. Liu, L. Wang, H. Lei, K. D. Pulgar Prieto, and D. Pan, “Homeostatic Control of Hpo/MST Kinase Activity through Autophosphorylation-Dependent Recruitment of the STRIPAK PP2A Phosphatase Complex,” *Cell Rep.*, vol. 21, no. 12, pp. 3612–3623, Dec. 2017, doi: 10.1016/j.celrep.2017.11.076.
- [80] S. Ma, Z. Meng, R. Chen, and K.-L. Guan, “The Hippo Pathway: Biology and Pathophysiology,” *Annu. Rev. Biochem.*, vol. 88, no. 1, pp. 577–604, Jun. 2019, doi: 10.1146/annurev-biochem-013118-111829.
- [81] A. Hamon, C. Masson, J. Bitard, L. Gieser, J. E. Roger, and M. Perron, “Retinal Degeneration Triggers the Activation of YAP/TEAD in Reactive Müller Cells,” *Investig. Ophthalmology Vis. Sci.*, vol. 58, no. 4, p. 1941, Apr. 2017, doi: 10.1167/iovs.16-21366.
- [82] G. Heimann *et al.*, “Changes in the Proliferative Program Limit Astrocyte Homeostasis in the Aged Post-Traumatic Murine Cerebral Cortex,” *Cereb. Cortex*, vol. 27, no. 8, pp. 4213–4228, Aug. 2017, doi: 10.1093/cercor/bhx112.
- [83] C. Simon, M. Götz, and L. Dimou, “Progenitors in the adult cerebral cortex: Cell cycle properties and regulation by physiological stimuli and injury,” *Glia*, vol. 59, no. 6, pp. 869–881, Jun. 2011, doi: 10.1002/glia.21156.
- [84] P. Zhang, Y. Sun, and L. Ma, “ZEB1: At the crossroads of epithelial-mesenchymal transition, metastasis and therapy resistance,” *Cell Cycle*, vol. 14, no. 4, Landes Bioscience, pp. 481–487, Feb. 16, 2015, doi: 10.1080/15384101.2015.1006048.
- [85] E. Sánchez-Tilló, O. de Barrios, L. Siles, M. Cuatrecasas, A. Castells, and A. Postigo, “ β -catenin/TCF4

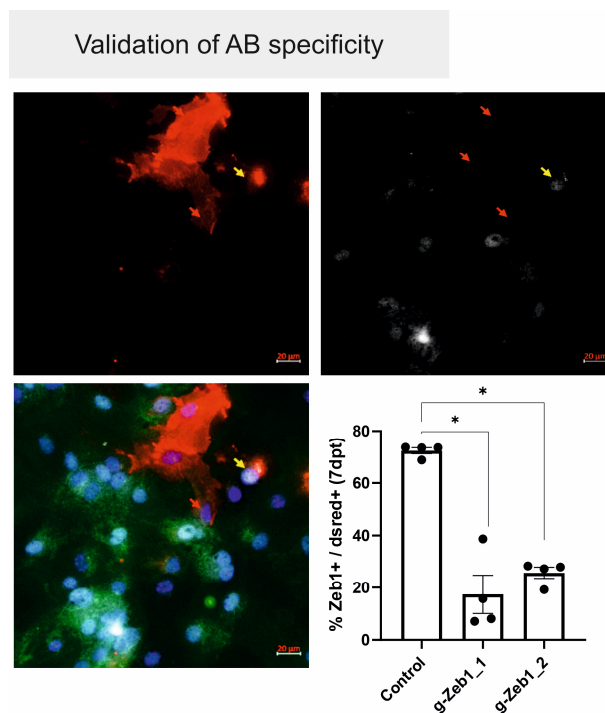
- complex induces the epithelial-to-mesenchymal transition (EMT)-activator ZEB1 to regulate tumor invasiveness.,” *Proc. Natl. Acad. Sci. U. S. A.*, vol. 108, no. 48, pp. 19204–9, Nov. 2011, doi: 10.1073/pnas.1108977108.
- [86] B. Gupta *et al.*, “The transcription factor ZEB1 regulates stem cell self-renewal and cell fate in the adult hippocampus,” *Cell Rep.*, vol. 36, no. 8, p. 109588, Aug. 2021, doi: 10.1016/j.celrep.2021.109588.
- [87] Y. Yang *et al.*, “Determination of a Comprehensive Alternative Splicing Regulatory Network and Combinatorial Regulation by Key Factors during the Epithelial-to-Mesenchymal Transition,” *Mol. Cell. Biol.*, vol. 36, no. 11, pp. 1704–1719, Jun. 2016, doi: 10.1128/MCB.00019-16.
- [88] X. Zhang *et al.*, “Cell-Type-Specific Alternative Splicing Governs Cell Fate in the Developing Cerebral Cortex,” *Cell*, vol. 166, no. 5, pp. 1147-1162.e15, Aug. 2016, doi: 10.1016/j.cell.2016.07.025.
- [89] S. Choi *et al.*, “RBFOX2-regulated TEAD1 alternative splicing plays a pivotal role in Hippo-YAP signaling,” *Nucleic Acids Res.*, vol. 50, no. 15, pp. 8658–8673, Aug. 2022, doi: 10.1093/nar/gkac509.
- [90] J. R. Wiśniewski, A. Zougman, N. Nagaraj, and M. Mann, “Universal sample preparation method for proteome analysis,” *Nat. Methods* 2009 65, vol. 6, no. 5, pp. 359–362, Apr. 2009, doi: 10.1038/nmeth.1322.
- [91] L. Käll, J. D. Canterbury, J. Weston, W. S. Noble, and M. J. MacCoss, “Semi-supervised learning for peptide identification from shotgun proteomics datasets,” *Nat. Methods*, vol. 4, no. 11, pp. 923–925, Oct. 2007, doi: 10.1038/nmeth1113.
- [92] R. J. Platt *et al.*, “CRISPR-Cas9 Knockin Mice for Genome Editing and Cancer Modeling,” *Cell*, vol. 159, no. 2, pp. 440–455, Oct. 2014, doi: 10.1016/j.cell.2014.09.014.
- [93] C. T. Breunig *et al.*, “One step generation of customizable gRNA vectors for multiplex CRISPR approaches through string assembly gRNA cloning (STAgR),” *PLoS One*, vol. 13, no. 4, Apr. 2018, doi: 10.1371/journal.pone.0196015.
- [94] N. Heins *et al.*, “Glial cells generate neurons: The role of the transcription factor Pax6,” *Nat. Neurosci.*, vol. 5, no. 4, pp. 308–315, 2002, doi: 10.1038/nn828.
- [95] A. Dobin *et al.*, “STAR: ultrafast universal RNA-seq aligner.,” *Bioinformatics*, vol. 29, no. 1, pp. 15–21, Jan. 2013, doi: 10.1093/bioinformatics/bts635.
- [96] R. Kolde, “CRAN - Package pheatmap,” 2019. <https://cran.r-project.org/web/packages/pheatmap/index.html> (accessed Sep. 21, 2021).
- [97] L. M. Blighe K., Rana S., “EnhancedVolcano: Publication-ready volcano plots with enhanced colouring and labeling.” 2022, [Online]. Available: <https://github.com/kevinblighe/EnhancedVolcano>.
- [98] A. Kassambara and F. Mundt, “Extract and Visualize the Results of Multivariate Data Analyses [R package factoextra version 1.0.7],” Apr. 01, 2020. <https://cloud.r-project.org/web/packages/factoextra/index.html> (accessed Sep. 21, 2021).
- [99] C. C. Aggarwal, A. Hinneburg, and D. A. Keim, “On the Surprising Behavior of Distance Metrics in High Dimensional Space,” in *Lecture Notes in Computer Science (including subseries Lecture Notes in Artificial Intelligence and Lecture Notes in Bioinformatics)*, vol. 1973, 2001, pp. 420–434.
- [100] B. Meunier, E. Dumas, I. Piec, D. Béchet, M. Hébraud, and J. F. Hocquette, “Assessment of hierarchical clustering methodologies for proteomic data mining,” *J. Proteome Res.*, vol. 6, no. 1, pp. 358–366, 2007, doi: 10.1021/pr060343h.
- [101] F. Murtagh and P. Legendre, “Ward’s Hierarchical Agglomerative Clustering Method: Which Algorithms Implement Ward’s Criterion?,” *J. Classif.*, vol. 31, no. 3, pp. 274–295, Oct. 2014, doi: 10.1007/s00357-014-9161-z.
- [102] S. P. Albaum *et al.*, “A guide through the computational analysis of isotope-labeled mass spectrometry-based quantitative proteomics data: an application study,” *Proteome Sci.*, vol. 9, no. 1, p. 30, Oct. 2011, doi: 10.1186/1477-5956-9-30.
- [103] A. Neueder and G. P. Bates, “A common gene expression signature in Huntington’s disease patient brain regions,” *BMC Med. Genomics*, vol. 7, no. 1, p. 60, Dec. 2014, doi: 10.1186/s12920-014-0060-2.
- [104] A. M. Yip and S. Horvath, “Gene network interconnectedness and the generalized topological overlap measure.,” *BMC Bioinformatics*, vol. 8, no. 1, p. 22, Jan. 2007, doi: 10.1186/1471-2105-8-22.
- [105] A. Sandelin, W. Alkema, P. Engström, W. W. Wasserman, and B. Lenhard, “JASPAR: An open-access database for eukaryotic transcription factor binding profiles,” *Nucleic Acids Res.*, vol. 32, no. DATABASE ISS., pp. 91D – 94, Jan. 2004, doi: 10.1093/nar/gkh012.
- [106] J. Schindelin *et al.*, “Fiji: an open-source platform for biological-image analysis,” *Nat. Methods*, vol. 9, no. 7, pp. 676–682, Jul. 2012, doi: 10.1038/nmeth.2019.



Supplemental Figure 1: Protein expression of marker genes as determined by MS/MS mass spectrometry on purified glial populations (black) and flow-through (grey) from the various brain regions. Bottom row shows the only three ependymal marker genes as defined by Ohlig et al. that were detected in our proteomic data set. Mean \pm SEM is plotted for each condition.



Supplemental Figure 2. **A:** Differentially expressed proteins that were enriched at least twofold in one region against all others. **B:** YAP1 protein expression as determined by MS/MS mass spectrometry on purified glial populations (black) and flow-through (grey) from the various brain regions. Mean \pm SEM is plotted for each condition.



Supplemental Figure 3: Validation of antibody specificity by KO of ZEB1 in primary astrocytes. Cortical astrocyte cultures from transgenic mice expressing wt-Cas9 transfected with control or gRNA plasmids against Zeb1 show efficient reduction in the expression of ZEB1. Red: tdTomato positive, successfully transfected cells, green: Cas9-GFP, white: ZEB1. Red arrows: transfected cells with successful ZEB1 KO, blue: DAPI. Yellow arrow: transfected cell with residual ZEB1 expression. Percentage Zeb1 positive cells among transfected cells shown as mean \pm SEM (n = 4, *p \leq 0.05)

RETINAL REGIONS SHAPE HUMAN AND MURINE MÜLLER CELL PROTEOME
PROFILE AND FUNCTIONALITY

Authors:

Kaplan L, Drexler C, Pfaller AM, Brenna S, Wunderlich KA, Dimitracopoulos A, Merl-Pham J, Perez M, Schlötzer-Schrehardt U, Enzmann V, Samardzija M, Puig B, Fuchs P, Franze K, Hauck SM, Grosche A

Author contributions:

Conceptualization: LK, PF, BP, KF, SMH, AG. *Methodology:* LK, CD, AMP, SB, KAW, AD, MP, US, VE, KF, SMH, AG. *Investigation:* LK, CD, AMP, SMH, AG. *Visualization:* LK, AG. *Supervision:* PF, BP, KF, SMH, AG. *Writing—original draft:* LK, AG. *Writing—review & editing:* LK, VE, MS, PF, BP, KF, SMH, AG.

License:





Attribution 4.0 International (CC BY 4.0)

Availability:

DOI: 10.1002/glia.24283

RESEARCH ARTICLE

Retinal regions shape human and murine Müller cell proteome profile and functionality

Lew Kaplan¹  | Corinne Drexler^{2,3} | Anna M. Pfaller¹ | Santra Brenna⁴  |
 Kirsten A. Wunderlich¹ | Andrea Dimitracopoulos⁵ | Juliane Merl-Pham⁶ |
 Maria-Theresa Perez^{7,8} | Ursula Schlötzer-Schrehardt⁹ | Volker Enzmann^{10,11}  |
 Marijana Samardzija¹² | Berta Puig⁴ | Peter Fuchs² | Kristian Franze^{5,13,14} |
 Stefanie M. Hauck⁶ | Antje Grosche¹ 

¹Department of Physiological Genomics, Ludwig-Maximilians-Universität München, Munich, Germany

²Max Perutz Labs, Department of Biochemistry and Cell Biology, University of Vienna, Vienna Biocenter Campus (VBC), Vienna, Austria

³Vienna Biocenter PhD Program, Doctoral School of the University of Vienna and Medical University of Vienna, Vienna, Austria

⁴Neurology Department, Experimental Research in Stroke and Inflammation (ERSI), University Medical Center Hamburg-Eppendorf, Hamburg, Germany

⁵Department of Physiology, Development and Neuroscience, University of Cambridge, Cambridge, UK

⁶Research Unit Protein Science and Metabolomics and Proteomics Core, Helmholtz Zentrum München, German Research Center for Environmental Health, Neuherberg, Germany

⁷Department of Clinical Sciences, Division of Ophthalmology, Lund University, Lund, Sweden

⁸NanoLund, Nanometer Structure Consortium, Lund University, Lund, Sweden

⁹Department of Ophthalmology, Friedrich-Alexander-Universität Erlangen-Nürnberg, Erlangen, Germany

¹⁰Department of Ophthalmology, Bern University Hospital, Inselspital, University of Bern, Bern, Switzerland

¹¹Department of BioMedical Research, University of Bern, Bern, Switzerland

¹²Department of Ophthalmology, University Hospital Zurich, University of Zurich, Zurich, Switzerland

¹³Institute of Medical Physics, Friedrich-Alexander-Universität Erlangen-Nürnberg, Erlangen, Germany

¹⁴Max-Planck-Zentrum für Physik und Medizin, Erlangen, Germany

Correspondence

Antje Grosche, Department of Physiological Genomics, Ludwig-Maximilians-Universität München, Munich, Germany.
 Email: antje.grosche@med.uni-muenchen.de

Funding information

Austrian Science Fund, Grant/Award Number: P30310; Deutsche Forschungsgemeinschaft, Grant/Award Numbers: GR 4403/1-1, GR 4403/5-1, GR 4403/7-1, HA 6014/5-1; ProRetina Foundation Germany, Grant/Award Numbers: Pro-Re/Seed/Grosche.1-2014, Pro-Re/Seed/Kaplan-Grosche.1-2019

Abstract

The human macula is a highly specialized retinal region with pit-like morphology and rich in cones. How Müller cells, the principal glial cell type in the retina, are adapted to this environment is still poorly understood. We compared proteomic data from cone- and rod-rich retinæ from human and mice and identified different expression profiles of cone- and rod-associated Müller cells that converged on pathways representing extracellular matrix and cell adhesion. In particular, epiplakin (EPPK1), which is thought to play a role in intermediate filament organization, was highly expressed in macular Müller cells. Furthermore, *EPPK1* knockout in a human Müller cell-derived cell line led to a decrease in traction forces as well as to changes in cell size, shape, and filopodia characteristics. We here identified *EPPK1* as a central molecular player in the region-specific architecture of the human retina, which likely enables specific functions under the immense mechanical loads in vivo.

This is an open access article under the terms of the [Creative Commons Attribution](https://creativecommons.org/licenses/by/4.0/) License, which permits use, distribution and reproduction in any medium, provided the original work is properly cited.

© 2022 The Authors. *GLIA* published by Wiley Periodicals LLC.

KEYWORDS

retina, macula, Müller cells, glial heterogeneity, EPPK1

1 | INTRODUCTION

A healthy retina is our most important gateway to the outside world, providing us with a major part of our sensory input to orient and interact with our environment quickly and efficiently (Hutmacher, 2019). For sharp vision in humans, most of the image information is focused on a tiny spot of the retina, the macula. Therefore, any damage in this area has catastrophic effects. The macula with its central fovea is characterized by a pit-like depression in which the somata of the inner retinal cells are displaced laterally so that light can strike the photoreceptors unimpeded. The outer nuclear layer in this region is increasingly dominated by cones. This culminates in the foveola, which contains almost exclusively cones, surrounded and supplied only by processes of a z-shaped subpopulation of Müller cells, the major macroglia of the retina. Finally, the retinal vasculature is completely absent from the fovea (Bringmann et al., 2018) and increased light exposure leads to a higher turn-over in metabolites and the production of reactive oxygen species (Handa, 2012).

Many known pathologies leading to visual impairment are caused by defects in photoreceptor, vasculature, or the retinal pigment epithelium (RPE) functions, which have been intensively studied in recent decades (Bhutto & Luty, 2012; Lenis et al., 2018; Verbakel et al., 2018). In contrast, despite their numerous important functions, Müller cells are still poorly understood. Originally thought to provide mainly structural support for retinal neurons, it has later been proposed that Müller cells shuttle not only metabolites like pyruvate and lactate, but are, to name just a few examples, also involved in glutamate recycling—similar to brain astrocytes (Hurley et al., 2015; Lu et al., 2006; Reichenbach & Bringmann, 2020; Toft-Kehler et al., 2018)—or even glutamate release to feedback on neurons (Slezak et al., 2012). Such functions are mediated by a myriad of Müller cell processes contacting all other retinal cell types. In addition, Müller glia, which extend across the entire thickness of the retina, are thought to conduct light through all cell layers to the photoreceptors on the light-averted side of the retina (Franze et al., 2007) and to be responsible not only for the biomechanical stability of the tissue, but also for the formation of the foveal pit (Bringmann et al., 2018; Bringmann et al., 2020; MacDonald et al., 2015). In zebrafish, it has been shown that Müller cells can acquire stem cell properties after injury, leading to complete tissue regeneration (Goldman, 2014; Wan & Goldman, 2016). Finally, while the canonical visual cycle involves the multistep enzymatic conversion of all-trans-retinol to 11-cis-retinal in the RPE, an alternative, cone-specific and Müller cell-dependent pathway has been described recently (Wang & Kefalov, 2011).

Although it is conceivable that the unique conditions of the human macula pose challenges for both photoreceptors and Müller

cells, many of these aspects have been studied in model systems that do not have the specifics of this region. This raises the question of how glial metabolism and metabolite exchange adapt to increased energy consumption, increased cone density, and lack of vascularization in the macula. Alternatively, what factors are necessary to provide the extremely long, Z-shaped Müller cells of the macula with the biomechanical properties needed to withstand the high mechanical stresses and tensile forces imposed by the vitreous to preserve the fragile tissue structure of this retinal region (Bringmann et al., 2021). To approach these questions at a broad molecular level, transcriptomic and especially proteomic profiling of human Müller cells are required. There have been efforts to use bulk RNA sequencing (RNAseq) (Whitmore et al., 2014), which provides excellent depth but is unable to distinguish between cell types, so that only general inter-regional differences are represented, an obstacle that has been solved by the advent of single-cell (sc)RNAseq (Chambers et al., 2019; Voigt et al., 2021). However, it is important to bear in mind that the final products in the cell are, in most cases, proteins that coordinate cellular metabolism, structural integrity, and intercellular communication. Many steps influence how much of the final functional protein results from a specific mRNA. These include regulation of mRNA translation, post-translational modifications, oligomerization, and stability issues of both the mRNA and the protein. However, whole retina mass proteomic analysis suffers from similar limitations as bulk RNAseq and single-cell proteomics is still under development (Brunner et al., 2022; Kelly, 2020). To tackle these challenges, we previously established a method to isolate pure, morphologically intact Müller cells from murine (Grosche et al., 2016) or human retina. We compared the proteomes of Müller cells isolated from the R91W/Nrl^{-/-} mice, representing Müller cells in a cone-rich environment similar to the macula, with the proteomes of control mice, representing Müller cells in the peripheral human retina, and of human Müller cells isolated from the macula and periphery. We found differentially expressed proteins converging on specific molecular pathways—a number of which were the same in both species. EPPK1, a selected novel protein candidate, was functionally characterized by studying a respective knockout in the human Müller cell-derived cell line MIO-M1. Our results indicate that EPPK1 participates in the constitution of macular Müller cell's tensile strength as well as morphology and has an influence on the secretion of extracellular vesicles.

The identification of the molecular and functional properties of retinal Müller cells of the macula is urgently needed to better understand and efficiently fight debilitating sight-threatening diseases in humans such as age-related macular degeneration. With this study, we provide the first insights into the heterogeneity of human retinal Müller cells at a protein level and point to potential directions for future research.

2 | MATERIALS AND METHODS

2.1 | Mouse lines and donor tissue

The all-cone Rpe65R91W;Nr1^{-/-} (R91W;Nr1) mouse model (Samardzija et al., 2014) and the Rpe65R91W single mutant mice (Samardzija et al., 2008) were bred at a specific pathogen-free barrier animal facility of the Helmholtz Center Munich in accordance with and with allowance by institutional as well as state and federal guidelines (5.1–568-Gas: Allowance to breed and kill animals for scientific purposes).

Eppk1 knockout mice of the C57BL/6 background (Spazierer et al., 2006; Szabo et al., 2015) and C57BL/6 wild-type mice were kept at the pathogen-free mouse facility of the Max Perutz Labs animal facility, Vienna, Austria, in accordance with Austrian Federal Government laws.

Eyes from adult male and female mice (3 to 6 months of age) were collected after animals were sacrificed via cervical dislocation. Eyes fixed in 4% PFA from *Gfap/Vim* double knockout mice (3 months of age) were kindly provided by Maria-Theresa Perez (Lund University, Lund, Sweden).

Samples for proteome profiling of human Müller cells were isolated from a set of five donor eyes. The Institutional Review Board at University of Regensburg approved the use of human tissues for this purpose. Five eyes from four non-diabetic Caucasian donors 58–89 years of age (2 males, 1 female, 1 of unknown gender) at a death-to-experimentation interval of <30 h were included in this analysis (Figure S1, Table S1). Ocular health histories were not available. Eyes were opened by eye bank recovery personnel using an 18 mm diameter corneal trephine and stored on ice for transfer to the laboratory for further processing.

To stain for EPPK1 in the macular and peripheral retina, human eyes (postmortem time <8–24 h, two eyes from two donors, Table S1) were cryosectioned. The research complies with the human research act (HRA) stating that small quantities of bodily substances removed in the course of transplantation may be anonymized for research purposes without consent (HRA chapter 5, paragraph 38, Switzerland).

2.2 | Proteomic profiling of MACS enriched retinal cell types

2.2.1 | Cell purification from human donor or murine retina

As described previously (Grosche et al., 2016), different retinal cell types were isolated either from whole murine retina or from 6 mm punches (from macula and from periphery) of human retina using magnetic activated cell sorting. First, the tissue was treated with papain (0.2 mg/ml; Roche) for 30 min at 37°C in PBS/Glucose (12 mM), washed and incubated in DNase I (200 U/ml in PBS/Glucose) for 4 min at RT. PBS/Glucose was removed and substituted with

extracellular solution (ECS, 136 mM NaCl, 3 mM KCl, 10 mM HEPES, 11 mM glucose, 1 mM MgCl₂ and 2 mM CaCl₂, pH 7.4) before dissociating the tissue using a firepolished glass Pasteur pipette. The cell suspension was sequentially depleted of microglia and vascular cells by incubating (15 min, 4°C) with anti-mouse/human CD11b and CD31 microbeads (Miltenyi Biotec), respectively, and passing through LS-columns according to manufacturer's protocol (Miltenyi Biotec). The resulting suspension was incubated (15 min, 4°C) with anti-CD29 biotinylated antibodies (0.1 mg/ml, Miltenyi Biotec), spun down, washed and the pellet resuspended in ECS containing anti-biotin ultra-pure MicroBeads (1:5; Miltenyi Biotec). The suspension was passed through a LS-column resulting in a neuron-rich flowthrough (CD29⁻), before the bound CD29⁺ Müller cells were finally eluted from the column. To prepare samples for immunostaining, 100 µl of each of the CD29⁺ and CD29⁻ fractions were fixed for 15 min in 4% paraformaldehyde (PFA) at RT, spun down, resuspended in 50 µl PBS and dropped onto a microscope slide.

2.2.2 | LC-MS/MS mass spectrometry analysis

Proteins were proteolysed with LysC and trypsin with filter-aided sample preparation procedure (FASP) as described (Grosche et al., 2016; Wiśniewski et al., 2009). Acidified eluted peptides were analyzed on a QExactive HF or HF-X mass spectrometer (Thermo Fisher Scientific) online coupled to a Ultimate 3000 RSLC nano-HPLC (Dionex) as described (Grosche et al., 2016). Briefly, samples were automatically injected and loaded onto the C18 trap cartridge and after 5 min eluted and separated on the C18 analytical column (nanoEase MZ HSS T3, 100 Å, 1.8 µm, 75 µm × 250 mm; Waters) by a 95 min nonlinear acetonitrile gradient at a flow rate of 250 nl/min. MS spectra were recorded at a resolution of 60,000 with an automatic gain control (AGC) target of 3e6 and a maximum injection time of 30 or 50 ms from 300 to 1500 m/z. From the MS scan, the 10 or 15 most abundant peptide ions were selected for fragmentation via HCD with a normalized collision energy of 27 or 28, an isolation window of 1.6 m/z, and a dynamic exclusion of 30 s. MS/MS spectra were recorded at a resolution of 15,000 with an AGC target of 1e5 and a maximum injection time of 50 ms. Unassigned charges, and charges of +1 and > +8 were excluded from precursor selection.

Acquired raw data were analyzed in the Proteome Discoverer software (versions 2.2 or 2.4, Thermo Fisher Scientific) for peptide and protein identification via a database search (Sequest HT search engine) against the SwissProt Mouse database (Release 2020_02, 17,061 sequences) or the SwissProt Human database (Release 2020_02, 20,435 sequences), considering full tryptic specificity, allowing for up to one missed tryptic cleavage site, precursor mass tolerance 10 ppm, fragment mass tolerance 0.02 Da. Carbamidomethylation of cysteine was set as a static modification. Dynamic modifications included deamidation of asparagine and glutamine, oxidation of methionine, and a combination of methionine loss with acetylation on protein N-terminus. The Percolator algorithm (Käll et al., 2007) was used for validating peptide spectrum matches and peptides. Only top-scoring identifications

for each spectrum were accepted, additionally satisfying a false discovery rate < 1% (high confidence). The final list of proteins satisfying the strict parsimony principle included only protein groups passing an additional protein confidence false discovery rate < 5% (target/decoy concatenated search validation).

Quantification of proteins, after precursor recalibration, was based on intensity values (at RT apex) for all unique peptides per protein. Peptide abundance values were normalized on total peptide amount. The protein abundances were calculated summing the abundance values for admissible peptides. The final protein ratio was calculated using median abundance values of five biological replicates each. The statistical significance of the ratio change was ascertained with ANOVA. For the MIO-M1 data sets, the statistical significance of the ratio change was ascertained employing the *t* test approach described in (Navarro et al., 2014) which is based on the presumption that we look for expression changes for proteins that are just a few in comparison to the number of total proteins being quantified. The quantification variability of the non-changing “background” proteins can be used to infer which proteins change their expression in a statistically significant manner.

2.3 | EV isolation from cell culture media and NTA analysis

After 72 h incubation, serum-free media was collected from both WT and *EPPK1* knockout MIO-M1 cells and immediately centrifuged at $300 \times g$, for 10 min at 4°C. The resulting supernatant was then centrifuged at $2000 \times g$, for 10 min at 4°C. The resulting supernatant was further centrifuged at $10,000 \times g$, for 30 min at 4°C. Lastly, the $10,000 \times g$ supernatant was spun at $100,000 \times g$ (24,000 rpm, sw40ti rotor) for 70 min at 4°C. The final pellet was resuspended in 30 μ l PBS with protease inhibitors (Roche). The cell numbers were assessed for each replicate well.

The final EVs suspension was diluted either 1:300 (WT) or 1:100 (KO cell lines). The measurement was done with the LM10 unit (Nanosight). The diluted samples were recorded with 10 videos, each 10 s long. Data analysis with NTA 3.0 software (Nanosight) was performed with the following settings: detection threshold = 6, screen gain = 2. Particle numbers were adjusted for dilution as well as cell number.

2.4 | Immunofluorescence staining and microscopy

Mouse eyes were fixed in 4% PFA for 1 h, cryoprotected, embedded in OCT compound and cut into sections of 20 μ m thickness using a cryostat. Human donor eyes were immersion-fixated with 4% paraformaldehyde (PFA) for 48 h. Thereafter, the central part of the eye cup containing the optic nerve head and the macula including the underlying RPE, choroid, and sclera was dissected. The tissue was submitted to cryoprotection, embedded in OCT and cut into 20 μ m thick sections. Retinal detachment from the RPE is an artifact commonly observed in cryosections.

Retinal sections were permeabilized (0.3% Triton X-100 plus 1.0% DMSO in PBS) and blocked (5% normal donkey serum with 0.3% Triton X-100 and 1.0% DMSO in PBS) for 2 h at room temperature. Primary antibodies (Table 1) were incubated overnight at 4°C. Sections were washed (1% bovine serum albumin [BSA] in PBS) and incubated with secondary antibodies (2 h at room temperature; Table 2). Cell nuclei were labeled with DAPI (1:1000; Life Technologies). Control experiments without primary antibodies showed no nonspecific labeling.

MIO-M1 cells were grown on sterile coverslips until desired confluency, washed with PBS and fixed for 15 min in 4% PFA. Cells were then permeabilized with 0.1% Triton X-100 in PBS for 10 min, washed with 1% BSA/PBS and incubated with primary antibodies for 2 h at RT. Coverslips were subsequently washed with PBS and incubated with secondary antibodies and DAPI for 1.5 h at RT and lastly mounted onto a microscope slide.

Confocal images were taken with a custom-made VisiScope CSU-X1 confocal system (Visitron Systems) equipped with high-resolution sCMOS camera (PCO AG).

Stimulated emission depletion (STED) microscopy was performed at the Core Facility Bioimaging of the Biomedical Center with an inverted Leica SP8X STED 3D microscope, equipped with a 405 nm Laser and a pulsed white light laser (470–670 nm). Gated-STED images were acquired with a 93x/1.30 glycerol objective, pixel size was around 30–32 nm. The following spectral settings were used: Abberior Star 580 (ex: 580 nm; em: 590–620 nm) and Abberior STAR 635P (ex: 635 nm; em: 645–702 nm). Signals were recorded with hybrid photo detectors (HyDs) in counting mode. Depletion laser wavelength was 775 nm.

2.5 | qPCR

Total RNA was isolated from peripheral retinal samples of three donors and from wild type MIO-M1 cells using PureLink™ RNA Mini Kit (ThermoFisher, 12183018A) following manufacturer's instructions; 50 ng of total RNA per sample were reverse transcribed with RevertAid Reverse Transcriptase (ThermoFisher, EP0441) with the help of random hexamer primers. Primers for qPCR were designed using the Universal ProbeLibrary Assay Design Center (Roche) to be used with the corresponding probes (Table 2). Since *EPPK1* mRNA consists of only one translated exon, an exon spanning assay was not possible. Final expression values were calculated via the Δ Ct method by taking the difference between *EPPK1* and a house keeper's (*PDHB*) Ct values and using the result as the power of two.

2.6 | Western blot analysis

A 100% confluent 10 cm cell culture dish was used for isolating protein lysates. The cells were washed two times with PBS and subsequently overlaid with 500 μ l of ice-cold protein lysis buffer (50 mM HEPES pH 7, 100 mM NaCl, 5 mM $MgCl_2$, 1 mM EGTA or EDTA,

TABLE 1 Antibodies used for immunofluorescence stainings

Primary antibody	Species	Company	Catalogue number/ reference	Dilution/ concentration
GLUL	Mouse	Merck	MAB302	1:500
CD9	Rat	BD Biosciences	553758	1:200
GFAP	Mouse	Sigma-Aldrich	G3893	1:500
EPPK1	Rabbit	gift from G. Wiche (Spazierer et al., 2003)	-	1:2000
VIM	Mouse	Santa Cruz	sc-373717	1:500
Secondary antibody				
Anti-rabbit-Cy3	Goat	Dianova	111-165-144	1:500
Anti-mouse-AF488	Goat	LifeTech	A-1109	1:500
Anti-rat-Cy3	Goat	Dianova	112-165-167	1:500
Anti-mouse-Abberior STAR 580	Goat	Abberior	2-0002-005-1	1:200
Anti-rabbit- Abberior STAR 635P	Goat	Abberior	2-0012-007-2	1:200

TABLE 2 qPCR primers

Primer	UPL probe #	Sequence (5'–3')
h_EPPK1_qpcr_for	32	CCACAAGAAGAGCTTTTCCAG
h_EPPK1_qpcr_rev	32	AGCCTGGCCTCTAGGAGT
h_PDHB_qpcr_for	17	AGAGCGCTTCTCACTGGAC
h_PDHB_qpcr_rev	17	CCAAGCAGAAATACCTTCTCATC

2.5% Triton X-100, 100 nM DTT, 0.5 mg/ml DNase I, 0.2 mg/ml RNase A, 1 mM PMSF, protease inhibitors [cOmplete ULTRA tablets, Roche]) before scraping them off. The solution was homogenized, transferred into an Eppendorf tube, and incubated for 5 min at room temperature and lastly sheared via a 27-gauge needle. For retinal samples, the tissue was snap frozen in liquid nitrogen and per 10 mg of tissue 200 µl of tissue protein lysate buffer (Tris pH 7.5; 10 mM NaCl; 150 mM EDTA; 5 mM Triton X-100; 1% SDS; 0.1% NP-40; 1% 1% phosphatase inhibitor cocktails 2 and 3 [Sigma-Aldrich, cat no. P5726 and P0044]; 100 µg/ml DNase I; 100 µg/ml RNase; 1 mM PMSF) was added. The tissue was homogenized using an IKA® ULTRA-TUR-RAX® disperser tool (IKA T10 basic), until a homogenized solution was observed. The suspension was incubated for 10 min at RT with periodic mixing to guarantee efficient cell lysis and ribonuclease digestion.

Samples were combined with SDS loading dye (390 mM Tris-HCl pH 6.8, 485 mM DTT, 10% SDS, 0.1% Bromophenol-Blue, 50% glycerol) and incubated at 95°C for 5 min before clearing the samples by centrifugation at 13800 g. Equal sample volumes were run on a 12% gel and stained with Coomassie dye to account for loading differences (Figure S2). Next, samples were loaded onto a combination of a stacking (4%) and resolving (6%) SDS polyacrylamide gel. The electrophoresis was run at 20 mA per gel until 1 h after the dye front ran out and the 250 kDa band of the protein ladder reached the bottom of the gel. Protein was transferred to a nitrocellulose membrane using a Mini

Trans-Blot machine (Biorad) at 4°C, 25 V overnight. Membranes were blocked in 5% BSA/PBS for 1 h, washed with PBS/0.05% Tween20 (PBS-T), and incubated with primary antibody diluted in 5% BSA/PBS-T for 3 hours at RT. After washing the membrane again and incubating it with HRP-conjugated secondary antibody (goat anti-rabbit, 1:20000, Vector Laboratories), protein bands were visualized using Clarity Max Western ECL Substrate (Biorad, 1705060 S). For human cell lines, we used a rabbit anti-EPPK1 primary antibody acquired from Thermo Fisher (PA5-66869) in a dilution of 1:2000, while samples stemming from mouse tissue were incubated with a rabbit anti-EPPK1 antibody (dilution 1:10000) generated in an earlier study (Spazierer et al., 2003).

2.7 | Cell culture and CRISPR approach to generate a EPPK1 knockout

MIO-M1 cells (Limb et al., 2002) were cultured in FBS containing medium (DMEM, high glucose, GlutaMAX™ Supplement, HEPES, 10% FBS, 1:100 Penicillin/Streptomycin; Gibco) at 37°C, 5% CO₂ unless stated otherwise.

We generated an EPPK1 knockout in MIO-M1 cells using pSpCas9(BB)-2A-Puro (PX459) V2.0 plasmid supplied by Addgene (plasmid # 6298) as suggested by the authors that deposited the plasmid (Ran et al., 2013). We first designed gRNAs using various tools (Benchling, (2021), CRISPRdirect (Naito et al., 2015)) targeted at a 1000 bp long region in the beginning of the translated exon and chose two guides each with minimal off-site reactivity (Table 3). Restriction digest of the plasmid with BbsI-HF (NEB) and subsequent ligation (T4 DNA Ligase, NEB) with the annealed, double stranded oligonucleotides yielded the final expression vectors, the correctness of which was confirmed by sequencing.

For the transfection, ~300,000 cells were seeded per well of a 6-well plate to receive a subconfluent culture on the next day. Cells were transfected with an equimolar mix of all four vectors using

TABLE 3 Guide RNAs designed for EPPK1 knockout in human MIO-M1 cells

	Designed gRNA sequence (5'–3')	Strand	Tool	Oligonucleotides ready for cloning (5'–3')
gRNA_1_top	GGCTATCCTGACCCCTACGG	+	Benchling	caccGGCTATCCTGACCCCTACGG
gRNA_1_bottom				aaacCCGTAGGGGTCAGGATAGCC
gRNA_2_top	ACGTGCACTCACGTCCACTG	–	Benchling	caccGACGTGCACTCACGTCCACTG
gRNA_2_bottom				aaacCAGTGGACGTGAGTGCACGT <u>C</u>
gRNA_3_top	CCAGAGTGTCTACGCCGCCA	+	CRISPRdirect	cacc <u>G</u> CCAGAGTGTCTACGCCGCCA
gRNA_3_bottom				aaacTGCGGGCGTAGACACTCTGG <u>C</u>
gRNA_4_top	CCTGGAGGGTACCGGCAGCG	+	CRISPRdirect	cacc <u>G</u> CCTGGAGGGTACCGGCAGCG
gRNA_4_bottom				aaacCGCTGCCGGTACCCTCCAGG <u>C</u>

Note: Lowercase letters indicate overhangs necessary for correct insertion into the digested vector backbone and are not part of the target sequence. A 5' G (underlined) was added to guides if not already present to increase transcription efficiency by the U6 promoter (Ran et al., 2013).

TABLE 4 Primers used to verify construct and knockout sequence

Primer	Usage	Sequence (5'–3')
hU6-F	Vector sequencing	GAGGGCCTATTTCATGATT
hEPPK1_PCRSeq_for	Target region amplification and sequencing	TAACCAGCCGTGTGTGATGAGT
hEPPK1_PCRSeq_rev	Target region amplification and sequencing	CCTGTCCACTAGCCCTTCTTC

jetOPTIMUS transfection reagent (Polyplus) according to manufacturer's protocol. Briefly, a total of 2.5 µg of plasmid mix was added to 200 µl of jetOPTIMUS buffer, which then was supplemented with 2.5 µl jetOPTIMUS reagent and incubated for 10 min. This transfection mix was added to the cells and incubated for 4 hours before exchanging the medium. Cells were allowed to recover for 48 h before moving to puromycin (3 µg/ml) containing selection medium. After 4 days the remaining transfected cells were harvested and seeded in a 96-well plate at a density of 5 cells/ml (100 µl containing 0.5 cells per well) ensuring that most wells would contain either zero or one cell. Thus, colonies grown in such wells would be originating from a single cell and yield monoclonal cell lines. After ~3 weeks, we saw colonies big enough to be harvested and further expanded two of them in bigger scale thereby generating the final monoclonal cell lines F7 and C9. Genomic DNA was isolated from these lines and used as input for a PCR with primers amplifying the 1000 bp target region in order to confirm the knockout on genomic level via sequencing (Table 4).

2.8 | Traction force microscopy

To perform traction force microscopy, we first produced acrylamide-based gels with a defined shear modulus of 1000 Pa as previously published by Bollmann et al. (2015) and applied them to culture dishes. Briefly, glass bottom dishes (µ-Dish 35 mm, high, Ibidi) were

first treated with (3-Aminopropyl) trimethoxysilane (APTMS) for 2–3 min and washed with distilled water. The glass surface was then covered with 2.5% glutaraldehyde for 30 min, washed and air-dried. Coverslips were prepared by cleaning in 80% ethanol and water and made hydrophobic by submerging them in RainX (Kracor Car Care International Ltd.) for 10 min. For the gels, we first made a master mix by combining 500 µl 40% acrylamide (Sigma-Aldrich) with 65 µl hydroxy-acrylamide (Sigma-Aldrich); 500 µl of this solution was added to 250 µl 2% bis-acrylamide (Fisher Scientific) to obtain the final master mix. In order to produce gels of 1000 Pa stiffness we mixed 75 µl master mix with 415 µl sterile PBS and 10 µl fluorescent beads (FluoSpheres carboxylate, 0.2 µm, crimson, Life Technologies). To ensure even dispersion of the beads, the gel solution was placed in an ultrasonic bath for 5 min and subsequently degassed in a desiccator for 10 min. Polymerization was initiated by the addition of 5 µl 10% APS and 1.5 µl of TEMED before adding 10 µl of the solution onto the treated glass bottom. By placing the prepared coverslip on top of the drop and immediately inverting the dish, we ensured an even distribution of the gel and the placement of the beads close to the imaging surface. After polymerization, PBS was added to the dish and the coverslip removed.

Two milliliter of a cell suspension containing 20,000 cells were seeded onto the gels and cultured over night before imaging. The dishes were imaged at the Core Facility Bioimaging of the Biomedical Center using an inverted Leica DMI8 Widefield microscope equipped with a Hamamatsu-Flash4 camera and a Lumencor SpectraX light engine using a 40x/0.60 objective. A motorized stage enabled the precise marking and revisiting of specific spots on the dish while an incubator enclosure and heated dish holder ensured cell culture conditions (37°C, 5% CO₂); 10 to 20 cells exhibiting a clear non-round morphology were selected per dish: Each cell position was scanned with phase contrast additionally to the fluorescence imaging (ex.: 625–655 nm, em.: 670–770 nm) to detect the location of the cell and the beads in the associated state. Gels were rinsed with PBS, incubated with trypsin, and rigorously rinsed again to ensure complete cell detachment but taking care not to move the dish. All positions were revisited to document the embedded beads in their relaxed state as well as the absence of the cell.

To calculate the traction stress and generate traction force maps we used several plugins for the ImageJ (Schindelin et al., 2012) software as well as custom written macros. Images of the beads were first enhanced in contrast, and then combined into a stack of which the background was subtracted using the rolling ball algorithm. The *Linear Stack Alignment with SIFT* (Lowe, 2004) plugin was then used to align both images of the stack to account for the x,y-drift when revisiting the cell positions. Next, each stack was processed with a plugin for particle image velocimetry (PIV) (Tseng, 2011; Tseng et al., 2012) using the template matching method with advanced settings. Traction forces and corresponding heat maps were calculated from the PIV vector matrices using a plugin for Fourier-transform traction cytometry (FTTC) (Tseng, 2011; Tseng et al., 2012). In some cases, the x,y-drift caused excessively high forces to be detected at the edges of a traction map, which is why we excluded all values in a 335-pixel wide frame. From the remaining values we calculated the average traction stress as the mean of all forces above a threshold set at 30% of the maximum value (peak traction stress) for each image analogous to the protocol developed by Bollmann et al. (2015). The custom ImageJ macros including the specific settings for the SIFT, PIV, and FTTC plugins are available upon request.

2.9 | Bioinformatic and statistical analyses

All statistical analyses were performed using the R programming language unless stated otherwise.

For differential protein expression analysis, we first excluded proteins that had missing values in more than two out of five Müller cell samples per group. Then, we chose only proteins that were significantly enriched in Müller cells in at least one group (RMG/neuron ratio >1, adjusted *p*-value <.05) yielding the Müller cell-specific proteins. The normalized abundance values were log transformed and used as an input to calculate differential protein expression with the *limma* package (Ritchie et al., 2015). PCA coordinates were calculated on log transformed normalized abundance values as input of the *prcomp* function and subsequently visualized via the *factoextra* (Kassambara & Mundt, 2020) package. Heat maps were produced on the basis of median centered, log transformed normalized abundances using the *heatmap* (Kolde, 2019) package. Other plots were created with *ggplot2* (Data S1).

Single-cell RNA sequencing data sets from Voigt (Voigt et al., 2019) and Cowan (Cowan et al., 2020) were downloaded as count matrices from Gene Expression Omnibus with the accession number GSE130636 or from <https://data.iob.ch/>, respectively. We used a standard pipeline relying on the Seurat (Hao et al., 2021; Stuart et al., 2019) package including normalization, scaling, identification of variable genes, dimensionality reduction, and cluster annotation based on known marker genes in line with the original studies. To mimic our proteomics approach, we then used the *FindMarkers* function to identify genes, that were specifically enriched (log2 fold change >0, adjusted *p*-value <.05) in the Müller cell clusters compared to retinal neurons including rods and cones as well as bipolar, amacrine,

horizontal, and ganglion cells. In the next step, we split the RMG clusters by region and performed differential gene expression analysis on the subclusters using the same function. For better comparison, we calculated the central to peripheral Müller cell expression ratio for each individual gene/protein and plotted the overlapping ones against each other in a scatter plot.

Quantification of morphological features as well as filopodia characteristics was performed with the CellProfiler (Jones et al., 2008; McQuin et al., 2018) software on the basis of actin staining of sparsely seeded cells across three independent experiments. First, individual cells were identified as primary objects, which were subsequently eroded to remove minor processes and filopodia and thus get the main cell body. The primary objects were then masked with the eroded objects and subsequently skeletonized to generate the outlines of cells without the body. Using the *MeasureObject* modules we quantified the branch parameters of the skeletonized outline for filopodia characterization and several other parameters of the primary objects representing the whole cells. The number of branch ends per cell was normalized to its perimeter as well as to the median number of detected branch ends per experiment to account for cell size and slight variation in contrast/image quality between experiments. The total branch lengths of a cell were additionally normalized to the number of its branch ends to get a measure of average filopodia length per cell.

Using CellProfiler, CD9 intensity was measured in three independent experiments by first identifying individual nuclei via DAPI staining as primary objects and the CD9 immunofluorescence as secondary objects around the nuclei. Intensity values per cell were normalized to median intensities per experiment.

We used the CytoScape (Shannon et al., 2003) software to create and explore gene/protein networks and perform pathway enrichment analysis via the StringApp plugin (Doncheva et al., 2019). Analysis scripts as well as CellProfiler pipelines are available upon request.

3 | RESULTS

3.1 | All-cone mice show generally healthy retinal layering with minor abnormalities in the outer retina

Grimm and colleagues described the generation and characterization of the R91W/Nrl^{-/-} (from here on just “all-cone”) mouse retina among others, in terms of structure, visual acuity and photoreceptor degeneration over time (Samardzija et al., 2014). To gauge its use as a model for the human macula, we wanted to test for possible differences between the all-cone retinal cytoarchitecture and its respective control carrying only the R91W mutation (from here on regarded as “control” in comparisons with all-cone samples). For this, we stained for cell type-specific markers, quantified the nuclei in the nuclear, and measured the thicknesses of the plexiform layers (Figure 1). Immunofluorescence staining for calretinin, a marker of inner retinal neurons including amacrine and ganglion cells, showed no significant difference between genotypes (Figure 1a,b), but the outer nuclear layer

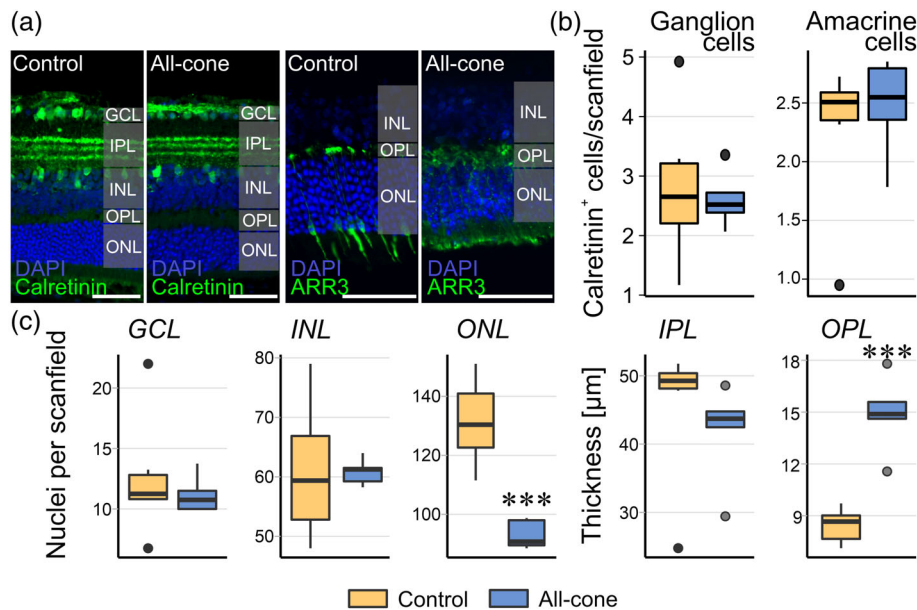


FIGURE 1 Morphological characterization of the all-cone mouse model. (a) Representative central retinal sections from control (R91W) and all-cone mice (R91W/*Nrl*^{-/-}). Cells of the inner retina were visualized by staining with calretinin, a ganglion and amacrine cell marker (left), while cones were delineated by staining for cone arrestin (ARR3, right). Scale bars, 50 μ m. (b) Quantification of calretinin-positive cells in the ganglion cell layer (GCL) that comprise primarily ganglion cells and some displaced amacrine cells and in the inner nuclear layer (INL) representing amacrine cells. (c) DAPI-positive nuclei were quantified in all three retinal nuclear layers. We found on average 30% less nuclei in the outer nuclear layer of all-cone mice, while there were no differences in the other layers. Additionally, all-cone mice showed an almost twofold thicker outer plexiform layer than the control. (b, c) Box plots represent data from $n = 6$ control and $n = 5$ all-cone animals, respectively. Compared with control: *** $p < .001$; ONL, outer nuclear layer; OPL, outer plexiform layer; IPL, inner plexiform layer

(ONL) of the all-cone mouse contained $\sim 30\%$ fewer cells (Figure 1c). Finally, we observed a significantly thicker outer plexiform layer (OPL) in the all-cone mice (Figure 1c). Cone arrestin (ARR3) staining in control mice showed the characteristic pattern of interspersed cone photoreceptors in the ONL ranging from synaptic terminals in the OPL to the outer segments thereby visualizing complete individual cells (Figure 1a). Individual cones were barely visible in the ONL of the all-cone mice, because of them being very densely packed, similar to what is observed in the human fovea. Additionally, we noticed abnormal outer segment morphology and rather disorganized cone pedicles in the OPL.

3.2 | Proteome profiling identifies differentially expressed proteins between cone- and rod-associated murine Müller cells

To enable the specific investigation of the Müller cell protein expression pattern from cone- or rod-rich mouse retina, we performed magnetic activated cell sorting (MACS) (Grosche et al., 2016; Pauly et al., 2019). This process of sequential cell depletion resulted in four cell populations—microglia (CD11b⁺), endothelial cells (CD31⁺), Müller cells (CD29⁺), and neurons (CD11b⁻, CD31⁻, CD29⁻). We confirmed the composition of the Müller cell fraction (CD29⁺) in comparison to the neuron-enriched flowthrough by staining drop samples for the Müller cell marker glutamine synthetase (GLUL) and found

comparable enrichment as published earlier (Grosche et al., 2016). Not only were Müller cells present in a high percentage of more than 70% in the CD29 fraction, but also there was an almost complete absence of glutamine synthetase (GLUL)-positive cells in the flowthrough, corroborating the good performance of the technique (Figure 2a). Importantly, the native elongated and arborized morphology of Müller cells was structurally preserved after the sorting (Figure 2a).

Tandem mass spectrometry was used to generate a complex proteomic data set with a total of ~ 6000 identified proteins. The expression pattern of known marker genes confirmed the predominant cell types in the respective sorting fractions (Figure 2b). While Müller cell markers GLUL, RDH10 (retinol dehydrogenase 10), and RLBP1 (retinaldehyde-binding protein 1) were highly enriched in the CD29⁺ fractions of all samples, the CD11b⁻ fractions showed the highest expression of the microglial marker allograft inflammatory factor 1 (AIF1 alias IBA1), while CLDN5 (claudin 5) was most strongly expressed in the endothelial-rich CD31 (alias PECAM1—platelet and endothelial cell adhesion molecule 1)-positive fractions (Figure 2b). The triple-negative flowthrough, depleted from microglia, vascular cells and Müller cells had the highest expression in neuronal markers, especially cone arrestin (ARR3) (Figure 2b), confirming that this fraction mostly consisted of photoreceptors and retinal neurons. As expected, there was a significant difference in the expression of ARR3 between control and all-cone mice, corroborating their distinct photoreceptor identity (rod- vs. cone-dominated composition) (Figure 2b).

Principal component analysis (PCA) revealed clear clustering by cell type. In addition, Müller cells and neuronal fractions showed a moderate subclustering also by genotype, while CD11b and CD31 samples from control and all-cone mice seemed to intermingle (Figure 2c).

Because we were primarily interested in Müller cells and their interactions with photoreceptors, we focused further analyses on the proteins that showed Müller cell-specific expression in both genotypes, a total of 1929 proteins. Identification of differentially expressed proteins

(DEPs) was performed using the *limma* package in R (Ritchie et al., 2015). We detected 253 DEPs with an adjusted *p*-value lower than .05, of which 209 (54 with a fold change greater 2) were higher and 44 (18 with a fold change greater 2) lower expressed in cone only mice (Figure 2d–f; Table S2). Particularly EPPK1 (epiplakin) caught our interest, because it showed one of the highest expression differences in our mouse model (log₂ fold change all-cone vs. control: 3.15, (Figure 2f)) while nothing is known about its function in the retina.

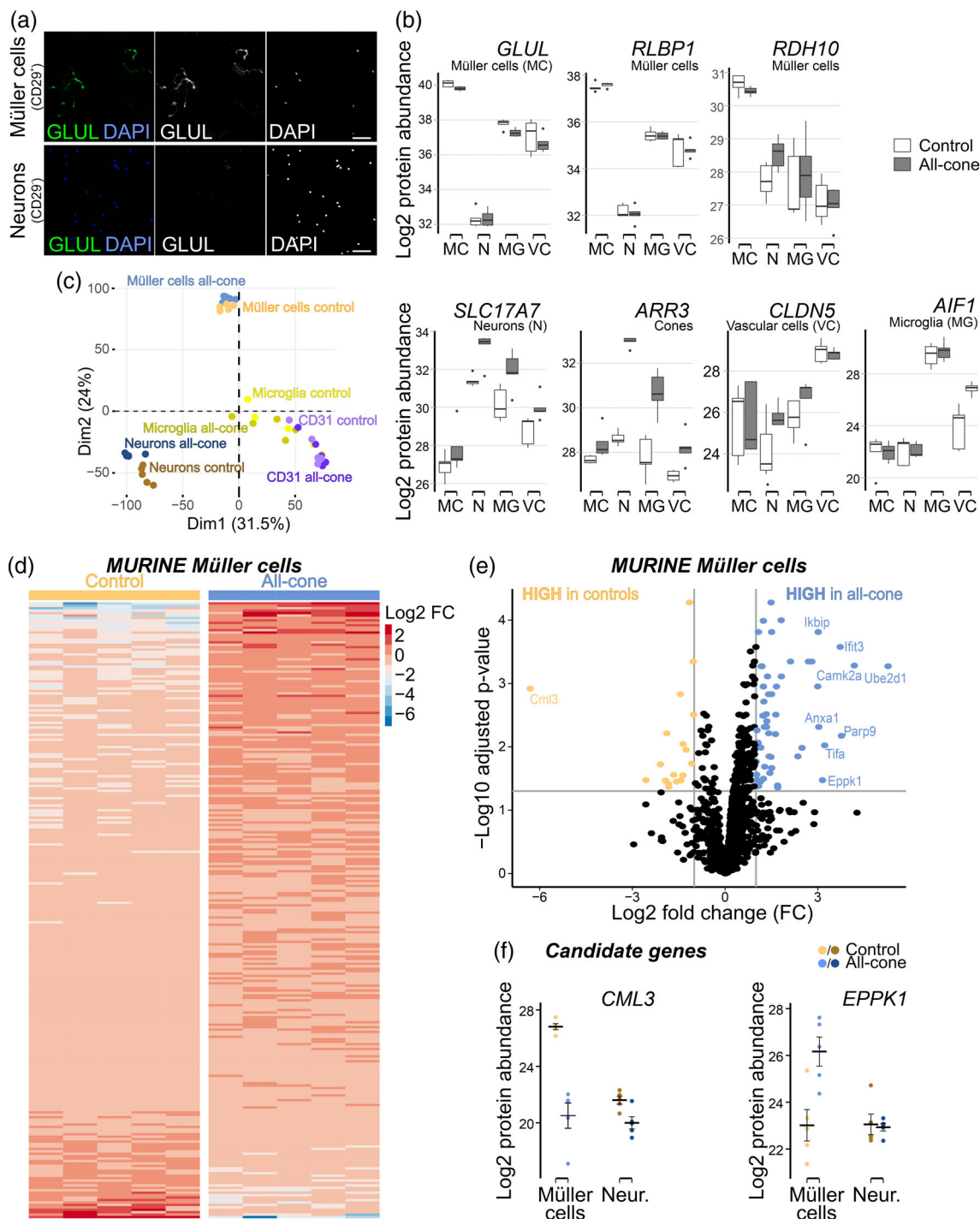


FIGURE 2 Legend on next page.

3.3 | Proteomic analysis identifies differentially expressed proteins between macular and peripheral human Müller cells

To compare differentially expressed proteins identified in the all-cone mouse model, we generated a comprehensive proteomic data set from Müller cells of the human macula (cone-rich) and periphery (rod-dominant). We collected postmortem retinal punches (6 mm in diameter) from the macula and periphery from 5 individual donor eyes (Figure S1), followed by MACS-based Müller cell isolation. As described for the mouse data set, we validated the purity of Müller cells and the photoreceptor-rich flowthrough by checking marker protein expression as determined by immunostaining and tandem mass spectrometry (Figure 3a,b). Müller cell markers *GLUL*, *RDH10*, and *RLBP1* were enriched in the CD29-positive fraction, while *ARR3*, *RHO*, and *PDE6G* had the highest expression in the flowthrough (CD11b⁻, CD31⁻, and CD29⁻) (Figure 3b). Samples were clearly separated by cell type/fraction in the PCA, with the central and peripheral Müller cell fractions clearly segregated, whereas the neuronal fractions isolated from respective retinal areas showed some overlap (Figure 3c).

Analysis via the *limma* package identified 81 proteins with higher and 136 with lower expression in macular Müller cells compared to peripheral ones (Table S3). Notably, we found that only six proteins (*S100A11*, *TTC39B*, *GLIPR2*, *BICD2*, *APOE*, *LMNA*) were consistently and significantly enriched both in human macular as well as in all-cone mice Müller cells. Two proteins (*ENO1*, *DHRS3*) showed congruent downregulation in human and mice and also vimentin, a classical Müller cell marker, showed a slightly lower expression in macular Müller cells (Figures 3e, S3A) which we were able to corroborate by immunostaining (Figure S3B). Apart from those, novel interesting human-specific candidate proteins could be identified. For example 11-beta-hydroxysteroid dehydrogenase 1 (*HSD11B1*), an enzyme involved in glucocorticoid metabolism was expressed at significantly

higher levels in the macular Müller cell subpopulation (Figure 3f). In the context of glucocorticoid signaling in diabetic retinopathy (Ghaseminejad et al., 2020), it might be interesting to follow up in future studies. *EPPK1*, even though not reaching significance in this data set as in cone-rich mouse retina, was among the proteins expressed at higher levels in macular Müller cells (Figure 3f).

The list of these 217 differentially expressed proteins (DEP) was subjected to evaluation using the STRING database in combination with the CytoScape network analysis tool to identify functional connections between candidate genes. This resulted in a network encompassing 133 proteins, while 84 proteins were disconnected. Gene set enrichment analysis of the whole network revealed the highest enrichment in pathways related to extracellular exosomes and the basement membrane for a majority of the proteins including up- and downregulated ones (Figure 3g). Other enriched pathways included proteins involved in adhesion to the extracellular matrix (ECM) like various integrins, collagens as well as focal adhesion proteins *TLN1* (Talin-1) and *TNS1* (Tensin-1), which were all upregulated in macular Müller cells. Furthermore, proteins involved in the biosynthesis and/or transport of retinoid species *RDH10*, *RLBP1*, *RBP1* (Retinol-binding protein 1) and *DHRS3* (Short-chain dehydrogenase/reductase 3) were downregulated in the macula, while another member, *RDH11*, showed the trend of an inverse expression pattern (Figure S3A). We validated the findings for *RDH10* of our proteomic screen via immunostaining of human retinal sections and showed a Müller cell-specific localization with a noticeably higher expression in peripheral regions (Figure S3B).

Recent advances in scRNAseq led to a growing number of publications studying tens of thousands of single cells from a variety of tissues including human retina. Our next question was whether the Müller cell heterogeneity suggested by our proteomic data was also reflected at the RNA level. We therefore explored publicly available resource data from Voigt et al. (2019) and Cowan et al. (2020) that profiled human retinal cells and compared them with respect to

FIGURE 2 Proteomic profiling of Müller cells isolated from rod- or cone-dominant murine retinae. (a) Sequential magnetic-activated cell sorting (MACS) based enrichment from all-cone and control (not shown) retinae yielded CD29⁺ cell fractions (top) that consisted almost exclusively of glutamine synthetase (*GLUL*)-positive cells with distinct morphology confirming their Müller cell identity. Flowthrough (CD11b⁻, CD31⁻, CD29⁻, bottom) was completely free of *GLUL* immunostaining thus consisting mostly of retinal neurons. Typically, ~300,000 Müller glia are isolated from two pooled retinae of each mouse and ~ 10 times more neurons. Scale bar, 50 μ m. (b) Label-free mass spectrometric analysis shows that Müller cell markers *GLUL*, *RLBP1* (retinaldehyde-binding protein 1) and retinol dehydrogenase 10 (*RDH10*) are highly expressed in the CD29⁺ retinal Müller cells (MC), while cone arrestin (*ARR3*) and vesicular glutamate transporter 1 (*SLC17A7*) are enriched in the triple-negative flowthrough, indicating that neurons (N) are the most abundant cell type here. *AIF1* (allograft inflammatory factor 1 alias *Iba1*) and *CLDN5* (Claudin-5) expression are highest in the CD11b⁺ and CD31⁺ fractions, respectively, thereby confirming their microglial (MG) and vascular cell (VC) composition. (c) Proteome profiling via mass spectrometry performed on the four cell fractions separated by MACS. Principal component analysis (PCA) shows a clear clustering of the samples primarily by cell type and especially for Müller cells and neurons also by genotype. (d) Heat map of 1929 Müller cell-specific, differentially expressed proteins identified by label-free tandem mass spectrometry. *Limma* identified 209 up- and 44 downregulated proteins in the all-cone mouse as compared to controls. Each vertical lane represents data from cells isolated from one individual animal ($n = 5$). (e) The volcano plot shows proteins that are significantly differentially expressed (adj. p -value < .05) between the genotypes. Blue: Upregulated >twofold in all-cone mice, yellow: Upregulated >twofold in control. proteins that show at least eight-fold upregulation are indicated by labels. (f) *CML3* (N-acetyltransferase family 8 member 3, *Nat8f3*) expression as determined by mass spectrometric profiling is around 80-fold higher in control animals than in the double mutants, while *EPPK1* is increased by more than eight-fold in cone-dominant retina error bars indicate mean plus standard error. Neur., neurons. (b–f) Label-free mass spectrometric analysis was performed on cell populations purified from retinae of 5 control and 5 all-cone mice, respectively

regional differences in the fovea and retinal periphery. We first identified genes that were enriched in Müller cells compared to neurons including cones, rods, bipolar, amacrine, and ganglion cells. The

resulting genes were then subjected to differential expression analysis by comparing Müller cells of foveal/macular origin with their peripheral counterparts resulting in 477 and 742 differentially expressed

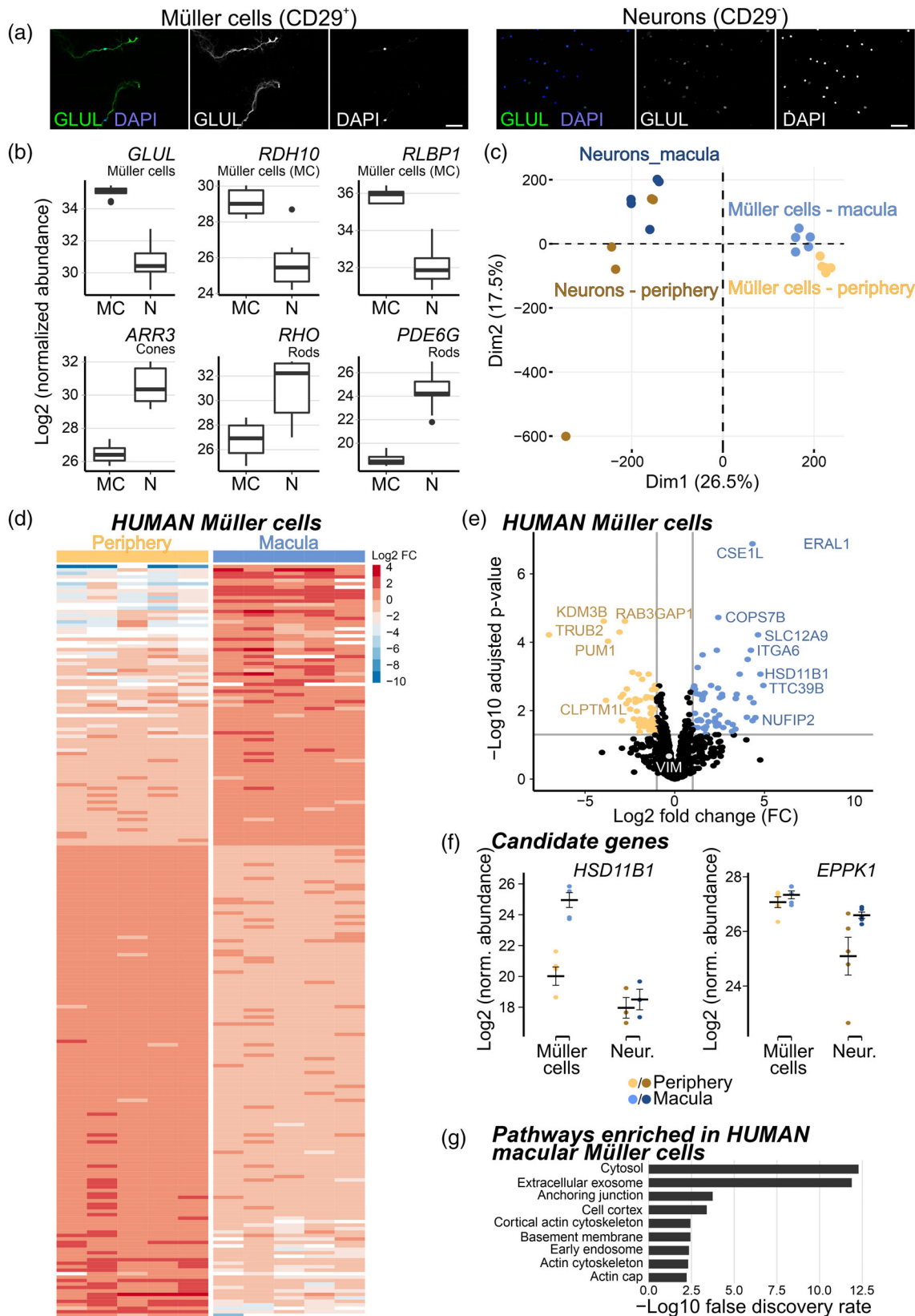


FIGURE 3 Legend on next page.

genes for the Voigt and Cowan studies, respectively. 33 and 68 of them, respectively, were also detected in our proteomic analysis, of which, importantly, the absolute majority (30 and 67, respectively) showed the same regionally distinct expression pattern (Figure 4a). Finally, a total of 29 genes with a congruent expression profile (11 up-, 18 downregulated in macula), were identified in all three data sets (Figure 4b).

Transcripts for EPPK1, our candidate with consistent expression profiles in human and mouse Müller cell proteomes, were identified only in Voigt et al. (2019). Because some transcripts were also detected in ganglion cells, they did not meet the above criteria for cross-validation of proteomes across scRNAseq data sets. However, a consistent trend toward higher EPPK1 transcript levels was observed in macular Müller cells compared with their peripheral counterparts (Figure S4).

3.4 | EPPK1 is specifically enriched in cone-associated Müller cells

Our study revealed high expression of EPPK1 protein in both mouse and human Müller cells (Figures 2 and 3). EPPK1, with a mass of around 500–700 kDa is a huge protein belonging to a family of cytoskeletal linkers like desmoplakin or plectin (Hu et al., 2018; Sonnenberg & Liem, 2007) and was shown to have domains that are capable to directly interact with intermediate filaments in hepatocytes or keratinocytes (Jang et al., 2005; Spazierer et al., 2008; Szabo et al., 2015; Wang et al., 2006). We found a similar EPPK1 expression pattern in humans and mice being specific to Müller cells and expressed stronger in glia isolated from cone-rich retina (Figure 2f, Figure 3f). While the interregional difference of EPPK1 protein expression was close to, but did not reach statistical significance in our human data set (one-tailed paired t-test p-value: 0.09), immunostaining on cryosections of human retina delineated a clear regional difference in the EPPK1 staining pattern, confirming its localization in

macular Müller cells (Figure 5a). In line with this finding, the EPPK1 staining was confined to Müller cell inner and outer stem processes in all-cone and control mice with a beads-on-a-string to fibrillar appearance (Figure 5a). The higher staining intensity for EPPK1 in Müller cells from all-cone mice is consistent with our findings from mass spectrometric analysis (Figure 5a). Moreover, Western blot analysis done on retinal extracts from control and all-cone mice provided additional proof that EPPK1 levels are higher in cone-rich retina (Figure 5b). Co-blotting of retinal samples from wild type and *Eppk1* knockout (*Eppk1*^{-/-}) mice demonstrated specificity of the antibody, as no specific signal was detected in EPPK1-deficient retina (Figure 5b).

To assess whether EPPK1 is mandatory for retinal integrity, we studied the retinal architecture in *Eppk1*^{-/-} mice. Notably, previous work showed that a knockout of *Eppk1* in mice did not lead to major phenotypic differences, even in tissues with high EPPK1 physiological expression levels, such as the skin (Goto et al., 2006; Spazierer et al., 2006), or to a disturbed keratin organization. A knockout in keratin 8, a close interaction partner of EPPK1, on the other hand, completely abolished the EPPK1 localization to the cellular periphery of wild-type hepatocytes demonstrating the dependence of a proper subcellular EPPK1 localization on keratin intermediate filaments (Szabo et al., 2015). Similarly, no obvious disturbance in retinal or Müller cell morphology was found in *Eppk1*^{-/-} mice (Figure 5c), nor did we detect a disorganization in vimentin (VIM), another intermediate filament, which is specifically expressed in Müller cells but is, in contrast to GFAP, detectable at high levels already in Müller cells of the healthy retina. Next, we analyzed the EPPK1 localization in *Gfap/Vim* double knockout mice. The long EPPK1-positive beads-on-a-string-like structures seen in the wild type (Figure 5d) were absent, but shorter structures and a slight accumulation in the Müller cell somata could be detected.

Studies in liver (Szabo et al., 2015) and pancreas (Wögenstein et al., 2014) suggest a role in the organization of the intermediate filament network in response to pathological tissue alterations. In

FIGURE 3 Proteomic profiling of rod- or cone-associated human Müller cells. (a) Punches of 6 mm in diameter were dissected from macular and peripheral regions of retinal tissue from human donors and subsequently subjected to MACS sorting as described for mouse. CD29⁺ fractions consisted almost entirely of glutamine synthetase (GLUL)-positive Müller cells that retained their intricate, elongated morphology, while cells of the flowthrough showed no staining for GLUL. Approximately 200,000 Müller glia are isolated from each 6 mm tissue punch and ~ 3–4 times more neurons. Scale bar, 50 μ m. (b) Neuronal (N)- and Müller cell (MC)-enriched cell fractions were analyzed using tandem mass spectrometry. Expression of retinal Müller glia markers GLUL, RDH10 and RLBP1 was found primarily in the CD29⁺ fractions, while cone-arrestin (ARR3), rhodopsin (RHO) and phosphodiesterase 6G (PDE6G) were enriched in the flowthrough, representative of high photoreceptor content of the neuronal cell population. (c) Protein expression profiles determined by tandem mass spectrometry were separated mainly by cell type in a PCA. Furthermore, Müller cells grouped into tight subclusters according to their region of origin, whereas the intraregional difference between neuronal fractions appeared less pronounced. (d) Heat map of differentially expressed proteins determined by limma analysis of the proteome profiles of Müller cell subpopulations. Each vertical lane represents data from one donor eye ($n = 5$). (e) A volcano plot shows proteins with at least twofold upregulation in Müller cells of the macula (63, blue) or periphery (67, yellow), respectively. Labels for proteins with a fold change higher than 8 and an adjusted p -value $< .01$ are provided. (f) Corticosteroid 11-beta-dehydrogenase isozyme 1 (HSD11B1) is specifically enriched in Müller cells in both regions with a 30-fold higher expression in Müller cells of the macula. EPPK1, while being significantly upregulated in all-cone versus control mice, shows a similar tendency in human, but does not reach significance (one-sided, paired t test: p -value = .09). Error bars indicate mean \pm standard error. Neur., neurons. (g) Pathway enrichment analysis on differentially regulated proteins from macular and peripheral human Müller cells presenting significantly enriched GO-term of cellular components. (b–f) Label-free mass spectrometric analysis was performed on cell populations purified from macular and peripheral retinal punches from five donor eyes

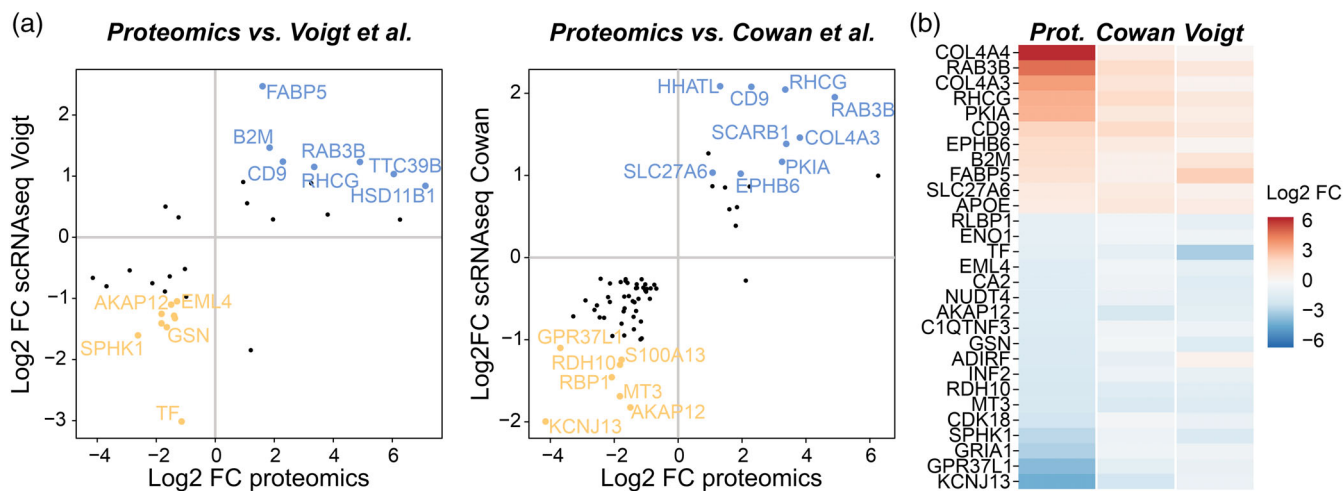


FIGURE 4 Comparison of human proteomic candidate genes identified as differentially expressed in Müller cell subpopulations with published human retinal scRNAseq datasets representing central (macula/fovea) and peripheral human retina. (a) From publicly available single-cell transcriptomic data sets generated by Voigt et al. as well as Cowan et al. (Cowan et al., 2020; Voigt et al., 2019) we identified genes that were specifically expressed in Müller cell clusters and showed significant difference between central and peripheral cells. Comparison of these differentially expressed genes with the proteomic data of the current study showed some degree of overlap with 33 genes from Voigt and 68 from Cowan being detected in both approaches. Genes/proteins that show a fold change (FC) of at least two on protein as well as on transcript level are colored, with blue indicating upregulation in macula and yellow upregulation in periphery. Most of the genes/proteins that were found to be differentially expressed in two methods also showed to be regulated in the same regional pattern. (b) Heat map showing a total of 29 genes/proteins differentially expressed in Müller cells (macula vs. peripheral region) that are shared among the three data sets

hepatocytes, keratin 8 is upregulated in parallel with EPPK1 (Szabo et al., 2015). In a similar fashion, one of the main intermediate filaments of Müller glia, GFAP, is upregulated during stress-induced gliosis such as transient retinal ischemia (Pannicke et al., 2018; Wunderlich et al., 2015). Accordingly, we examined EPPK1 localization in postischemic retinas exhibiting high GFAP expression in Müller cells, a model established by our group in another study (Mages et al., 2019). Indeed, we observed a more intense EPPK1 staining of gliotic Müller cells (Figure 5e,f) and super-resolution microscopy revealed a spot-like EPPK1 co-localization with GFAP filaments in the inner Müller glia stem processes (Figure 5e).

In sum, the concordant findings on the expression of EPPK1 in mouse and human retina make it a very interesting candidate that we have identified in our cross-species proteomic approach.

3.5 | EPPK1 knockout leads to morphological and biophysical changes of the human immortalized MIO-M1 Müller cell line

To date, the functional role of EPPK1 in glial cells or the retina in general has not been studied. Consequently, we sought to investigate EPPK1 function and its role in the central human retina. Due to the scarcity of human donor samples and the poor performance of primary Müller cells *in vitro* in regard to proliferation, morphological stability and accessibility for genetic manipulation, we chose the immortalized human MIO-M1 cell line (Limb et al., 2002) to start functional studies of EPPK1 in glia cells. Real-time quantitative PCR

(qPCR) analysis of RNA isolated from MIO-M1 cells and human donor retina revealed the presence of EPPK1 mRNA in MIO-M1 cells, albeit at significantly lower levels than in human retinal extracts (Figure 6a). Consistent with this, EPPK1 protein was also identified by tandem mass spectrometry analysis of cell lysates from MIO-M1. (Figure 6b).

Next, we designed a CRISPR/Cas9-based genetic knockout (KO) approach to delete EPPK1 for subsequent functional analysis. Peculiarly, despite its huge size of more than 20,000 bp, the genetic locus of EPPK1 contains only two exons of which only the second is translated into protein. We defined a region of 1000 bps, starting with an annotated keratin binding site at the beginning of exon 2, to be targeted by our knockout strategy employing 4 guide RNAs (Figure 6c). The latter were designed to assure deletions stretching several dozens or hundreds of base pairs and thus ensuring either the generation of a premature stop codon or the creation of a truncated non-functional protein. After selection of puromycin-resistant transfected cells, two monoclonal colonies were chosen for further expansion.

Genotyping by PCR confirmed that these two cell lines, named C9 and F7, carried a deletion in their EPPK1 gene (Figure 6d). Both showed a heterozygous genotype with one smaller (~500 bp) and one larger band (~1000 bp). The absence of a wild type band confirmed the absence of wild type cells in the monoclonal cultures. Sequencing of the two longer mutant DNA fragments revealed precise combined cuts of gRNA3 and gRNA1 that resulted in a deletion of 199 bp followed by a premature stop codon at amino acid position 143. The shorter mutant bands were the result of cuts by gRNAs 3 and 4 that resulted in an excision of 678 bp and a premature stop codon at amino acid 127. Lack of EPPK1 expression in C9 and F7 cell lines was

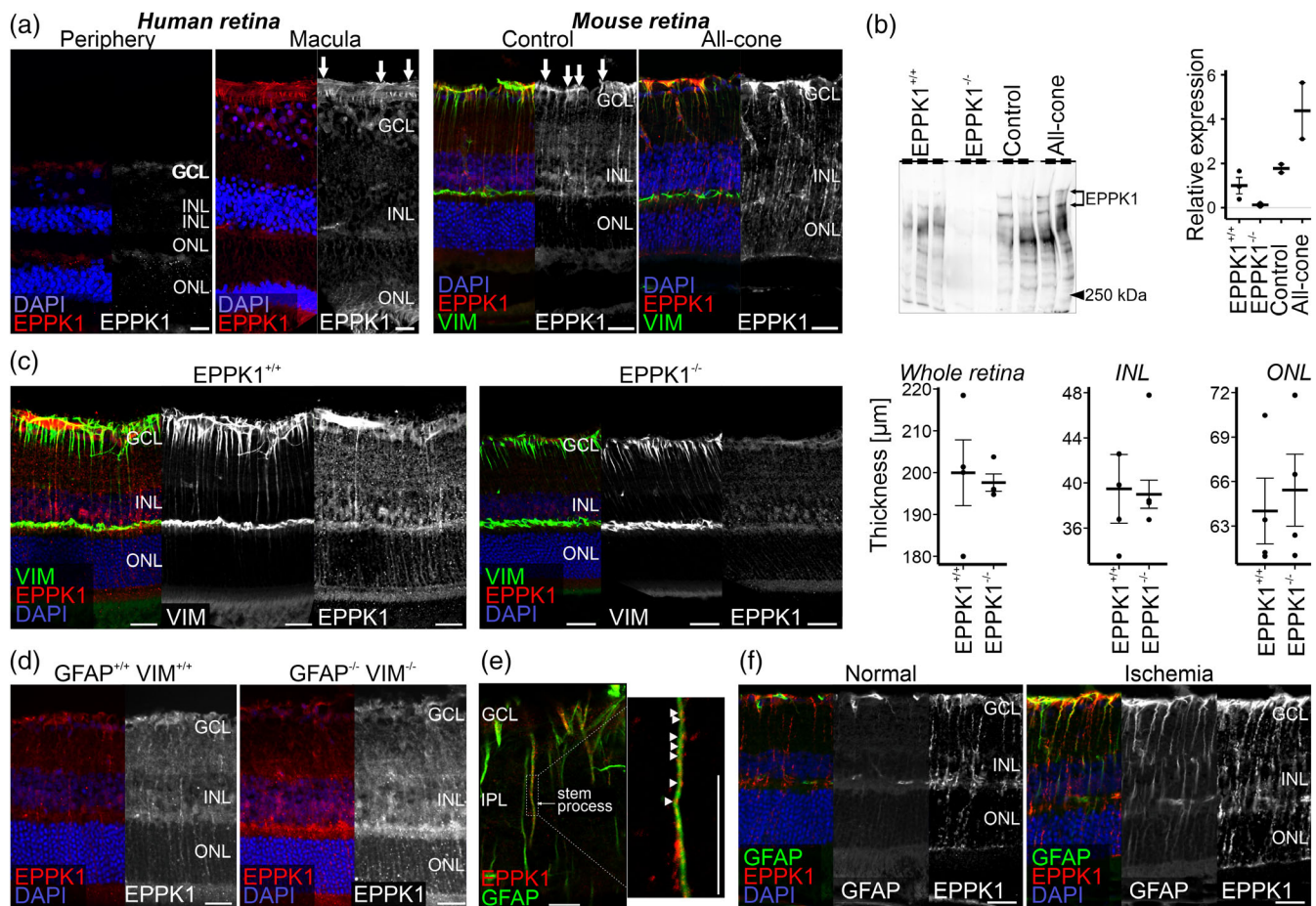


FIGURE 5 EPPK1 expression and localization in human retina and various genetic mouse models. (a) Immunostaining of EPPK1 in human retina showed signal in macular Müller cells, primarily in their endfeet (arrows), while such staining was almost completely absent in the periphery. A comparable staining pattern was observed in mouse retina, where EPPK1 also has a specific localization in Müller cells extending from their basal endfeet (arrows) to their stem processes extending into the outer retina. Co-labeling of vimentin, a classical Müller cell marker, and EPPK1 in mouse retinal sections shows that EPPK1 is mainly localized in Müller cell processes. Scale bars, 50 µm. (b) The implemented anti-EPPK1 antibody shows protein specific binding in Western blot analysis with several bands in wild type due to protein degradation as frequently observed in protein lysates derived from mouse tissues. However, no immune-reactive bands were detected in samples from Eppk1 knockout (Eppk1^{-/-}) retina. Increased EPPK1 protein expression was confirmed for all-cone versus control retina. Quantification was performed on the upper two bands (arrows) showing molecular weights expected for intact mouse EPPK1 protein variants (Ueo et al., 2021). (c) Left, representative images of retinal sections stained for EPPK1 and the intermediate filament vimentin. Genetic Eppk1 ablation has no gross effect on the organization or localization of vimentin in Müller cells. Right, quantification of the thickness of the whole central retina or the respective layers shows comparable gross retinal architecture in Eppk1^{-/-} retina compared to controls. Data is represented as mean and standard error from four individuals per group. (d) Immunostaining of EPPK1 in retinas lacking both main glial intermediate filaments GFAP and vimentin indicate a shift from a filamentous to a more disorganized EPPK1 localization associated with a displacement into the somata of Müller cells. Scale bars, 20 µm. (e) EPPK1 seemed to be upregulated in a retinal pathology model (transient ischemia) and can be seen to co-localize spot-like (arrowheads) with GFAP-positive Müller cell stem processes visualized by STED microscopy. Scale bar, 10 µm (f) high intraocular pressure led to reactive gliosis of Müller cells and thus to an upregulation of GFAP (right), while it is usually not detectable in healthy cells (left). GCL, ganglion cell layer; INL, inner nuclear layer; ONL, outer nuclear layer

confirmed by qPCR at transcript (Figure 6e) and by Western blot at protein level (Figure 6f).

We then used proteomic profiling to assess possible molecular perturbations of EPPK1 knockout Müller cells and/or their secretome. We harvested the cell lysates and conditioned medium from mutant and wild type cells and performed tandem mass spectrometric analysis. Checking for the cell lysates first, we found a downregulation of cell adhesion and extracellular matrix proteins like collagens, aggrecan

core protein, and fibronectin (Table S4), analogous to human peripheral Müller cells. Similarly, pathway enrichment analysis revealed a dysregulation of vesicle-related pathways (Figure 6g). Regarding the secretome, we observed a downregulation of extracellular matrix proteins like collagens, fibronectin, chondroitin sulfate proteins and other adhesion molecules (Table S5). Accordingly, pathway enrichment analysis clearly points toward a reduced secretion of components of the extracellular matrix via extracellular vesicles (Figure 6g).

Next, we characterized potential effects of the *EPPK1* knockout on cell morphology by staining the actin cytoskeleton using phalloidin (Figure 7a). We noticed a reduction in cell size as well as an increased

number of fine filopodia (Figure 7a,b). The outlines of the cells were segmented using CellProfiler software and various parameters such as cell area, solidity, elongation, form factor, and others were quantified.

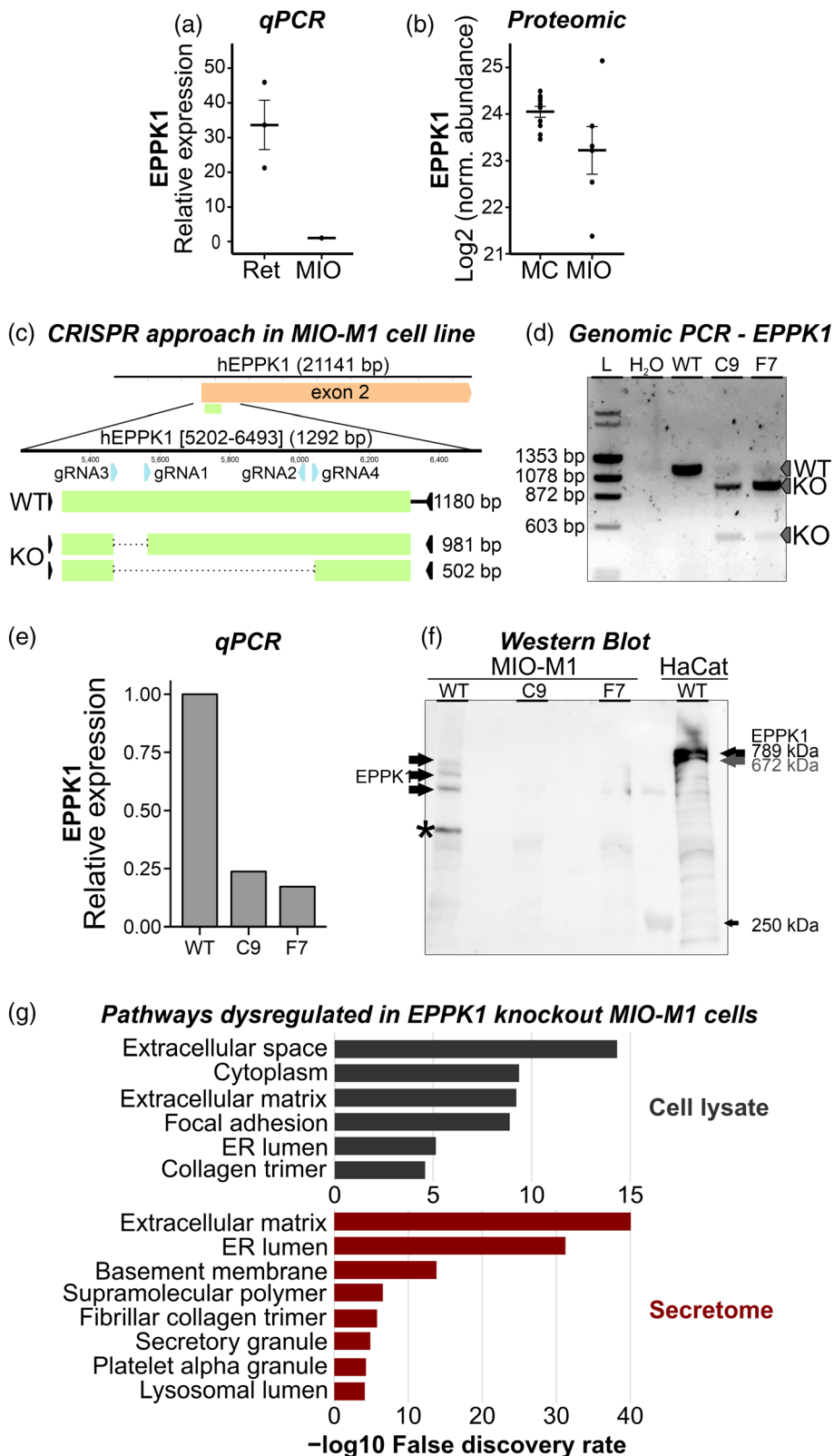


FIGURE 6 Legend on next page.

Most notably, we identified a significant and consistent decrease of the overall cell area in both knockout lines of around 35% (Figure 7b). Another prominent parameter was solidity, which is the ratio between the area of the cell and its convex hull which is spread out by its protrusions. It can thus be used as an indirect measure of the cell's morphology, e.g., their complexity, with values closer to 1 indicating roundish, regularly shaped cells and values closer to 0 indicating cells with many complex processes (Janssen et al., 2022; Lobo et al., 2016). Although we observed some variation in the shape of the cells of all genotypes, C9 and F7 exhibited a more regular morphology with fewer large projections. This was reflected in their significantly higher solidity (Figure 7b).

Additionally, through an image-processing pipeline that included segmentation, erosion, masking, and skeletonization, we were able to robustly segment filopodia of individual cells (Figure 7a). This allowed us to count the number of filopodia per cell and calculate their average length. *EPPK1* knockout resulted in an increase in the number of filopodia with a simultaneous decrease in filopodia length (Figure 7c).

As cell morphology and filopodial dynamics are mainly regulated through the cytoskeleton, which also generates forces critical for cell function and retinal tissue integrity (MacDonald et al., 2015), we investigated the dependence of force generation by Müller cells on *EPPK1* using traction force microscopy. For this, we grew cells on polyacrylamide substrates with a shear modulus of $G' = 1000$ Pa (~ 3000 Pa Young's modulus), which is in the range of reported moduli for retina (Ferrara et al., 2021), but which is much softer than tissue culture plastics ($G' \sim$ GPa) (Akhmanova et al., 2015) and found cells of various morphologies in both mutant cell lines and controls. While about half of the cells (49%–59%) displayed a spherical morphology and a smaller part (6%–27%) showed more arborized structure, we focused on bipolar cells (24%–34%) as shown in Figure 7d for our measurements. We analyzed the displacement of the embedded fluorescent beads after removal of the cells and subsequent relaxation of the gels to calculate the forces required for the initial deformation. The highest contractile forces were generated at the cell poles. *EPPK1*-deficient cells exerted significantly lower forces on their substrate than control cells, with a reduction of about 30% to 40% (Figure 7d).

Given the morphological and biomechanical changes in the absence of *EPPK1* in MIO-M1 cells and the implication of exocytotic pathways (Figure 6g), we wanted to investigate whether knockout of *EPPK1* affects extracellular vesicle transport. There is evidence that intracellular exosome trafficking requires interaction with intermediate filaments in glial cells (Margiotta & Bucci, 2016; Potokar et al., 2007). Interestingly, tetraspanin CD9, a common vesicle-associated protein (Escola et al., 1998; Théry et al., 1999; Théry et al., 2018), was specifically expressed by Müller cells and enriched in the Müller cell subpopulation of the macular region (Figure S3)—a pattern that was also consistent in two scRNAseq data sets (Figure 4b). Immunostaining of MIO-M1 knockout cells for CD9 revealed that *EPPK1* knockout cells exhibited significantly lower staining intensity (Figure 7e). Proteomic analysis of knockout and wild type MIO-M1 cells corroborated these findings, showing that as in human peripheral Müller cells, indeed CD9 protein abundance is lower in *EPPK1*-ablated cells (Figure 7f).

Finally, we wondered whether the difference in intracellular CD9 expression depends primarily on a decreased protein synthesis or on a general shift in exocytosis. While we saw no difference in CD9 protein amounts in the secretome of *EPPK1* knockout and WT (Table S5), nanoparticle tracking analysis of conditioned medium showed a decrease in the secretion of small extracellular vesicles (<200 nm) from both knockout cell lines, with C9 cells releasing about three times less particles into the medium than the control (Figure 7g).

4 | DISCUSSION

The human macula is a peculiar structure essential for sharp vision, but unfortunately, also very susceptible to diseases like age-related macular degeneration (AMD), diabetic macular edema or macular telangiectasia type 2 (MacTel2). To date, many studies have focused on the role of different retinal cell types like microglia (Altmann & Schmidt, 2018) or the vasculature (Yeo et al., 2019) in the macula in pathological as well as in healthy conditions. Although morphological and functional differences between macular and peripheral Müller glia were addressed in few studies (Syrbe et al., 2018; Wang &

FIGURE 6 Generation and validation of *EPPK1*-deficient MIO-M1 Müller cell lines. Comparison of *EPPK1* expression between human donor retina and the immortalized human Müller cell derived cell line MIO-M1, shows that transcript (a) as well as protein (b) is detectable in the latter, albeit at a lower level than in native tissue. Error bars indicate mean \pm standard error. (c) The human *EPPK1* locus (top) consists of one small, untranslated and one huge, $\sim 16,000$ bp long exon that encodes for the whole translated region. For CRISPR/Cas9 mediated knockout (KO), we designed guide RNAs to target a 1000 bp long region at the beginning of a predicted keratin binding site. To ensure complete knockout of the gene, we transfected the cells with a combination of four guide RNAs and generated two monoclonal cell lines, C9 and F7. (d) PCR amplification of the target region resulted in one band with the expected size of 1180 bp for wild type cells, while the mutant lines showed two bands each. Sequencing of the mutant PCR fragments revealed cuts by gRNA3, gRNA1, and gRNA3, gRNA4 leading to a deletion of 199 bp and 678 bp, respectively (c, bottom). Quantitative PCR (e), mean of two technical replicates) and Western blot analysis (f) confirmed successful knockout of *EPPK1* in the mutant cell lines. Wild type MIO-M1 cells showed three high molecular bands, maybe due to the triploidy of chromosome 8 (Limb et al., 2002), on which *EPPK1* is encoded. a fourth band, visible in the wild type (asterisk), might be a degradation artifact. The HaCat wild-type cell line (keratinocyte origin) was used as a positive control showing two immune-reactive bands at the expected molecular weight (789 and 672 k Da, respectively). The respective *EPPK1* knockout lines (C9, F7) lacked any immune-reactive bands. Size differences of *EPPK1* may occur between samples originating from non-isogenic individuals (Ishikawa et al., 2018). (g) the plot shows GO terms (cellular components) for proteins found at different levels in cell lysate or the secretome of control and *EPPK1*-deficient MIO-M1 lines. ER, endoplasmatic reticulum

Kefalov, 2009; Zhang et al., 2019), there is no deeper understanding of molecular protein pathways involved in regional Müller cell heterogeneity. In this study, we used multiple models in a multiomic approach to start closing this knowledge gap and to identify specific proteins that shape functional differences between central and peripheral Müller cells. Using the all-cone mice, we first studied differences between Müller glia in a cone-rich retina, compared to rod-rich

normal controls in order to characterize this aspect of regional differences in photoreceptor subtype distribution in the human macular and peripheral retina, respectively. It has been shown that all-cone mice are capable of functional vision and have normal retinal layering (Samardzija et al., 2014). Nevertheless, we performed additional in-depth characterization of the cellular composition as well as morphometric quantification of all retinal layers, in order to exclude possible

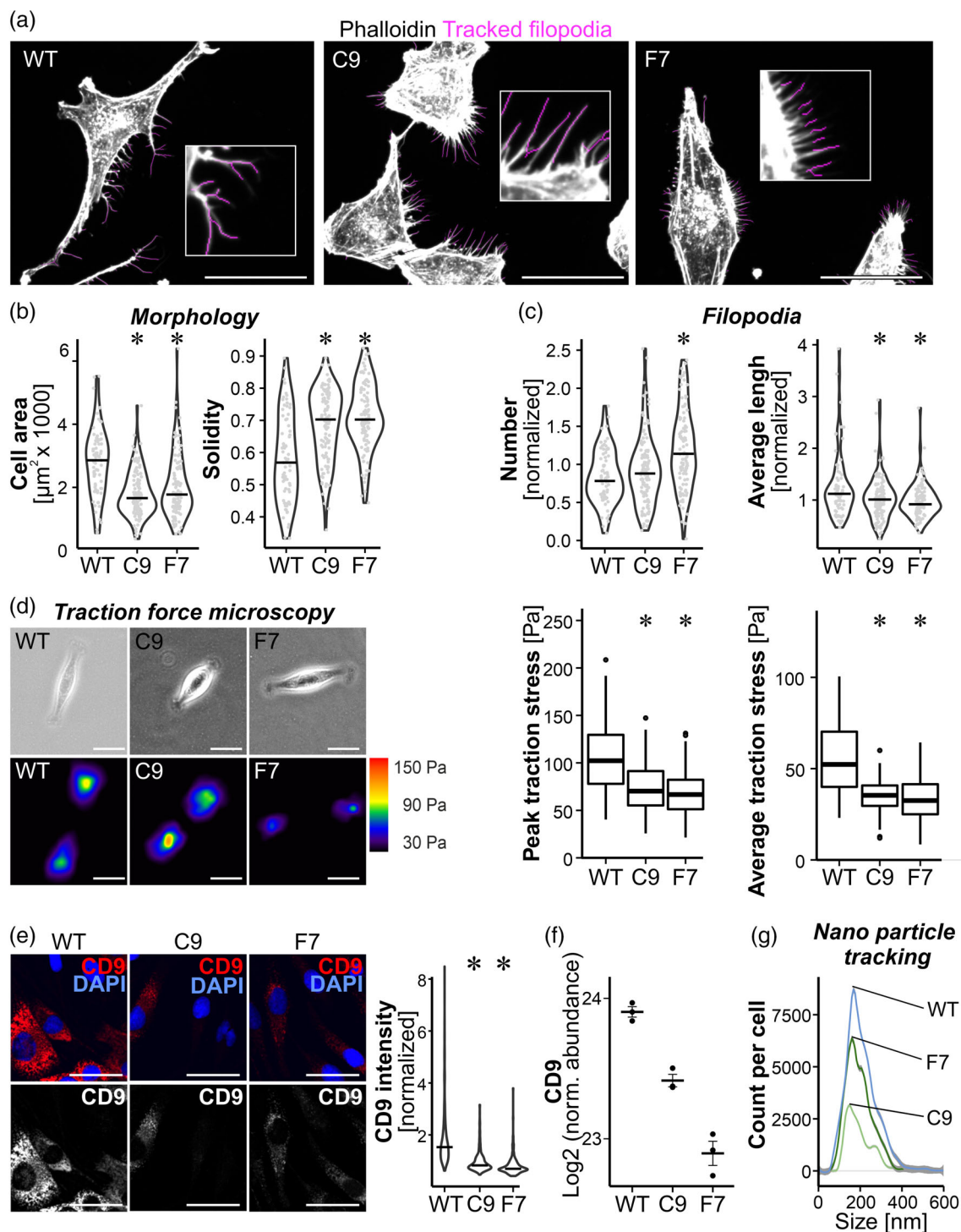


FIGURE 7 Legend on next page.

confounding factors from cone-independent retinal changes, like inner neuron composition. Complementary to the morphological analysis performed by Samardzija et al. (2014), we found minor alterations of the outer nuclear layer, with a lower number of nuclei in the all-cone retina. It is unclear whether this discrepancy develops during embryonal stages, maybe due to inefficient cone differentiation, or whether it is a sign of photoreceptor degeneration after birth as a result of the double mutation (Samardzija et al., 2014).

The increased thickness of the outer plexiform layer might be explained by cone pedicles, the synaptic structures relaying signals to the neurons of the inner nuclear layer, being bigger than the corresponding rod spherules (Hoon et al., 2014; Kolb, 1995; Wässle et al., 2002). Although the exact wiring and signal transduction remain elusive and require further studies on this model, we did not find any obvious changes of the inner retinal layers in terms of thickness and gross cellular composition.

Although the all-cone mouse retina may yield some insights regarding Müller cell-cone interaction, it does not reproduce key characteristics of the human macula like the pit-like morphology and avascular zone of the fovea, as well as a gradient of cone diversity and distribution. Still, we assessed whether at least some aspects of human cone-associated Müller cell heterogeneity could be modeled. Therefore, we examined the proteome of Müller cells from the macula and periphery of human donor retinas for comparison. Indeed, in our proteomic approach, we found only eight proteins to be significantly differentially expressed in both datasets. This suggests that although there does not seem to be a broad congruence between all-cone and macular Müller cells, there seems to be some core proteins important for Müller cell cone interaction like APOE (Apolipoprotein E), LMNA (Prelamin-A/C), ENO1 (Alpha-enolase) or DHRS3.

Comparing our proteome data with two published single cell RNAseq datasets, we found several differentially expressed genes consistently detected in both transcriptomic and proteomic profiles. Although there is increasing evidence that protein levels can be uncoupled from the synthesis of their transcript by a variety of mechanisms (Liu et al., 2016; Noya et al., 2019; Sharma et al., 2015;

Vogel & Marcotte, 2012), we found that genes that overlap in the datasets analyzed here were mostly regulated in the same manner—29 genes showed a consistent regulatory pattern across all three data sets. These included *CD9*, a member of the tetraspanin family involved in the biogenesis of extracellular vesicles, as well as *RDH10* and *RLBP1*. Unexpectedly, *RDH10*, *RLBP1*, *RBP1* and *DHRS3*, all bona fide proteins of the visual cycle, were higher expressed in peripheral Müller cells. This seems counterintuitive, as studies report that cones, which are present in exceptionally high number in the macular retina, specifically rely on the function of these Müller cell-specific genes/proteins for the regeneration of their photopigment (Kaylor et al., 2013; Wang & Kefalov, 2009; Xue et al., 2015). However, because there are no rods with long outer segments in the fovea to keep the RPE at a distance from the cones and also because the outer segments of the cones are exceptionally longer in the fovea (Domdei et al., 2021; Tschulakow et al., 2018; Yuodelis & Hendrickson, 1986) than in the peripheral retina, the RPE can potentially take care of the cones better in the fovea than in the periphery. Notably, *DHRS3*, an enzyme that opposes *RDH10* in the synthesis of retinaldehyde (Adams et al., 2014; Belyaeva et al., 2019), was one of eight proteins consistently lower in cone-rich samples of both, human and mouse Müller cells. An ablation of *Dhrs3* during development was shown to lead to an accumulation of all-trans retinoic acid (ATRA) with a concurrent reduction of the retinol pool resulting in embryonic lethality (Billings et al., 2013). The same study found a downregulation of *Rdh10* in response to *Dhrs3* knockout, leading the authors to hypothesize this to be a measure to counter increased ATRA levels. Since ATRA is a known transcriptional regulator involved in a multitude of gene regulatory networks (Balmer & Blomhoff, 2002; da Silva & Cepko, 2017; Kam et al., 2012; Thompson et al., 2019), it is crucial to tightly control its synthesis, which might be a major function of *RDH10* and *DHRS3* in Müller cells. In agreement with this, several knockout experiments in cones, Müller cells, and the whole retina have shown, that *RDH10* is not required for proper cone function (Xue et al., 2017), leading to the assumption that other retinol dehydrogenase family proteins must be involved in the Müller cell-dependent

FIGURE 7 Morphological, molecular, and functional signature of the human Müller cell line MIO-M1 deficient for EPPK1. (a) MIO-M1 cells cultured on glass coverslips and stained with phalloidin to visualize actin filaments and thereby the general morphology including fine filopodia (insets). Using the CellProfiler image analysis software, we were able to quantify several cell morphological characteristics including filopodia length (highlighted in purple) and number. (b) Measurements of cell area as well as solidity, which can be seen as a proxy for cell branching with higher values meaning less cell processes, showed a significant decrease in cell size and complexity of both EPPK1 knockout (KO) lines C9 and F7. (c) EPPK1 knockout cells had significantly shorter, but more filopodia. The bar inside violin plots represents the median. (d) Wild type and knockout MIO-M1 cells were cultured on polyacrylamide gels with a shear modulus of 1000 Pa and embedded fluorescent beads. Comparing the positions of the beads between cell-associated and relaxed state (cells were removed), allowed the calculation of traction stress exerted by the cells. Polar cells of all lineages, wild type or EPPK1 knockout (top), imposed primarily traction forces on the gel at their poles, which pulled in the direction of their soma (bottom). Compared to wild types, EPPK1 knockout cells exerted weaker peak as well as average stress onto their gel substrate. n: Peak traction stress: C9 = 31, F7 = 38, WT = 33; average traction stress: C9 = 29, F7 = 38, WT = 33. (e) Left, staining of *CD9* localized primarily around nuclei and showed a decreased signal in EPPK1 knockout cell lines C9 and F7. Right, intensity measurements of *CD9* staining per nucleus confirms a significantly lower expression in mutant cells. The bar inside violin plots represents the median. (f) *CD9* protein expression is significantly reduced in both EPPK1 knockout MIO-M1 lines as determined by mass spectrometric protein quantification. Error bars indicate mean \pm standard error. (g) Nano particle tracking analysis (NTA) of medium supernatant collected from wild type as well as knockout cells (mean of two technical replicates) suggests a decrease in the secretion of extracellular vesicles by the C9 and F7 lines. (a, d, e) scale bars, 50 μ m. (b, c, d, e) $p < .05$; compared with WT control

cone visual cycle. In this context, RDH11 would be an interesting candidate, since it has similar enzymatic activity (Belyaeva et al., 2019) and tends to be higher expressed in foveal Müller cells (Figure S3). Which isomerization and/or oxidation steps of the cone visual cycle actually occur in Müller cells and which proteins catalyze these reactions have not yet been completely elucidated, but the data provided in this study can serve as a starting point.

As pointed out before, hundreds of Müller cell-specific proteins were found to be differentially regulated. EPPK1 showed one of the highest expression differences in the all-cone mouse model. Immunofluorescence staining for EPPK1 confirmed its Müller cell-specific expression pattern as well as a beads-on-a-string-like co-localization with the glial intermediate filaments vimentin and GFAP. Previously, EPPK1 was shown to not only co-localize with a variety of keratins and vimentin, but also to be able to physically bind to them in *in vitro* studies (Jang et al., 2005; Spazierer et al., 2008; Szabo et al., 2015; Wang et al., 2006). The effect of EPPK1 deficiency in mice seems to be dependent on cell type and tissue health, with no obvious phenotype in normal epidermal and hepatic cells, whereas it leads to a disruption of intermediate filaments in HeLa cells and to impaired disease-induced keratin network reorganization in disease models of liver and pancreas (Jang et al., 2005; Spazierer et al., 2006; Szabo et al., 2015; Wögenstein et al., 2014). Likewise, we did neither find morphological defects in the retina of healthy *Eppk1* knockout mice nor in the vimentin network of their Müller cells. Since the ablation in this mouse line is of constitutive nature, it could be that EPPK1 deficiency is compensated either by other members of the plakin family or proteins similarly involved in the formation of cytoskeletal morphology and/or adhesion as has been suggested for envoplakin, periplakin, and keratins (Inaba et al., 2020; Tonoike et al., 2011). In *Gfap/Vim* double knockout retinae, we found a disruption of the filamentous structure of the EPPK1 staining pattern with a concurrent increased localization in Müller cell somata, suggesting that EPPK1 is not required for intermediate filament organization in wild-type retinae, whereas GFAP and/or vimentin appear to be required for proper EPPK1 localization. This finding is in line with an observation in keratin 8 knockout cells, where EPPK1 was completely delocalized, while there seemed to be no effect of *Eppk1* knockout on keratin 8 (Szabo et al., 2015). But what might this mean for primarily cone-associated Müller cells in the retina where EPPK1 showed an increased expression?

Although EPPK1 transcripts seem to be rare and are detected only at very low levels in Müller cells and to some extent also in ganglion cells in the scRNAseq datasets of human donor retinas (Voigt et al., 2019), we confirmed by immunostaining that the protein is specifically expressed in human Müller cells, whereas a low level of expression in ganglion cell axons cannot be completely excluded. Additionally, qPCR, mass spectrometry, and Western blot analysis showed EPPK1 expression in the human Müller glia derived cell line MIO-M1. *In vivo*, Müller cells are thought to confer mechanical stability to the retina (MacDonald et al., 2015). However, in the parafoveal region Müller cells in particular must meet special biomechanical requirements to maintain the structural integrity of the tissue because of at least two factors: (i) their elongated and z-shaped morphology resulting in large Müller cells and (ii) the potentially increased

mechanical strain, for example, employed by the vitreous body that is especially tightly attached to the macular retina (Syrbe et al., 2018). Moreover, it has even been speculated that Müller cells help maintain or even form the foveal pit (Bringmann et al., 2018, 2020). Here, we found evidence that EPPK1 might be involved in these functions, as its knockout in MIO-M1 cells led to (i) smaller cells with fewer protrusions and (ii) weaker traction forces. This, in turn, indicates that increased EPPK1 expression in macular Müller cells may contribute to the formation of their larger, more complex morphology as well as to the ability to exert the increased mechanical forces required to shape the fovea. In line with the discussed theory, we also found an increase in extracellular matrix proteins and adhesion molecules in macular Müller cells consistent with published scRNAseq datasets. Thus, it appears that Müller cells in the macula have not only enhanced expression of proteins like EPPK1 that seem to be key for the exertion of higher traction forces and cell-ECM interaction, but also ECM components themselves. Several collagens (COL4A1, COL4A3, COL4A4) and other ECM associated proteins (ITGA6 [Integrin alpha-6], LMNA) together with lipid binding proteins such as APOE and FABP5 (Fatty acid-binding protein 5) are highest expressed in macular Müller cells, suggesting a remodeling of the microenvironment in regard to intercellular transport of metabolites (Liu et al., 2017; Napoli, 2012), ECM composition and stiffness (Bachmann et al., 2019; Bourgot et al., 2020). Importantly, EPPK1 seems to be deeply embedded into this functional network as demonstrated by the perturbances of cell morphology and function of its knockout in the human Müller cell-derived cell line.

The massive downregulation of CD9 after *EPPK1* knockout might reveal another, perhaps indirect, function of EPPK1. CD9 is one of the proteins with the most consistent expression profiles at both the transcript and protein levels in human retina, with significantly higher expression (like EPPK1) in cone-associated Müller cells. Previously, intermediate filaments were associated with vesicular transport (Margiotta & Bucci, 2016; Potokar et al., 2007, 2020) and EPPK1 was shown to bind directly to several intermediate filaments, including vimentin (Jang et al., 2005; Wang et al., 2006). Therefore, EPPK1 might affect vesicle transport either directly, by promoting the binding of intermediate filaments and vesicles, or indirectly, by modifying the rigidity/density of the cytoskeletal meshwork. In contrast to the cell lysate, we did not find a difference in CD9 abundance in the secretome of EPPK1-ablated cells, but an overall decrease in the number of released small extracellular vesicles (EVs). We thus hypothesize that most vesicles shed from the Müller cell line carry CD9 making it an interesting candidate to follow up on mechanisms of Müller cell secretion, while CD9-dependent EV biogenesis seems EPPK1-independent. In contrast, intracellular trafficking of structures relevant for EV shedding were disrupted, as we observed less EVs in the supernatant. Together with the finding that proteins of the ECM (collagens, fibronectin, and chondroitin sulfate proteins) were highly abundant in the secretome of wild type cells, but significantly downregulated in both EPPK1-deficient MIO-M1 lines, this could imply that EPPK1 does not only confer mechanical stability to those huge z-shaped macular Müller cells, but also coordinates transport and release of proteins

across long distances in those Müller cells. The pronounced deposition of ECM components by Müller cells could be the central basis for the intense interaction with associated tissues or cells including the vitreous body especially in the macula. In line with this, there have even been reports of CD9 promoting cell–cell adhesion through direct interaction with other cell surface proteins like integrins (Reyes et al., 2018) or ICAM1 (Intercellular adhesion molecule 1) (Franz et al., 2016) in a vesicle-independent manner—an additional research strand that should be further pursued in future studies to understand the very specific biomechanical microenvironment of the human macula achieved by the cells located there.

Several studies suggested genes involved in serine biosynthesis like *PHGDH* (D-3-phosphoglycerate dehydrogenase) as well as glycolytic pathways to be risk factors for MacTel2 (Gantner et al., 2019; Scerri et al., 2017). Subsequently, Zhang et al. were able to show that the same proteins were indeed differentially expressed between Müller cells of foveal and peripheral origin already in a healthy state (Zhang et al., 2019). Looking at our data, we did not see any changes in *PHGDH* between macular and peripheral Müller cells. This discrepancy might stem from the different source material, being acutely and specifically isolated Müller cells in our case, and Müller cells growing out of retinal pieces after weeks in culture for Zhang et al. (2019), where massive metabolic changes can occur. Interestingly, another finding was the notably different morphology of cultured central and peripheral Müller cells and a subsequent differential expression of pathways related to extracellular matrix organization in line with our observations. In contrast to our findings, Zhang and colleagues noticed smaller cells with less complexity concomitant with an upregulation in ECM pathways in Müller cells of macular origin. The source of this discrepancy is unclear, but it is worthwhile following up for example in the context of macular holes emerging during MacTel2 disease (Heeren et al., 2020), which might not be explained with a difference in serine biosynthesis.

5 | CONCLUSION

Previous studies showed that the central human retina not only presents a microenvironment with specific characteristics that produces challenges to the inhabitant cells different to the periphery, but that it is also highly susceptible to debilitating diseases. Here, we focused on Müller cells and were able to uncover differentially regulated pathways mainly, but not exclusively, linked to secretory and cell adhesion systems. Furthermore, we identified EPPK1 and CD9 to be enriched in macular Müller cells, implicating a role in the cells' biophysical properties as well as intracellular vesicle trafficking and their release. Nevertheless, future studies need to clarify the exact mode of interaction between EPPK1 and CD9 and their potential role in macular pathological processes.

AUTHOR CONTRIBUTIONS

Conceptualization: Lew Kaplan, Peter Fuchs, Berta Puig, Kristian Franze, Stefanie M. Hauck, Antje Grosche. **Methodology:** Lew Kaplan,

Corinne Drexler, Anna M. Pfaller, Santra Brenna, Kirsten A. Wunderlich, Andrea Dimitracopoulos, Maria-Theresa Perez, Ursula Schlötzer-Schrehardt, Volker Enzmann, Kristian Franze, Stefanie M. Hauck, Antje Grosche. **Investigation:** Lew Kaplan, Corinne Drexler, Anna M. Pfaller, Stefanie M. Hauck, Antje Grosche. **Visualization:** Lew Kaplan, Antje Grosche. **Supervision:** Peter Fuchs, Berta Puig, Kristian Franze, Stefanie M. Hauck, Antje Grosche. **Writing—original draft:** Lew Kaplan, Antje Grosche. **Writing—review & editing:** Lew Kaplan, Volker Enzmann, Marijana Samardzija, Peter Fuchs, Berta Puig, Kristian Franze, Stefanie M. Hauck, Antje Grosche.

ACKNOWLEDGMENTS

We thank Magdalena Götz for her support and inspiring discussions. We also thank Gabriele Jäger and Fabian Gruhn for excellent technical assistance and the Core Facilities Metabolomics and Proteomics Core (CF-MPC) and Laboratory Animal Services (CF-LAS) at Helmholtz Center Munich for providing services, expertise, and data recording and analyses. Open Access funding enabled and organized by Projekt DEAL.

FUNDING INFORMATION

German Research Foundation grant GR 4403/1-1; GR 4403/5-1; GR 4403/7-1 (Antje Grosche) and HA 6014/5-1 (Stefanie M. Hauck). Pro Retina-Stiftung Germany grants Pro-Re/Seed/Grosche.1-2014 (Antje Grosche) and Pro-Re/Seed/Kaplan-Grosche.1-2019 (Lew Kaplan, Antje Grosche). Austrian Science Fund (FWF) grant P30310 (Corinne Drexler, Peter Fuchs).

CONFLICT OF INTEREST

The authors declare that they have no competing interests.

DATA AVAILABILITY STATEMENT

All data relevant to this work are included in the manuscript and supplemental data. The raw data of the proteomic analysis (e.g., for cell types from all-cone mice, human retina, MIO-M1 cell lysate, and secretome) will be provided by the authors upon request.

ORCID

Lew Kaplan  <https://orcid.org/0000-0003-4336-2768>

Santra Brenna  <https://orcid.org/0000-0001-8233-2110>

Volker Enzmann  <https://orcid.org/0000-0003-4384-4855>

Antje Grosche  <https://orcid.org/0000-0003-0338-7530>

REFERENCES

- Adams, M. K., Belyaeva, O. V., Wu, L., & Kedishvili, N. Y. (2014). The retinaldehyde reductase activity of *dhrs3* is reciprocally activated by retinol dehydrogenase 10 to control retinoid homeostasis. *The Journal of Biological Chemistry*, 289, 14868–14880.
- Akhmanova, M., Osidak, E., Domogatsky, S., Rodin, S., & Domogatskaya, A. (2015). Physical, spatial, and molecular aspects of extracellular matrix of *In vivo* niches and artificial scaffolds relevant to stem cells research. *Stem Cells International*, 2015, 1–35.
- Altmann, C., & Schmidt, M. (2018). The role of microglia in diabetic retinopathy: Inflammation, microvasculature defects and neurodegeneration. *International Journal of Molecular Sciences*, 19, 110.

- Bachmann, M., Kukkurainen, S., Hytönen, V. P., & Wehrle-Haller, B. (2019). Cell adhesion by Integrins. *Physiological Reviews*, 99, 1655–1699.
- Balmer, J. E., & Blomhoff, R. (2002). Gene expression regulation by retinoic acid. *Journal of Lipid Research*, 43, 1773–1808.
- Belyaeva, O. V., Adams, M. K., Popov, K. M., & Kedishvili, N. Y. (2019). Generation of retinaldehyde for retinoic acid biosynthesis. *Biomolecules*, 10, 5.
- Benchling. (2021). Cloud-based informatics platform for life sciences R&D | Benchling.
- Bhutto, I., & Luty, G. (2012). Understanding age-related macular degeneration (AMD): Relationships between the photoreceptor/retinal pigment epithelium/Bruch's membrane/choriocapillaris complex. *Molecular Aspects of Medicine*, 33, 295–317.
- Billings, S. E., Pierzchalski, K., Tjaden, N. E. B., Pang, X.-Y., Trainor, P. A., Kane, M. A., & Moise, A. R. (2013). The retinaldehyde reductase DHRS3 is essential for preventing the formation of excess retinoic acid during embryonic development. *The FASEB Journal*, 27, 4877–4889.
- Bollmann, L., Koser, D. E., Shahapure, R., Gautier, H. O. B., Holzapfel, G. A., Scarcelli, G., Gather, M. C., Ulbricht, E., & Franze, K. (2015). Microglia mechanics: Immune activation alters traction forces and durotaxis. *Frontiers in Cellular Neuroscience*, 9, 363.
- Bourgot, I., Primac, I., Louis, T., Noël, A., & Maquoi, E. (2020). Reciprocal interplay between Fibrillar collagens and collagen-binding Integrins: Implications in cancer progression and metastasis. *Frontiers in Oncology*, 10, 1488.
- Bringmann, A., Syrbe, S., Görner, K., Kacza, J., Francke, M., Wiedemann, P., & Reichenbach, A. (2018). The primate fovea: Structure, function and development. *Progress in Retinal and Eye Research*, 66, 49–84.
- Bringmann, A., Unterlauff, J. D., Wiedemann, R., Barth, T., Rehak, M., & Wiedemann, P. (2020). Two different populations of Müller cells stabilize the structure of the fovea: An optical coherence tomography study. *International Ophthalmology*, 40, 2931–2948.
- Bringmann, A., Unterlauff, J. D., Wiedemann, R., Barth, T., Rehak, M., & Wiedemann, P. (2021). Degenerative lamellar macular holes: Tractional development and morphological alterations. *International Ophthalmology*, 41, 1203–1221.
- Brunner, A.-D., Thielert, M., Vasilopoulou, C., Ammar, C., Coscia, F., Mund, A., Hoerning, O. B., Bache, N., Apalategui, A., Lubeck, M., Richter, S., Fischer, D. S., Raether, O., Park, M. A., Meier, F., Theis, F. J., & Mann, M. (2022). Ultra-high sensitivity mass spectrometry quantifies single-cell proteome changes upon perturbation. *Molecular Systems Biology*, 18, e10798.
- Chambers, D. C., Carew, A. M., Lukowski, S. W., & Powell, J. E. (2019). Transcriptomics and single-cell RNA-sequencing. *Respirology*, 24, 29–36.
- Cowan, C. S., Renner, M., De Gennaro, M., Gross-Scherf, B., Goldblum, D., Hou, Y., Munz, M., Rodrigues, T. M., Krol, J., Szikra, T., Papasaikas, P., Cuttat, R., Waldt, A., Diggelmann, R., Patino-Alvarez, C. P., Gerber-Hollbach, N., Schuierer, S., Hou, Y., Srdanovic, A., ... Roska, B. (2020). Cell types of the human retina and its organoids at single-cell resolution. *Cell*, 182, 1623–1640.e34.
- da Silva, S., & Cepko, C. L. (2017). Fgf8 expression and degradation of retinoic acid are required for patterning a high-acuity area in the retina. *Developmental Cell*, 42, 68–81.e6.
- Domdei, N., Reiniger, J. L., Holz, F. G., & Harmening, W. M. (2021). The relationship between visual sensitivity and eccentricity, cone density and outer segment length in the human Foveola. *Investigative Ophthalmology & Visual Science*, 62, 31.
- Doncheva, N. T., Morris, J. H., Gorodkin, J., & Jensen, L. J. (2019). Cytoscape StringApp: Network analysis and visualization of proteomics data. *Journal of Proteome Research*, 18, 623–632.
- Escola, J. M., Kleijmeer, M. J., Stoorvogel, W., Griffith, J. M., Yoshie, O., & Geuze, H. J. (1998). Selective enrichment of tetraspan proteins on the internal vesicles of multivesicular endosomes and on exosomes secreted by human B-lymphocytes. *The Journal of Biological Chemistry*, 273, 20121–20127.
- Ferrara, M., Lugano, G., Sandinha, M. T., Kearns, V. R., Geraghty, B., & Steel, D. H. W. (2021). Biomechanical properties of retina and choroid: A comprehensive review of techniques and translational relevance. *Eye*, 35, 1818–1832.
- Franz, J., Brinkmann, B. F., König, M., Hüve, J., Stock, C., Ebnet, K., & Riethmüller, C. (2016). Nanoscale imaging reveals a Tetraspanin-CD9 coordinated elevation of endothelial ICAM-1 clusters. *PLoS One*, 11, e0146598.
- Franze, K., Grosche, J., Skatchkov, S. N., Schinking, S., Foja, C., Schild, D., Uckermann, O., Travis, K., Reichenbach, A., & Guck, J. (2007). Müller cells are living optical fibers in the vertebrate retina. *Proceedings of the National Academy of Sciences*, 104, 8287–8292.
- Gantner, M. L., Eade, K., Wallace, M., Handzlik, M. K., Fallon, R., Trombley, J., Bonelli, R., Giles, S., Harkins-Perry, S., Heeren, T. F. C., Sauer, L., Ideguchi, Y., Baldini, M., Scheppke, L., Dorrell, M. I., Kitano, M., Hart, B. J., Cai, C., Nagasaki, T., ... Friedlander, M. (2019). Serine and lipid metabolism in macular disease and peripheral neuropathy. *The New England Journal of Medicine*, 381, 1422–1433.
- Ghaseminejad, F., Kaplan, L., Pfaller, A. M., Hauck, S. M., & Grosche, A. (2020). The role of Müller cell glucocorticoid signaling in diabetic retinopathy. *Graefes Archive for Clinical and Experimental Ophthalmology*, 258, 221–230.
- Goldman, D. (2014). Müller glial cell reprogramming and retina regeneration. *Nature Reviews Neuroscience*, 15, 431–442.
- Goto, M., Sumiyoshi, H., Sakai, T., Fassler, R., Ohashi, S., Adachi, E., Yoshioka, H., & Fujiwara, S. (2006). Elimination of Epiplakin by gene targeting results in acceleration of keratinocyte migration in mice. *Molecular and Cellular Biology*, 26, 548–558.
- Grosche, A., Hauser, A., Lepper, M. F., Mayo, R., von Toerne, C., Merl-Pham, J., & Hauck, S. M. (2016). The proteome of native adult Müller glial cells from murine retina. *Molecular & Cellular Proteomics*, 15, 462–480.
- Handa, J. T. (2012). How does the macula protect itself from oxidative stress? *Molecular Aspects of Medicine*, 33, 418–435.
- Hao, Y., Hao, S., Andersen-Nissen, E., Mauck, W. M., Zheng, S., Butler, A., Lee, M. J., Wilk, A. J., Darby, C., Zager, M., Hoffman, P., Stoeckius, M., Papalexi, E., Mimitou, E. P., Jain, J., Srivastava, A., Stuart, T., Fleming, L. M., Yeung, B., ... Satija, R. (2021). Integrated analysis of multimodal single-cell data. *Cell*, 184, 3573–3587.e29.
- Heeren, T. F. C., Chew, E. Y., Clemons, T., Fruttiger, M., Balaskas, K., Schwartz, R., Egan, C. A., & Charbel Issa, P. (2020). Macular telangiectasia type 2: Visual acuity, disease end stage, and the MacTel area. *Ophthalmology*, 127, 1539–1548.
- Hoon, M., Okawa, H., Della Santina, L., & Wong, R. O. L. (2014). Functional architecture of the retina: Development and disease. *Progress in Retinal and Eye Research*, 42, 44–84.
- Hu, L., Huang, Z., Wu, Z., Ali, A., & Qian, A. (2018). Mammalian plakins, giant cytolinkers: Versatile biological functions and roles in cancer. *International Journal of Molecular Sciences*, 19, 974.
- Hurley, J. B., Lindsay, K. J., & Du, J. (2015). Glucose, lactate, and shuttling of metabolites in vertebrate retinas. *Journal of Neuroscience Research*, 93, 1079–1092.
- Hutmacher, F. (2019). Why is there so much more research on vision than on any other sensory modality? *Frontiers in Psychology*, 10, 2246.
- Inaba, Y., Chauhan, V., van Loon, A. P., Choudhury, L. S., & Sagasti, A. (2020). Keratins and the plakin family cytolinker proteins control the length of epithelial microridge protrusions. *eLife*, 9, 1–27.
- Ishikawa, K., Furuhashi, M., Sasaki, T., Kudoh, J., Tsuchisaka, A., Hashimoto, T., Sasaki, T., Yoshioka, H., Eshima, N., Matsuda-Hirose, H., Sakai, T., Hatano, Y., & Fujiwara, S. (2018). Intragenic copy number variation within human epiplakin 1 (EPPK1) generates variation of molecular size of epiplakin. *Journal of Dermatological Science*, 91, 228–231.



- Jang, S.-I., Kalinin, A., Takahashi, K., Marekov, L. N., & Steinert, P. M. (2005). Characterization of human epiplakin: RNAi-mediated epiplakin depletion leads to the disruption of keratin and vimentin IF networks. *Journal of Cell Science*, *118*, 781–793.
- Janssen, A. F. J., Breusegem, S. Y., & Larriue, D. (2022). Current methods and pipelines for image-based quantitation of nuclear shape and nuclear envelope abnormalities. *Cell*, *11*, 347.
- Jones, T. R., Kang, I. H., Wheeler, D. B., Lindquist, R. A., Papallo, A., Sabatini, D. M., Golland, P., & Carpenter, A. E. (2008). CellProfiler analyst: Data exploration and analysis software for complex image-based screens. *BMC Bioinformatics*, *9*, 482.
- Käll, L., Canterbury, J. D., Weston, J., Noble, W. S., & MacCoss, M. J. (2007). Semi-supervised learning for peptide identification from shotgun proteomics datasets. *Nature Methods*, *4*, 923–925.
- Kam, R. K. T., Deng, Y., Chen, Y., & Zhao, H. (2012). Retinoic acid synthesis and functions in early embryonic development. *Cell & Bioscience*, *2*, 11.
- Kassambara A. & Mundt F. (2020). Extract and visualize the results of multivariate data analyses [R package factextra version 1.0.7].
- Kaylor, J. J., Yuan, Q., Cook, J., Sarfare, S., Makshanoff, J., Miu, A., Kim, A., Kim, P., Habib, S., Roybal, C. N., Xu, T., Nusinowitz, S., & Travis, G. H. (2013). Identification of DES1 as a vitamin A isomerase in Müller glial cells of the retina. *Nature Chemical Biology*, *9*, 30–36.
- Kelly, R. T. (2020). Single-cell proteomics: Progress and prospects. *Molecular & Cellular Proteomics*, *19*, 1739–1748.
- Kolb H. (1995). Photoreceptors University of Utah Health Sciences Center.
- Kolde R. (2019). CRAN - Package pheatmap.
- Lenis, T. L., Hu, J., Ng, S. Y., Jiang, Z., Sarfare, S., Lloyd, M. B., Esposito, N. J., Samuel, W., Jaworski, C., Bok, D., Finnemann, S. C., Radeke, M. J., Redmond, T. M., Travis, G. H., & Radu, R. A. (2018). Expression of ABCA4 in the retinal pigment epithelium and its implications for stargardt macular degeneration. *Proceedings of the National Academy of Sciences of the United States of America*, *115*, E11120–E11127.
- Limb, G. A., Salt, T. E., Munro, P. M. G., Moss, S. E., & Khaw, P. T. (2002). In vitro characterization of a spontaneously immortalized human Müller cell line (MIO-M1). *Investigative Ophthalmology & Visual Science*, *43*, 864–869.
- Liu, L., MacKenzie, K. R., Putluri, N., Maletić-Savatić, M., & Bellen, H. J. (2017). The glia-neuron lactate shuttle and elevated ROS promote lipid synthesis in neurons and lipid droplet accumulation in glia via APOE/D. *Cell Metabolism*, *26*, 719–737.e6.
- Liu, Y., Beyer, A., & Aebersold, R. (2016). On the dependency of cellular protein levels on mRNA abundance. *Cell*, *165*, 535–550.
- Lobo, J., See, E. Y.-S., Biggs, M., & Pandit, A. (2016). An insight into morphometric descriptors of cell shape that pertain to regenerative medicine. *Journal of Tissue Engineering and Regenerative Medicine*, *10*, 539–553.
- Lowe, D. G. (2004). Distinctive image features from scale-invariant keypoints. *International Journal of Computer Vision*, *60*, 91–110.
- Lu, Y.-B., Franze, K., Seifert, G., Steinhäuser, C., Kirchhoff, F., Wolburg, H., Guck, J., Janmey, P., Wei, E.-Q., Käs, J., & Reichenbach, A. (2006). Viscoelastic properties of individual glial cells and neurons in the CNS. *Proceedings of the National Academy of Sciences of the United States of America*, *103*, 17759–17764.
- MacDonald, R. B., Randlett, O., Oswald, J., Yoshimatsu, T., Franze, K., & Harris, W. A. (2015). Müller glia provide essential tensile strength to the developing retina. *The Journal of Cell Biology*, *210*, 1075–1083.
- Mages, K., Grassmann, F., Jäggle, H., Rupprecht, R., Weber, B. H. F., Hauck, S. M., & Grosche, A. (2019). The agonistic TSPO ligand XBD173 attenuates the glial response thereby protecting inner retinal neurons in a murine model of retinal ischemia. *Journal of Neuroinflammation*, *16*, 43.
- Margiotta, A., & Bucci, C. (2016). Role of intermediate filaments in vesicular traffic. *Cell*, *5*, 20.
- McQuin, C., Goodman, A., Chernyshev, V., Kamensky, L., Cimini, B. A., Karhohs, K. W., Doan, M., Ding, L., Rafelski, S. M., Thirstrup, D., Wieggraabe, W., Singh, S., Becker, T., Caicedo, J. C., & Carpenter, A. E. (2018). CellProfiler 3.0: Next-generation image processing for biology. *PLoS Biology*, *16*, e2005970.
- Naito, Y., Hino, K., Bono, H., & Ui-Tei, K. (2015). CRISPRdirect: Software for designing CRISPR/Cas guide RNA with reduced off-target sites. *Bioinformatics*, *31*, 1120–1123.
- Napoli, J. L. (2012). Physiological insights into all-trans-retinoic acid biosynthesis. *Biochimica et Biophysica Acta, Molecular and Cell Biology of Lipids*, *1821*, 152–167.
- Navarro, P., Trevisan-Herraz, M., Bonzon-Kulichenko, E., Núñez, E., Martínez-Acedo, P., Pérez-Hernández, D., Jorge, I., Mesa, R., Calvo, E., Carrascal, M., Hernández, M. L., García, F., Bárcena, J. A., Ashman, K., Abian, J., Gil, C., Redondo, J. M., & Vázquez, J. (2014). General statistical framework for quantitative proteomics by stable isotope labeling. *Journal of Proteome Research*, *13*, 1234–1247.
- Noya, S. B., Colameo, D., Brüning, F., Spinnler, A., Mircsof, D., Opitz, L., Mann, M., Tyagarajan, S. K., Robles, M. S., & Brown, S. A. (2019). The forebrain synaptic transcriptome is organized by clocks but its proteome is driven by sleep. *Science* (80-), *366*, eaav2642.
- Pannicke, T., Wagner, L., Reichenbach, A., & Grosche, A. (2018). Electro-physiological characterization of Müller cells from the ischemic retina of mice deficient in the leukemia inhibitory factor. *Neuroscience Letters*, *670*, 69–74.
- Pauly, D., Agarwal, D., Dana, N., Schäfer, N., Biber, J., Wunderlich, K. A., Jabri, Y., Straub, T., Zhang, N. R., Gautam, A. K., Weber, B. H. F., Hauck, S. M., Kim, M., Curcio, C. A., Stambolian, D., Li, M., & Grosche, A. (2019). Cell-type-specific complement expression in the healthy and diseased retina. *Cell Reports*, *29*, 2835–2848.e4.
- Potokar, M., Kreft, M., Li, L., Daniel Andersson, J., Pangršič, T., Chowdhury, H. H., Pekny, M., & Zorec, R. (2007). Cytoskeleton and vesicle mobility in astrocytes. *Traffic*, *8*, 12–20.
- Potokar, M., Morita, M., Wiche, G., & Jorgačevski, J. (2020). The diversity of intermediate filaments in astrocytes. *Cell*, *9*, 1604.
- Ran, F. A., Hsu, P. D., Wright, J., Agarwala, V., Scott, D. A., & Zhang, F. (2013). Genome engineering using the CRISPR-Cas9 system. *Nature Protocols*, *8*, 2281–2308.
- Reichenbach, A., & Bringmann, A. (2020). Glia of the human retina. *Glia*, *68*, 768–796.
- Reyes, R., Cardeñes, B., Machado-Pineda, Y., & Cabañas, C. (2018). Tetraspanin CD9: A key regulator of cell adhesion in the immune system. *Frontiers in Immunology*, *9*, 863.
- Ritchie, M. E., Phipson, B., Wu, D., Hu, Y., Law, C. W., Shi, W., & Smyth, G. K. (2015). Limma powers differential expression analyses for RNA-sequencing and microarray studies. *Nucleic Acids Research*, *43*, e47.
- Samardžija, M., Caprara, C., Heynen, S. R., DeParis, S. W., Meneau, I., Traber, G., Agca, C., von Lintig, J., & Grimm, C. (2014). A mouse model for studying cone photoreceptor pathologies. *Investigative Ophthalmology and Visual Science*, *55*, 5304–5313.
- Samardžija, M., Von Lintig, J., Tanimoto, N., Oberhauser, V., Thiersch, M., Seeliger, M., Remé, C. E., Grimm, C., & Wenzel, A. (2008). R91W mutation in Rpe65 leads to milder early-onset retinal dystrophy due to the generation of low levels of 11-cis-retinal. *Human Molecular Genetics*, *17*, 281–292.
- Scerri, T. S., Quaglieri, A., Cai, C., Zernant, J., Matsunami, N., Baird, L., Schepke, L., Bonelli, R., Yannuzzi, L. A., Friedlander, M., MacTel Project Consortium, Egan, C. A., Fruttiger, M., Leppert, M., Allikmets, R., & Bahlo, M. (2017). Genome-wide analyses identify common variants associated with macular telangiectasia type 2. *Nature Genetics*, *49*, 559–567.
- Schindelin, J., Arganda-Carreras, I., Frise, E., Kaynig, V., Longair, M., Pietzsch, T., Preibisch, S., Rueden, C., Saalfeld, S., Schmid, B., Tinevez, J. Y., White, D. J., Hartenstein, V., Eliceiri, K., Tomancak, P., &

- Cardona, A. (2012). Fiji: An open-source platform for biological-image analysis. *Nature Methods*, 9, 676–682.
- Shannon, P., Markiel, A., Ozier, O., Baliga, N. S., Wang, J. T., Ramage, D., Amin, N., Schwikowski, B., & Ideker, T. (2003). Cytoscape: A software environment for integrated models of biomolecular interaction networks. *Genome Research*, 13, 2498–2504.
- Sharma, K., Schmitt, S., Bergner, C. G., Tyanova, S., Kannaiyan, N., Manrique-Hoyos, N., Kongi, K., Cantuti, L., Hanisch, U.-K., Phillips, M.-A., Rossner, M. J., Mann, M., & Simons, M. (2015). Cell type- and brain region-resolved mouse brain proteome. *Nature Neuroscience*, 18, 1819–1831.
- Slezak, M., Grosche, A., Niemiec, A., Tanimoto, N., Pannicke, T., Münch, T. A., Crocker, B., Isope, P., Härtig, W., Beck, S. C., Huber, G., Ferracci, G., Perraut, M., Reber, M., Miehe, M., Demais, V., Lévêque, C., Metzger, D., Szklarczyk, K., ... Priefer, F. W. (2012). Relevance of Exocytotic glutamate release from retinal glia. *Neuron*, 74, 504–516.
- Sonnenberg, A., & Liem, R. K. H. (2007). Plakins in development and disease. *Experimental Cell Research*, 313, 2189–2203.
- Spazierer, D., Fuchs, P., Pröll, V., Janda, L., Oehler, S., Fischer, I., Hauptmann, R., & Wiche, G. (2003). Epiplakin gene analysis in mouse reveals a single exon encoding a 725-kDa protein with expression restricted to epithelial tissues. *The Journal of Biological Chemistry*, 278, 31657–31666.
- Spazierer, D., Fuchs, P., Reipert, S., Fischer, I., Schmuth, M., Lassmann, H., & Wiche, G. (2006). Epiplakin is dispensable for skin barrier function and for integrity of keratin network cytoarchitecture in simple and stratified epithelia. *Molecular and Cellular Biology*, 26, 559–568.
- Spazierer, D., Raberger, J., Groß, K., Fuchs, P., & Wiche, G. (2008). Stress-induced recruitment of epiplakin to keratin networks increases their resistance to hyperphosphorylation-induced disruption. *Journal of Cell Science*, 121, 825–833.
- Stuart, T., Butler, A., Hoffman, P., Hafemeister, C., Papalexi, E., Mauck, W. M., Hao, Y., Stoeckius, M., Smibert, P., & Satija, R. (2019). Comprehensive integration of single-cell data. *Cell*, 177, 1888–1902.e21.
- Syrbe, S., Kuhrt, H., Gärtner, U., Habermann, G., Wiedemann, P., Bringmann, A., & Reichenbach, A. (2018). Müller glial cells of the primate foveola: An electron microscopical study. *Experimental Eye Research*, 167, 110–117.
- Szabo, S., Wögenstein, K. L., Österreicher, C. H., Guldiken, N., Chen, Y., Doler, C., Wiche, G., Boor, P., Haybaeck, J., Strnad, P., & Fuchs, P. (2015). Epiplakin attenuates experimental mouse liver injury by chaperoning keratin reorganization. *Journal of Hepatology*, 62, 1357–1366.
- Théry, C., Regnault, A., Garin, J., Wolfers, J., Zitvogel, L., Ricciardi-Castagnoli, P., Raposo, G., & Amigorena, S. (1999). Molecular characterization of dendritic cell-derived exosomes: Selective accumulation of the heat shock protein hsc73. *The Journal of Cell Biology*, 147, 599–610.
- Théry, C., Witwer, K. W., Aikawa, E., Alcaraz, M. J., Anderson, J. D., Andriantsitohaina, R., Antoniou, A., Arab, T., Archer, F., Atkin-Smith, G. K., Ayre, D. C., Bach, J. M., Bachurski, D., Baharvand, H., Balaj, L., Baldacchino, S., Bauer, N. N., Baxter, A. A., Bebawy, M., ... Zuba-Surma, E. K. (2018). Minimal information for studies of extracellular vesicles 2018 (MISEV2018): A position statement of the International Society for Extracellular Vesicles and update of the MISEV2014 guidelines. *Journal of Extracellular Vesicles*, 7, 1535750.
- Thompson, B., Katsanis, N., Apostolopoulos, N., Thompson, D. C., Nebert, D. W., & Vasiliou, V. (2019). Genetics and functions of the retinoic acid pathway, with special emphasis on the eye. *Human Genomics*, 13, 61.
- Toft-Kehler, A. K., Skytt, D. M., & Kolko, M. (2018). A perspective on the Müller cell-neuron metabolic partnership in the inner retina. *Molecular Neurobiology*, 55, 5353–5361.
- Tonoike, Y., Matsushita, K., Tomonaga, T., Katada, K., Tanaka, N., Shimada, H., Nakatani, Y., Okamoto, Y., & Nomura, F. (2011). Adhesion molecule periplakin is involved in cellular movement and attachment in pharyngeal squamous cancer cells. *BMC Cell Biology*, 12, 41.
- Tschulakow, A. V., Oltrup, T., Bende, T., Schmelzle, S., & Schraermeyer, U. (2018). The anatomy of the foveola reinvestigated. *PeerJ*, 6, e4482.
- Tseng Q. (2011). Etude d'architecture multicellulaire avec le microenvironnement cellulaire.
- Tseng, Q., Duchemin-Pelletier, E., Deshiere, A., Bolland, M., Guilloud, H., Filhol, O., & Théry, M. (2012). Spatial organization of the extracellular matrix regulates cell-cell junction positioning. *Proceedings of the National Academy of Sciences of the United States of America*, 109, 1506–1511.
- Ueo, D., Furuhashi, M., Sasaki, T., Kudoh, J., Parry, D. A. D., Winter, D. J., Sasaki, T., Hashimoto, T., Tsuruta, D., & Fujiwara, S. (2021). Intragenic copy number variation in mouse epiplakin 1 (Eppk1) and the conservation of the repeat structures in the lower vertebrates. *Journal of Dermatological Science*, 103, 186–189.
- Verbakel, S. K., van Huet, R. A. C., Boon, C. J. F., den Hollander, A. I., Collin, R. W. J., Klaver, C. C. W., Hoyng, C. B., Roepman, R., & Klevering, B. J. (2018). Non-syndromic retinitis pigmentosa. *Progress in Retinal and Eye Research*, 66, 157–186.
- Vogel, C., & Marcotte, E. M. (2012). Insights into the regulation of protein abundance from proteomic and transcriptomic analyses. *Nature Reviews Genetics*, 13, 227–232.
- Voigt, A. P., Mullin, N. K., Stone, E. M., Tucker, B. A., Scheetz, T. E., & Mullins, R. F. (2021). Single-cell RNA sequencing in vision research: Insights into human retinal health and disease. *Progress in Retinal and Eye Research*, 83, 100934.
- Voigt, A. P., Whitmore, S. S., Flamme-Wiese, M. J., Riker, M. J., Wiley, L. A., Tucker, B. A., Stone, E. M., Mullins, R. F., & Scheetz, T. E. (2019). Molecular characterization of foveal versus peripheral human retina by single-cell RNA sequencing. *Experimental Eye Research*, 184, 234–242.
- Wan, J., & Goldman, D. (2016). Retina regeneration in zebrafish. *Current Opinion in Genetics & Development*, 40, 41–47.
- Wang, J. S., & Kefalov, V. J. (2009). An alternative pathway mediates the mouse and human cone visual cycle. *Current Biology*, 19, 1665–1669.
- Wang, J.-S., & Kefalov, V. J. (2011). The cone-specific visual cycle. *Progress in Retinal and Eye Research*, 30, 115–128.
- Wang, W., Sumiyoshi, H., Yoshioka, H., & Fujiwara, S. (2006). Interactions between epiplakin and intermediate filaments. *The Journal of Dermatology*, 33, 518–527.
- Wässle, H., Haverkamp, S., & Grünert, U. (2002). The cone pedicle a complex synapse in the retina. *The Keio Journal of Medicine*, 51, 19–20.
- Whitmore, S. S., Wagner, A. H., DeLuca, A. P., Drack, A. V., Stone, E. M., Tucker, B. A., Zeng, S., Braun, T. A., Mullins, R. F., & Scheetz, T. E. (2014). Transcriptomic analysis across nasal, temporal, and macular regions of human neural retina and RPE/choroid by RNA-Seq. *Experimental Eye Research*, 129, 93–106.
- Wiśniewski, J. R., Zougman, A., Nagaraj, N., & Mann, M. (2009). Universal sample preparation method for proteome analysis. *Nature Methods*, 6(6), 359–362.
- Wögenstein, K. L., Szabo, S., Lunova, M., Wiche, G., Haybaeck, J., Strnad, P., Boor, P., Wagner, M., & Fuchs, P. (2014). Epiplakin deficiency aggravates murine caerulein-induced acute pancreatitis and favors the formation of acinar keratin granules. *PLoS One*, 9, e108323.
- Wunderlich, K. A., Tanimoto, N., Grosche, A., Zrenner, E., Pekny, M., Reichenbach, A., Seeliger, M. W., Pannicke, T., & Perez, M.-T. (2015). Retinal functional alterations in mice lacking intermediate filament proteins glial fibrillary acidic protein and vimentin. *The FASEB Journal*, 29, 4815–4828.
- Xue, Y., Sato, S., Razafsky, D., Sahu, B., Shen, S. Q., Potter, C., Sandell, L. L., Corbo, J. C., Palczewski, K., Maeda, A., Hodzic, D., & Kefalov, V. J. (2017). The role of retinol dehydrogenase 10 in the cone visual cycle. *Scientific Reports*, 7, 2390.



- Xue, Y., Shen, S. Q., Jui, J., Rupp, A. C., Byrne, L. C., Hattar, S., Flannery, J. G., Corbo, J. C., & Kefalov, V. J. (2015). CRALBP supports the mammalian retinal visual cycle and cone vision. *The Journal of Clinical Investigation*, *125*, 727–738.
- Yeo, N. J. Y., Chan, E. J. J., & Cheung, C. (2019). Choroidal neovascularization: Mechanisms of endothelial dysfunction. *Frontiers in Pharmacology*, *10*, 1363.
- Yuodelis, C., & Hendrickson, A. (1986). A qualitative and quantitative analysis of the human fovea during development. *Vision Research*, *26*, 847–855.
- Zhang, T., Zhu, L., Madigan, M. C., Liu, W., Shen, W., Cherepanoff, S., Zhou, F., Zeng, S., Du, J., & Gillies, M. C. (2019). Human macular Müller cells rely more on serine biosynthesis to combat oxidative stress than those from the periphery. *eLife*, *8*, 1–19.

SUPPORTING INFORMATION

Additional supporting information can be found online in the Supporting Information section at the end of this article.

How to cite this article: Kaplan, L., Drexler, C., Pfaller, A. M., Brenna, S., Wunderlich, K. A., Dimitracopoulos, A., Merl-Pham, J., Perez, M.-T., Schlötzer-Schrehardt, U., Enzmann, V., Samardzija, M., Puig, B., Fuchs, P., Franze, K., Hauck, S. M., & Grosche, A. (2022). Retinal regions shape human and murine Müller cell proteome profile and functionality. *Glia*, 1–24. <https://doi.org/10.1002/glia.24283>

RELEASE OF VAMP5-POSITIVE EXTRACELLULAR VESICLES BY RETINAL MÜLLER GLIA IN VIVO

Authors:

Demais V, Pohl A, Wunderlich KA, Pfaller AM, **Kaplan L**, Barthélémy A, Dittrich R, Puig B, Giebel B, Hauck SM, Pfriederger FW, Grosche A

Author contributions:

VD: performed electron microscopy-related work, acquired and analyzed electron micrographs. AP: performed immunofluorescence microscopy-related work, qPCR experiments and analyses, immunoblots for VAMP expression in the healthy and ischemic retina, established protocols for primary Müller cell cultures, performed EV purification, and edited the manuscript. KAW: performed EV purification from primary Müller cell cultures and immunoblot analyses, analyzed EV marker localization via STED microscopy, and edited the manuscript. AMP: generated purified EVs for mass spectrometric analysis, and edited the manuscript. **LK**: performed EV isolation and bioinformatic analysis of proteomic data, and edited the manuscript. AB: performed immunohistochemical staining with selected antibodies to prepare immunogold staining. RD: performed NTA. BP: set up the EV isolation protocol, analyzed results, edited the manuscript. BG: analyzed NTA results and edited the manuscript. SMH: performed mass spectrometric analysis of retinal cell types and purified EVs, analyzed protein expression levels, and edited the manuscript. AG: designed experiments, analyzed results, prepared figures, and edited the manuscript. FWP: designed experiments, analyzed results, prepared figures, and wrote the manuscript.





License:

Attribution-NonCommercial 4.0 International (CC BY-NC 4.0)

Availability:

DOI: 10.1002/jev2.12254

Release of VAMP5-positive extracellular vesicles by retinal Müller glia in vivo

Valerie Demais¹  | Anne Pohl^{2,3} | Kirsten A. Wunderlich²  | Anna M. Pfaller² |
 Lew Kaplan²  | Amelie Barthélémy⁴ | Robin Dittrich⁵ | Berta Puig⁶  |
 Bernd Giebel⁵  | Stefanie M. Hauck⁷  | Frank W. Pfrieger^{1,4}  | Antje Grosche² 

¹Plateforme Imagerie In Vitro, CNRS UAR 3156, Neuropôle, University of Strasbourg, Strasbourg, France

²Department of Physiological Genomics, BioMedical Center BMC, Ludwig-Maximilian University, Planegg-Martinsried, Germany

³Institute of Human Genetics, University of Regensburg, Regensburg, Germany

⁴Centre National de la Recherche Scientifique, Université de Strasbourg, Institut des Neurosciences Cellulaires et Intégratives, Strasbourg, France

⁵Institute for Transfusion Medicine, University Hospital Essen, University of Duisburg-Essen, Essen, Germany

⁶Neurology Department, Experimental Research in Stroke and Inflammation (ERSI), University Medical Center Hamburg-Eppendorf, Hamburg, Germany

⁷Metabolomics and Proteomics Core and Research Unit Protein Science, Helmholtz-Zentrum München, München, Germany

Correspondence

Frank Pfrieger, Plateforme Imagerie In Vitro, CNRS UAR 3156, Neuropôle, University of Strasbourg, Strasbourg 67000, France.
 Email: fw-pfrieger@gmx.de

Antje Grosche, Department of Physiological Genomics, BioMedical Center BMC, Ludwig-Maximilian University, Planegg-Martinsried 82152, Germany.
 Email: antje.grosche@med.uni-muenchen.de

Valerie Demais and Anne Pohl are equally contributing first authors.

Funding information

Université de Strasbourg, Grant/Award Number: UPR3212; ProRetina Foundation Germany, Grant/Award Numbers: Pro-Re/Seed/Grosche.1-2014, Pro-Re/Seed/Kaplan-Grosche.1-2019; Centre National de la Recherche Scientifique, Grant/Award Number: UPR3212; Deutsche Forschungsgemeinschaft, Grant/Award Numbers: GR 4403/1-1, GR 4403/5-1, GR 4403/7-1, HA 6014/5-1; Agence Nationale de la Recherche, Grant/Award Number: GLIAVAMP

Abstract

Cell-cell interactions in the central nervous system are based on the release of molecules mediating signal exchange and providing structural and trophic support through vesicular exocytosis and the formation of extracellular vesicles. The specific mechanisms employed by each cell type in the brain are incompletely understood. Here, we explored the means of communication used by Müller cells, a type of radial glial cells in the retina, which forms part of the central nervous system. Using immunohistochemical, electron microscopic, and molecular analyses, we provide evidence for the release of distinct extracellular vesicles from endfeet and microvilli of retinal Müller cells in adult mice in vivo. We identify VAMP5 as a Müller cell-specific SNARE component that is part of extracellular vesicles and responsive to ischemia, and we reveal differences between the secretomes of immunoaffinity-purified Müller cells and neurons in vitro. Our findings suggest extracellular vesicle-based communication as an important mediator of cellular interactions in the retina.

KEYWORDS

neuroglia, exosomes, tetraspanin, gliosis, SNARE complex, secretome, vitreous body, microvillus

This is an open access article under the terms of the [Creative Commons Attribution-NonCommercial License](https://creativecommons.org/licenses/by-nc/4.0/), which permits use, distribution and reproduction in any medium, provided the original work is properly cited and is not used for commercial purposes.

© 2022 The Authors. *Journal of Extracellular Vesicles* published by Wiley Periodicals, LLC on behalf of the International Society for Extracellular Vesicles.

1 | INTRODUCTION

Glial cells control the development (Araujo et al., 2019; Lago-Baldaia et al., 2020; Tan et al., 2021) and function (García-Cáceres et al., 2019; Kofuji & Araque, 2021; Nave & Werner, 2021) of neurons, and they influence the outcome of pathologic conditions due to disease or injury (Kim et al., 2020; Linnerbauer et al., 2020; Patel et al., 2019; Raiders et al., 2021; Wilton & Stevens, 2020; Wilton et al., 2019). During the last years, much has been learned about glia-neuron interactions. Neurons and different types of glial cells communicate via intercellular contacts and via the release of molecules fulfilling multiple functions that range from structural, energy and trophic support to cell signalling (Giaume et al., 2021; Illes et al., 2019; Jha & Morrison, 2020; Seifert & Steinhäuser, 2018; Shen et al., 2017; Sultan et al., 2015). Molecules of the secretome that are contained in intracellular vesicles can be released directly into the extracellular space following fusion of the vesicular membrane with the plasma membrane (Fiacco & McCarthy, 2018; Mielnicka & Michaluk, 2021; Murat & García-Cáceres, 2021; Savtchouk & Volterra, 2018; Vardjan et al., 2019). Alternatively, they can be released as molecular assemblies contained in extracellular vesicles (EVs) harbouring a context- and cell type-specific host of proteins, lipids, and nucleic acids (Kalluri & LeBleu, 2020; Mathieu et al., 2019; Pfrieger & Vitale, 2018; Pistono et al., 2020; Théry et al., 2018; Van Niel et al., 2022; Yates et al., 2022). EVs have been discussed as potential means of cell-cell communication in the normal and diseased central nervous system (CNS) (Aires et al., 2021; Budnik et al., 2016; Li et al., 2019; Liu et al., 2020; Lizarraga-Valderrama & Sheridan, 2021; Mahjoum et al., 2021; Pascual et al., 2020; Schnatz et al., 2021; You & Ikezu, 2019), but knowledge about their presence, origin, and composition in nervous tissues *in vivo* is still incomplete (Brenna et al., 2021). Here, we explored possible mechanisms of glial communication in the CNS using the mouse retina as model tissue. We focus on Müller cells, a prominent type of radial glial cell that spans the entire retina (Wang et al., 2017) and impacts retinal development and function by diverse mechanisms (Reichenbach & Bringmann, 2020). Previous studies suggested that these cells employ vesicular release of molecules (Slezak et al., 2012; Wagner et al., 2017), but the full range of their intercellular communication capacity is unknown. Our findings suggest that Müller cells release EVs from their endfeet facing the vitreous body and from their microvilli surrounding photoreceptor segments. We show that Müller cell-derived EVs bear a characteristic protein composition that differs substantially from those secreted by neurons. Moreover, we uncover that in retinæ of adult mice, vesicle-associated membrane protein 5 (VAMP5), a component of soluble N-ethylmaleimide-sensitive factor attachment proteins receptor (SNARE) complexes, is specifically expressed by Müller cells and contained in a subset of their EVs.

2 | MATERIALS AND METHODS

2.1 | Animals

All experiments were performed with adult C57BL/6J mice in accordance with the European Community Council Directive 2010/63/EU and the ARVO Statement for the Use of Animals in Ophthalmic and Vision Research. Animals were housed in a 12h light/dark cycle with ~400 lux with *ad libitum* access to drinking water and food.

2.2 | Transient retinal ischemia

The protocols for induction of transient retinal ischemia were approved by the local Bavarian authorities (55.2 DMS-2532-2-182, Germany). Ischemia was induced in one eye of 8-weeks-old male and female mice using the high intraocular pressure (HIOP) method (Pannicke et al., 2014; Wagner et al., 2016). The untreated contralateral eye served as internal control. This approach reduced the number of animals used in these experiments as demanded by the 3R rules. Anaesthesia was induced by intraperitoneal injection of ketamine (100 mg/kg body weight; Ratiopharm, Ulm, Germany) and xylazine (5 mg/kg; Bayer Vital, Leverkusen, Germany). Pupillary dilation was induced by atropine sulphate (100 mg/kg; Braun, Melsungen, Germany). The anterior chamber of the test eye was cannulated from the pars plana with a 30-gauge infusion needle connected to a bottle containing saline (0.9% NaCl). The intraocular pressure was increased transiently to 160 mm Hg by elevating the bottle for 90 min. After removing the needle, animals were returned to cages and sacrificed after indicated periods of time for tissue analyses using carbon dioxide.

2.3 | Immunoaffinity-based cell purification

Specific cell types were enriched from retinal cell suspensions as described previously using immunomagnetic separation (Grosche et al., 2016; Pauly et al., 2019). Briefly, retinæ were treated with papain (0.2 mg/ml; Roche Molecular Biochemicals) for 30 min at 37°C in the dark in calcium- and magnesium-free extracellular solution (140 mM NaCl, 3 mM KCl, 10 mM HEPES, 11 mM glucose, pH 7.4). After several rinses and 4 min of incubation with DNase I (200 U/ml), retinæ were triturated in

extracellular solution with 1 mM MgCl₂ and 2 mM CaCl₂ added. The retinal cell suspension was subsequently incubated with CD11b- and CD31-binding microbeads to remove microglia and vascular cells, respectively, according to the manufacturer's instructions (Miltenyi Biotec, Bergisch Gladbach, Germany). The respective binding cells were depleted from the retinal suspension using large cell (LS)-columns, prior to Müller cell enrichment. To select Müller cells, the cell suspension was incubated in extracellular solution containing biotinylated anti-CD29 (0.1 mg/ml, Miltenyi Biotec) for 15 min at 4°C. Cells were washed in extracellular solution, spun down, resuspended in the presence of anti-biotin MicroBeads (1:5; Miltenyi Biotec) and incubated for 15 min at 4°C. After washing, CD29-positive Müller cells were enriched using LS columns according to the manufacturer's instructions (Miltenyi Biotec). Cells in the flow-through of the last sorting step – depleted of microglia, vascular cells, and Müller cells – were considered as mixed neuronal population.

2.4 | Immunohistochemical and -cytochemical staining

For immunohistochemical staining, enucleated eyes were immersion-fixed (4% paraformaldehyde for 2h), washed with phosphate-buffered saline (PBS), cryoprotected in sucrose, embedded in Tissue-Tek O.C.T. compound (Sakura Finetek, Staufen, Germany), and cut in 20 µm sections using a cryostat. Retinal sections were permeabilized (0.3% Triton X-100 w1% DMSO in PBS) and blocked (5% normal goat serum with 0.3% Triton X-100 and 1% DMSO in PBS) for 2h at room temperature (RT). For immunocytochemical staining, acutely isolated or cultured cells were fixed (4% paraformaldehyde for 15 min), washed with PBS, permeabilized (0.3% Triton X-100 plus 1% DMSO in PBS) and blocked (5% normal goat serum with 0.3% Triton X-100 and 1% DMSO in PBS; 30 min at RT). Sections or fixed cells were incubated with primary antibodies (Table S1) in bovine serum albumine (BSA; 1% in PBS) overnight at 4°C. Samples were washed (1% BSA) and incubated with secondary antibodies (2h at RT; 1% BSA). In some experiments, cell nuclei were labelled with DAPI (1:1000; Life Technologies). Samples were mounted in Aqua-Poly/Mount (Polysciences, Hirschberg, Germany). Control experiments without primary antibodies indicated absence of unspecific labelling except for the goat-anti-mouse secondary antibody that labelled blood vessels (not shown). Images of stained sections and cells were acquired with a custom-made VisiScope CSU-X1 confocal system (Visitron Systems, Puchheim, Germany) equipped with a high-resolution sCMOS camera (PCO AG, Kehlheim, Germany). For super resolution microscopy, fixed retinal sections were permeabilized with Triton X-100 (0.5 % in 2% BSA in PBS) for 2h before incubation with primary antibodies in blocking solution (overnight at 4°C). After washing with PBS, sections were incubated with secondary antibodies (Abberior Star) and DAPI for 2h in blocking solution at RT, subsequently washed with PBS, and briefly rinsed with distilled water before being mounted with ProLong Gold antifade reagent (Invitrogen, Life Technologies). Stimulated emission depletion (STED) microscopy was performed at the Core Facility Bioimaging of the Biomedical Centre of the LMU München with an inverted Leica SP8 STED X WLL microscope using appropriate lasers for fluorophore excitation (405 nm; pulsed white light laser 470–670 nm). Images were acquired with a 93x/1.3 NA glycerol immersion objective with the pixel size set to 23 nm. The following spectral settings were used: DAPI (excitation: 405 nm; emission: 415–450 nm; PMT), AbberiorStar 580 (580 nm; 590–620 nm; HyD; depletion laser: pulsed 775 nm, at 12% intensity), AbberiorStar 635P (635 nm; 645–702 nm; HyD; depletion laser: pulsed 775 nm, at 12% intensity). Recording of colour channels was performed sequentially to avoid bleed-through. Image brightness and contrast were adjusted with the open source software FIJI (Schindelin et al., 2012).

2.5 | Immunoblotting of proteins from acutely isolated, immunoaffinity-purified cells

Pellets of enriched cell populations from pooled pairs of mouse eyes were redissolved in reducing radioimmunoprecipitation assay (RIPA) buffer, denatured, and sonicated. Protein amounts were quantified using the Bradford or the RC DC Protein assays (BioRad, Feldkirchen, Germany) according to the manufacturer's instructions. Equal amounts of protein per sample were loaded to compare levels of selected VAMPs in cells (2.5 or 5 µg depending on the VAMP). Samples were separated by 12% SDS-PAGE and immunodetection of proteins was performed as described (Schäfer et al., 2017) using primary and secondary antibodies (Table S1) diluted in blocking solution (5% BSA in Tris-buffered saline with Tween 20). Blots were developed with WesternSure PREMIUM Chemiluminescent Substrate (LI-COR, Bad Homburg, Germany).

2.6 | Test of VAMP5 antibody specificity by immunoprecipitation

Retinae were dissected from adult mice and lysed mechanically and chemically in RIPA buffer. The protein concentration was determined by the RC DC Protein Assay (BioRad). For immunoprecipitation, to each sample (1 mg of total extract from four mouse retinae), 5 µg of anti-VAMP5 antibody or a rabbit IgG-control antibody was added (Table S1) and the antibody-lysate mix was incubated on the rotator at 4°C for 4h. For affinity purification, 25 µl of Protein G Sepharose (Merck, Darmstadt, Germany) were resuspended three times in TBS (0.5% NP40) and then centrifuged at 2000g for 5 min. Beads were added to the

antibody-lysate mix and incubated on the rotator at 4°C overnight. The complexes formed by antibody, antigen, and Protein G Sepharose were pelleted (4000g for 5 min) two times, and washed in TBS. Proteins were eluted in Laemmli buffer for 10 min at 37°C and spun down at 4000g. Supernatant was collected and stored at -20°C until mass spectrometric analysis.

2.7 | Transcript profiling of acutely isolated, immunoaffinity-purified cells by RNAseq

Total RNA was isolated from pellets of enriched cell populations using the PureLink RNA Micro Scale Kit (Thermo Fisher Scientific, Schwerte, Germany). Validation of RNA integrity and quantification of RNA concentrations were performed using the Agilent RNA 6000 Pico chip analyser according to the manufacturer's instructions (Agilent Technologies, Waldbronn, Germany). Enrichment of mRNA, library preparation (Nextera XT, Clontech), quantification (KAPA Library Quantification Kit Illumina, Kapa Biosystems, Inc., Woburn, MA, USA) and sequencing on an Illumina platform (NextSeq 500 High Output Kit v2; 150 cycles) were performed at the service facility of the KFB Centre of Excellence for Fluorescent Bioanalytics (Regensburg, Germany; www.kfb-regensburg.de). After de-multiplexing, at least 20 million reads per sample were detected. Quality control (QC) of the reads and quantification of transcript abundance were performed with the Tuxedo suite software (Langmead et al., 2009; Trapnell et al., 2009). To this end, the cutadapt routine was used to remove adapter sequences (Martin, 2011) and several QC measures were obtained with the fastqc routine. Next, the trimmed reads were aligned to the reference genome/transcriptome (GRCm38) with HISAT2 (Kim et al., 2015). Transcript abundance was estimated with the stringtie routine (Pertea et al., 2015) and expressed as fragments per kilobase pairs of transcripts per million reads (fragments per kilobase million, fpkm).

2.8 | Quantitative reverse-transcriptase polymerase chain reaction (qRT-PCR) of acutely isolated, immunoaffinity-purified cells

Total RNA was isolated from pellets of enriched cell populations using the PureLink RNA Micro Scale Kit (Thermo Fisher Scientific, Schwerte, Germany). An on-column DNase digestion step (PureLink DNase mixture, Thermo Fisher Scientific, for 20 min at RT) was included to remove genomic DNA (Roche Molecular Systems, Mannheim, Germany). RNA integrity was validated using the Agilent RNA 6000 Pico Assay according to the manufacturer's instructions (Agilent Technologies, Waldbronn, Germany). First-strand cDNAs from the total RNA purified from each cell population were synthesized using the RevertAid H Minus First-Strand cDNA Synthesis Kit (Fermentas by Thermo Fisher Scientific, Schwerte, Germany). Primers were designed using the Universal ProbeLibrary Assay Design Centre (Roche, Table S2) and transcript levels of candidate genes were measured by qRT-PCR using the TaqMan hPSC Scorecard Panel (384 well, ViiA7, Life Technologies, Darmstadt, Germany) according to the manufacturer's instructions.

2.9 | TUNEL staining of cultured cells

Immunoaffinity-purified cells were plated on coverslips, placed in 24-well plates and cultured under chemically defined, serum-free conditions in DMEM-F12 GlutaMax supplemented with Gibco Antibiotic-Antimycotic (1:100; Thermo Fischer Scientific) and NeuroBrews (1:50; Miltenyi Biotec). After 24h or 48h, cells were fixed (4% PFA, 15 min at RT), permeabilized (0.25% Triton X-100 in PBS, 20 min at RT), washed twice with de-ionized water and pretreated for 10 min at RT in TdT reaction buffer (Click-iT Plus TUNEL Assay, Alexa Fluor 594 dye, ThermoFisher Scientific, Schwerte, Germany), before the enzyme mix was added and incubated for 60 min at 37°C. After two washes in 3% BSA/PBS (2 min each), the Click iT reaction cocktail was added and incubated for another 30 min at RT. Subsequent staining for the Müller cell marker glutamine synthetase (GLUL) and DAPI co-staining was performed as described in the section 'Immunohistochemical and -cytochemical staining', after coverslips were washed two times (3% BSA/PBS for 5 min at RT). Images of cells were taken with a custom-made VisiScope CSU-X1 confocal system (Visitron Systems, Puchheim, Germany).

2.10 | Preparation of immunoaffinity-purified EVs from cultured cells

Approximately 600,000 and 300,000 immunomagnetically sorted neurons and Müller cells, respectively, were seeded on individual wells of a 48-well-plate and cultured under chemically defined, serum-free conditions in 400 µl DMEM-F12 GlutaMax supplemented with Gibco Antibiotic-Antimycotic (1:100; Thermo Fischer Scientific) and NeuroBrews (1:50; Miltenyi Biotec). Small samples of cells were fixed and air-dried on glass slides to control for cell purity by immunocytochemical staining of GLUL. After 48h to 60h, conditioned medium (CM) was collected from individual wells of culture plates and preserved for subsequent analyses of released material. As reference, cells were also harvested from individual wells, pelleted by centrifugation, and

immediately lysed in hot SDS (0.1 % in distilled water) for mass spectrometry or in RIPA buffer for immunoblotting and frozen at -80°C until further processing. CM was cleared by several centrifugation steps with increasing speed and duration (600g for 10 min; 2000g for 30 min; 10,000g for 45 min) as described (Théry et al., 2006). The supernatant of the last centrifugation step was subjected to immunomagnetic separation of secreted material positive for the surface markers CD63 and CD9 (Miltenyi) following the manufacturer's instructions. Immunoaffinity-purified material containing EVs was characterized at the molecular and structural level according to the MISEV2018 guidelines (Théry et al., 2018). For protein analyses, proteins in material enriched from CM by immunomagnetic separation were directly eluted and lysed from the μ -columns still in the magnet either with hot SDS (0.1% in distilled water) for mass spectrometry or in RIPA buffer for immunoblotting. The material in the flow-through of the washing steps was pelleted by ultracentrifugation (at 100,000g for 2h; Optima MAX -XP Ultracentrifuge from Beckman Coulter equipped with a TLA55 rotor) before lysis as described (Théry et al., 2006). Each lysed fraction was frozen at -80°C until further use.

2.11 | Immunoblotting of proteins from EVs, flow-through and corresponding cell lysates

Immunoaffinity-purified material from CM, flow-through and lysates of each cell type were diluted in Laemmli sample buffer, and separated using SDS-PAGE (15%). Semidry blotting was performed using TRISbase (2.5 mM with 192% glycine and 20% methanol) as transfer buffer. PVDF membranes were blocked using non-fat dry milk (5% in TBS with 0.1% Tween 20) and incubated with primary and secondary antibodies. Blots were developed with Clarity Max™ Western ECL substrate (Bio-Rad Medical Diagnostics GmbH, Dreieich, Germany).

2.12 | Nanoparticle tracking analysis

EV-containing samples from CM were characterized by nanoparticle tracking analysis (NTA) allowing for particle quantification and average size estimation (Dragovic et al., 2011; Sokolova et al., 2011). The ZetaView™ platform (ParticleMetrix, Meerbusch, Germany) was calibrated with polystyrene beads of 100 nm diameter (Thermo Fisher). Analyses were performed exactly as described (Görgens et al., 2019). Briefly, with five repetitions, videos were recorded at all 11 positions. The machine's sensitivity was set to 75, the shutter to 75 and the framerate to 30.

2.13 | Quantitative proteomics - LC-MSMS analysis, label-free quantification and data analysis

Proteins from immunoaffinity-purified EVs, flow-through and lysates of cultured cells were proteolysed with LysC and trypsin with the filter-aided sample preparation procedure as described (Grosche et al., 2016; Wiśniewski et al., 2009). Acidified eluted peptides were analysed on a Q Exactive HF-X mass spectrometer (Thermo Fisher Scientific) online coupled to an Ultimate 3000 RSLC nano-HPLC (Dionex). Samples were automatically injected and loaded onto the C18 trap cartridge and after 5 min eluted and separated on the C18 analytical column (Acquity UPLC M-Class HSS T3 Column, 1.8 μm , 75 μm \times 250 mm; Waters) by a 95 min non-linear acetonitrile gradient at a flow rate of 250 nl/min. MS spectra were recorded at a resolution of 60,000 with an automatic gain control (AGC) target of 3×10^6 and a maximum injection time of 30 ms from 300 to 1500 m/z. From the MS scan, the 15 most abundant peptide ions were selected for fragmentation via HCD with a normalized collision energy of 28, an isolation window of 1.6 m/z, and a dynamic exclusion of 30s. MS/MS spectra were recorded at a resolution of 15,000 with a AGC target of 10^5 and a maximum injection time of 50 ms. Unassigned charges and charges of +1 and $>+8$ were excluded from precursor selection. Acquired raw data were analysed in the Proteome Discoverer 2.4 SP1 software (Thermo Fisher Scientific; version 2.4.1.15) for peptide and protein identification via a database search (Sequest HT search engine) against the SwissProt Mouse database (Release 2020_02, 17061 sequences), considering full tryptic specificity, allowing for up to one missed tryptic cleavage site, precursor mass tolerance 10 ppm, fragment mass tolerance 0.02 Da. Carbamidomethylation of cysteine was set as a static modification. Dynamic modifications included deamidation of asparagine and glutamine, oxidation of methionine, and a combination of methionine loss with acetylation on protein N-terminus. The Percolator algorithm (Käll et al., 2007) was used to validate peptide spectrum matches and peptides. Only top-scoring identifications for each spectrum were accepted, additionally satisfying a false discovery rate $<1\%$ (high confidence). The final list of proteins satisfying the strict parsimony principle included only protein groups passing an additional protein confidence false discovery rate $<5\%$ (target/decoy concatenated search validation). Quantification of proteins, after precursor recalibration, was based on intensity values (at RT apex) for all unique peptides per protein. Peptide abundance values were normalized to the total peptide amount. The protein abundances were calculated summing the abundance values for admissible peptides. To compare proteins in EVs and lysate, the final protein ratio was calculated using median abundance values of five biological replicates each. The statistical significance of the ratio change was tested with ANOVA. *P* values were adjusted for multiple testing by the Benjamini-Hochberg correction. Proteins

with an adjusted P value <0.05 were deemed significant. To generate the heatmaps using open source programming language R (Team, 2021), mass spectrometric data were first filtered to include only proteins that were detected in at least three of five biological replicates of the CD9- or CD63-positive EV fractions of neurons or Müller cells. Moreover, proteins had to be enriched by 1.25 fold in the respective EV sample compared to the corresponding lysate. To generate an abundance heatmap, normalized abundance values were log₂-transformed and the Manhattan distances between the samples and proteins, respectively, were calculated. Using hierarchical clustering with the ward.D2 method, dendrograms were generated that were separated in 11 clusters for the proteins and two clusters for the samples. The heatmap itself including annotations was created with the pheatmap package (<https://cran.r-project.org/web/packages/pheatmap/index.html>). The smaller 11 clusters were then combined into four major clusters, for which gene enrichment analysis was performed using g:Profiler (ordered query, g:SCS threshold of a P -value <0.05) (Raudvere et al., 2019). Venn diagrams were created using R (Team, 2021) with proteins showing a more than 2-fold increase in the respective CD9- or CD63-positive EV fraction compared to corresponding cell lysates prepared in parallel. Proteins were ranked based on abundance values in respective CD9- or CD63-positive EV fractions relative to values in cell lysates. To highlight established EV markers, protein data were downloaded from the Vesiclepedia website (version 4.1) (Pathan et al., 2019) and restricted to components that were detected by at least three independent experimental approaches.

2.14 | Immunogold labelling of retinae and transmission electron microscopy

Retinae were fixed (PFA 4%, glutaraldehyde 0.1% in PBS at pH 7.4 for 1h at RT), washed in PBS, incubated with saponin (0.1% in PBS for 1h), and washed with BSA (2% in PBS, five times for 10 min each). Retina were incubated overnight at 4°C with an antibody against VAMP5 (1:100), CD63 (1:50) or CD9 (1:50; 0.1% BSA in PBS). After washing (2% BSA in PBS), retinae were incubated with ultrasmall nanogold F(ab') fragments of goat anti-rabbit or goat anti-mouse (1:100, 0.1% BSA in PBS; Aurion), rinsed (0.1% BSA in PBS) and then washed in PBS and water. Gold particles were silver-enhanced using the R-Gent SE-EM kit (Aurion, Wageningen, Netherlands). For double-immunogold labelling, retinae were washed again several times in distilled water and phosphate buffer (PB; 0.1M NaH₂PO₄; pH 7.4), blocked (5% normal goat serum in PBS) and incubated overnight at 4°C with an additional antibody. After washing (5% normal goat serum in PBS), retinae were incubated with ultrasmall nanogold F(ab') fragments of goat anti-rat (1:100, 0.1% normal goat serum in PBS; Aurion). After several rinses in phosphate buffer, retina were fixed (2.5% glutaraldehyde in PB) and washed in PB and in distilled water. The second round of gold particles was silver enhanced using the R-Gent SE-EM kit (Aurion) until they showed distinct sizes from the first ones. Immunogold-labelled retinae were postfixed (0.5% OsO₄ in distilled water) for 15 min. Finally, samples were dehydrated in graded ethanol series and embedded in Embed 812 (EMS). Ultrathin sections were cut with an ultramicrotome (Leica), stained with uranyl acetate [1% (w/v) in 50% ethanol], and examined by transmission electron microscopy (TEM; Hitachi H7500 equipped with an AMT Hamamatsu digital camera).

2.15 | Electron microscopic analysis of EVs secreted in vitro

To determine the size and shape of EV-like material secreted by cultured Müller cells and neurons, corresponding CM was subjected to differential ultracentrifugation (600g for 10 min; 2000g for 30 min; 10,000g for 45 min; 100,000g for 2h) as described (Théry et al., 2006). Pellets of the last step were fixed (2% glutaraldehyde in PBS for 1h), dried overnight on glass coverslips (rinsed with distilled water, dehydrated in graded ethanol series, desiccated in hexamethyldisilazane, and air-dried before use), carbon-coated and examined by scanning electron microscopy (SEM) at 15kV (Hitachi S800). For electron microscopic inspection of immunogold-labelled EVs, immunoaffinity-purified material was fixed (4% PFA, 0.1% glutaraldehyde in PBS at pH 7.4 for 1h), washed (PBS), dried overnight on glass coverslips for scanning electron microscopy (SEM) or on formvar-carbon grids for TEM and washed (BSA 2% in PBS, five times for 10 min each). EV samples were incubated overnight at 4°C with antibodies against VAMP5 (1:100) and CD63 (1:50) or CD9 (1:50; 0.1% BSA in PBS), washed (2% BSA in PBS), and incubated for 1h with nanogold F(ab') fragments (1:100 in PBS with 0.1% BSA, Aurion) with different particle sizes and secondary antibodies (goat anti-rabbit: 40 nm for SEM and 5 nm for TEM; goat anti-mouse or goat anti-rat: 25 nm for SEM or 15 nm for TEM). After several rinses in PB, EVs were fixed in glutaraldehyde (2.5% in PB), washed in PB and postfixed in OsO₄ (0.5% in PB for 15 min). Finally, all samples were rinsed in distilled water, dehydrated in graded ethanol series, desiccated in hexamethyldisilazane, and air-dried. TEM samples were stained with uranyl acetate [1% (w/v) in distilled water] and examined (Hitachi H7500 equipped with an AMT Hamamatsu digital camera). For SEM analysis, immunogold-labelled samples were carbon-coated and examined at 15kV (Hitachi S800). Secondary electron and backscatter electron images were collected simultaneously by corresponding detectors.

2.16 | Statistical analysis

Statistical analyses were performed with indicated tests using GraphPad Prism software (version 7). In figures, significance levels are indicated by asterisks (*, $P < 0.05$; **, $P < 0.01$; ***, $P < 0.001$). Whiskers in figures indicate standard error of the mean.

3 | RESULTS

We explored vesicle-based communication by retinal Müller cells using adult mice as experimental model. As a first step, we determined which vesicle-associated membrane proteins (VAMPs) are expressed by retinal Müller cells *in vivo* using immunohistochemical staining of retinal sections. We focused on the VAMP family as these proteins are part of the SNARE complex, which mediates membrane fusion and thereby enables the cellular release of molecules and vesicles (Südhof & Rothman, 2009; Urbina & Gupton, 2020).

3.1 | Expression of selected VAMPs in retinal Müller cells and their post-ischemic upregulation

As shown in Figure 1a, each member of the VAMP family showed a distinct expression pattern in the adult mouse retina. Notably, we observed an overlap of cellubrevin/VAMP3, myobrevin/VAMP5 and VAMP8 with the Müller cell-specific markers GLUL or retinaldehyde binding protein 1 (RLBP1). On the other hand, VAMP1, 2, 7 were present in plexiform layers containing synaptic connections, whereas VAMP4 labelled cell somata in the ganglion cell and inner nuclear layer (Figure 1a). We validated the glial expression of VAMP3, 5 and 8 using independent experimental approaches (Figure 1b, c). Cell-specific transcript analyses by RNAseq and qRT-PCR using lysates of immunoaffinity-purified cells (Grosche et al., 2016; Pauly et al., 2019) corroborated our results obtained by immunohistochemical staining (Figure 1b). Müller cells expressed *Vamp3*, *Vamp5* and *Vamp8*, whereas *Synaptobrevin/Vamp2*, a component of synapses, was enriched in neurons indicating the validity of cell-specific profiles. We also examined the presence of VAMP proteins in immunoaffinity-purified cells by immunoblotting (Figure 1c) and its cellular distribution by immunocytochemical staining of acutely isolated Müller cells (Figure 1d). These experiments revealed that Müller cells express VAMP3 and VAMP5 and that both VAMPs show a punctate distribution indicating their presence in vesicle-like structures (Figure 1d). The validity of the VAMP5 antibody (Table S1) was indicated by previously published observations that VAMP5-deficient mice show strongly reduced signals in immunoblots and after immunohistochemical staining performed with the same antibody (Ikezawa et al., 2018). Moreover, our work revealed VAMP5 as a top-enriched protein in immunoprecipitated retinal lysates analysed by mass spectrometry (Data S1).

Glial cells react swiftly to injury and disease with prominent and context-specific changes in their expression profiles (Escartin et al., 2021; Pekny et al., 2016; Zamanian et al., 2012). To test whether expression levels of *Vamp3*, 5 and 8 in Müller cells change during gliosis, we used an established model of transient retinal ischemia (Pannicke et al., 2014; Wagner et al., 2016). We observed several-fold increases of these glia-specific *Vamp* transcripts in acutely isolated, immunoaffinity-purified Müller cells from ischemic retinae compared to cells from control tissue of contralateral eyes (Figure 2a). Immunohistochemical staining revealed that transient ischemia enhanced levels of VAMP3 in processes of Müller cells in the plexiform layers and in structures located in the layer containing photoreceptor segments. VAMP5 levels rose in both plexiform layers and at the external limiting membrane. VAMP8 expression increased across all plexiform layers. (Figure 2b). Transcript levels of other members of the VAMP family were not altered. Taken together, these results showed that Müller cells express a subset of VAMPs, whose levels increase under pathologic conditions.

3.2 | Presence of VAMP5 in multivesicular bodies of retinal Müller cells and in the extracellular space facing the internal and external limiting membranes *in vivo*

The unexpectedly strong expression of VAMP5 in Müller cells prompted us to focus on this member of the VAMP family and to scrutinize its subcellular distribution using TEM. To facilitate comprehension of electron micrographs, morphologic features of Müller cells and their location with respect to the different retinal layers are shown schematically (Figure 3a) together with representative transmission electron micrographs of their compartments in the inner and outer retina (Figure 3b). Immunogold staining of retinal sections combined with TEM corroborated the presence of VAMP5 in Müller cells (Figure 4). We detected the protein in distinct intracellular structures resembling vesicles and multivesicular bodies. These structures were located in endfeet of Müller cells and in their radial processes apposed to the external limiting membrane (ELM) of the outer retina

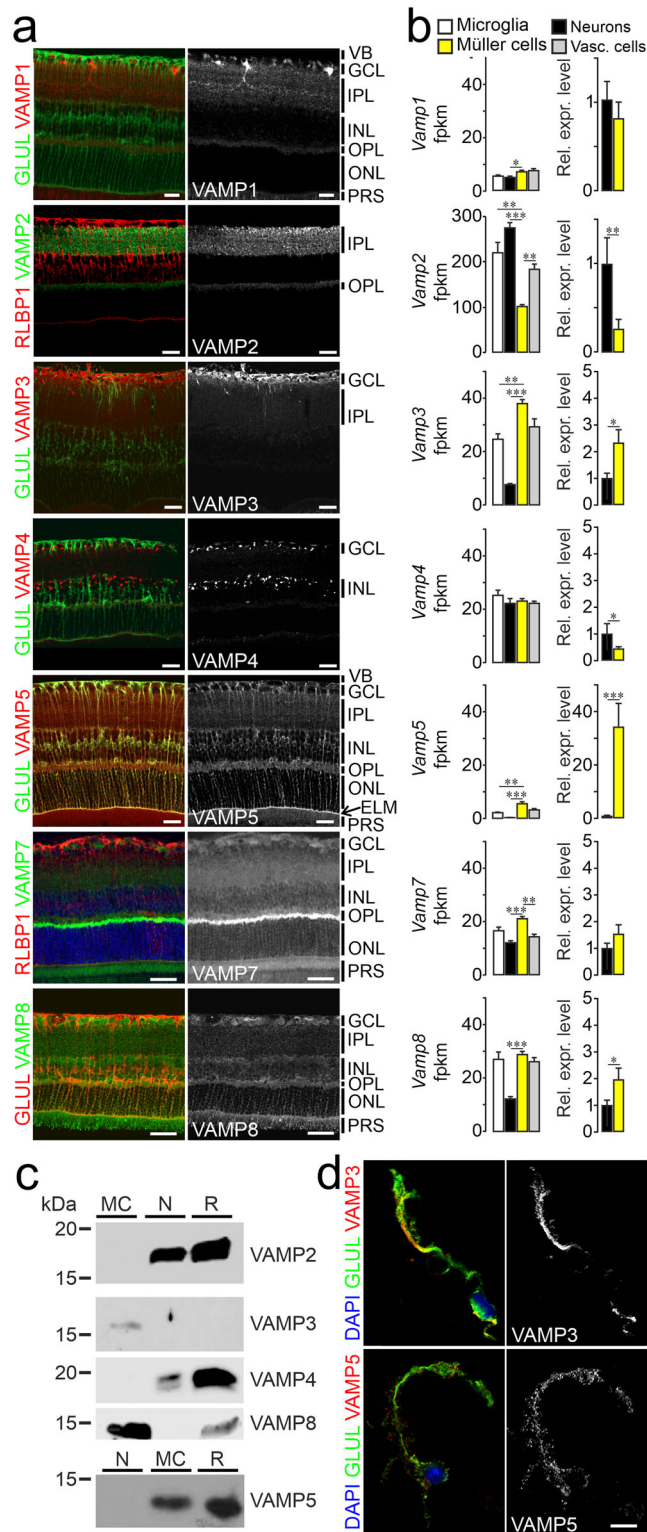


FIGURE 1 Expression of VAMP3, 5 and 8 by retinal Müller cells (a) False-colour and greyscale confocal micrographs of retinal sections from adult mice subjected to double-immunohistochemical staining of the indicated VAMPs and of the Müller cell markers GLUL and RLBPI. Positions of selected ocular structures and retinal layers are indicated: VB, vitreous body; GCL, ganglion cell layer; IPL, inner plexiform layer; INL, inner nuclear layer; OPL, outer plexiform layer; ONL, outer nuclear layer; ELM, external limiting membrane (arrow); PRS, photoreceptor segments. Scale bars: 20 μm . (b) Left, average counts of indicated *Vamp* transcripts obtained by RNAseq from lysates of indicated types of acutely isolated, immunoaffinity-purified retinal cells ($n = 3-4$ preparations; Mann-Whitney test; whiskers indicate SEM). Fpkkm, fragments per kilobase million. Right, mean relative expression levels of indicated *Vamps* in Müller cells compared to neurons. (c) Representative immunoblots showing the presence of selected VAMPs in indicated populations of acutely isolated immunoaffinity-purified retinal cells (MC, Müller cells; N, neurons; R, retinal lysates). For each protein tested, equal amounts of total protein from indicated samples were loaded. (d) False-colour and greyscale micrographs of acutely isolated immunoaffinity-purified Müller cells subjected to nuclear (blue) and double-immunocytochemical staining of VAMP3 and VAMP5 (red) and GLUL (green). Scale bar: 10 μm .

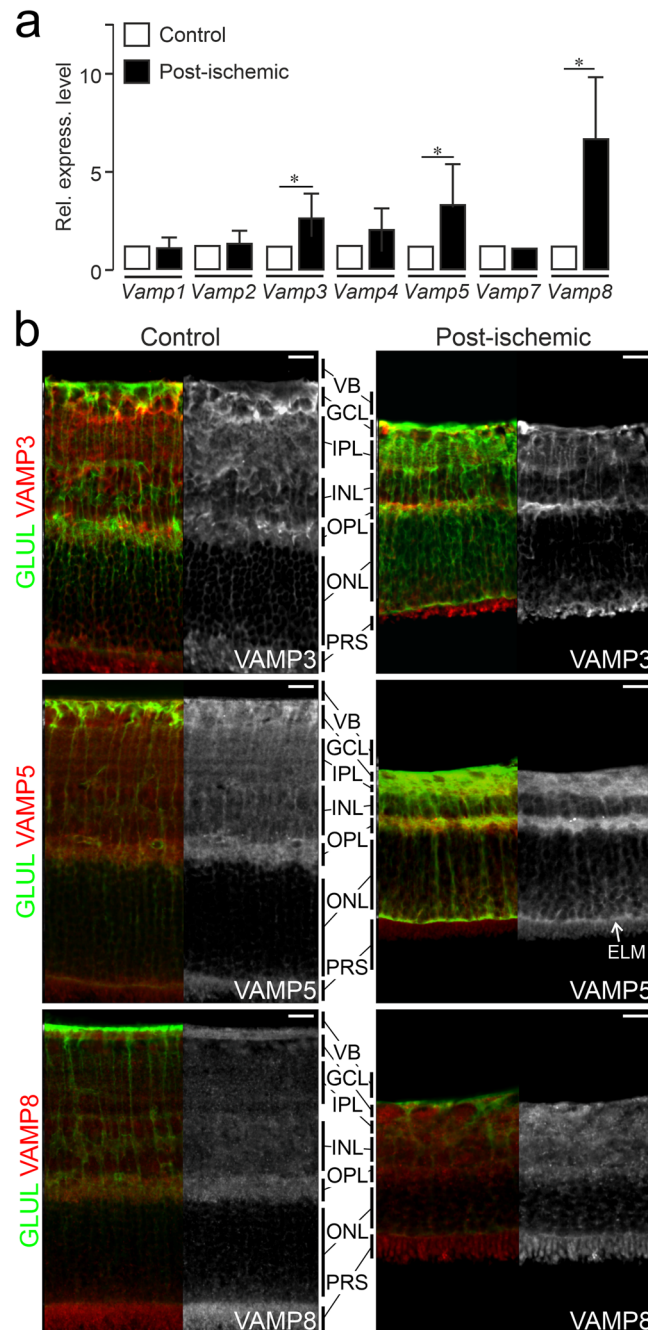


FIGURE 2 Ischemia-induced increase of *Vamp3*, *Vamp5* and *Vamp8* expression in retinal Müller cells (a) Mean relative levels of indicated transcripts as determined by qRT-PCR in acutely isolated, immunoaffinity-purified Müller cells from retinæ at 7 days after transient ischemia (post-ischemic). Levels were normalized to those in Müller cells isolated from untreated control eyes ($n = 3$ preparations; whiskers indicate SEM; Mann-Whitney test). (b) False-colour and greyscale confocal micrographs of retinal sections from control eyes and from eyes at 7 days after transient ischemia followed by double-immunohistochemical staining of the indicated VAMPs (red) and of GLUL-positive Müller cells (green). VB, vitreous body; GCL, ganglion cell layer; IPL, inner plexiform layer; INL, inner nuclear layer; OPL, outer plexiform layer; ONL, outer nuclear layer; ELM, external limiting membrane; PRS, photoreceptor segments. Scale bar: 20 μm .

(Figure 4). Interestingly, we also observed VAMP5-positive vesicle-like structures on the extracellular side of the internal limiting membrane facing the vitreous body and around apical microvilli of Müller cells reaching into the subretinal space surrounding photoreceptor segments (Figure 4). Together, our ultrastructural observations revealed the presence of VAMP5 in vesicular structures located in the cytoplasm of Müller cells and in the extracellular space facing the internal and external limiting membrane in vivo.

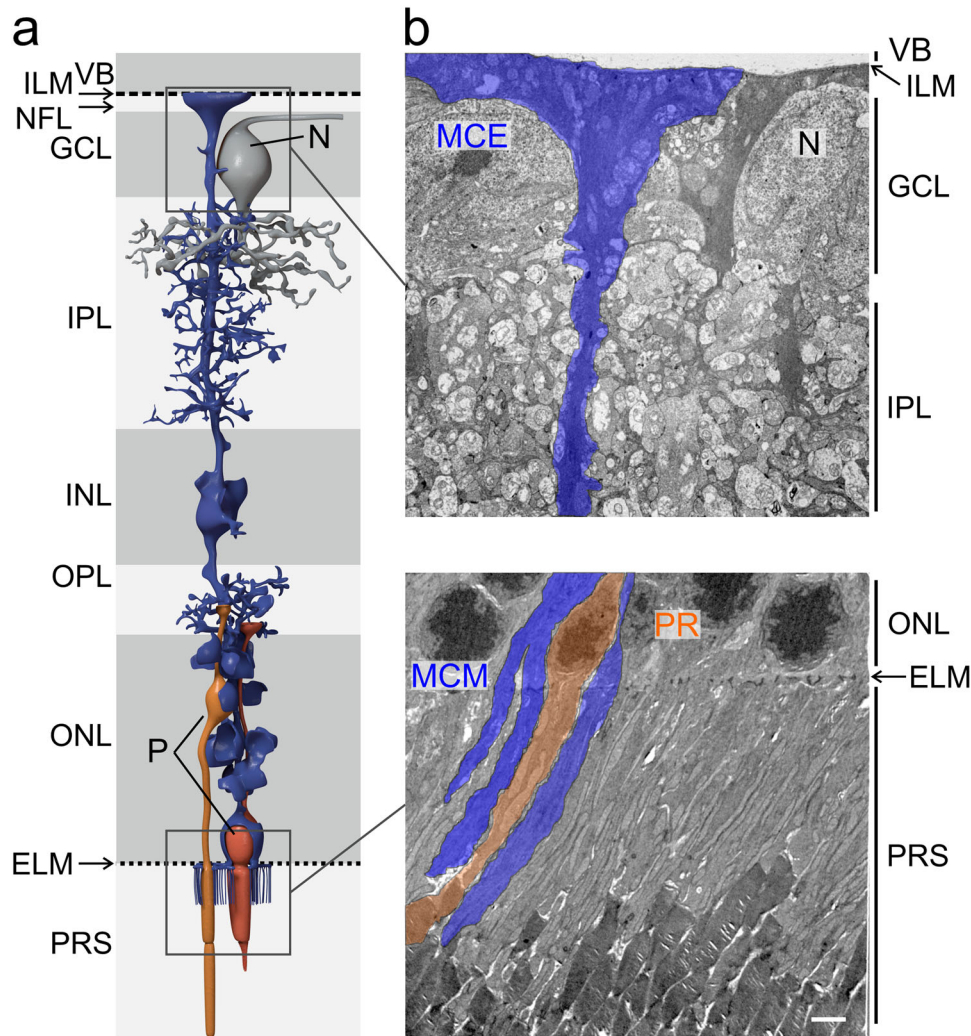


FIGURE 3 Location of Müller cells and ultrastructure of selected compartments in the inner and outer retina. (a) Schematic representation of a Müller cell and its position with respect to the different layers of the mouse retina. VB, vitreous body; ILM, internal limiting membrane; NFL, nerve fiber layer; GCL, ganglion cell layer; N, soma of a neuron; IPL, inner plexiform layer; INL, inner nuclear layer; OPL, outer plexiform layer; ONL, outer nuclear layer; ELM, external limiting membrane; P, soma of a photoreceptor; PRS, photoreceptor segments. (b) Representative transmission electron micrographs showing layers of the inner (top) and outer (bottom) retina and the location of Müller cell elements. In the inner retina (top), endfeet of Müller cells (MCE) face the vitreous body (VB), form the inner limiting membrane (ILM) and surround large somata of neurons (N) in the ganglion cell layer (GCL). Their processes traverse and interweave the inner plexiform layer (IPL; top). In the outer retina (bottom), Müller cell processes traverse the outer nuclear layer (ONL) containing nuclei (P) of photoreceptors (PR) and send apical microvilli (MCM) from the external limiting membrane (ELM) into the subretinal space where they interweave with photoreceptor segments (PRS). Scale bar: $2\ \mu\text{m}$.

3.3 | Presence of EV markers in specialized domains of retinal Müller cells

Our ultrastructural findings raised the question whether VAMP5 is associated with EVs secreted by Müller cells. To explore this, we studied the distribution of CD81 (TSPAN28), CD9 (TSPAN29) and CD63 (TSPAN30) in Müller cells. These transmembrane proteins are ubiquitously expressed members of the tetraspanin family, located in distinct cellular compartments and contained in distinct types of EVs (Escola et al., 1998; Théry et al., 1999; Théry et al., 2018). Immunohistochemical and -cytochemical detection of the selected tetraspanins in retinal sections (Figure 5a) and in acutely isolated immunoaffinity-purified Müller cells (Figure 5b), respectively, revealed a distinct distribution of each protein along GLUL-positive Müller cells. The cell surface component CD9 decorated their endfeet facing the vitreous body, structures in the outer plexiform layer and notably their apical microvilli extending into the subretinal space (Figure 5a). CD81 was strongly expressed in the outer plexiform layer and on apical microvilli of Müller cells. CD63, which is also present in the endosomal-lysosomal system (Escola et al., 1998; Kobayashi et al., 2000; Pols & Klumperman, 2009), showed a distinct distribution. This protein was present in the endfeet of Müller cells and nearly absent from their apical microvilli (Figure 5a). Inspection of acutely isolated Müller cells showed limited overlap of CD9 and CD81 and some colocalization of CD9 and CD63 (Figure 5b). CD9 and CD63 also showed punctate staining not

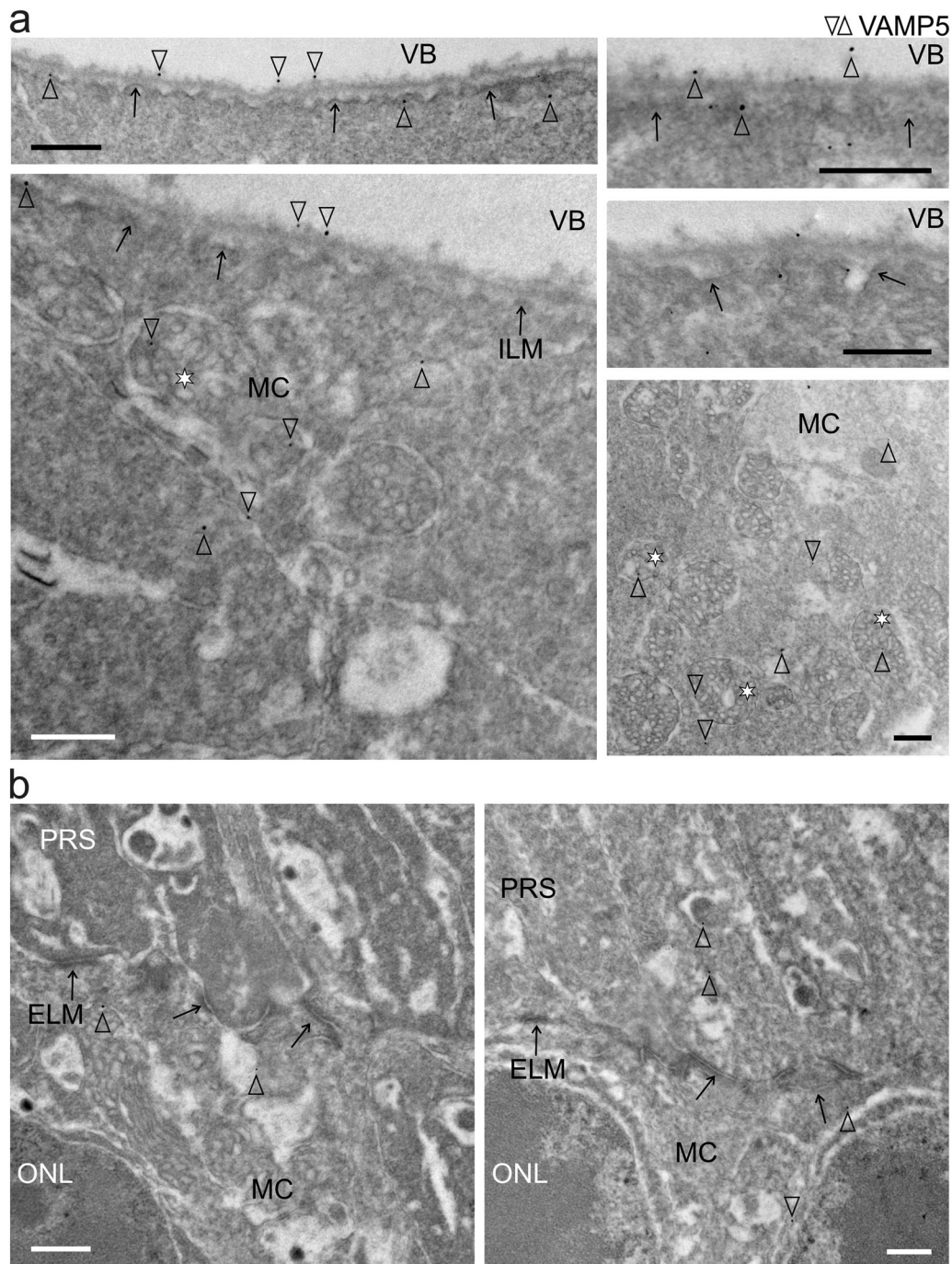


FIGURE 4 Subcellular and extracellular location of VAMP5 in the retina (a) Transmission electron micrographs of the inner retina showing the presence of VAMP5 (empty arrowheads) in endfeet of Müller cells (MC), notably in multivesicular bodies (asterisks), at the intra- and extracellular side of the internal limiting membrane (ILM, black arrows) and in the vitreous body (VB). (b) Electron micrographs of the outer retina showing the presence of VAMP5 in processes of Müller cells (MC) in the outer nuclear layer (ONL) and on their apical microvilli extending beyond the external limiting membrane (ELM, black arrows) into the subretinal space containing photoreceptor segments (PRS). Retinal sections were subjected to immunogold labelling of VAMP5. Selected nanogold particles are indicated by empty arrowheads. Scale bars: 500 nm.

associated with GLUL (Figure 5a) raising the question whether these proteins were expressed by other types of retinal cells. To address this question, we compared expression levels between retinal cell types using transcriptome (RNAseq) and proteome (mass spectrometry) analyses of acutely isolated and immunoaffinity-purified cells (Figure 6). For each tetraspanin tested, transcript and protein levels were highest in Müller cells compared to other cells with the notable exception of CD81, which was also

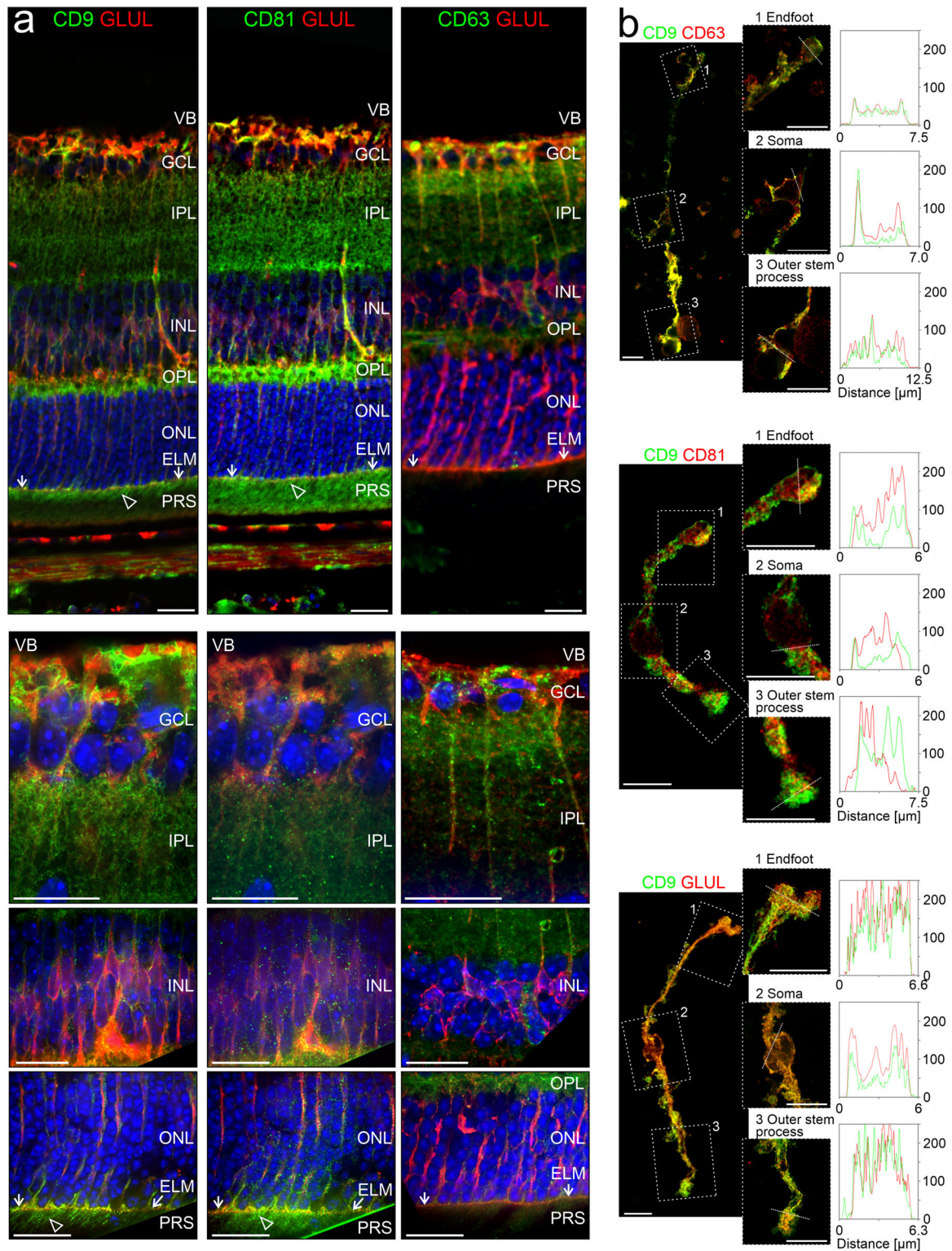


FIGURE 5 Distribution of EV markers in the retina (a) False-colour confocal micrographs of retinal sections subjected to double-immunohistochemical staining of GLUL-positive retinal Müller cells and of the tetraspanins CD9, CD81 or CD63. Empty arrowheads indicate presence of CD9 and CD81 on apical microvilli of Müller cells extending beyond the external limiting membrane (ELM, white allows) in the subretinal space containing photoreceptor segments (PRS). VB, vitreous body; GCL, ganglion cell layer; IPL, inner plexiform layer; INL, inner nuclear layer; OPL, outer plexiform layer; ONL, outer nuclear layer; RPE, retinal pigment epithelium. Scale bars: 20 μm . (b) False-colour confocal (left) and STED (right) micrographs of acutely isolated, immunoaffinity-purified Müller cells showing entire cells and selected compartments, indicated by rectangles, at higher magnification. The terms “endfoot” and “outer stem process” indicate the Müller cell compartments that are apposed to the internal and external limiting membrane in the intact retina, respectively. Fixed cells were subjected to double-immunocytochemical staining of CD9, CD63 or CD81 and of GLUL. Scale bars: 10 μm . Plots show fluorescence intensities [in analog-digital units] of respective proteins across the selected compartments with the location of the line scans indicated by white dashed lines.

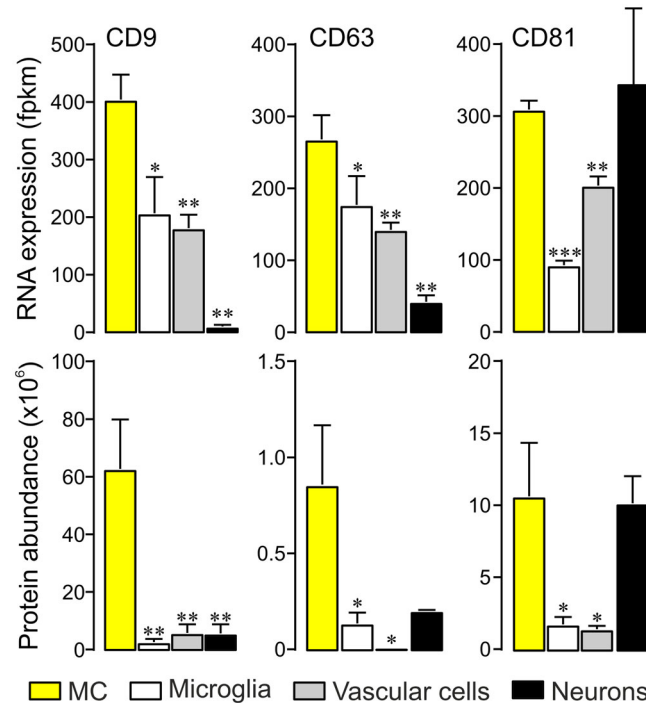


FIGURE 6 Cell-specific expression of tetraspanins in selected retinal cells Transcript (top) and protein levels (bottom) of indicated tetraspanins in acutely isolated immunoaffinity-purified retinal cells ($n = 3-5$; whiskers: SEM; Mann-Whitney test) as determined by RNAseq and mass spectrometry, respectively. Fpkm, fragments per kilobase million. MC, Müller cells.

abundant in neurons (Figure 6). Taken together, these results revealed a domain-specific presence of the selected tetraspanins with CD63 expressed on Müller cell endfeet facing the vitreous body, and CD9 and CD81 strongly present on apical microvilli of Müller cells extending into the subretinal space.

3.4 | Ultrastructural and molecular characterization of EVs secreted by Müller cells in vitro

Our observations in vivo suggested that Müller cells secrete EVs. Among the tetraspanins detected in the retina, we focused on CD63 and CD9 given their strong expression by glial cells, and their presence in Müller cell endfeet and microvilli representing highly specialized compartments of these cells. To characterize glia-derived EVs, we purified Müller cells from retinal cell suspensions by immunomagnetic separation, cultured them for maximally 60h under chemically defined, serum-free conditions and prepared secreted material contained in CM as outlined below. For comparison, we also analysed material in CM of affinity-purified retinal neurons. To determine cell viability during the indicated culture periods, we first performed TUNEL assays. This approach revealed absence of TUNEL-positive in GLUL-positive Müller cells indicating high viability of Müller cells. Among GLUL-negative cells representing in part neurons, a fraction of cells was TUNEL-positive indicating a lower, but stable viability of these cells during the culture period (Figure 7a). Next, we characterized material secreted by retinal Müller cells and neurons by established methods (Théry et al., 2018). As first step, we enriched EV-like material contained in Müller cell- and neuron-derived CM by differential ultracentrifugation (Théry et al., 2006) and inspected its form and size by SEM. We observed round, vesicle-like structures (Figure 7b) with diameters between 30 and 150 nm (Figure 7c, top panel), which is within the established size range of EVs. Independent information about the size of these structures was obtained by NTA, which also informed about particle concentrations (Figure 7c, bottom panel). To this end, we enriched material secreted by cultured Müller cells and neurons by immunomagnetic separation of CM using an antibody against CD9. These samples showed a narrower size range than the ultracentrifugation-enriched material inspected by SEM probably due to the immunoaffinity-based selection (Figure 7c). Notably, NTA revealed a ~1000-fold higher concentration of particles in affinity-purified samples compared to CM thus indicating efficient enrichment of EV-like material (Figure 7c, insert). We next probed whether Müller cells secrete VAMP5. To this end, we purified CD63- and CD9-positive material from Müller cell- and neuron-derived CM and subjected the samples to immunoblotting. Flow-through lacking EVs and cell or retinal lysates served as negative and positive controls, respectively. This approach revealed the presence of VAMP5 – albeit at low levels – in CD9-positive material secreted by Müller cells, but not in material secreted by neurons and not in CD63-positive material from either cell population probably due to limited quantities

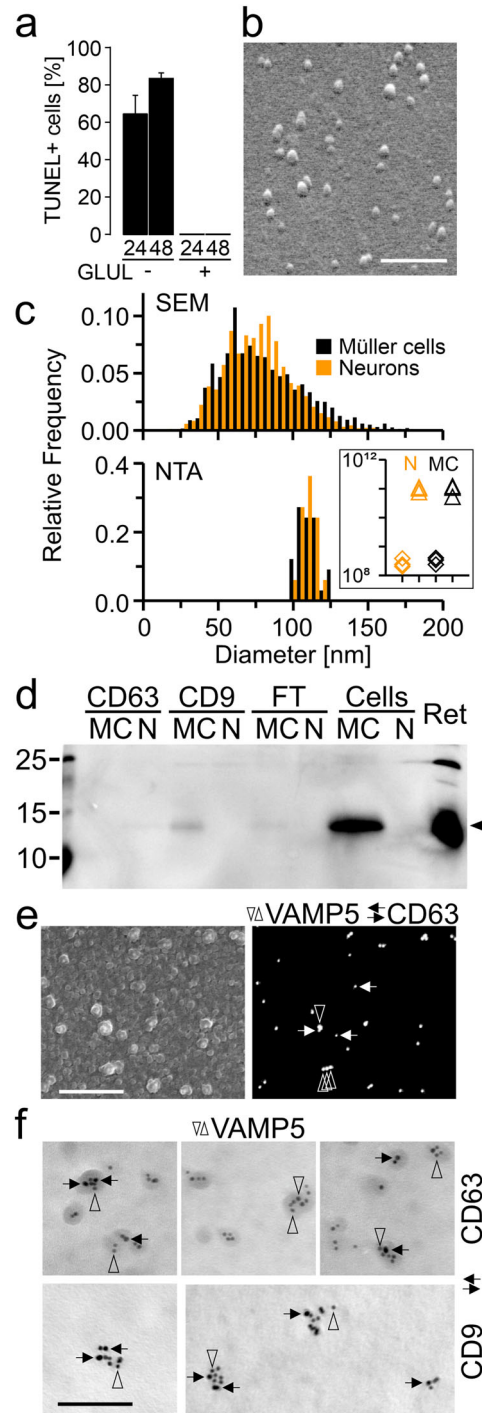


FIGURE 7 Characterization of EVs secreted by Müller cells in vitro (a) Cell death among GLUL-positive Müller cells and GLUL-negative neurons after indicated periods (in hours) in serum-free culture estimated by TUNEL staining. Note the absence of TUNEL-positive cells in cultures of GLUL-positive cells. (b) Scanning electron micrograph of vesicle-like structures released by immunoaffinity-purified Müller cells cultured for 60h under serum-free conditions. Secreted material contained in CM was enriched by ultracentrifugation prior to processing for SEM. Scale bar: 600 nm. (c) Diameters of vesicle-like structures shown in (b) as determined by SEM (top; $n = 3091 / 2361$ particles from neurons / Müller cells; $n = 3$ culture preparations each; 10 images each preparation) and of CD9-positive EVs determined by NTA (bottom; $n = 3$ independent cultures). Orange and black bars indicate neuronal and glia-derived material, respectively. Insert, particle concentration per mL in CM (diamonds) and immunoaffinity-purified EV samples (triangles) from neurons (N, orange) and Müller cells (MC, black). (d) Immunoblots probing the presence of VAMP5 in CD63- or CD9-positive EVs secreted by cultured Müller cells (MC) and neurons (N), in the flow-through (FT), in cell lysates (Cells) and in the retina (Ret). (e) Scanning electron micrographs of secondary (left) and backscatter electrons (right) showing the surface and proteins, respectively of EVs immunoaffinity purified from CM of Müller cells and subjected to double-immunogold labelling of VAMP5 (vertical empty arrowheads; 40 nm) and CD63 (horizontal black arrows; 25 nm) using gold nanoparticles of different sizes. Scale bar: 750 nm. (f) Transmission electron micrographs showing colocalization of indicated proteins on affinity-purified EVs secreted by Müller cells in vitro. Ultrathin sections were subjected to double-immunogold labelling of VAMP5 (vertical empty arrowheads) and of CD63 or CD9 (horizontal black arrows) using gold nanoparticles of different sizes (VAMP5/CD9: 5/10 nm; VAMP5/CD63: 10/5 nm). Scale bar: 100 nm.

(Figure 7d). To test directly whether VAMP5 is present on EV-like structures, we subjected CD9- and CD63-positive material secreted by cultured Müller cells to double-immunogold staining followed by SEM or TEM. Electron microscopic inspection revealed the colocalization of VAMP5 with CD63 and with CD9 on EV-like structures (Figure 7e,f).

3.5 | Distinct proteomic profiles of CD9- and CD63-positive EVs secreted by neurons and Müller cells in vitro

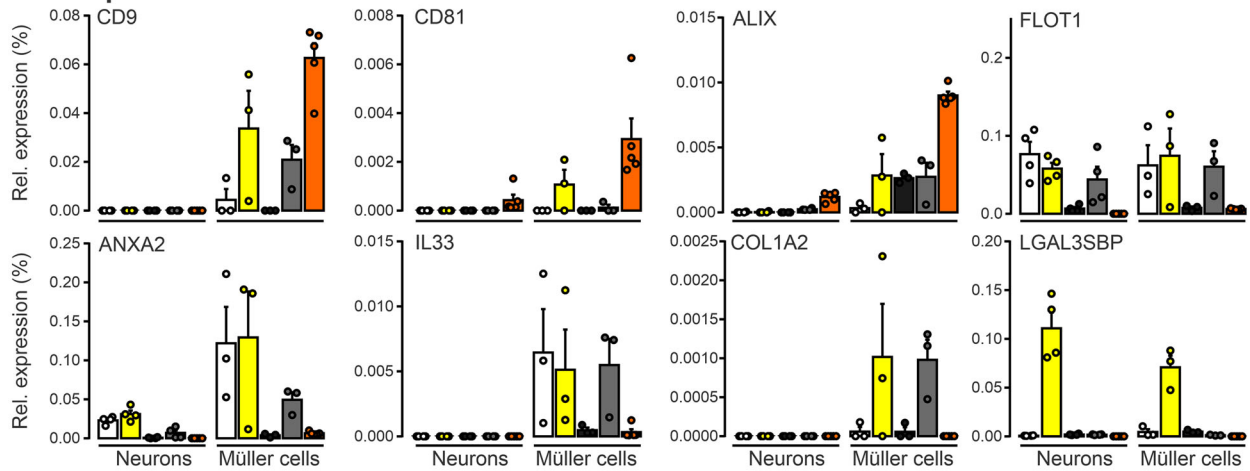
We next determined the protein composition of immunoaffinity-purified material secreted by Müller cells and neurons in serum-free primary cultures using label-free mass spectrometry (Figure 8). As controls, we analysed the protein content of non-binding flow-through of CM and of lysates of cultured and of acutely isolated cells, each from Müller cells and neurons (Figure 8). The mass spectrometric data revealed an enrichment of established (CD9, CD81, ALIX, FLOT1, ANXA2) and of more specific EV components (COL1A2: Velázquez-Enríquez et al., 2021; LGALS3BP: Luga et al., 2012) in the CD9- and CD63-affinity purified samples compared to flow-through of media and to cell lysates (Figure 8). On the other hand, proteins of organelles unrelated to EVs were only present in lysates, but absent from secreted material (Figure 8). This observation excluded the presence of contaminating material and indicated the quality of our EV preparations. Glial and neuronal markers were enriched in the respective lysates confirming their cell-specific origin (Figure 8). Among these proteins, the cytoplasmic components GLUL and MAPIB were also present in material immunoaffinity-purified from CM (Figure 8). To explore the cell- and subtype-specific protein composition of presumed EVs, abundance values of proteins were subjected to hierarchical clustering (Figure 9). The resulting sample clusters (columns) recapitulated the experimental groups indicating distinct compositions of neuron- and glia-secreted material and differences among CD9- and CD63-positive EV samples. The approach assigned proteins detected in EV samples (rows) to four principal groups (Figure 9): Cluster 1 and cluster 2 contained either Müller cell- or and neuron-specific components, respectively. Two additional clusters contained proteins that were expressed in both neurons and Müller cells at high levels (Cluster 3) and at distinct levels (Cluster 4) across all experimental groups. Notably, all clusters contained EV components as shown by GO term analysis (Figure 9). To further explore the diversity of glia- and neuron-derived EVs, we compared the protein contents of CD9- and CD63-positive material in CM from Müller cells and from neurons. As shown in Figure 10(a), between 59% and 64% of proteins detected in EV-like structures secreted by Müller cells or neurons were non-overlapping and thus specific to the cell of origin. The fraction was similarly large in CD9- and CD63-positive material. This finding indicated that neurons and Müller cells secrete EVs with partially distinct protein contents. A comparison of proteins in CD9- and CD63-positive EVs from neurons and Müller cells revealed 80% and 60% overlap, respectively (Figure 10b) indicating that the two populations of EVs secreted by glial cells have a more distinct protein content than those secreted by neurons. A comparison of our proteomic data with entries in the Vesiclepedia database (Pathan et al., 2019) revealed that half of the proteins detected in neuron- and Müller cells-derived EVs are established markers (Figure 10). Notably, we found CD81 and diazepam binding inhibitor (DBI) exclusively in CD9-positive EVs from Müller cells, whereas the fibrinogen beta chain (FGB) was only detected in their CD63-positive counterparts. The EV component galectin 3 binding protein (LGALS3BP) was present in neuronal and Müller cell-derived CD9-positive EVs (Figure 10). Among the new proteins strongly enriched in Müller-derived EVs are centrosomal protein 290 (CEP290) and carbonic anhydrase (CA3). Taken together, our findings revealed that immunoaffinity-purified Müller cells secrete EVs in vitro that have a distinct protein composition from those secreted by neurons. Moreover, CD9- and CD63-positive EVs from Müller cells show limited protein overlap indicating distinct subsets.

3.6 | Colocalization of VAMP5 with tetraspanins in the extracellular space of the inner and outer retina in vivo

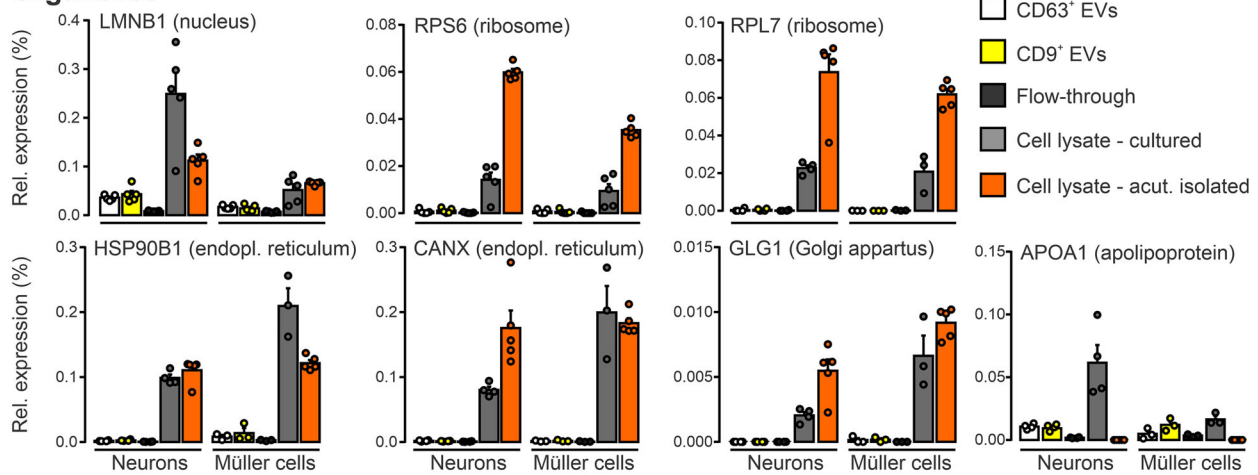
Our finding that VAMP5 and selected tetraspanins are present on EV-like material secreted by Müller cells in vitro prompted us to examine their colocalization on extracellular structures in retinae in vivo using light and electron microscopy. Immunohistochemical staining of retinal sections revealed an overlapping distribution of VAMP5 with CD63 at Müller cell endfeet (Figure 11a) and with CD9 in apical microvilli (Figure 11b). The apposition of CD63 and VAMP5 in Müller cell endfeet was corroborated by super-resolution light microscopy (Figure 11c, d). The post-ischemic increase of VAMP5 expression (Figure 2) prompted us to test whether induction of transient ischemia affected the distribution of VAMP5 and CD9 at two distinct time points. Previous reports showed already an increase of retinal CD9 at 7 days post-injury (Iwagawa et al., 2020; Vázquez-Chona et al., 2004) similar as reported here for VAMP5 after induction of ischemia (Figure 2). Ischemia induced time-dependent changes in the distribution of CD9 and VAMP5 in layers of the inner (Figure 12a) and outer (Figure 12b) retina. CD9 showed a more increased presence on plasma membranes, especially in apical microvilli of Müller cells, whereas VAMP5 showed a more wide-spread expression in post-ischemic retinae (Figure 12).

Our light microscopic observations indicated overlap of VAMP5 and of tetraspanins in specialized domains of Müller cells situated in the inner and outer retina, but we could not distinguish intra- and extracellular structures. To address this crucial

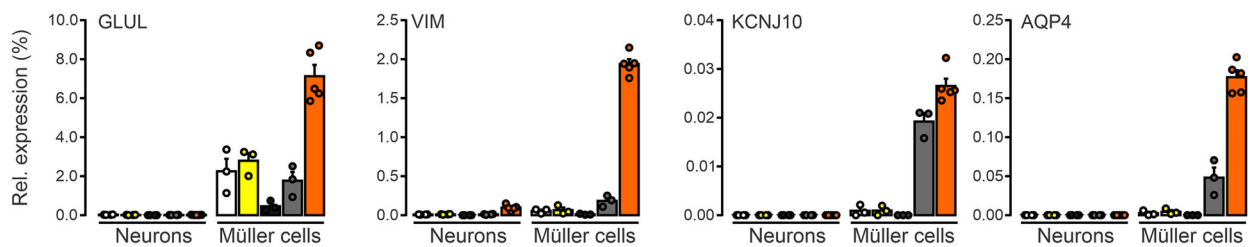
EV components



Organelles



Müller cells



Neurons

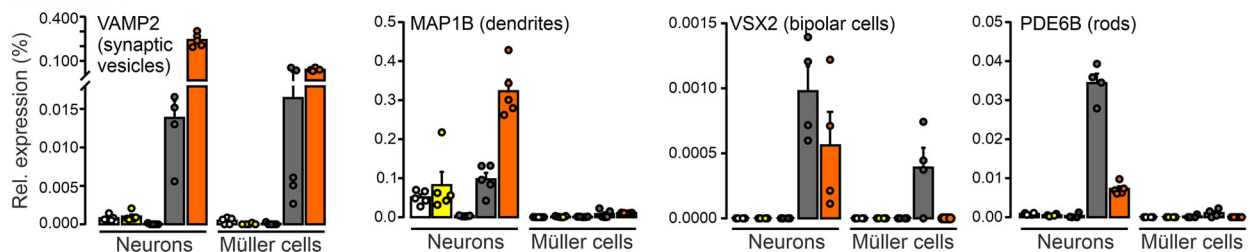


FIGURE 8 Presence of established markers in EVs secreted by Müller cells and neurons in vitro. Relative expression levels of selected proteins contained in EVs, organelles, Müller cells and neurons in CD9- and CD63-positive EVs purified from CM, in material of the flow-through, and in lysates of cultured and of acutely isolated neurons and Müller cells determined by mass spectrometry. Protein levels were normalized to total abundance of protein detected in respective samples. Symbols represent individual preparations. Bars and whiskers represent average values and SEM, respectively ($n = 5$ preparations).

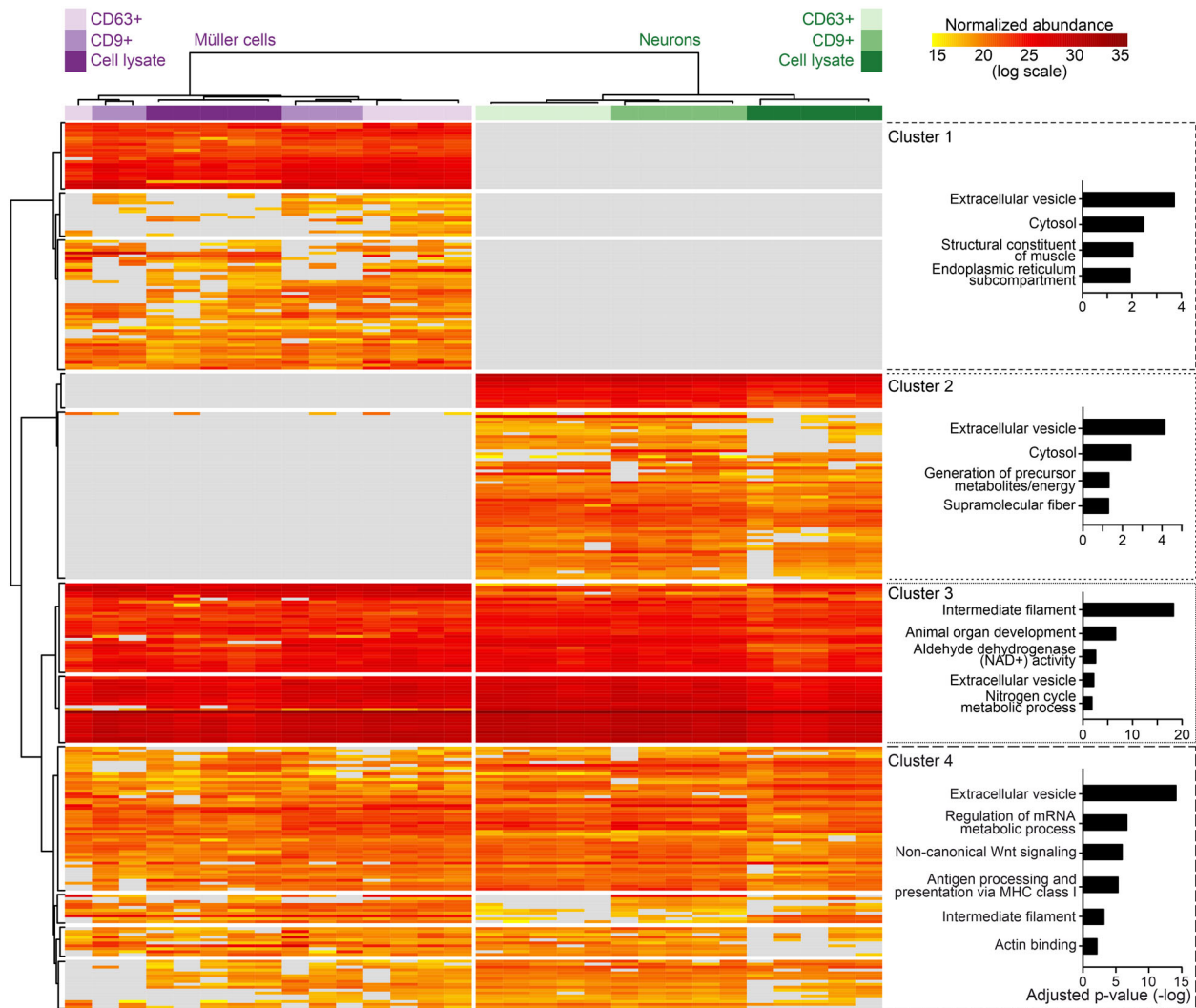


FIGURE 9 Protein profiles of CD9- and CD63-positive EVs from Müller cells and neurons Heatmap showing the normalized abundances of proteins detected in EVs by mass spectrometry and dendrograms showing grouping of columns (experimental conditions) and of rows (proteins) generated by unsupervised hierarchical clustering. Plots on the right show GO terms in four largest protein clusters and respective adjusted P values.

point, we performed double-immunogold labelling of respective proteins in ultrathin retinal sections using gold nanoparticles of distinct sizes (to facilitate orientation see also Figure 3b). TEM inspection revealed close apposition of VAMP5 and CD63 in the extracellular space forming the vitreous body suggesting their presence on vesicle-like structures (Figure 13a). Notably, we observed regularly vesicle-like structures decorated with VAMP5 and CD9 in the extracellular space intercalated between photoreceptor segments and Müller cell microvilli at variable distance from the external limiting membrane (Figure 13b).

4 | DISCUSSION

Our study provides first evidence that Müller cells release distinct EV-like structures from specialized compartments in the inner and outer retina of adult mice. Until now, EVs have mainly been studied after isolation from biological fluids or cell culture media. Here, we report their detection in an intact biological tissue *in vivo*, which has represented a key challenge in the field (Van Niel et al., 2022; Verweij et al., 2021). Previously, EVs have been found in various ocular structures and fluids including acutely isolated retinae from mice (Mighty et al., 2020; Wooff et al., 2020), liquid biopsies of the human vitreous body (Zhao et al., 2018) and aqueous humour (Hsiao et al., 2021), the conjunctival mucin layer of rats (Tendler & Panshin, 2020), the retinal pigment epithelium of aged mice (Wang et al., 2009) and drusen of patients with age-related macular degeneration (Grillo et al., 2021). However, the cellular origin of these EVs remained unclear. Our findings point to Müller cells as a source of EVs in the retina and indicate that the release occurs at two prominent compartments of these cells. Müller cells are highly polarized showing

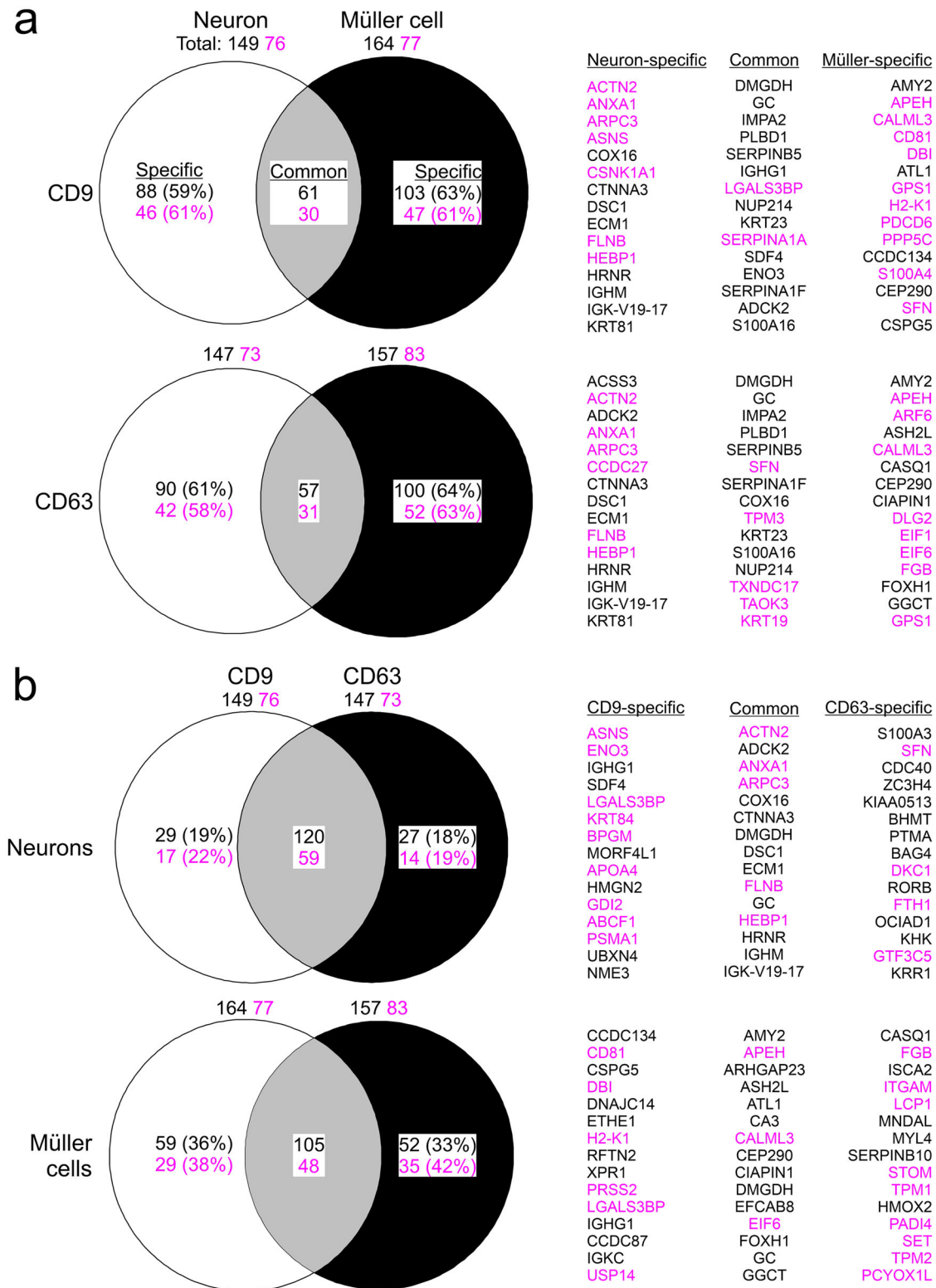


FIGURE 10 Diversity of neuron- and Müller cell-derived EVs based on protein content Venn diagrams showing differences and overlaps in protein content between neurons and Müller cells for CD9- (top) and CD63-positive (bottom) EVs (a) and between CD9- and CD63-positive EVs from neurons (top) and from Müller cells (bottom) (b). Numbers indicate counts of all proteins that were detected in respective samples (total), that were present in both samples (common) and that were only present in either sample (specific). Indicated percentages were calculated compared to total number of detected proteins. Names of specific and common proteins showing highest enrichment in EVs compared to lysate (top 15) are indicated on the right. Numbers and names in magenta highlight established EV components listed in the Vesiclepedia database.

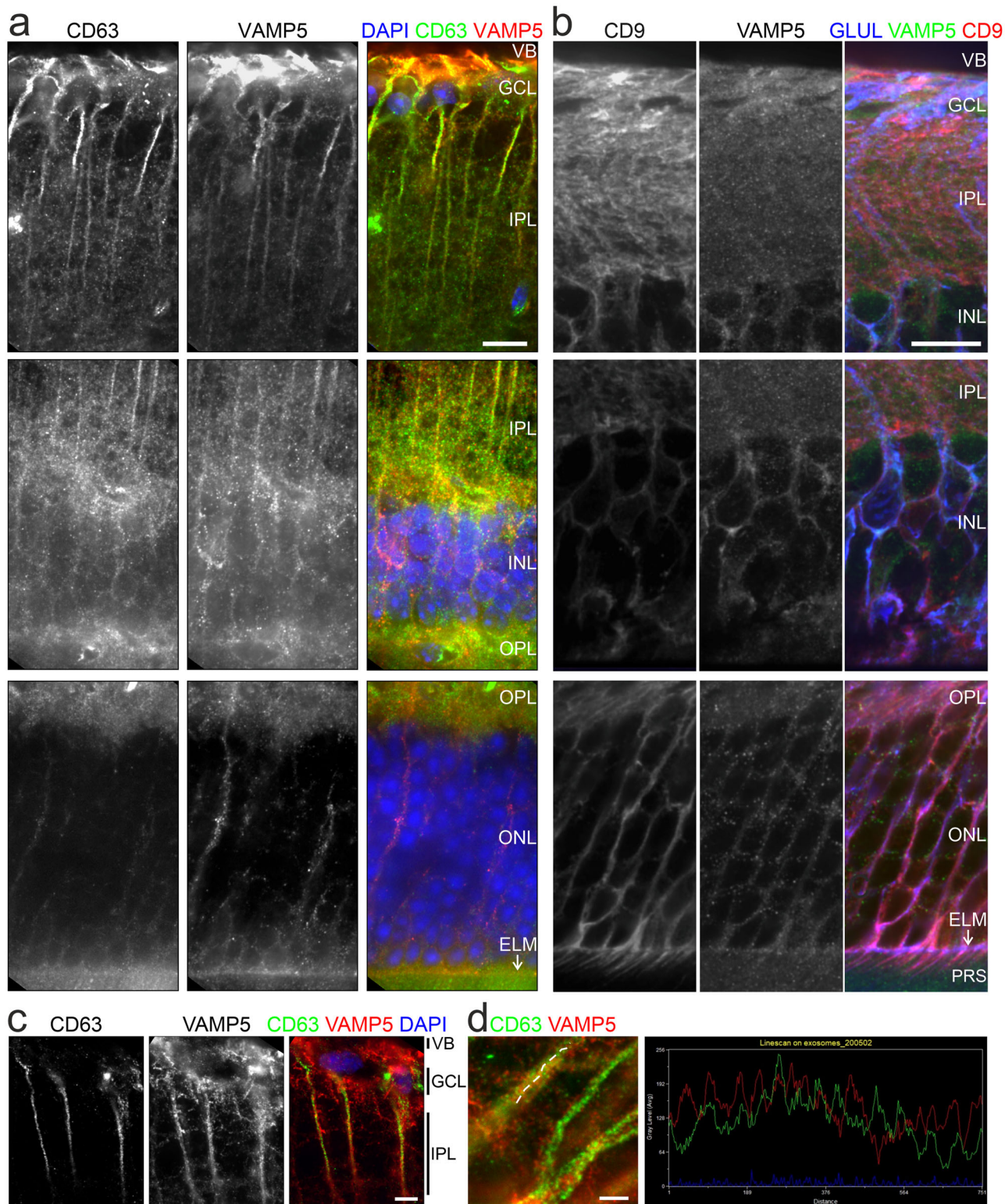


FIGURE 11 Colocalization of VAMP5 and EV markers in retinal cells in vivo. Greyscale and false-colour confocal micrographs of retinal sections subjected to double-immunohistochemical staining of VAMP5 and of CD63 (a) or CD9 (b). VB, vitreous body; GCL, ganglion cell layer; IPL, inner plexiform layer; INL, inner nuclear layer; OPL, outer plexiform layer; ONL, outer nuclear layer; ELM, external limiting membrane (white arrows); PRs, photoreceptor segments. Scale bars: 10 μm . (c) Greyscale and false-colour STED micrographs of retinal sections after double-immunohistochemical staining of CD63 and VAMP5. Scale bar: 5 μm . (d) STED micrographs at higher magnification showing Müller cell processes (left). Plot of fluorescence intensities along the line scan indicated in the micrograph (dashed white line) (right). Scale bar: 5 μm .

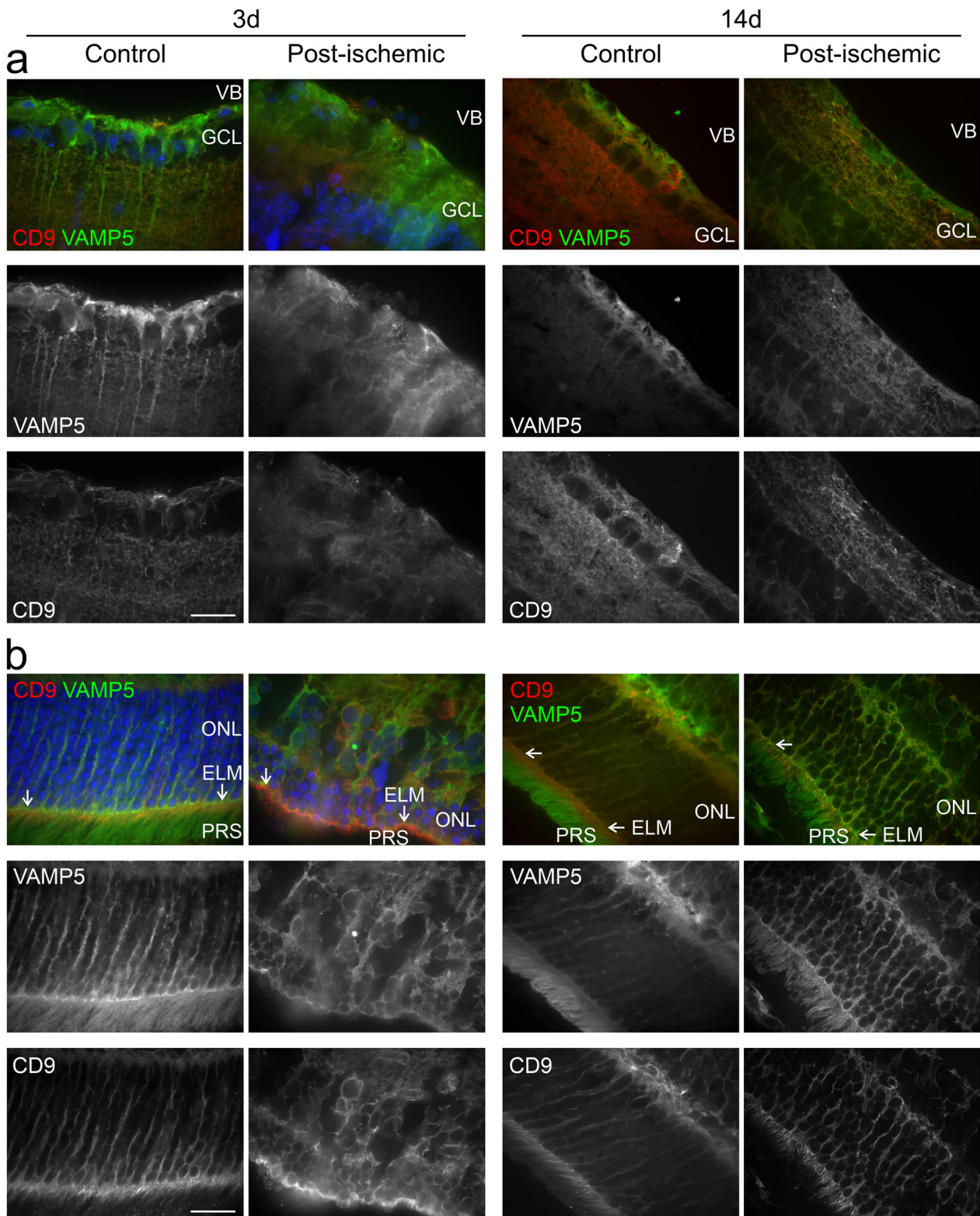


FIGURE 12 Post-ischemic changes in the retinal distribution of VAMP5 and CD9. False-colour and corresponding greyscale confocal micrographs showing the inner (a) and outer (b) retinae from control eyes and from post-ischemic eyes at 3 (left) and 14 (right) days after transient ischemia. Retinal sections were subjected to double-immunohistochemical staining of VAMP5 (green) and of CD9 (red). VB, vitreous body; GCL, ganglion cell layer; ONL, outer nuclear layer; ELM, external limiting membrane (white arrows); PRS, photoreceptor segments. Scale bar: 40 μm .

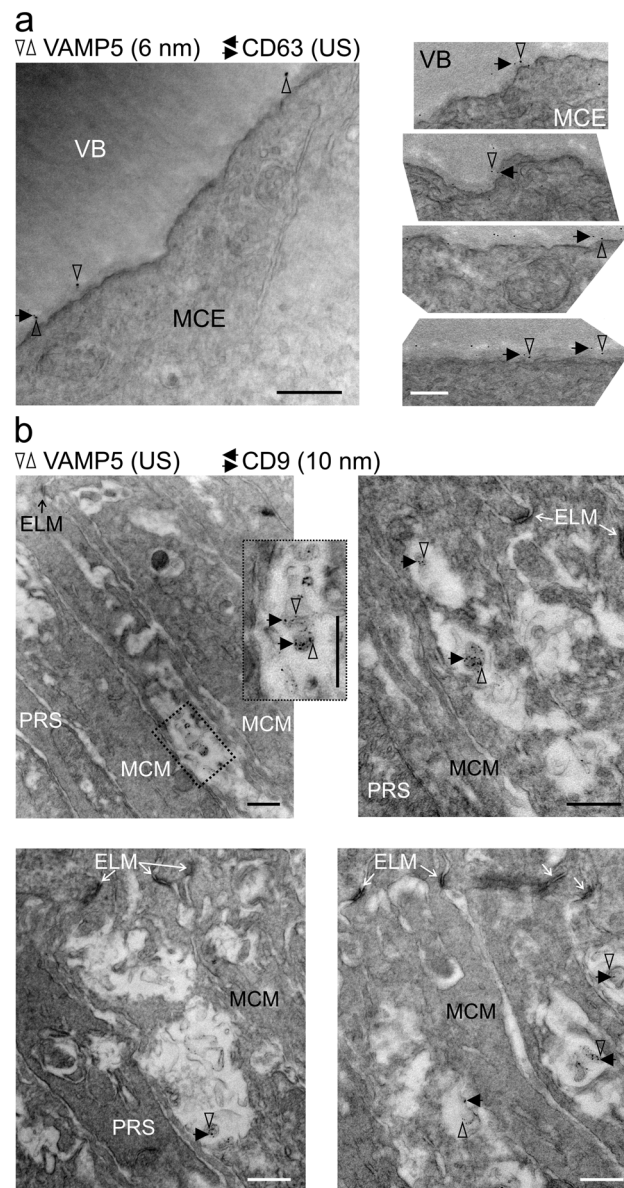


FIGURE 13 Colocalization of tetraspanins and VAMP5 on extracellular vesicular structures in the retina Representative transmission electron micrographs of retinal sections revealing colocalization of CD63 (a) and of CD9 (b) with VAMP5 in the extracellular space (a) apposed to endfeet forming the vitreous body and (b) close to microvilli of Müller cells surrounding photoreceptor segments, respectively. Retinal ultrathin sections were subjected to double-immunogold labelling of the indicated proteins using gold nanoparticles of distinct sizes (as indicated; US, ultrasmall ~ 0.8 nm). VB, vitreous body; MCE, Müller cell endfoot; ELM, external limiting membrane; MCM, Müller cell microvillus; PRS, photoreceptor segment. VAMP5: vertical empty arrowheads; CD63 and CD9: horizontal black arrows. Scale bars: 500 nm.

distinct morphologic and functional specializations at their business ends: endfeet facing the vitreous body and apical microvilli surrounding photoreceptor segments (Derouiche et al., 2012; Reichenbach, 1989). Our results suggest that Müller cells secrete subsets of EVs from these compartments possibly by distinct mechanisms based on their tetraspanin content: The presence of CD63 in multivesicular bodies of endfeet and in the apposed extracellular space suggests that EVs in this compartment originate from intraluminal vesicles. The presence of CD9 on EVs in the subretinal space suggests that these structures originate from apical microvilli. Müller cell-derived EVs thus resemble exosome and ectosomes bearing CD63 and CD9, respectively. Their distinct subcellular origin and content have been exposed by a recent study on HeLa cell-derived material (Mathieu et al., 2021). Our hypothesis that Müller cells release EVs from their apical microvilli in the subretinal space is supported by the notion that many cell types shed EV-like structures from their specialized plasma membrane protrusions such as cilia, microvilli and filopodia (Hara et al., 2010; Marzesco et al., 2005; Salinas et al., 2017; Wang, Silva et al., 2014; Wood et al., 2013; for review see Rilla, 2021). The presence of CD81 (Clarke & Geisert, 1998) and CD9 (Iwagawa et al., 2020) in Müller cell compartments of the

inner and outer retina is supported by earlier reports. So far, the retinal distribution of CD63 has remained unknown. We report its enrichment in Müller cell endfeet. With respect to other retinal cells, this ubiquitously expressed tetraspanin has been studied in cultured human retinal pigment epithelial cells as part of their EVs (Sreekumar et al., 2010) and in rodent retinal ganglion cells as component of the endosomal-lysosomal system (Demais et al., 2016).

Until now, EVs secreted by primary Müller cells *in vitro* have not been characterized except for a recent report showing the presence of micro RNAs in these structures (Akamine et al., 2021). In fact, Müller cells have been mainly studied as target of EVs (Didiano et al., 2020; Eastlake et al., 2021; Kamalden et al., 2017; Ke et al., 2021; Peng et al., 2018; Wassmer et al., 2017; Zhang et al., 2020). Probably the best studied source of retinal EVs are cultured pigment epithelial cells (Ahn et al., 2021; Flores-Bellver et al., 2021; Kang et al., 2014; Klingeborn et al., 2017; Mukai et al., 2021; Otsuki et al., 2021; Sreekumar et al., 2010; Toyofuku et al., 2012). Few studies characterized EVs secreted by other types of retinal cells *in vitro* including precursor cells (Zhou et al., 2018), astrocytes (Hajrasouliha et al., 2013), retinal ganglion cells (Wang et al., 2021) and photoreceptors (Kalargyrou et al., 2021). Microvesicle release from photoreceptors was reported *in vivo* (Ropelewski & Imanishi, 2020). Here, we provide the first direct comparison of neuronal and glial secretomes and of the respective cell lysates. Our analysis reveals that Müller cells and retinal neurons secrete EVs with distinct protein compositions showing less than 40% overlap. We uncovered several Müller cell-specific EV components. DBI is a putative endogenous ligand of translocator protein 18 kDa (TSPO) thought to mediate interactions of Müller cells and microglia in the retina (Wang, Wang et al., 2014). Carbonic anhydrase was detected on apical microvilli of Müller cells in the mouse retina (Nagelhus et al., 2005; Ochrietor et al., 2005) supporting the release of EVs from these structures. CEP290/NPHP6, a ciliary component, has not been associated with EVs, but its deficiency causes retinal diseases (Chen et al., 2021). EVs secreted by cultured neurons (Chivet et al., 2014; Fauré et al., 2006; Lachenal et al., 2011; Morel et al., 2013; Yuyama et al., 2012) and glial cells (Frühbeis et al., 2013; Gabrielli et al., 2015; Glebov et al., 2015; Guitart et al., 2016; Hooper et al., 2012; Potolicchio et al., 2005) from other parts of the CNS have been characterized, but their proteomic profiles have not been compared. Notably, the limited overlap of proteins found in CD9- and CD63-positive EVs from Müller cells supports the notion that a given cell type produces distinct subtypes of EVs (Jeppesen et al., 2019; Kowal et al., 2016) and corroborates our idea that Müller cells secrete distinct types of EVs from distinct compartments.

Our analysis of VAMPs revealed Müller cell-specific expression of VAMP5. Up to now, the distribution of this protein in the retina has remained unknown. Previous reports detected VAMP5 in skeletal muscle and other organs, but not in the brain (Takahashi et al., 2013; Zeng et al., 1998). A more recent study identified *Vamp5* as miRNA-regulated gene in the retina supporting our finding that the protein is present in this part of the CNS (Olivares et al., 2017). Our finding that VAMP5 is associated with EVs is supported by several lines of evidence. Electron microscopic inspection of muscle cell lines revealed its localization at the plasma membrane, in vesicular structures, and in multivesicular bodies (Tajika et al., 2014; Zeng et al., 1998) in line with our immunogold data. Moreover, VAMP5 was detected in EVs of the murine lung (Choudhary et al., 2021), from cultured myotubes (Forterre et al., 2014), mesenchymal stem cells (Salomon et al., 2013) and tumoural Jurkat T cells (Bosque et al., 2016). A hint towards the function of VAMP5 in EVs comes from a recent observation that components of the SNARE complex can be transferred intercellularly via EVs enabling vesicular release in target cells (Vilcaes et al., 2021). VAMP5 has also been shown to be part of the machinery that mediates EV-dependent cytokine release from mesenchymal stem cells *in vitro* (Kou et al., 2018). VAMP5 did not mediate fusion of vesicular and plasma membrane containing specific tSNAREs in an artificial exocytosis assay (Hasan et al., 2010), but deletion of VAMP5 from mice causes developmental defects in the respiratory and urinary systems and perinatal death (Ikezawa et al., 2018). The observed upregulation of VAMP5 and the changes in CD9 distribution under ischemic conditions suggest that VAMP5 is part of the gliotic reaction to injury and disease and that ischemia affects EV secretion in the retina. Ischemia-induced changes in brain cells releasing EVs have been reported previously (Brenna et al., 2020). On the other hand, EVs are explored as therapeutic approaches to mitigate post-ischemic pathologic changes (Doepfner et al., 2015).

In summary, our data support the idea of EV-based communication between cells in the CNS and suggest Müller cells as a key actor in the retina.

AUTHOR CONTRIBUTIONS

Valerie Demais: performed electron microscopy-related work, acquired and analysed electron micrographs. Anne Pohl: performed immunofluorescence microscopy-related work, qPCR experiments and analyses, immunoblots for VAMP expression in the healthy and ischemic retina, established protocols for primary Müller cell cultures, performed EV purification, and edited the manuscript. Kirsten A. Wunderlich: performed EV purification from primary Müller cell cultures and immunoblot analyses, analysed EV marker localization via STED microscopy, and edited the manuscript. Anne Maria Pfaller: generated purified EVs for mass spectrometric analysis, and edited the manuscript. Lew Kaplan: performed EV isolation and bioinformatic analysis of proteomic data, and edited the manuscript. Amelie Barthélémy: performed immunohistochemical staining with selected antibodies to prepare immunogold staining. Robin Dittrich: performed NTA. Berta Puig: set up the EV isolation protocol, analysed results, edited the manuscript. Bernd Giebel: analysed NTA results and edited the manuscript. Stefanie M. Hauck: performed mass spectrometric analysis of retinal cell types and purified EVs, analysed protein expression levels, and edited the manuscript. Antje Grosche: designed experiments, analysed results, prepared figures, and edited the manuscript. Frank W. Pfrieger: designed

experiments, analysed results, prepared figures, and wrote the manuscript. The authors thank Jens Grosche for the schematic drawing of retinal cells, and Alexandra Hauser, Dirkje Felder and Gabrielle Jäger for excellent technical assistance.

ACKNOWLEDGEMENTS

Part of this work was supported by the Centre National de la Recherche Scientifique under grant UPR3212 (Frank W. Pfrieder), the Université de Strasbourg under grant UPR3212 (Frank W. Pfrieder), the Agence National de la Recherche Scientifique under grant GLIIVAMP (Frank W. Pfrieder), the Deutsche Forschungsgemeinschaft under grants GR 4403/1-1; GR 4403/5-1; GR 4403/7-1 (Antje Grosche) and HA 6014/5-1 (Stefanie M. Hauck) and the ProRetina Foundation Germany under grants Pro-Re/Seed/Grosche.1-2014 (Antje Grosche) and Pro-Re/Seed/Kaplan-Grosche.1-2019 (Lew Kaplan, Antje Grosche).

Open access funding enabled and organized by Projekt DEAL.

CONFLICT OF INTEREST

The authors report no conflict of interest.

DATA AVAILABILITY STATEMENT

Data are available on request from the authors.

ORCID

Valerie Demais  <https://orcid.org/0000-0003-1328-1115>

Kirsten A. Wunderlich  <https://orcid.org/0000-0002-4927-1851>

Lew Kaplan  <https://orcid.org/0000-0003-4336-2768>

Berta Puig  <https://orcid.org/0000-0002-2255-8393>

Bernd Giebel  <https://orcid.org/0000-0003-2446-948X>

Stefanie M. Hauck  <https://orcid.org/0000-0002-1630-6827>

Frank W. Pfrieder  <https://orcid.org/0000-0001-7085-1431>

Antje Grosche  <https://orcid.org/0000-0003-0338-7530>

REFERENCES

- Ahn, J. Y., Datta, S., Bandeira, E., Cano, M., Mallick, E., Rai, U., Powell, B., Tian, J., Witwer, K. W., Handa, J. T., & Paulaitis, M. E. (2021). Release of extracellular vesicle miR-494-3p by ARPE-19 cells with impaired mitochondria. *Biochimica et Biophysica Acta General Subjects*, 1865, 129598. <https://doi.org/10.1016/j.bbagen.2020.129598>
- Aires, I. D., Ribeiro-Rodrigues, T., Boia, R., Ferreira-Rodrigues, M., Girão, H., Ambrósio, A. F., & Santiago, A. R. (2021). Microglial extracellular vesicles as vehicles for neurodegeneration spreading. *Biomolecules*, 11, 770. <https://doi.org/10.3390/biom11060770>
- Akamine, P. S., Lima, C. R., Lustoza-Costa, G. J., Fuziwara, C. S., Del Debbio, C. B., Kimura, E. T., Santos, M. F., & Hamassaki, D. E. (2021). Age-related increase of let-7 family microRNA in rat retina and vitreous. *Experimental Eye Research*, 204, 108434. <https://doi.org/10.1016/j.exer.2020.108434>
- Araujo, A. P. B., Carpi-Santos, R., & Gomes, F. C. A. (2019). The role of astrocytes in the development of the cerebellum. *Cerebellum (London, England)*, 18, 1017–1035. <https://doi.org/10.1007/s12311-019-01046-0>
- Bosque, A., Dietz, L., Gallego-Lleyda, A., Sanclemente, M., Iturralde, M., Naval, J., Alava, M. A., Martínez-Lostao, L., Thierse, H. J., & Anel, A. (2016). Comparative proteomics of exosomes secreted by tumoral Jurkat T cells and normal human T cell blasts unravels a potential tumorigenic role for valosin-containing protein. *Oncotarget*, 7, 29287–29305. <https://doi.org/10.18632/oncotarget.8678>
- Brenna, S., Altmepfen, H. C., Mohammadi, B., Rissiek, B., Schlink, F., Ludewig, P., Krisp, C., Schlüter, H., Failla, A. V., Schneider, C., Glatzel, M., Puig, B., & Magnus, T. (2020). Characterization of brain-derived extracellular vesicles reveals changes in cellular origin after stroke and enrichment of the prion protein with a potential role in cellular uptake. *Journal of Extracellular Vesicles*, 9, 1809065. <https://doi.org/10.1080/20013078.2020.1809065>
- Brenna, S., Krisp, C., Altmepfen, H. C., Magnus, T., & Puig, B. (2021). Brain-derived extracellular vesicles in health and disease: A methodological perspective. *International Journal of Molecular Sciences*, 22, 1365. <https://doi.org/10.3390/ijms22031365>
- Budnik, V., Ruiz-Cañada, C., & Wendler, F. (2016). Extracellular vesicles round off communication in the nervous system. *Nature Reviews Neuroscience*, 17, 160–172. <https://doi.org/10.1038/nrn.2015.29>
- Chen, H. Y., Kelley, R. A., Li, T., & Swaroop, A. (2021). Primary cilia biogenesis and associated retinal ciliopathies. *Seminars in Cell & Developmental Biology*, 110, 70–88. <https://doi.org/10.1016/j.semcldb.2020.07.013>
- Chivet, M., Javalet, C., Laulagnier, K., Blot, B., Hemming, F. J., & Sadoul, R. (2014). Exosomes secreted by cortical neurons upon glutamatergic synapse activation specifically interact with neurons. *Journal of Extracellular Vesicles*, 3, 24722. <https://doi.org/10.3402/jev.v3.24722>
- Choudhary, I., Vo, T., Paudel, K., Wen, X., Gupta, R., Kesimer, M., Patial, S., & Saini, Y. (2021). Vesicular and extravesicular protein analyses from the airspaces of ozone-exposed mice revealed signatures associated with mucoinflammatory lung disease. *Science Reports*, 11, 23203. <https://doi.org/10.1038/s41598-021-02256-5>
- Clarke, K., & Geisert, E. E., Jr (1998). The target of the antiproliferative antibody (TAPA) in the normal and injured rat retina. *Molecular Vision*, 4, 3.
- Demais, V., Barthélémy, A., Perraut, M., Ungerer, N., Keime, C., Reibel, S., & Pfrieder, F. W. (2016). Reversal of pathologic lipid accumulation in NPC1-deficient neurons by drug-promoted release of LAMP1-coated lamellar inclusions. *Journal of Neuroscience*, 36, 8012–8025. <https://doi.org/10.1523/jneurosci.0900-16.2016>
- Derouiche, A., Pannicke, T., Haseleu, J., Blaess, S., Grosche, J., & Reichenbach, A. (2012). Beyond polarity: Functional membrane domains in astrocytes and Muller cells. *Neurochemical Research*, 37, 2513–2523. <https://doi.org/10.1007/s11064-012-0824-z>

- Didiano, D., Abner, J. J., Hinger, S. A., Flickinger, Z., Kent, M., Clement, M. A., Balaiya, S., Liu, Qi., Dai, X., Levine, E. M., & Patton, J. G. (2020). Induction of a proliferative response in the zebrafish retina by injection of extracellular vesicles. *Experimental Eye Research*, *200*, 108254. <https://doi.org/10.1016/j.exer.2020.108254>
- Doepfner, T. R., Herz, J., Görgens, A., Schlechter, J., Ludwig, A. K., Radtke, S., De Miroshedji, K., Horn, P. A., Giebel, B., & Hermann, D. M. (2015). Extracellular vesicles improve post-stroke neuroregeneration and prevent posts ischemic immunosuppression. *Stem Cells Translational Medicine*, *4*, 1131–1143. <https://doi.org/10.5966/sctm.2015-0078>
- Dragovic, R. A., Gardiner, C., Brooks, A. S., Tannetta, D. S., Ferguson, D. J. P., Hole, P., Carr, B., Redman, C. W. G., Harris, A. L., Dobson, P. J., Harrison, P., & Sargent, I. L. (2011). Sizing and phenotyping of cellular vesicles using nanoparticle tracking analysis. *Nanomedicine*, *7*, 780–788. <https://doi.org/10.1016/j.nano.2011.04.003>
- Eastlake, K., Lamb, W. D. B., Luis, J., Khaw, P. T., Jayaram, H., & Limb, G. A. (2021). Prospects for the application of Müller glia and their derivatives in retinal regenerative therapies. *Progress in Retinal and Eye Research*, *85*, 100970. <https://doi.org/10.1016/j.preteyeres.2021.100970>
- Escartin, C., Galea, E., Lakatos, A., O'Callaghan, J. P., Petzold, G. C., Serrano-Pozo, A., Steinhäuser, C., Volterra, A., Carmignoto, G., Agarwal, A., Allen, N. J., Araque, A., Barbeito, L., Barzilai, A., Bergles, D. E., Bonvento, G., Butt, A. M., Chen, W. T., Cohen-Salmon, M., ... Verkhratsky, A. (2021). Reactive astrocyte nomenclature, definitions, and future directions. *Nature Neuroscience*, *24*, 312–325. <https://doi.org/10.1038/s41593-020-00783-4>
- Escola, J. M., Kleijmeer, M. J., Stoorvogel, W., Griffith, J. M., Yoshie, O., & Geuze, H. J. (1998). Selective enrichment of tetraspan proteins on the internal vesicles of multivesicular endosomes and on exosomes secreted by human B-lymphocytes. *Journal of Biological Chemistry*, *273*, 20121–20127. <https://doi.org/10.1074/jbc.273.32.20121>
- Fauré, J., Lachenal, G., Court, M., Hirrlinger, J., Chatellard-Causse, C., Blot, B., Grange, J., Schoehn, G., Goldberg, Y., Boyer, V., Kirchhoff, F., Raposo, G., Garin, J., & Sadoul, R. (2006). Exosomes are released by cultured cortical neurones. *Molecular and Cellular Neuroscience*, *31*, 642–648. <https://doi.org/10.1016/j.mcn.2005.12.003>
- Fiacco, T. A., & Mccarthy, K. D. (2018). Multiple lines of evidence indicate that gliotransmission does not occur under physiological conditions. *Journal of Neuroscience*, *38*, 3–13. <https://doi.org/10.1523/jneurosci.0016-17.2017>
- Flores-Bellver, M., Mighty, J., Aparicio-Domingo, S., Li, K. V., Shi, C., Zhou, J., Cobb, H., Mcgrath, P., Michelis, G., Lenhart, P., Bilousova, G., Heissel, S., Rudy, M. J., Coughlan, C., Goodspeed, A. E., Becerra, S. P., Redenti, S., & Canto-Soler, M. V. (2021). Extracellular vesicles released by human retinal pigment epithelium mediate increased polarised secretion of drusen proteins in response to AMD stressors. *Journal of Extracellular Vesicles*, *10*, e12165. <https://doi.org/10.1002/jev2.12165>
- Forterre, A., Jalabert, A., Berger, E., Baudet, M., Chikh, K., Errazuriz, E., De Larichaudy, J., Chanon, S., Weiss-Gayet, M., Hesse, A. M., Record, M., Geloën, A., Lefai, E., Vidal, H., Couté, Y., & Rome, S. (2014). Proteomic analysis of C2C12 myoblast and myotube exosome-like vesicles: A new paradigm for myoblast-myotube cross talk? *Plos One*, *9*, e84153. <https://doi.org/10.1371/journal.pone.0084153>
- Frühbeis, C., Fröhlich, D., Kuo, W. P., Amphornrat, J., Thilemann, S., Saab, A. S., Kirchhoff, F., Möbius, W., Goebels, S., Nave, K. A., Schneider, A., Simons, M., Klugmann, M., Trotter, J., & Krämer-Albers, E. M. (2013). Neurotransmitter-triggered transfer of exosomes mediates oligodendrocyte-neuron communication. *Plos Biology*, *11*, e1001604. <https://doi.org/10.1371/journal.pbio.1001604>
- Gabrielli, M., Battista, N., Riganti, L., Prada, I., Antonucci, F., Cantone, L., Matteoli, M., Maccarrone, M., & Verderio, C. (2015). Active endocannabinoids are secreted on extracellular membrane vesicles. *Embo Reports*, *16*, 213–220. <https://doi.org/10.15252/embr.201439668>
- García-Cáceres, C., Ballard, E., Prevot, V., Luquet, S., Woods, S. C., Koch, M., Horvath, T. L., Yi, C. X., Chowen, J. A., Verkhratsky, A., Araque, A., Bechmann, I., & Tschöp, M. H. (2019). Role of astrocytes, microglia, and tanycytes in brain control of systemic metabolism. *Nature Neuroscience*, *22*, 7–14. <https://doi.org/10.1038/s41593-018-0286-y>
- Giaume, C., Naus, C. C., Sáez, J. C., & Leybaert, L. (2021). Glial connexins and pannexins in the healthy and diseased brain. *Physiological Reviews*, *101*, 93–145. <https://doi.org/10.1152/physrev.00043.2018>
- Glebov, K., Löchner, M., Jabs, R., Lau, T., Merkel, O., Schloss, P., Steinhäuser, C., & Walter, J. (2015). Serotonin stimulates secretion of exosomes from microglia cells. *Glia*, *63*, 626–634. <https://doi.org/10.1002/glia.22772>
- Görgens, A., Bremer, M., Ferrer-Tur, R., Murke, F., Tertel, T., Horn, P. A., Thalmann, S., Welsh, J. A., Probst, C., Guerin, C., Boulanger, C. M., Jones, J. C., Hanenberg, H., Erdbrügger, U., Lannigan, J., Ricklefs, F. L., El-Andaloussi, S., & Giebel, B. (2019). Optimisation of imaging flow cytometry for the analysis of single extracellular vesicles by using fluorescence-tagged vesicles as biological reference material. *Journal of Extracellular Vesicles*, *8*, 1587567. <https://doi.org/10.1080/20013078.2019.1587567>
- Grillo, S. L., Etzel, J. D., Weber, S. R., Ondeck, C., Wang, W., Zhao, Y., Barber, A. J., & Sundstrom, J. M. (2021). Descriptive analysis of Fibulin-3 and the extracellular vesicle marker, Alix, in drusen from a small cohort of postmortem human eyes. *Experimental Eye Research*, *203*, 108422. <https://doi.org/10.1016/j.exer.2020.108422>
- Grosche, A., Hauser, A., Lepper, M. F., Mayo, R., Von Toerne, C., Merl-Pham, J., & Hauck, S. M. (2016). The proteome of native adult müller glial cells from murine retina. *Molecular & Cellular Proteomics*, *15*, 462–480. <https://doi.org/10.1074/mcp.M115.052183>
- Guitart, K., Loers, G., Buck, F., Bork, U., Schachner, M., & Kleene, R. (2016). Improvement of neuronal cell survival by astrocyte-derived exosomes under hypoxic and ischemic conditions depends on prion protein. *Glia*, *64*, 896–910. <https://doi.org/10.1002/glia.22963>
- Hajrasouliha, A. R., Jiang, G., Lu, Q., Lu, H., Kaplan, H. J., Zhang, H. G., & Shao, H. (2013). Exosomes from retinal astrocytes contain antiangiogenic components that inhibit laser-induced choroidal neovascularization. *Journal of Biological Chemistry*, *288*, 28058–28067. <https://doi.org/10.1074/jbc.M113.470765>
- Hara, M., Yanagihara, T., Hirayama, Y., Ogasawara, S., Kurosawa, H., Sekine, S., & Kihara, I. (2010). Podocyte membrane vesicles in urine originate from tip vesiculation of podocyte microvilli. *Human Pathology*, *41*, 1265–1275. <http://doi.org/10.1016/j.humpath.2010.02.004>
- Hasan, N., Corbin, D., & Hu, C. (2010). Fusogenic pairings of vesicle-associated membrane proteins (VAMPs) and plasma membrane t-SNAREs–VAMP5 as the exception. *Plos One*, *5*, e14238. <https://doi.org/10.1371/journal.pone.0014238>
- Hooper, C., Sainz-Fuertes, R., Lynham, S., Hye, A., Killick, R., Warley, A., Bolondi, C., Pocock, J., & Lovestone, S. (2012). Wnt3a induces exosome secretion from primary cultured rat microglia. *Bmc Neuroscience [Electronic Resource]*, *13*, 144. <https://doi.org/10.1186/1471-2202-13-144>
- Hsiao, Y. P., Chen, C., Lee, C. M., Chen, P. Y., Chung, W. H., Wang, Y. P., Hung, Y. C., Cheng, C. M., Chen, C., Ko, B. H., & Hsu, M. Y. (2021). Differences in the quantity and composition of extracellular vesicles in the aqueous humor of patients with retinal neovascular diseases. *Diagnostics (Basel)*, *11*, 1276. <https://doi.org/10.3390/diagnostics11071276>
- Ikezawa, M., Tajika, Y., Ueno, H., Murakami, T., Inoue, N., & Yorifuji, H. (2018). Loss of VAMP5 in mice results in duplication of the ureter and insufficient expansion of the lung. *Developmental Dynamics*, *247*, 754–762. <https://doi.org/10.1002/dvdy.24618>
- Illes, P., Burnstock, G., & Tang, Y. (2019). Astroglia-derived ATP modulates CNS neuronal circuits. *Trends in Neuroscience (Tins)*, *42*, 885–898. <https://doi.org/10.1016/j.tins.2019.09.006>

- Iwagawa, T., Aihara, Y., Umutohi, D., Baba, Y., Murakami, A., Miyado, K., & Watanabe, S. (2020). Cd9 protects photoreceptors from injury and potentiates Edn2 expression. *Investigative Ophthalmology & Visual Science*, *61*, 7. <https://doi.org/10.1167/iovs.61.3.7>
- Jeppesen, D. K., Fenix, A. M., Franklin, J. L., Higginbotham, J. N., Zhang, Q., Zimmerman, L. J., Liebler, D. C., Ping, J., Liu, Q., Evans, R., Fissell, W. H., Patton, J. G., Rome, L. H., Burnette, D. T., & Coffey, R. J. (2019). Reassessment of exosome composition. *Cell*, *177*, 428–445.e18. <https://doi.org/10.1016/j.cell.2019.02.029>
- Jha, M. K., & Morrison, B. M. (2020). Lactate transporters mediate glia-neuron metabolic crosstalk in homeostasis and disease. *Frontiers in Cellular Neuroscience*, *14*, 589582. <https://doi.org/10.3389/fncel.2020.589582>
- Kalargyrou, A. A., Basche, M., Hare, A., West, E. L., Smith, A. J., Ali, R. R., & Pearson, R. A. (2021). Nanotube-like processes facilitate material transfer between photoreceptors. *Embo Reports*, *22*, e53732. <https://doi.org/10.15252/embr.202153732>
- Käll, L., Canterbury, J. D., Weston, J., Noble, W. S., & Maccoss, M. J. (2007). Semi-supervised learning for peptide identification from shotgun proteomics datasets. *Nature Methods*, *4*, 923–925. <https://doi.org/10.1038/nmeth1113>
- Kalluri, R., & Lebleu, V. S. (2020). The biology, function, and biomedical applications of exosomes. *Science*, *367*, eAau6977. <https://doi.org/10.1126/science.aau6977>
- Kamalden, T. A., Macgregor-Das, A. M., Kannan, S. M., Dunkerly-Eyring, B., Khaliddin, N., Xu, Z., Fusco, A. P., Yazib, S. A., Chow, R. C., Duh, E. J., Halushka, M. K., Steenbergen, C., & Das, S. (2017). Exosomal MicroRNA-15a transfer from the pancreas augments diabetic complications by inducing oxidative stress. *Antiox Redox Signalling*, *27*, 913–930. <https://doi.org/10.1089/ars.2016.6844>
- Kang, G. Y., Bang, J. Y., Choi, Ae J., Yoon, J., Lee, W. C., Choi, S., Yoon, S., Kim, H. C., Baek, J. H., Park, H. S., Lim, H. J., & Chung, H. (2014). Exosomal proteins in the aqueous humor as novel biomarkers in patients with neovascular age-related macular degeneration. *Journal of Proteome Research*, *13*, 581–595. <https://doi.org/10.1021/pr400751k>
- Ke, Y., Fan, X., Hao, R., Dong, L., Xue, M., Tan, L., Yang, C., Li, X., & Ren, X. (2021). Human embryonic stem cell-derived extracellular vesicles alleviate retinal degeneration by upregulating Oct4 to promote retinal Müller cell retrodifferentiation via HSP90. *Stem Cell Research Therapy*, *12*, 21–21. <https://doi.org/10.1186/s13287-020-02034-6>
- Kim, D., Langmead, B., & Salzberg, S. L. (2015). HISAT: A fast spliced aligner with low memory requirements. *Nature Methods*, *12*, 357–360. <https://doi.org/10.1038/nmeth.3317>
- Kim, Y. S., Choi, J., & Yoon, B. E. (2020). Neuron-glia interactions in neurodevelopmental disorders. *Cells*, *9*, 2176. <https://doi.org/10.3390/cells9102176>
- Klingeborn, M., Dismuke, W. M., Skiba, N. P., Kelly, U., Stamer, W. D., & Bowes Rickman, C. (2017). Directional exosome proteomes reflect polarity-specific functions in retinal pigmented epithelium monolayers. *Science Reports*, *7*, 4901. <https://doi.org/10.1038/s41598-017-05102-9>
- Kobayashi, T., Vischer, U. M., Rosnoble, C., Lebrand, C., Lindsay, M., Parton, R. G., Kruithof, E. K., & Gruenberg, J. (2000). The tetraspanin CD63/lamp3 cycles between endocytic and secretory compartments in human endothelial cells. *Molecular Biology of the Cell*, *11*, 1829–1843. <https://doi.org/10.1091/mbc.11.5.1829>
- Kofuji, P., & Araque, A. (2021). Astrocytes and behavior. *Annual Review of Neuroscience*, *49*–67. <https://doi.org/10.1146/annurev-neuro-101920-112225>
- Kou, X., Xu, X., Chen, C., Sanmillan, M. L., Cai, T., Zhou, Y., Giraudo, C., Le, A., & Shi, S. (2018). The Fas/Fap-1/Cav-1 complex regulates IL-1RA secretion in mesenchymal stem cells to accelerate wound healing. *Science Translational Medicine*, *10*, eaai8524. <https://doi.org/10.1126/scitranslmed.aai8524>
- Kowal, J., Arras, G., Colombo, M., Jouve, M., Morath, J. P., Primdal-Bengtson, B., Dingli, F., Loew, D., Tkach, M., & Thery, C. (2016). Proteomic comparison defines novel markers to characterize heterogeneous populations of extracellular vesicle subtypes. *PNAS*, *113*, E968–E977. <https://doi.org/10.1073/pnas.1521230113>
- Lachenal, G., Pernet-Gallay, K., Chivet, M., Hemming, F. J., Belly, A. S., Bodon, G., Blot, B., Haase, G., Goldberg, Y., & Sadoul, R. (2011). Release of exosomes from differentiated neurons and its regulation by synaptic glutamatergic activity. *Molecular and Cellular Neuroscience*, *46*, 409–418. <https://doi.org/10.1016/j.mcn.2010.11.004>
- Lago-Baldaia, I., Fernandes, V. M., & Ackerman, S. D. (2020). More than mortar: Glia as architects of nervous system development and disease. *Frontiers in Cell and Developmental Biology*, *8*, 611269. <https://doi.org/10.3389/fcell.2020.611269>
- Langmead, B., Trapnell, C., Pop, M., & Salzberg, S. L. (2009). Ultrafast and memory-efficient alignment of short DNA sequences to the human genome. *Genome Biology*, *10*, R25. <https://doi.org/10.1186/gb-2009-10-3-r25>
- Li, H., Luo, Y., Zhu, L., Hua, W., Zhang, Y., Zhang, H., Zhang, L., Li, Z., Xing, P., Zhang, Y., Hong, B., Yang, P., & Liu, J. (2019). Glia-derived exosomes: Promising therapeutic targets. *Life Sciences*, *239*, 116951. <https://doi.org/10.1016/j.lfs.2019.116951>
- Linnerbauer, M., Wheeler, M. A., & Quintana, F. J. (2020). Astrocyte crosstalk in CNS inflammation. *Neuron*, *108*, 608–622. <https://doi.org/10.1016/j.neuron.2020.08.012>
- Liu, J., Jiang, F., Jiang, Y., Wang, Y., Li, Z., Shi, X., Zhu, Y., Wang, H., & Zhang, Z. (2020). Roles of exosomes in ocular diseases. *International Journal of Nanomedicine*, *15*, 10519–10538. <https://doi.org/10.2147/IJN.S277190>
- Lizarraga-Valderrama, L. R., & Sheridan, G. K. (2021). Extracellular vesicles and intercellular communication in the central nervous system. *Febs Letters*, *595*, 1391–1410. <https://doi.org/10.1002/1873-3468.14074>
- Luga, V., Zhang, L., Vilorio-Petit, A. M., Ogunjimi, A. A., Inanlou, M. R., Chiu, E., Buchanan, M., Hosein, A. N., Basik, M., & Wrana, J. L. (2012). Exosomes mediate stromal mobilization of autocrine Wnt-PCP signaling in breast cancer cell migration. *Cell*, *151*, 1542–1556. <https://doi.org/10.1016/j.cell.2012.11.024>
- Mahjoub, S., Rufino-Ramos, D., Pereira De Almeida, L. S., Broekman, M. L. D., Breakefield, X. O., & Van Solinge, T. S. (2021). Living proof of activity of extracellular vesicles in the central nervous system. *International Journal of Molecular Sciences*, *22*, 7294. <http://doi.org/10.3390/ijms22147294>
- Martin, M. (2011). Cutadapt removes adapter sequences from high-throughput sequencing reads. *EMBnetjournal*, *17*, 10–12. <https://doi.org/10.14806/ej.17.1.200>
- Marzesco, A. M., Janich, P., Wilsch-Bräuninger, M., Dubreuil, V., Langenfeld, K., Corbeil, D., & Huttner, W. B. (2005). Release of extracellular membrane particles carrying the stem cell marker prominin-1 (CD133) from neural progenitors and other epithelial cells. *Journal of Cell Science*, *118*, 2849–2858. <http://doi.org/10.1242/jcs.02439>
- Mathieu, M., Martin-Jaular, L., Lavieu, G., & Théry, C. (2019). Specificities of secretion and uptake of exosomes and other extracellular vesicles for cell-to-cell communication. *Nature Cell Biology*, *21*, 9–17. <https://doi.org/10.1038/s41556-018-0250-9>
- Mathieu, M., Névo, N., Jouve, M., Valenzuela, J. I., Maurin, M., Verweij, F. J., Palmulli, R., Lankar, D., Dingli, F., Loew, D., Rubinstein, E., Boncompain, G., Perez, F., & Théry, C. (2021). Specificities of exosome versus small ectosome secretion revealed by live intracellular tracking of CD63 and CD9. *Nature Communication*, *12*, 4389. <http://doi.org/10.1038/s41467-021-24384-2>
- Mielnicka, A., & Michaluk, P. (2021). Exocytosis in astrocytes exocytosis in astrocytes. *Biomolecules*, *11*, 1367. <http://doi.org/10.3390/biom11091367>
- Mighty, J., Zhou, J., Benito-Martin, A., Sauma, S., Hanna, S., Onwumere, O., Shi, C., Muntzel, M., Sauane, M., Young, M., Molina, H., Cox, D., & Redenti, S. (2020). Analysis of adult neural retina extracellular vesicle release, RNA transport and proteomic cargo. *Investigative Ophthalmology & Visual Science*, *61*, 30. <https://doi.org/10.1167/iovs.61.2.30>
- Morel, L., Regan, M., Higashimori, H., Ng, S. K., Esau, C., Vidensky, S., Rothstein, J., & Yang, Y. (2013). Neuronal exosomal miRNA-dependent translational regulation of astroglial glutamate transporter GLT1. *Journal of Biological Chemistry*, *288*, 7105–7116. <https://doi.org/10.1074/jbc.M112.410944>

- Mukai, A., Otsuki, Y., Ito, E., Fujita, T., Ueno, M., Maeda, T., Kinoshita, S., Sotozono, C., & Hamuro, J. (2021). Mitochondrial miRNA494-3p in extracellular vesicles participates in cellular interplay of iPSC-Derived human retinal pigment epithelium with macrophages. *Experimental Eye Research*, 208, 108621. <https://doi.org/10.1016/j.exer.2021.108621>
- Murat, C. B., & García-Cáceres, C. (2021). Astrocyte gliotransmission in the regulation of systemic metabolism. *Metabolites*, 11, 732. <https://doi.org/10.3390/metabol1110732>
- Nagelhus, E. A., Mathiisen, T. M., Bateman, A. C., Haug, F. M., Ottersen, O. P., Grubb, J. H., Waheed, A., & Sly, W. S. (2005). Carbonic anhydrase XIV is enriched in specific membrane domains of retinal pigment epithelium, Müller cells, and astrocytes. *PNAS*, 102, 8030–8035. <http://doi.org/10.1073/pnas.0503021102>
- Nave, K. A., & Werner, H. B. (2021). Ensheathment and myelination of axons: Evolution of glial functions. *Annual Review of Neuroscience*, 44, 197–219. <https://doi.org/10.1146/annurev-neuro-100120-122621>
- Ochrietor, J. D., Clamp, M. F., Moroz, T. P., Grubb, J. H., Shah, G. N., Waheed, A., Sly, W. S., & Linser, P. J. (2005). Carbonic anhydrase XIV identified as the membrane CA in mouse retina: Strong expression in Müller cells and the RPE. *Experimental Eye Research*, 81, 492–500. <https://doi.org/10.1016/j.exer.2005.03.010>
- Olivares, A. M., Jelcick, A. S., Reinecke, J., Leehy, B., Haider, A., Morrison, M. A., Cheng, L., Chen, D. F., Deangelis, M. M., & Haider, N. B. (2017). Multimodal regulation orchestrates normal and complex disease states in the Retina. *Science Reports*, 7, 690. <https://doi.org/10.1038/s41598-017-00788-3>
- Otsuki, Y., Ito, E., Mukai, A., Ueno, M., Yamawaki, T., Sotozono, C., Kinoshita, S., & Hamuro, J. (2021). CD63+ extracellular vesicles from retinal pigment epithelial cells participate in crosstalk with macrophages in the innate inflammatory axis. *Experimental Eye Research*, 205, 108496. <https://doi.org/10.1016/j.exer.2021.108496>
- Pannicke, T., Frommherz, I., Biedermann, B., Wagner, L., Sauer, K., Ulbricht, E., Härtig, W., Krügel, U., Ueberham, U., Arendt, T., Illes, P., Bringmann, A., Reichenbach, A., & Grosche, A. (2014). Differential effects of P2Y1 deletion on glial activation and survival of photoreceptors and amacrine cells in the ischemic mouse retina. *Cell Death & Disease*, 5, e1353. <https://doi.org/10.1038/cddis.2014.317>
- Pascual, M. A., Ibáñez, F., & Guerri, C. (2020). Exosomes as mediators of neuron-glia communication in neuroinflammation. *Neural Regeneration Research*, 15, 796–801. <https://doi.org/10.4103/1673-5374.268893>
- Patel, D. C., Tewari, B. P., Chaunsali, L., & Sontheimer, H. (2019). Neuron-glia interactions in the pathophysiology of epilepsy. *Nature Reviews Neuroscience*, 20, 282–297. <https://doi.org/10.1038/s41583-019-0126-4>
- Pathan, M., Fonseka, P., Chitti, S. V., Kang, T., Sanwlani, R., Van Deun, J., Hendrix, A., & Mathivanan, S. (2019). Vesiclepedia 2019: A compendium of RNA, proteins, lipids and metabolites in extracellular vesicles. *Nucleic Acids Research*, 47, D516–D519. <https://doi.org/10.1093/nar/gky1029>
- Pauly, D., Agarwal, D., Dana, N., Schäfer, N., Biber, J., Wunderlich, K. A., Jabri, Y., Straub, T., Zhang, N. R., Gautam, A. K., Weber, B. H. F., Hauck, S. M., Kim, M., Curcio, C. A., Stambolian, D., Li, M., & Grosche, A. (2019). Cell-type-specific complement expression in the healthy and diseased retina. *Cell Reports*, 29, 2835–2848. <https://doi.org/10.1016/j.celrep.2019.10.084>
- Pekna, M., Pekna, M., Messing, A., Steinhäuser, C., Lee, J. M., Parpura, V., Hol, E. M., Sofroniew, M. V., & Verkhratsky, A. (2016). Astrocytes: A central element in neurological diseases. *Acta Neuropathologica*, 131, 323–345. <https://doi.org/10.1007/s00401-015-1513-1>
- Peng, Y., Baulier, E., Ke, Y., Young, A., Ahmedli, N. B., Schwartz, S. D., & Farber, D. B. (2018). Human embryonic stem cells extracellular vesicles and their effects on immortalized human retinal Müller cells. *Plos One*, 13, e0194004. <https://doi.org/10.1371/journal.pone.0194004>
- Pertea, M., Pertea, G. M., Antonescu, C. M., Chang, T. C., Mendell, J. T., & Salzberg, S. L. (2015). StringTie enables improved reconstruction of a transcriptome from RNA-seq reads. *Nature Biotechnology*, 33, 290–295. <https://doi.org/10.1038/nbt.3122>
- Pfrieger, F. W., & Vitale, N. (2018). Cholesterol and the journey of extracellular vesicles. *Journal of Lipid Research*, 59, 2255–2261. <https://doi.org/10.1194/jlr.R084210>
- Pistono, C., Bister, N., Stanová, I., & Malm, T. (2020). Glia-derived extracellular vesicles: Role in central nervous system communication in health and disease. *Frontiers in Cell and Developmental Biology*, 8, 623771. <https://doi.org/10.3389/fcell.2020.623771>
- Pols, M. S., & Klumperman, J. (2009). Trafficking and function of the tetraspanin CD63. *Experimental Cell Research*, 315, 1584–1592. <https://doi.org/10.1016/j.yexcr.2008.09.020>
- Potolichio, I., Carven, G. J., Xu, X., Stipp, C., Riese, R. J., Stern, L. J., & Santambrogio, L. (2005). Proteomic analysis of microglia-derived exosomes: Metabolic role of the aminopeptidase CD13 in neuropeptide catabolism. *Journal of Immunology*, 175, 2237–2243. <https://doi.org/10.4049/jimmunol.175.4.2237>
- Raiders, S., Han, T., Scott-Hewitt, N., Kucenas, S., Lew, D., Logan, M. A., & Singhvi, A. (2021). Engulfed by glia: Glial pruning in development, function, and injury across species. *Journal of Neuroscience*, 41, 823–833. <https://doi.org/10.1523/jneurosci.1660-20.2020>
- Raudvere, U., Kolberg, L., Kuzmin, I., Arak, T., Adler, P., Peterson, H., & Vilo, J. (2019). g:Profiler: A web server for functional enrichment analysis and conversions of gene lists (2019 update). *Nucleic Acids Research*, 47, W191–W198. <https://doi.org/10.1093/nar/gkz369>
- Reichenbach, A. (1989). Attempt to classify glial cells by means of their process specialization using the rabbit retinal Müller cell as an example of cytotopographic specialization of glial cells. *Glia*, 2, 250–259. <https://doi.org/10.1002/glia.440020406>
- Reichenbach, A., & Bringmann, A. (2020). Glia of the human retina. *Glia*, 68, 768–796. <https://doi.org/10.1002/glia.23727>
- Rilla, K. (2021). Diverse plasma membrane protrusions act as platforms for extracellular vesicle shedding. *Journal of Extracellular Vesicles*, 10, e12148. <https://doi.org/10.1002/jev2.12148>
- Ropelewski, P., & Imanishi, Y. (2020). RPE cells engulf microvesicles secreted by degenerating rod photoreceptors. *eNeuro*, 7, 3. <http://doi.org/10.1523/ENEURO.0507-19.2020>
- Salinas, R. Y., Pearing, J. N., Ding, J. D., Spencer, W. J., Hao, Y., & Arshavsky, V. Y. (2017). Photoreceptor discs form through peripherin-dependent suppression of ciliary ectosome release. *Journal of Cell Biology*, 216, 1489–1499. <http://doi.org/10.1083/jcb.201608081>
- Salomon, C., Ryan, J., Sobrevia, L., Kobayashi, M., Ashman, K., Mitchell, M., & Rice, G. E. (2013). Exosomal signaling during hypoxia mediates microvascular endothelial cell migration and vasculogenesis. *Plos One*, 8, e68451. <https://doi.org/10.1371/journal.pone.0068451>
- Savtchouk, I., & Volterra, A. (2018). Gliotransmission: Beyond black-and-white. *Journal of Neuroscience*, 38, 14–25. <https://doi.org/10.1523/JNEUROSCI.0017-17.2017>
- Schäfer, N., Grosche, A., Schmitt, S. I., Braunger, B. M., & Pauly, D. (2017). Complement components showed a time-dependent local expression pattern in constant and acute white light-induced photoreceptor damage. *Frontiers in Molecular Neuroscience*, 10, 197. <https://doi.org/10.3389/fnmol.2017.00197>
- Schindelin, J., Arganda-Carreras, I., Frise, E., Kaynig, V., Longair, M., Pietzsch, T., Preibisch, S., Rueden, C., Saalfeld, S., Schmid, B., Tinevez, J. Y., White, D. J., Hartenstein, V., Eliceiri, K., Tomancak, P., & Cardona, A. (2012). Fiji: An open-source platform for biological-image analysis. *Nature Methods*, 9, 676–682. <https://doi.org/10.1038/nmeth.2019>
- Schnatz, A., Müller, C., Brahmer, A., & Albers, E. M. K. (2021). Extracellular vesicles in neural cell interaction and CNS homeostasis. *FASEB Bioadvances*, 3, 577–592. <https://doi.org/10.1096/fba.2021-00035>
- Seifert, G., & Steinhäuser, C. (2018). Heterogeneity and function of hippocampal macroglia. *Cell and Tissue Research*, 373, 653–670. <https://doi.org/10.1007/s00441-017-2746-1>

- Shen, W., Nikolic, L., Meunier, C., Pfrieger, F., & Audinat, E. (2017). An autocrine purinergic signaling controls astrocyte-induced neuronal excitation. *Science Reports*, 7, 11280. <https://doi.org/10.1038/s41598-017-11793-x>
- Slezak, M., Grosche, A., Niemiec, A., Tanimoto, N., Pannicke, T., Münch, T. A., Crocker, B., Isope, P., Härtig, W., Beck, S. C., Huber, G., Ferracci, G., Perraut, M., Reber, M., Mieke, M., Demais, V., Lévêque, C., Metzger, D., Szklarczyk, K., ... Pfrieger, F. W. (2012). Relevance of exocytotic glutamate release from retinal glia. *Neuron*, 74, 504–516. <https://doi.org/10.1016/j.neuron.2012.03.027>
- Sokolova, V., Ludwig, A. K., Hornung, S., Rotan, O., Horn, P. A., Epple, M., & Giebel, B. (2011). Characterisation of exosomes derived from human cells by nanoparticle tracking analysis and scanning electron microscopy. *Colloids and Surfaces. B, Biointerfaces*, 87, 146–150. <https://doi.org/10.1016/j.colsurfb.2011.05.013>
- Sreekumar, P. G., Kannan, R., Kitamura, M., Spee, C., Barron, E., Ryan, S. J., & Hinton, D. R. (2010). α B crystallin is apically secreted within exosomes by polarized human retinal pigment epithelium and provides neuroprotection to adjacent cells. *Plos One*, 5, e12578. <https://doi.org/10.1371/journal.pone.0012578>
- Südhof, T. C., & Rothman, J. E. (2009). Membrane fusion: Grappling with SNARE and SM proteins. *Science*, 323, 474–477. <https://doi.org/10.1126/science.1161748>
- Sultan, S., Li, L., Moss, J., Petrelli, F., Cassé, F., Gebara, E., Lopatar, J., Pfrieger, F. W., Bezzi, P., Bischofberger, J., & Toni, N. (2015). Synaptic integration of adult-born hippocampal neurons is locally controlled by astrocytes. *Neuron*, 88, 957–972. <https://doi.org/10.1016/j.neuron.2015.10.037>
- Tajika, Y., Takahashi, M., Khairani, A. F., Ueno, H., Murakami, T., & Yorifuji, H. (2014). Vesicular transport system in myotubes: Ultrastructural study and signposting with vesicle-associated membrane proteins. *Histochemistry and Cell Biology*, 141, 441–454. <https://doi.org/10.1007/s00418-013-1164-z>
- Takahashi, M., Tajika, Y., Khairani, A. F., Ueno, H., Murakami, T., & Yorifuji, H. (2013). The localization of VAMP5 in skeletal and cardiac muscle. *Histochemistry and Cell Biology*, 139, 573–582. <https://doi.org/10.1007/s00418-012-1050-0>
- Tan, C. X., Burrus Lane, C. J., & Eroglu, C. (2021). Role of astrocytes in synapse formation and maturation. *Current Topics in Developmental Biology*, 142, 371–407. <https://doi.org/10.1016/bs.ctdb.2020.12.010>
- Team RC (2021). <https://www.R-project.org/>
- Tendler, Y., & Panshin, A. (2020). Features of p53 protein distribution in the corneal epithelium and corneal tear film. *Science Reports*, 10, 10051. <https://doi.org/10.1038/s41598-020-67206-z>
- Théry, C., Regnault, A., Garin, J., Wolfers, J., Zitvogel, L., Ricciardi-Castagnoli, P., Raposo, G., & Amigorena, S. (1999). Molecular characterization of dendritic cell-derived exosomes: Selective accumulation of the heat shock protein Hsc73. *Journal of Cell Biology*, 147, 599–610. <https://doi.org/10.1083/jcb.147.3.599>
- Théry, C., Amigorena, S., Raposo, G., & Clayton, A. (2006). Isolation and characterization of exosomes from cell culture supernatants and biological fluids. *Current Protocols in Cell Biology*, 30, 3.22.21–3.22.29. <https://doi.org/10.1002/0471143030.cb0322s30>
- Théry, C., Witwer, K. W., Aikawa, E., Alcaraz, M. J., Anderson, J. D., Andriantsitohaina, R., Antoniou, A., Arab, T., Archer, F., Atkin-Smith, G. K., Ayre, D. C., Bach, J. M., Bachurski, D., Baharvand, H., Balaj, L., Baldacchino, S., Bauer, N. N., Baxter, A. A., Bebawy, M., ... Zuba-Surma, E. K. (2018). Minimal information for studies of extracellular vesicles 2018 (MISEV2018): A position statement of the International Society for Extracellular Vesicles and update of the MISEV2014 guidelines. *Journal of Extracellular Vesicles*, 7, 1535750. <https://doi.org/10.1080/20013078.2018.1535750>
- Toyofuku, T., Nojima, S., Ishikawa, T., Takamatsu, H., Tsujimura, T., Uemura, A., Matsuda, J., Seki, T., & Kumanogoh, A. (2012). Endosomal sorting by Semaphorin 4A in retinal pigment epithelium supports photoreceptor survival. *Genes & Development*, 26, 816–829. <https://doi.org/10.1101/gad.184481.111>
- Trapnell, C., Pachter, L., & Salzberg, S. L. (2009). TopHat: Discovering splice junctions with RNA-Seq. *Bioinformatics*, 25, 1105–1111. <https://doi.org/10.1093/bioinformatics/btp120>
- Urbina, F. L., & Gupton, S. L. (2020). SNARE-mediated exocytosis in neuronal development. *Frontiers in Molecular Neuroscience*, 13, 133. <https://doi.org/10.3389/fnmol.2020.00133>
- Van Niel, G., Carter, D. R. F., Clayton, A., Lambert, D. W., Raposo, G., & Vader, P. (2022). Challenges and directions in studying cell–cell communication by extracellular vesicles. *Nature Reviews Molecular Cell Biology*, 23, 369–382. <https://doi.org/10.1038/s41580-022-00460-3>
- Vardjan, N., Parpura, V., Verkhratsky, A., & Zorec, R. (2019). Gliocrine system: Astroglia as secretory cells of the CNS. *Advances in Experimental Medicine and Biology*, 1175, 93–115. https://doi.org/10.1007/978-981-13-9913-8_4
- Vázquez-Chona, F. L., Song, B. K., & Geisert, E. E. (2004). Temporal changes in gene expression after injury in the rat retina. *Investigative Ophthalmology & Visual Science*, 45, 2737–2746. <http://doi.org/10.1167/iovs.03-1047>
- Velázquez-Enríquez, J. M., Santos-Álvarez, J. C., Ramírez-Hernández, A. A., Reyes-Jiménez, E., López-Martínez, A., Pina-Canseco, S., Aguilar-Ruiz, S. R., Romero-Tlalolini, M. L. Á., Castro-Sánchez, L., Arellanes-Robledo, J., Vázquez-Garzón, V. R., & Baltiérrez-Hoyos, R. (2021). Proteomic analysis reveals key proteins in extracellular vesicles cargo associated with idiopathic pulmonary fibrosis in vitro. *Biomedicine*, 9, 1058. <https://doi.org/10.3390/biomedicine9081058>
- Verweij, F. J., Balaj, L., Boulanger, C. M., Carter, D. R. F., Compeer, E. B., D'Angelo, G., El Andaloussi, S., Goetz, J. G., Gross, J. C., Hyenne, V., Krämer-Albers, E. M., Lai, C. P., Loyer, X., Marki, A., Momma, S., Nolte-t Hoen, E. N. M., Pegtel, D. M., Peinado, H., Raposo, G., ... Van Niel, G. (2021). The power of imaging to understand extracellular vesicle biology in vivo. *Nature Methods*, 18, 1013–1026. <https://doi.org/10.1038/s41592-021-01206-3>
- Vilcaes, A. A., Chanaday, N. L., & Kavalali, E. T. (2021). Interneuronal exchange and functional integration of synaptobrevin via extracellular vesicles. *Neuron*, 109, 971–983.e5. <https://doi.org/10.1016/j.neuron.2021.01.007>
- Wagner, L., Pannicke, T., Frommherz, I., Sauer, K., Chen, J., & Grosche, A. (2016). Effects of IP3R2 receptor deletion in the ischemic mouse retina. *Neurochemical Research*, 41, 677–686. <https://doi.org/10.1007/s11064-015-1735-6>
- Wagner, L., Pannicke, T., Rupprecht, V., Frommherz, I., Volz, C., Illes, P., Hirrlinger, J., Jäggle, H., Egger, V., Haydon, P. G., Pfrieger, F. W., & Grosche, A. (2017). Suppression of SNARE-dependent exocytosis in retinal glial cells and its effect on ischemia-induced neurodegeneration. *Glia*, 65, 1059–1071. <https://doi.org/10.1002/glia.23144>
- Wang, A. L., Lukas, T. J., Yuan, M., Du, N., Tso, M. O., & Neufeld, A. H. (2009). Autophagy and exosomes in the aged retinal pigment epithelium: Possible relevance to drusen formation and age-related macular degeneration. *Plos One*, 4, e4160. <https://doi.org/10.1371/journal.pone.0004160>
- Wang, J., Silva, M., Haas, L. A., Morsci, N. S., Nguyen, K. C. Q., Hall, D. H., & Barr, M. M. (2014a). *C. elegans* ciliated sensory neurons release extracellular vesicles that function in animal communication. *Current Biology*, 24, 519–525. <https://doi.org/10.1016/j.cub.2014.01.002>
- Wang, M., Wang, X., Zhao, L., Ma, W., Rodriguez, I. R., Fariss, R. N., & Wong, W. T. (2014b). Microglia-microglia interactions via TSPO signaling regulates microglial activation in the mouse retina. *Journal of Neuroscience*, 34, 3793–3806. <http://doi.org/10.1523/JNEUROSCI.3153-13.2014>
- Wang, J., O'Sullivan, M. L., Mukherjee, D., Puñal, V. M., Farsi, S., & Kay, J. N. (2017). Anatomy and spatial organization of Müller glia in mouse retina. *Journal of Comparative Neurology*, 525, 1759–1777. <http://doi.org/10.1002/cne.24153>
- Wang, T., Li, Y., Guo, M., Dong, X., Liao, M., Du, M., Wang, X., Yin, H., & Yan, H. (2021). Exosome-mediated delivery of the neuroprotective peptide PACAP38 promotes retinal ganglion cell survival and axon regeneration in rats with traumatic optic neuropathy. *Frontiers in Cell and Developmental Biology*, 9, 659783. <https://doi.org/10.3389/fcell.2021.659783>

- Wassmer, S. J., Carvalho, L. S., György, B., Vandenberghe, L. H., & Maguire, C. A. (2017). Exosome-associated AAV2 vector mediates robust gene delivery into the murine retina upon intravitreal injection. *Science Reports*, 7, 45329. <https://doi.org/10.1038/srep45329>
- Wilton, D. K., Dissing-Olesen, L., & Stevens, B. (2019). Neuron-glia signaling in synapse elimination. *Annual Review of Neuroscience*, 42, 107–127. <https://doi.org/10.1146/annurev-neuro-070918-050306>
- Wilton, D. K., & Stevens, B. (2020). The contribution of glial cells to Huntington's disease pathogenesis. *Neurobiology of Disease*, 143, 104963. <https://doi.org/10.1016/j.nbd.2020.104963>
- Wiśniewski, J. R., Zougman, A., Nagaraj, N., & Mann, M. (2009). Universal sample preparation method for proteome analysis. *Nature Methods*, 6, 359–362. <https://doi.org/10.1038/nmeth.1322>
- Wood, C. R., Huang, K., Diener, D. R., & Rosenbaum, J. L. (2013). The cilium secretes bioactive ectosomes. *Current Biology*, 23, 906–911. <http://doi.org/10.1016/j.cub.2013.04.019>
- Woo, Y., Cioanca, A. V., Chu-Tan, J. A., Aggio-Bruce, R., Schumann, U., & Natoli, R. (2020). Small-medium extracellular vesicles and their miRNA cargo in retinal health and degeneration: Mediators of homeostasis, and vehicles for targeted gene therapy. *Frontiers in Cellular Neuroscience*, 14, 160. <https://doi.org/10.3389/fncel.2020.00160>
- Yates, A. G., Pink, R. C., Erdbrügger, U., Siljander, P. R. M., Dellar, E. R., Pantazi, P., Akbar, N., Cooke, W. R., Vatish, M., Neto, E. D., Anthony, D. C., & Couch, Y. (2022). In sickness and in health: The functional role of extracellular vesicles in physiology and pathology in vivo. *Journal of Extracellular Vesicles*, 11, e12151. <https://doi.org/10.1002/jev2.12151>
- You, Y., & Ikezu, T. (2019). Emerging roles of extracellular vesicles in neurodegenerative disorders. *Neurobiology of Disease*, 130, 104512. <https://doi.org/10.1016/j.nbd.2019.104512>
- Yuyama, K., Sun, H., Mitsutake, S., & Igarashi, Y. (2012). Sphingolipid-modulated exosome secretion promotes clearance of amyloid- β by microglia. *Journal of Biological Chemistry*, 287, 10977–10989. <https://doi.org/10.1074/jbc.M111.324616>
- Zamarian, J. L., Xu, L., Foo, L. C., Nouri, N., Zhou, L., Giffard, R. G., & Barres, B. A. (2012). Genomic analysis of reactive astrogliosis. *Journal of Neuroscience*, 32, 6391–6410. <https://doi.org/10.1523/jneurosci.6221-11.2012>
- Zeng, Q., Subramaniam, V. N., Wong, S. H., Tang, B. L., Parton, R. G., Rea, S., James, D. E., & Hong, W. (1998). A novel synaptobrevin/VAMP homologous protein (VAMP5) is increased during in vitro myogenesis and present in the plasma membrane. *Molecular Biology of the Cell*, 9, 2423–2437. <https://doi.org/10.1091/mbc.9.9.2423>
- Zhang, W., Jiang, H., & Kong, Y. (2020). Exosomes derived from platelet-rich plasma activate YAP and promote the fibrogenic activity of Müller cells via the PI3K/Akt pathway. *Experimental Eye Research*, 193, 107973. <https://doi.org/10.1016/j.exer.2020.107973>
- Zhao, Y., Weber, S. R., Lease, J., Russo, M., Siedlecki, C. A., Xu, L. C., Chen, H., Wang, W., Ford, M., Simó, R., & Sundstrom, J. M. (2018). Liquid biopsy of vitreous reveals an abundant vesicle population consistent with the size and morphology of exosomes. *Transl Vis Sci Technol*, 7, 6. <https://doi.org/10.1167/tvst.7.3.6>
- Zhou, J., Benito-Martin, A., Mighty, J., Chang, L., Ghoroghi, S., Wu, H., Wong, M., Guariglia, S., Baranov, P., Young, M., Gharbaran, R., Emerson, M., Mark, M. T., Molina, H., Canto-Soler, M. V., Selgas, H. P., & Redenti, S. (2018). Retinal progenitor cells release extracellular vesicles containing developmental transcription factors, microRNA and membrane proteins. *Science Reports*, 8, 2823. <https://doi.org/10.1038/s41598-018-20421-1>

SUPPORTING INFORMATION

Additional supporting information can be found online in the Supporting Information section at the end of this article.

How to cite this article: Demais, V., Pohl, A., Wunderlich, K. A., Pfaller, A. M., Kaplan, L., Barthélémy, A., Dittrich, R., Puig, B., Giebel, B., Hauck, S. M., Pfrieger, F. W., & Grosche, A. (2022). Release of VAMP5-positive extracellular vesicles by retinal Müller glia in vivo. *Journal of Extracellular Vesicles*, 11, e12254. <https://doi.org/10.1002/jev2.12254>

III. DISCUSSION

WITH GREAT DATA COMES GREAT COMPUTATION

My data analysis posed specific technical challenges that can all have an influence on the end result and most importantly the final interpretation. Omic data like RNAseq, proteomics and single cell RNAseq in particular are prone to generate zero-inflated expression matrices. Such matrices contain a high amount of genes/proteins with zero or missing expression values across many samples. The degree of the zero inflation in part depends on the sensitivity of the technique but also on the analyzed samples, resulting in two basic origins of zero values: biological and technical. Biological zeros represent a true missing of a protein or transcript and are the result of a difference between the analyzed samples, for example between cells of different type or state. Technical zeros generally can occur amongst others due to material loss during isolation/preparation steps or insufficient sensitivity of the counting method. Tandem mass spectrometry, as used in our proteomic investigations, has a number of complex variables causing technical zeros. These can range from instrumentation-related differences in HPLC columns, acquisition mode, scan speeds and database annotation, but also intersample variation in post-translational modifications. As data dependent acquisition (DDA) might miss peptides if they do not show the top intensities among precursor ions, we used data independent acquisition (DIA) for its superior protein identification rate although both can have issues detecting protein isoforms. To tackle some of the challenges of zero inflation in proteomics, imputation methods have been developed and were employed in our studies before statistical analysis but remain controversial [64], [65]. To further ensure meaningful interpretation and to increase robustness, I filtered the identified proteins to include only those that were found in three out of five biological replicates of glial samples.

Once I generated a satisfactory expression matrix, the primary target was the identification of differentially expressed genes or proteins for which I considered a variety of statistical tests implemented for example in packages for R. These include

Welch's t-test, analysis of variance (ANOVA), DESeq2 [66], limma [67], or SAM [68] but the identified genes/proteins differed in part significantly, as was previously reported [65], [69]. Thus, a careful deliberation was necessary to choose the right method depending on factors like sample size and distribution.

Even after the successful identification of differentially expressed proteins, the computational biologist is often left with long lists of gene names which might not immediately reveal their functional implications. To extract candidates for further investigation, one can boil down such lists to few select genes by applying – generally arbitrary – thresholds e.g. to a fold change or a p-value. Another possibility to better grasp the underlying meaning is the categorization by pathway enrichment analysis, which can give a hint in which contexts such genes might play a role. Amongst others, this can reveal the cellular localization, enzymatic activity, protein family, disease association or possible binding partners and thus guide further investigation. Common problems are the one-to-many relationship of genes to pathways, the deterioration of the importance of p-value/q-value [70] and the granularity of pathway terms [71]. The latter can not only alter statistics, but also aggravate interpretation if the enriched terms are too general/unspecific. Some strategies that I used if not to overcome, but to alleviate some of these challenges, were the selection of lists of interconnected genes by WGCNA [51], utilization of the meta database STRING [58], [59] and the visualization via Cytoscape. Additionally, I employed subclustering of the networks generated by STRING before pathway enrichment analysis to gain smaller lists of genes with better interpretable terms. The combination of these tools allowed me to identify pathways as well as specific proteins that seem to play a role in the heterogeneity of various glial subtypes.

The complexity increased even more when comparing (differential) expression between transcriptomic and proteomic technologies. Various post-transcriptional regulatory mechanism like stability of mRNA or protein, differential ribosome usage or translation on demand can lead to a divergence between transcript and protein levels [72], [73]. In the present work, I looked at the interregional differences on transcript and protein level in comparable samples. Since these methods rely on vastly different technologies, the comparison of the expression values, that may be orders of magnitude apart in their absolute numbers, is rather difficult. To alleviate this, one can use relative values or ratios to normalize for technological variation. As relative read-outs I chose for example the ratio between Müller cells' and neurons' expression levels, when comparing Müller cell populations in the retina or expression above median when several CNS regions were to be contrasted. Indeed, I found only weak Spearman correlation between 0.12 and 0.34 (53 % to 61 % concordant regulation) between bulk

RNAseq and proteomics when comparing glial subpopulations in murine central nervous system. In contrast, differential protein expression between human central and peripheral Müller cells was conserved to a higher degree on single cell transcriptomic level with most genes/proteins that were detected in both methods showing concordant regulation (> 90%). Studies report correlation values between 0.4 to 0.7 [72]–[75], but the higher values could only be achieved in direct comparison of tightly controlled, rather homogeneous samples. Thus, it seems that very defined conditions (e.g. same tissue, same cell type, same comparisons, precise quantification methods) need to be met to achieve an enhanced concordance regarding differential gene expression at both transcript and protein level. Consequently, Vogel and Marcotte [72] suggested a model where mRNA levels are seen as a broad genetic switch, while post-transcriptional regulation is responsible for the fine tuning of protein levels that are reflected in proteomics. A strong correlation would thus be seen only during a steady state. Defining a steady-state however can get difficult, considering that even in the healthy organism gene expression levels cycle constantly between different states at transcript and protein level [76], [77].

Bioinformatic analyses based on omic data remain an increasingly powerful tool to look at a plethora of cellular variables and allow the identification of genes of interest opening new avenues for investigation. Nevertheless, such *in silico* analyses may predict relationships based on mathematical models to a degree of certainty and are only as informative as the underlying data and thus do not reflect the whole biological picture. For example, interconnection between proteins can be indicated by correlated expression in proteomic data sets or by their membership in a biochemical pathway in a pathway enrichment analysis. But information about the manner of interaction, quaternary structure, alternative functions, cellular localization, or posttranslational modifications are missing. In consequence, no definitive statement can be made about their function.

In conclusion, bioinformatics helps uncover patterns hidden to the naked eye and spark novel ideas, but (molecular) biological tools are necessary to prove their relevance *in vitro* and ideally also *in vivo*, thus providing definitive evidence for hypotheses originally made using bioinformatics tools.

COMMON PROTEOMIC PATTERNS SHAPE GLOBAL AND LOCAL GLIAL IDENTITY

The mammalian CNS contains amongst others two major cell types: the glia and the neurons. While the latter have been intensively studied for many years and were successfully divided into many functional and regional subtypes, glia cells were long thought to play a secondary role. It is now clear that they fulfill a plethora of tissue-specific functions in the CNS including the retina. The degree to which glial functions are conserved or divergent between regions of the CNS or defining characteristics of subclasses have previously been studied and extensively reviewed but often lack the comparison with the retina [15], [28], [29], [78]–[86]. In the first manuscript, I focused on the relationship between brain astrocytes and their retinal siblings, the Müller cells, in an attempt to uncover similarities and differences of their proteomic landscape. In the second study, I explored the possibility and indeed provided some evidence of the existence of Müller cell subtypes in the human retina.

Comparing the proteomic data between Müller cells and brain astrocyte-enriched fractions from gray matter, white matter and diencephalon I found some proteins to be expressed in a consistent macroglia-specific manner. These included known glial markers like Glial fibrillary acidic protein (GFAP), Vimentin (VIM), GLAST (SLC1A3), Aquaporin 4 (AQP4), Glutamine synthetase (GLUL) and 10-formyltetrahydrofolate dehydrogenase (ALDH1L1). GFAP did not show a significantly different expression in the mass spectrometry data across all studied CNS regions. This is rather surprising, as it is generally accepted that GFAP is barely detectable by immunostaining in homeostatic Müller cells or cortical astrocytes, but is upregulated during pathology while being constitutively present in white matter and retinal astrocytes [87]. One reason for this finding could be a contamination of the purified Müller cell fraction by retinal astrocytes, even though Müller cells by far outnumber astrocytes in the retina. Another explanation could be that mechanical stress due to the isolation protocol triggers Müller cells and cortical astrocytes to initiate their response program to tissue damage signals and thus to upregulate GFAP. Finally, the use of human GFAP promotor-driven reporter expression does result in labeling of some Müller cells in non-injured tissue which implies that they indeed, even though at low levels, do express GFAP in the homeostatic retina [88].

On the other side, ALDH1L1 is regarded as a panastrocytic marker [87] but showed 8-fold higher expression in grey compared to white matter astrocytes. Generally, it is unclear whether and how proteomic differences translate to detectable

changes in immunostaining signals [89], [90], since this antibody-based technique involves several steps to visualize a target and generate a signal that is not necessarily correlated with protein expression values. The intra- and intercellular localization, post translational modifications, protein isoform composition and changes in epitope tertiary structure may all influence the detection by antibodies but are not necessarily picked up by mass spectrometry, depending on the mode or sample preparation [37]. Additionally, it is not apparent how much actual change in protein amount would lead to a measurable shift in immunofluorescence signal making it difficult to quantify reliably. Along these lines, (immuno-)fluorescence based quantification in transgenic mouse strains using ALDH1L1 as a driver for eGFP or Cre recombinase indicate an ubiquitous expression across the brain albeit with a slightly lower recombination efficiency in corpus callosum [87], [91]. Thus, these two methods, immunofluorescence staining and tandem mass spectrometry, need to be seen as complementary rather than congruent in respect to their evidence. On a different note, there are indications that the MACS sorting approach based on ACSA2 selection results in contamination with oligodendrocytes and ependymal cells to varying degrees between the three brain regions [16], which might result in a slight skew in marker expression that cannot be ruled out completely.

Nevertheless, we found transcription factors of the nuclear factor 1 family (NFI), NFIA and NFIX to be widely expressed specifically by glial cells of the central nervous system – and also the human retina – at comparable levels. NFIA seems to be involved in directing cell fate towards the glial lineage during development as it has been shown to be sufficient to stimulate gliogenesis and suppress neurogenesis in spinal cord [92], [93]. Similarly, a recent, extensive multispecies study reported that NFI transcription factors promote the quiescent state of Müller cells after injury, while leading to enhanced proliferation and the generation of neuron-like cells when deleted [94]. Interestingly, NFI factors showed a Müller cell-specific expression also in the human retina in our study with a tendency of a higher expression in macular glia compared to peripheral ones. In this context, increased NFI expression might lead to strengthened glial phenotype concomitant with a lack in proliferative and regenerative potential. Together our data and previous reports suggest a common regulatory network between Müller cells and astrocytes of the central nervous system that dictates glial versus neuronal identity not only during development but also in adult individuals.

DISTINCT PROTEOMIC PATTERNS BETWEEN REGIONS OF THE CNS CONVERGE ON YAP1 SIGNALING

Although I found a set of proteins with equal expression across Müller cells and astrocytes among the studied CNS regions, many more of the protein expression profiles were characteristic for specific glial subpopulations representing diverse molecular pathways. The sum of these revealed a close relationship between Müller cell and diencephalic astrocytes and distinct proteomic profiles for all subgroups. For example, gray matter and white matter glia were both enriched in ribosomal and ribosome-associated proteins, respectively, but each was enriched in different members of these protein families. Looking at mitochondrial proteins, I noticed a subset to be differentially regulated between grey matter and diencephalic glia, while having comparable levels between Müller cells and white matter.

Interestingly, when I compared various pathways with interregional regulation differences, it became clear that many seemed to converge onto Hippo pathway, which has an inhibitory function on YAP1 (Figure 4) [95], [96]. Several biomechanical signals cause YAP1 protein translocation from cytoplasm to nucleus [97], [98] and thus to transcriptional activation of a multitude of genes involved amongst others in cell cycle progression and proliferation.

In our context, Müller cells and diencephalic glia, shared a common set of equally expressed proteins, which indicates that their common ancestry, the diencephalic secondary vesicle, can still be traced in adult animals. Both showed increased expression of GTPases of the RAS family as well as other proto-oncogenes like MTOR or SRC in comparison to grey and white matter. The mutant, constitutive activation of these genes was implicated in unchecked growth and cell division, a hallmark of cancer [99], [100]. Additionally, there are reports providing some evidence for a complex interaction of RAS and SRC with YAP1 [101], [102]. As both glial subpopulations do express YAP1 on protein level, it might physiologically be similarly involved in the proliferative potential of diencephalic astrocytes and Müller cells. However, there is a discrepancy in their ability to proliferate. Müller cells do not divide in uninjured adult mouse retina, while diencephalic astrocytes to some degree do [16]. Here the strong and highly specific expression of Sarcolemmal Membrane-Associated Protein (SLMAP) that we found in Müller cells might allow some insights. This protein, too, participates in the Hippo pathway as it mediates the interaction of the striatin-interacting phosphatase and kinase (STRIPAK) complex to MST1/2, dephosphorylating them. Hence MST1/2 cannot activate LATS1/2 which finally leads to the translocation of YAP1

to the nucleus [96], [103]. Conversely, recent multispecies studies revealed that although YAP1 is upregulated in gliotic Müller cells of mice and xenopus, only amphibian cells constantly increase cell-cycle entry and proliferation. This barrier in the mammalian retina was abolished when a Hippo-inhibition-insensitive YAP1 species was overexpressed [104]–[106]. Thus SLMAP/STRIPAK independent signaling might lead to YAP1 inhibition and the difference in proliferation found between retina and diencephalon. Upstream of YAP1, this could be mediated, for example, by thousand-and-one kinases (TAO) or Ras association domain-containing protein 1 (RASSF1A), both of which have activating effects on MST1/2, whereas AMPK could directly inhibit YAP1 [96].

In grey matter, a brain region with limited, injury-induced proliferation of astrocytes [107], [108], I identified ZEB1 to have highest protein expression. This transcription factor, known to trigger epithelial to mesenchymal transition (EMT) [109]–[111] and recently shown to be involved in cell fate determination in hippocampus [112], may also act as a transcriptional coactivator of YAP1 [113], [114]. As YAP1 levels are also increased in grey matter, this expression pattern would indicate enhanced proliferative character, which was however shown to be less prominent when compared to diencephalon [16]. Another function of ZEB1 that might be of interest in this context is its role in alternative splicing during EMT [115]. Not only were proteins of mRNA processing and splicing upregulated in grey matter astrocytes, I also found proteins with a putative ZEB1 binding site and correlated expression to be also belonging to these pathways. This type of posttranscriptional regulation is involved in cortical cell lineage determination via RNA binding protein fox-1 homolog (RBFOX) proteins [116]. RBFOX2 in turn was shown to be able to confer alternative splicing of Transcriptional enhancer factor TEF-1 (TEAD1), a major DNA-binding YAP1 coactivator inducing an isoform dependent variation in cell growth [117].

In summary, it seems that glial subpopulations utilize various signaling cascades and posttranscriptional modification to modulate YAP1 target gene expression while a fine-tuned combination of these potentially generate the observed discrepancy in proliferative character. Follow-up studies to validate this working hypothesis would therefore be very interesting.

Proteins differentially regulated between regions converge on Hippo signaling

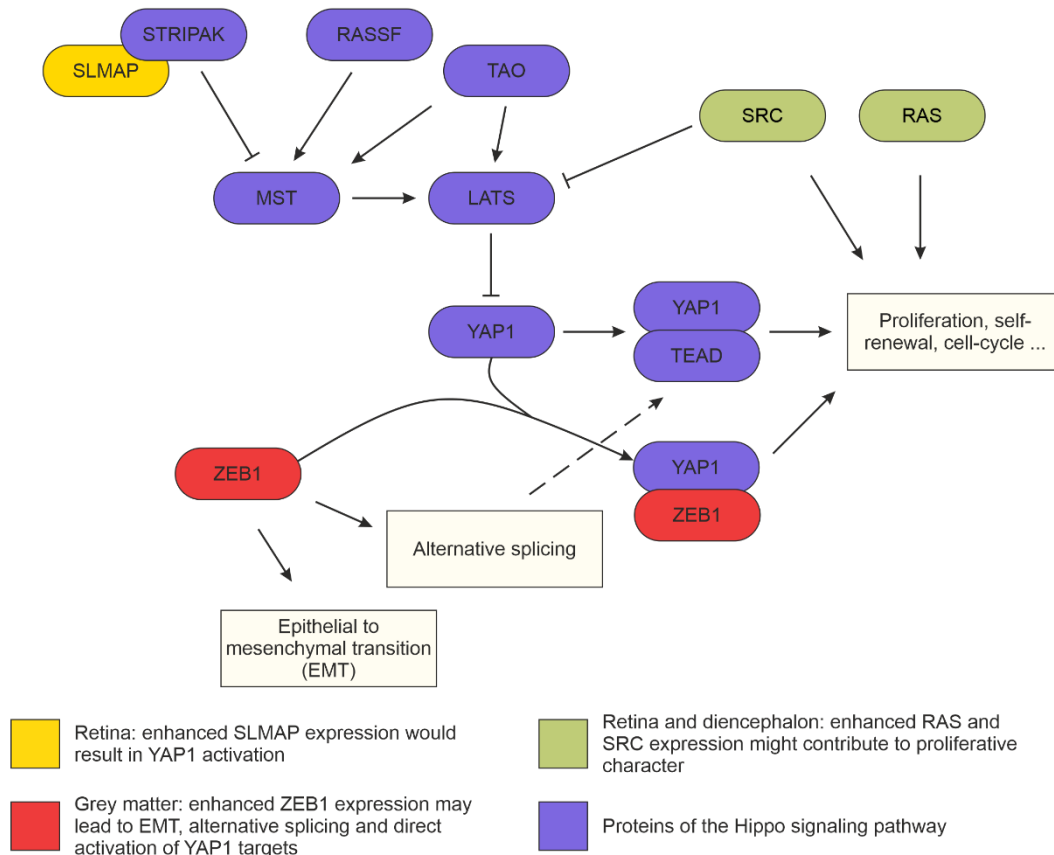


Figure 4: Several pathways that showed differential regulation between regions of the murine central nervous system seemed to converge onto Hippo signaling. Increased expression of SLMAP in retinal Müller cells might contribute to inhibitive MST dephosphorylation and thus to YAP1 activation. Proto-oncogenes SRC and RAS GTPases were enriched in Müller cells and glia from diencephalon and are thought to be involved in pathways enhancing cell proliferation. Grey matter showed highest expression in ZEB1, a protein that triggers EMT and concomitant alternative splicing. It was reported to be able to physically interact with YAP1 and activate its target genes. Furthermore, alternative splicing of YAP1 coactivator TEAD has been implicated in the modulation of transcriptional regulation of YAP1 targets.

The first part of my thesis focused on broader contemplation of astrocytes of various murine brain regions and retinal Müller glia thereby establishing distinctive but also uniting proteomic profiles of these related glia. In contrast to that, the macula presents a spot in the human retina where a steep tissue heterogeneity unfolds across relatively small spatial distance (within a diameter of ~ 5-6 mm, Figure 3). While this poses the challenge of a limited number of cells and thus sample material, it at the same time provides the advantage of an accessible and very defined area. This region is characterized by an enrichment in cones and Müller cells prompting us to look specifically on the interaction of these cell types using the all-cone mouse model [118] that mimics this exclusive Müller cell-cone interaction in a first step. Indeed, I found differentially expressed proteins between Müller cells which are mainly in contact with cone photoreceptors and such in a rod-rich environment. This murine model, however,

does not appropriately reproduce other important aspects of the macular area such as decreased vascularization, increased and direct light exposure of photoreceptors, and morphologically different Müller cells. Consequently, I sought to directly compare macular Müller cells with their peripheral counterparts and generated a proteomic dataset from Müller cells isolated from human donor tissue. Focusing on the aspect of Müller cell cone interaction, I compared the differentially expressed proteins from the all-cone mouse model with the human proteomic analysis. I found minimal overlap of only eight differentially expressed proteins shared across species. Thus, it seems that the proteomic changes on Müller cells evoked by the pure cone- vs. rod-association are either poorly conserved between the models or that they play only a minor or indirect role in Müller cell heterogeneity. Nevertheless, there seems to be a core set of proteins that specifically represents Müller cell-cone interaction in mouse which is conserved in human. They might be involved in functions like the intercellular transport of energy metabolites or signaling molecules, cell-cell adhesion or photo pigment recycling.

Examining the proteins that were enriched in human macular Müller cells, I found predominantly members of extracellular matrix, cell adhesion, and vesicular pathways hinting towards a shift in the extracellular milieu and biomechanical cell properties. Accordingly, I decided to focus on epiplakin (EPPK1), a member of plakin cytolinkers, for its exceptionally high expression in cone-associated Müller cells – both in mouse and human retina. To uncover basic cell biological functions of EPPK1 in Müller cells, I chose the human Müller cell-derived cell line MIO-M1 and assessed the impact of CRISPR/Cas9-mediated EPPK1 knockout. Interestingly, I found a phenotype not unlike to peripheral Müller cells with smaller, less complex cell protrusions and a reduced expression of extracellular and cell-adhesion proteins. In addition, traction force microscopy revealed that cells lacking EPPK1 exerted less traction stress on their substrate. This in turn implies that elevated EPPK1 levels, as they are found in macular Müller cells, might contribute not only to the generation of large cells with their characteristic z-shaped morphology but also to their ability to exert or resist the local mechanical strain [119]–[121]. As drusen (subretinal deposits of proteins and lipids), edema and macular holes are a common pathology in retinal diseases like age-related macular degeneration or macular telangiectasia type 2 [122]–[124], it might be worthwhile considering EPPK1 as a target to increase tissue stability.

As mentioned above, EPPK1 knockout cells exhibited a dysregulation of extracellular protein expression, which included a downregulation of CD9, an extracellular vesicle(EV)-associated protein of the tetraspanin family [125]–[127]. We corroborated this finding using immunofluorescence stainings. CD9 was also found to be specifically expressed by Müller cells and enriched in the macula in our human

proteomics data as well as in two published single cell RNAseq data sets [128], [129]. Furthermore, my collaborators and I showed secretion of CD9-positive EVs specifically from isolated murine Müller cells. Proteomic analyses of EVs purified from supernatants of cultured retinal cells revealed the presence of cell-type and vesicle-subpopulation-specific protein cargo indicating functional specialization. Additionally, as I found EPPK1 KO cells to release fewer EVs but with the same relative amount of CD9 in their secretome, I hypothesize that MIO-M1 cells mostly secrete CD9-containing vesicles. Consequently, EPPK1 KO might not lead to a disturbance of CD9-EV biogenesis but rather to a downregulation of intracellular mechanisms of EV shedding, like transport or fusion. These findings allude to a possibly indirect function of EPPK1, in which higher EPPK1 expression in macular Müller cells might contribute to an increased EV secretion. As extracellular matrix protein was increased in central Müller cells and decreased in the secretome of EPPK1 KO cells, one can speculate that EPPK1-dependent EV secretion is involved in the modification of the foveal extracellular matrix.

In summary, we found a subset of proteins that is conserved across glial cells of different regions of the CNS even across species. At the same time there is region-specific protein expression that seems to define or correspond to the glial functional niche. Further studies are necessary to dive deeper and elucidate which functional ramifications are rooted within these proteomic profiles.

IV. MAIN CONCLUSIONS & OUTLOOK

In my thesis project, I focused on the dissection of the glial character in different regions of the CNS to better define and understand their common and distinct functions. Looking at murine Müller cells and astrocytes enriched from grey matter, white matter and diencephalon, I found not only that all subpopulations share a core pan-glial proteome. I also demonstrated that even spatially distantly located glial cells from retina and diencephalon can be closer related on proteome level than glia from the same organ, like grey matter and diencephalic astrocytes. Furthermore, I presented a proteomic foundation for an explanation why there is an apparent variation in proliferative and stem cell potential between subsets of astroglia. In this regard, the pathways I analyzed seemed to converge on Hippo signaling. In consequence, I hypothesized how it might be specifically tuned by region-enriched proteins to activate or deactivate YAP1-dependent transcriptional regulation. Future studies should address whether or upon which cues ZEB1-mediated alternative splicing persists in the adult brain and how it influences YAP1/TEAD1 activation or the ability of cortical astrocytes to perform EMT. Similarly, I found that Müller cells express high amounts of putatively YAP1-activating SLMAP and SRC, although YAP1 activity has been reported to be lacking in murine Müller cells. This implies that either endogenous levels of YAP1 are just not high enough to produce enhanced proliferation or that there are other yet unknown strong Hippo signaling members to inhibit YAP1. Conversely, experimentally upregulated YAP1 signaling has led to enhanced Müller cell proliferation. Based on the insights I gained by comparing glial subpopulation of the CNS in this study, one might use similar paradigms in astrocytes of the brain to increase proliferation and eventually regeneration.

In the human retina, I was able to identify major protein pathways on which Müller cell heterogeneity between macula and periphery is grounded. The most prominent

pathways comprise proteins of the extracellular matrix, cytoskeleton or focal adhesion, which may be involved in ensuring mechanical stability and are therefore upregulated in the macular retina, which is inherently very fragile due to its particular cellular composition. As one example, I investigated EPPK1 as a protein that might contribute not only to biomechanical properties of Müller cells but also to their size and morphology. Additionally, secretory proteins showed differential regulation hinting towards a variance in intercellular signaling and material exchange. The combination of these results hints towards a very distinct extracellular milieu of the macula, which could prompt future projects probing, for example, Müller cell stiffness or extracellular vesicle cargo. With these studies, I was able to lay a fundamental foundation for the cell biological and molecular understanding of Müller cells in the most important area of the human retina, which is at the same time unfortunately very susceptible to pathological changes.

All in all, my colleagues and I produced enormous amounts of data, the analysis of which is not yet fully exhausted. In fact, many more interesting pathways or proteins with specific features can be identified on their basis and then be used as a starting point for future investigations.

V. REFERENCES

- [1] G. Rathnasamy, W. S. Foulds, E.-A. Ling, and C. Kaur, "Retinal microglia – A key player in healthy and diseased retina," *Prog. Neurobiol.*, vol. 173, pp. 18–40, Feb. 2019, doi: 10.1016/j.pneurobio.2018.05.006.
- [2] A. Reichenbach and A. Bringmann, "Glia of the human retina," *Glia*, vol. 68, no. 4, pp. 768–796, Apr. 2020, doi: 10.1002/glia.23727.
- [3] A. Bringmann *et al.*, "Müller cells in the healthy and diseased retina.," *Prog. Retin. Eye Res.*, vol. 25, no. 4, pp. 397–424, Jul. 2006, doi: 10.1016/j.preteyeres.2006.05.003.
- [4] C.-J. Jeon, E. Strettoi, and R. H. Masland, "The Major Cell Populations of the Mouse Retina," *J. Neurosci.*, vol. 18, no. 21, pp. 8936–8946, Nov. 1998, doi: 10.1523/JNEUROSCI.18-21-08936.1998.
- [5] A. Reichenbach and S. R. Robinson, "Phylogenetic constraints on retinal organisation and development," *Prog. Retin. Eye Res.*, vol. 15, no. 1, pp. 139–171, Jan. 1995, doi: 10.1016/1350-9462(95)00008-9.
- [6] W. Lindenau, H. Kuhrt, E. Ulbricht, K. Körner, A. Bringmann, and A. Reichenbach, "Cone-to-Müller cell ratio in the mammalian retina: A survey of seven mammals with different lifestyle," *Exp. Eye Res.*, vol. 181, pp. 38–48, Apr. 2019, doi: 10.1016/j.exer.2019.01.012.
- [7] P. D. J. Gordon Betts, Kelly A. Young, James A. Wise, Eddie Johnson, Brandon Poe, Dean H. Kruse, Oksana Korol, Jody E. Johnson, Mark Womble, "13.1 The Embryologic Perspective – Anatomy and Physiology - Secondary Vesicles," 2013. <https://openstax.org/books/anatomy-and-physiology/pages/13-1-the-embryologic-perspective> (accessed Jun. 15, 2022).
- [8] A. Bringmann, A. Grosche, T. Pannicke, and A. Reichenbach, "GABA and Glutamate Uptake and Metabolism in Retinal Glial (Müller) Cells," *Front. Endocrinol. (Lausanne)*, vol. 4, p. 48, 2013, doi: 10.3389/fendo.2013.00048.
- [9] I. Farhy-Tselnicker and N. J. Allen, "Astrocytes, neurons, synapses: a tripartite view on cortical circuit development.," *Neural Dev.*, vol. 13, no. 1, p. 7, 2018, doi: 10.1186/s13064-018-0104-y.
- [10] L. Liu, K. R. MacKenzie, N. Putluri, M. Maletić-Savatić, and H. J. Bellen, "The Glia-Neuron Lactate Shuttle and Elevated ROS Promote Lipid Synthesis in Neurons and Lipid Droplet Accumulation in Glia via APOE/D," *Cell Metab.*, vol. 26, no. 5, pp. 719-737.e6, 2017, doi: 10.1016/j.cmet.2017.08.024.
- [11] J. B. Hurley, K. J. Lindsay, and J. Du, "Glucose, lactate, and shuttling of metabolites in vertebrate retinas," *J. Neurosci. Res.*, vol. 93, no. 7, pp. 1079–1092, Jul. 2015, doi: 10.1002/jnr.23583.
- [12] A. K. Toft-Kehler, D. M. Skytt, and M. Kolko, "A Perspective on the Müller Cell-Neuron Metabolic Partnership in the Inner Retina," *Mol. Neurobiol.*, vol. 55, no. 6, pp. 5353–5361, Jun. 2018, doi: 10.1007/s12035-017-0760-7.
- [13] J. Wan and D. Goldman, "Retina regeneration in zebrafish," *Curr. Opin. Genet. Dev.*, vol. 40, pp. 41–47, Oct. 2016, doi: 10.1016/J.GDE.2016.05.009.
- [14] G. Masserdotti, S. Gascón, and M. Götz, "Direct neuronal reprogramming: learning from and for development," *Development*, vol. 143, no. 14, pp. 2494–2510, Jul. 2016, doi: 10.1242/dev.092163.
- [15] B. E. Clarke, D. M. Taha, G. E. Tyzack, and R. Patani, "Regionally encoded functional heterogeneity of astrocytes in health and disease: A perspective," *Glia*, vol. 69, no. 1, pp. 20–27, Jan. 2021, doi: 10.1002/glia.23877.

- [16] S. Ohlig *et al.*, "Molecular diversity of diencephalic astrocytes reveals adult astrogenesis regulated by Smad4," *EMBO J.*, vol. 40, no. 21, Nov. 2021, doi: 10.15252/embj.2020107532.
- [17] J.-S. Wang and V. J. Kefalov, "The Cone-specific visual cycle," *Prog. Retin. Eye Res.*, vol. 30, no. 2, pp. 115–128, Mar. 2011, doi: 10.1016/j.preteyeres.2010.11.001.
- [18] J. S. Wang and V. J. Kefalov, "An Alternative Pathway Mediates the Mouse and Human Cone Visual Cycle," *Curr. Biol.*, vol. 19, no. 19, pp. 1665–1669, 2009, doi: 10.1016/j.cub.2009.07.054.
- [19] K. Franze *et al.*, "Müller cells are living optical fibers in the vertebrate retina," *Proc. Natl. Acad. Sci.*, vol. 104, no. 20, pp. 8287–8292, May 2007, doi: 10.1073/PNAS.0611180104.
- [20] R. B. MacDonald, O. Randlett, J. Oswald, T. Yoshimatsu, K. Franze, and W. A. Harris, "Müller glia provide essential tensile strength to the developing retina," *J. Cell Biol.*, vol. 210, no. 7, pp. 1075–1083, 2015, doi: 10.1083/jcb.201503115.
- [21] E. A. Turovsky *et al.*, "Mechanosensory signaling in astrocytes," *J. Neurosci.*, vol. 40, no. 49, pp. 9364–9371, Dec. 2020, doi: 10.1523/JNEUROSCI.1249-20.2020.
- [22] A. L. Placone, P. M. McGuiggan, D. E. Bergles, H. Guerrero-Cazares, A. Quiñones-Hinojosa, and P. C. Searson, "Human astrocytes develop physiological morphology and remain quiescent in a novel 3D matrix," *Biomaterials*, vol. 42, pp. 134–143, Feb. 2015, doi: 10.1016/j.biomaterials.2014.11.046.
- [23] C. L. Wilson, S. L. Hayward, and S. Kidambi, "Astrogliosis in a dish: Substrate stiffness induces astrogliosis in primary rat astrocytes," *RSC Adv.*, vol. 6, no. 41, pp. 34447–34457, Apr. 2016, doi: 10.1039/c5ra25916a.
- [24] A. Bizanti, P. Chandrashekar, and R. Steward, "Culturing astrocytes on substrates that mimic brain tumors promotes enhanced mechanical forces," *Exp. Cell Res.*, vol. 406, no. 2, p. 112751, Sep. 2021, doi: 10.1016/j.yexcr.2021.112751.
- [25] P. Moshayedi *et al.*, "Mechanosensitivity of astrocytes on optimized polyacrylamide gels analyzed by quantitative morphometry," *J. Phys. Condens. Matter*, vol. 22, no. 19, p. 194114, May 2010, doi: 10.1088/0953-8984/22/19/194114.
- [26] A. Verkhratsky, N. Bush, M. Nedergaard, and A. Butt, "The Special Case of Human Astrocytes," *Neuroglia*, vol. 1, no. 1, pp. 21–29, Mar. 2018, doi: 10.3390/neuroglia1010004.
- [27] L. Morel *et al.*, "Molecular and Functional Properties of Regional Astrocytes in the Adult Brain," *J. Neurosci.*, vol. 37, no. 36, pp. 8706–8717, Sep. 2017, doi: 10.1523/JNEUROSCI.3956-16.2017.
- [28] J. García-Marqués and L. López-Mascaraque, "Clonal identity determines astrocyte cortical heterogeneity," *Cereb. Cortex*, vol. 23, no. 6, pp. 1463–1472, Jun. 2013, doi: 10.1093/cercor/bhs134.
- [29] M. Bugiani, B. C. Plug, J. H. K. Man, M. Breur, and M. S. van der Knaap, "Heterogeneity of white matter astrocytes in the human brain," *Acta Neuropathol.*, vol. 143, no. 2, pp. 159–177, Feb. 2022, doi: 10.1007/s00401-021-02391-3.
- [30] A. Bringmann *et al.*, "The primate fovea: Structure, function and development," *Prog. Retin. Eye Res.*, vol. 66, no. November 2017, pp. 49–84, Sep. 2018, doi: 10.1016/j.preteyeres.2018.03.006.
- [31] N. T. Ingram, G. L. Fain, and A. P. Sampath, "Elevated energy requirement of cone photoreceptors," *Proc. Natl. Acad. Sci.*, no. 2, p. 202001776, 2020, doi: 10.1073/pnas.2001776117.
- [32] J. T. Handa, "How does the macula protect itself from oxidative stress?," *Mol. Aspects Med.*, vol. 33, no. 4, pp. 418–435, Aug. 2012, doi: 10.1016/j.mam.2012.03.006.
- [33] S. Syrbe *et al.*, "Müller glial cells of the primate foveola: An electron microscopical study," *Exp. Eye Res.*, vol. 167, pp. 110–117, 2018, doi: 10.1016/j.exer.2017.12.004.
- [34] A. Bringmann, J. D. Unterlauff, R. Wiedemann, T. Barth, M. Rehak, and P. Wiedemann, "Two different populations of Müller cells stabilize the structure of the fovea: an optical coherence tomography study," *Int. Ophthalmol.*, vol. 40, no. 11, pp. 2931–2948, Nov. 2020, doi: 10.1007/s10792-020-01477-3.
- [35] M. B. Powner *et al.*, "Perifoveal müller cell depletion in a case of macular telangiectasia type 2," *Ophthalmology*, vol. 117, no. 12, pp. 2407–16, Dec. 2010, doi: 10.1016/j.ophtha.2010.04.001.
- [36] M. B. Powner, M. C. Gillies, M. Zhu, K. Vevis, A. P. Hunyor, and M. Fruttiger, "Loss of Müller's cells and photoreceptors in macular telangiectasia type 2," *Ophthalmology*, vol. 120, no. 11, pp. 2344–2352, Nov. 2013, doi: 10.1016/j.ophtha.2013.04.013.

- [37] R. Aebersold and M. Mann, "Mass-spectrometric exploration of proteome structure and function," *Nature*, vol. 537, no. 7620. Nature Publishing Group, pp. 347–355, Sep. 14, 2016, doi: 10.1038/nature19949.
- [38] K. A. Neilson *et al.*, "Less label, more free: Approaches in label-free quantitative mass spectrometry," *Proteomics*, vol. 11, no. 4. John Wiley & Sons, Ltd, pp. 535–553, Feb. 01, 2011, doi: 10.1002/pmic.201000553.
- [39] T. Shi *et al.*, "Advances in targeted proteomics and applications to biomedical research," *Proteomics*, vol. 16, no. 15–16, pp. 2160–2182, 2016, doi: 10.1002/pmic.201500449.
- [40] A. Hu, W. S. Noble, and A. Wolf-Yadlin, "Technical advances in proteomics: new developments in data-independent acquisition," *F1000Research*, vol. 5, p. 419, Mar. 2016, doi: 10.12688/f1000research.7042.1.
- [41] J. Schindelin *et al.*, "Fiji: an open-source platform for biological-image analysis," *Nat. Methods*, vol. 9, no. 7, pp. 676–682, Jul. 2012, doi: 10.1038/nmeth.2019.
- [42] T. R. Jones *et al.*, "CellProfiler Analyst: data exploration and analysis software for complex image-based screens," *BMC Bioinformatics*, vol. 9, no. 1, p. 482, Dec. 2008, doi: 10.1186/1471-2105-9-482.
- [43] C. McQuin *et al.*, "CellProfiler 3.0: Next-generation image processing for biology.," *PLoS Biol.*, vol. 16, no. 7, p. e2005970, 2018, doi: 10.1371/journal.pbio.2005970.
- [44] M. Molbay, Z. I. Kolabas, M. I. Todorov, T. Ohn, and A. Ertürk, "A guidebook for DISCO tissue clearing," *Mol. Syst. Biol.*, vol. 17, no. 3, p. 9807, Mar. 2021, doi: 10.15252/MSB.20209807.
- [45] J. Cox and M. Mann, "MaxQuant enables high peptide identification rates, individualized p.p.b.-range mass accuracies and proteome-wide protein quantification," *Nat. Biotechnol.*, vol. 26, no. 12, pp. 1367–1372, Nov. 2008, doi: 10.1038/nbt.1511.
- [46] B. Li and C. N. Dewey, "RSEM: Accurate transcript quantification from RNA-Seq data with or without a reference genome," *BMC Bioinformatics*, vol. 12, no. 1, pp. 1–16, Aug. 2011, doi: 10.1186/1471-2105-12-323/TABLES/6.
- [47] N. L. Bray, H. Pimentel, P. Melsted, and L. Pachter, "Near-optimal probabilistic RNA-seq quantification," *Nat. Biotechnol.* 2016 345, vol. 34, no. 5, pp. 525–527, Apr. 2016, doi: 10.1038/nbt.3519.
- [48] F. A. Wolf, P. Angerer, and F. J. Theis, "SCANPY: Large-scale single-cell gene expression data analysis," *Genome Biol.*, vol. 19, no. 1, pp. 1–5, Feb. 2018, doi: 10.1186/S13059-017-1382-0/FIGURES/1.
- [49] T. Stuart *et al.*, "Comprehensive Integration of Single-Cell Data," *Cell*, vol. 177, no. 7, pp. 1888–1902.e21, Jun. 2019, doi: 10.1016/J.CELL.2019.05.031.
- [50] Y. Hao *et al.*, "Integrated analysis of multimodal single-cell data," *Cell*, vol. 184, no. 13, pp. 3573–3587.e29, Jun. 2021, doi: 10.1016/J.CELL.2021.04.048.
- [51] P. Langfelder and S. Horvath, "WGCNA: an R package for weighted correlation network analysis.," *BMC Bioinformatics*, vol. 9, p. 559, Dec. 2008, doi: 10.1186/1471-2105-9-559.
- [52] P. D. Thomas *et al.*, "PANTHER: A Library of Protein Families and Subfamilies Indexed by Function," *Genome Res.*, vol. 13, no. 9, pp. 2129–2141, Sep. 2003, doi: 10.1101/GR.772403.
- [53] M. Ashburner *et al.*, "Gene Ontology: tool for the unification of biology," *Nat. Genet.*, vol. 25, no. 1, p. 25, May 2000, doi: 10.1038/75556.
- [54] S. Carbon *et al.*, "The Gene Ontology resource: Enriching a GOld mine," *Nucleic Acids Res.*, vol. 49, no. D1, pp. D325–D334, Jan. 2021, doi: 10.1093/nar/gkaa1113.
- [55] M. Kanehisa and S. Goto, "KEGG: Kyoto Encyclopedia of Genes and Genomes," *Nucleic Acids Research*, vol. 28, no. 1. Oxford Academic, pp. 27–30, Jan. 01, 2000, doi: 10.1093/nar/28.1.27.
- [56] M. Kanehisa, "Toward understanding the origin and evolution of cellular organisms," *Protein Science*, vol. 28, no. 11. John Wiley & Sons, Ltd, pp. 1947–1951, Nov. 01, 2019, doi: 10.1002/pro.3715.
- [57] M. Kanehisa, M. Furumichi, Y. Sato, M. Ishiguro-Watanabe, and M. Tanabe, "KEGG: Integrating viruses and cellular organisms," *Nucleic Acids Res.*, vol. 49, no. D1, pp. D545–D551, Jan. 2021, doi: 10.1093/nar/gkaa970.
- [58] B. Snel, G. Lehmann, P. Bork, and M. A. Huynen, "String: A web-server to retrieve and display the repeatedly occurring neighbourhood of a gene," *Nucleic Acids Res.*, vol. 28, no. 18, pp. 3442–3444, Sep. 2000, doi: 10.1093/nar/28.18.3442.
- [59] D. Szklarczyk *et al.*, "STRING v11: protein-protein association networks with increased coverage, supporting functional discovery in genome-wide experimental datasets.,"

- Nucleic Acids Res.*, vol. 47, no. D1, pp. D607–D613, Jan. 2019, doi: 10.1093/nar/gky1131.
- [60] R. C. Gentleman *et al.*, “Bioconductor: open software development for computational biology and bioinformatics,” *Genome Biol.*, vol. 5, no. 10, p. R80, 2004, doi: 10.1186/gb-2004-5-10-r80.
- [61] W. Huber *et al.*, “Orchestrating high-throughput genomic analysis with Bioconductor,” *Nat. Methods*, vol. 12, no. 2, pp. 115–121, Feb. 2015, doi: 10.1038/nmeth.3252.
- [62] “Anaconda Software Distribution,” *Anaconda Documentation*, 2020. <https://docs.anaconda.com/> (accessed May 03, 2022).
- [63] “Docker.” <https://www.docker.com/> (accessed May 03, 2022).
- [64] B.-J. M. Webb-Robertson *et al.*, “Review, Evaluation, and Discussion of the Challenges of Missing Value Imputation for Mass Spectrometry-Based Label-Free Global Proteomics,” *J. Proteome Res.*, vol. 14, no. 5, pp. 1993–2001, May 2015, doi: 10.1021/pr501138h.
- [65] J. Wang *et al.*, “In-depth method assessments of differentially expressed protein detection for shotgun proteomics data with missing values,” *Sci. Rep.*, vol. 7, no. 1, pp. 1–8, 2017, doi: 10.1038/s41598-017-03650-8.
- [66] M. I. Love, W. Huber, and S. Anders, “Moderated estimation of fold change and dispersion for RNA-seq data with DESeq2,” *Genome Biol.*, vol. 15, no. 12, p. 550, Dec. 2014, doi: 10.1186/s13059-014-0550-8.
- [67] M. E. Ritchie *et al.*, “limma powers differential expression analyses for RNA-sequencing and microarray studies,” *Nucleic Acids Res.*, vol. 43, no. 7, pp. e47–e47, Apr. 2015, doi: 10.1093/nar/gkv007.
- [68] B. A. P. Roxas and Q. Li, “Significance analysis of microarray for relative quantitation of LC/MS data in proteomics,” *BMC Bioinformatics*, vol. 9, no. 1, p. 187, Dec. 2008, doi: 10.1186/1471-2105-9-187.
- [69] F. Seyednasrollah, A. Laiho, and L. L. Elo, “Comparison of software packages for detecting differential expression in RNA-seq studies,” *Brief. Bioinform.*, vol. 16, no. 1, pp. 59–70, 2013, doi: 10.1093/bib/bbt086.
- [70] W. Li, A. Shih, Y. Freudenberg-Hua, W. Fury, and Y. Yang, “Beyond standard pipeline and $p < 0.05$ in pathway enrichment analyses,” *Comput. Biol. Chem.*, vol. 92, p. 107455, Jun. 2021, doi: 10.1016/j.compbiolchem.2021.107455.
- [71] P. D. Karp, P. E. Midford, R. Caspi, and A. Khodursky, “Pathway size matters: the influence of pathway granularity on over-representation (enrichment analysis) statistics,” *BMC Genomics*, vol. 22, no. 1, p. 191, Dec. 2021, doi: 10.1186/s12864-021-07502-8.
- [72] C. Vogel and E. M. Marcotte, “Insights into the regulation of protein abundance from proteomic and transcriptomic analyses,” *Nat. Rev. Genet.*, vol. 13, no. 4, pp. 227–232, Apr. 2012, doi: 10.1038/nrg3185.
- [73] Y. Liu, A. Beyer, and R. Aebersold, “On the Dependency of Cellular Protein Levels on mRNA Abundance,” *Cell*, vol. 165, no. 3, pp. 535–550, Apr. 2016, doi: 10.1016/j.cell.2016.03.014.
- [74] E. Lundberg *et al.*, “Defining the transcriptome and proteome in three functionally different human cell lines,” *Mol. Syst. Biol.*, vol. 6, no. 1, p. 450, Jan. 2010, doi: 10.1038/msb.2010.106.
- [75] T. Maier, M. Güell, and L. Serrano, “Correlation of mRNA and protein in complex biological samples,” *FEBS Lett.*, vol. 583, no. 24, pp. 3966–3973, Dec. 2009, doi: 10.1016/j.febslet.2009.10.036.
- [76] J. Z. Li *et al.*, “Circadian patterns of gene expression in the human brain and disruption in major depressive disorder,” *Proc. Natl. Acad. Sci.*, vol. 110, no. 24, pp. 9950–9955, Jun. 2013, doi: 10.1073/pnas.1305814110.
- [77] M. Brancaccio *et al.*, “Cell-autonomous clock of astrocytes drives circadian behavior in mammals,” *Science (80-.)*, vol. 363, no. 6423, pp. 187–192, Jan. 2019, doi: 10.1126/science.aat4104.
- [78] P. Hasel, I. V. L. Rose, J. S. Sadick, R. D. Kim, and S. A. Liddelow, “Neuroinflammatory astrocyte subtypes in the mouse brain,” *Nat. Neurosci.*, vol. 24, no. 10, pp. 1475–1487, Oct. 2021, doi: 10.1038/s41593-021-00905-6.
- [79] J. Jo *et al.*, “Regional heterogeneity of astrocyte morphogenesis dictated by the formin protein, Daam2, modifies circuit function,” *EMBO Rep.*, vol. 22, no. 12, p. e53200, Dec. 2021, doi: 10.15252/embr.202153200.
- [80] L. Morel *et al.*, “Molecular and Functional Properties of Regional Astrocytes in the Adult Brain,” *J. Neurosci.*, vol. 37, no. 36, pp. 8706–8717, Sep. 2017, doi: 10.1523/JNEUROSCI.3956-16.2017.

- [81] S. J. Miller, "Astrocyte Heterogeneity in the Adult Central Nervous System.," *Front. Cell. Neurosci.*, vol. 12, p. 401, Nov. 2018, doi: 10.3389/fncel.2018.00401.
- [82] Y. Yang and R. Jackson, "Astrocyte identity: evolutionary perspectives on astrocyte functions and heterogeneity," *Current Opinion in Neurobiology*, vol. 56. Elsevier Current Trends, pp. 40–46, Jun. 01, 2019, doi: 10.1016/j.conb.2018.11.006.
- [83] W. T. Farmer and K. Murai, "Resolving astrocyte heterogeneity in the CNS," *Front. Cell. Neurosci.*, vol. 11, p. 300, Sep. 2017, doi: 10.3389/fncel.2017.00300.
- [84] F. Pestana, G. Edwards-Faret, T. G. Belgard, A. Martirosyan, and M. G. Holt, "No Longer Underappreciated: The Emerging Concept of Astrocyte Heterogeneity in Neuroscience," *Brain Sci.*, vol. 10, no. 3, p. 168, Mar. 2020, doi: 10.3390/brainsci10030168.
- [85] J. Kjell *et al.*, "Defining the Adult Neural Stem Cell Niche Proteome Identifies Key Regulators of Adult Neurogenesis," *Cell Stem Cell*, vol. 26, no. 2, pp. 277–293.e8, 2020, doi: 10.1016/j.stem.2020.01.002.
- [86] K. Sharma *et al.*, "Cell type- and brain region-resolved mouse brain proteome.," *Nat. Neurosci.*, vol. 18, no. 12, pp. 1819–31, Dec. 2015, doi: 10.1038/nn.4160.
- [87] Y. Yang *et al.*, "Molecular comparison of GLT1+ and ALDH1L1+ astrocytes in vivo in astroglial reporter mice," *Glia*, vol. 59, no. 2, pp. 200–207, Feb. 2011, doi: 10.1002/glia.21089.
- [88] L. Wagner *et al.*, "Suppression of SNARE-dependent exocytosis in retinal glial cells and its effect on ischemia-induced neurodegeneration," *Glia*, vol. 65, no. 7, pp. 1059–1071, Jul. 2017, doi: 10.1002/glia.23144.
- [89] J. Padden *et al.*, "Immunohistochemical Markers Distinguishing Cholangiocellular Carcinoma (CCC) from Pancreatic Ductal Adenocarcinoma (PDAC) Discovered by Proteomic Analysis of Microdissected Cells," *Mol. Cell. Proteomics*, vol. 15, no. 3, pp. 1072–1082, Mar. 2016, doi: 10.1074/mcp.M115.054585.
- [90] T. B. M. Schaaïj-Visser *et al.*, "Differential Proteomics Identifies Protein Biomarkers That Predict Local Relapse of Head and Neck Squamous Cell Carcinomas," *Clin. Cancer Res.*, vol. 15, no. 24, pp. 7666–7675, Dec. 2009, doi: 10.1158/1078-0432.CCR-09-2134.
- [91] K. A. Nave *et al.*, "Inducible targeting of CNS astrocytes in Aldh1l1-CreERT2 BAC transgenic mice," *F1000Research*, vol. 5, 2016, doi: 10.12688/F1000RESEARCH.10509.1.
- [92] B. Deneen, R. Ho, A. Lukaszewicz, C. J. Hochstim, R. M. Gronostajski, and D. J. Anderson, "The Transcription Factor NFIA Controls the Onset of Gliogenesis in the Developing Spinal Cord," *Neuron*, vol. 52, no. 6, pp. 953–968, Dec. 2006, doi: 10.1016/j.neuron.2006.11.019.
- [93] P. Kang *et al.*, "Sox9 and NFIA Coordinate a Transcriptional Regulatory Cascade during the Initiation of Gliogenesis," *Neuron*, vol. 74, no. 1, pp. 79–94, Apr. 2012, doi: 10.1016/j.neuron.2012.01.024.
- [94] T. Hoang *et al.*, "Gene regulatory networks controlling vertebrate retinal regeneration," *Science (80-.)*, vol. 370, no. 6519, p. eabb8598, Nov. 2020, doi: 10.1126/science.abb8598.
- [95] G. T. K. Boopathy and W. Hong, "Role of Hippo Pathway-YAP/TAZ Signaling in Angiogenesis," *Front. Cell Dev. Biol.*, vol. 7, no. APR, p. 49, Apr. 2019, doi: 10.3389/fcell.2019.00049.
- [96] S. Ma, Z. Meng, R. Chen, and K.-L. Guan, "The Hippo Pathway: Biology and Pathophysiology," *Annu. Rev. Biochem.*, vol. 88, no. 1, pp. 577–604, Jun. 2019, doi: 10.1146/annurev-biochem-013118-111829.
- [97] A. Totaro, T. Panciera, and S. Piccolo, "YAP/TAZ upstream signals and downstream responses," *Nat. Cell Biol.*, vol. 20, no. 8, pp. 888–899, Aug. 2018, doi: 10.1038/s41556-018-0142-z.
- [98] T. Panciera, L. Azzolin, M. Cordenonsi, and S. Piccolo, "Mechanobiology of YAP and TAZ in physiology and disease," *Nat. Rev. Mol. Cell Biol.*, vol. 18, no. 12, pp. 758–770, 2017, doi: 10.1038/nrm.2017.87.
- [99] H. Lavoie, J. Gagnon, and M. Therrien, "ERK signalling: a master regulator of cell behaviour, life and fate," *Nat. Rev. Mol. Cell Biol.*, vol. 21, no. 10, pp. 607–632, Oct. 2020, doi: 10.1038/s41580-020-0255-7.
- [100] D. Hanahan and R. A. Weinberg, "Hallmarks of cancer: The next generation," *Cell*, vol. 144, no. 5, pp. 646–674, 2011, doi: 10.1016/j.cell.2011.02.013.
- [101] Y. Si *et al.*, "Src Inhibits the Hippo Tumor Suppressor Pathway through Tyrosine Phosphorylation of Lats1," *Cancer Res.*, vol. 77, no. 18, pp. 4868–4880, Sep. 2017, doi:

- 10.1158/0008-5472.CAN-17-0391.
- [102] D. D. Shao *et al.*, "KRAS and YAP1 Converge to Regulate EMT and Tumor Survival," *Cell*, vol. 158, no. 1, pp. 171–184, Jul. 2014, doi: 10.1016/j.cell.2014.06.004.
- [103] Y. Zheng, B. Liu, L. Wang, H. Lei, K. D. Pulgar Prieto, and D. Pan, "Homeostatic Control of Hpo/MST Kinase Activity through Autophosphorylation-Dependent Recruitment of the STRIPAK PP2A Phosphatase Complex," *Cell Rep.*, vol. 21, no. 12, pp. 3612–3623, Dec. 2017, doi: 10.1016/j.celrep.2017.11.076.
- [104] A. Hamon, C. Masson, J. Bitard, L. Gieser, J. E. Roger, and M. Perron, "Retinal Degeneration Triggers the Activation of YAP/TEAD in Reactive Müller Cells," *Investig. Ophthalmology Vis. Sci.*, vol. 58, no. 4, p. 1941, Apr. 2017, doi: 10.1167/iovs.16-21366.
- [105] A. Hamon *et al.*, "Linking YAP to Müller Glia Quiescence Exit in the Degenerative Retina," *Cell Rep.*, vol. 27, no. 6, pp. 1712–1725.e6, May 2019, doi: 10.1016/j.celrep.2019.04.045.
- [106] E. M. Rueda *et al.*, "The Hippo Pathway Blocks Mammalian Retinal Müller Glial Cell Reprogramming," *Cell Rep.*, vol. 27, no. 6, pp. 1637–1649.e6, May 2019, doi: 10.1016/j.celrep.2019.04.047.
- [107] G. Heimann *et al.*, "Changes in the Proliferative Program Limit Astrocyte Homeostasis in the Aged Post-Traumatic Murine Cerebral Cortex," *Cereb. Cortex*, vol. 27, no. 8, pp. 4213–4228, Aug. 2017, doi: 10.1093/cercor/bhx112.
- [108] C. Simon, M. Götz, and L. Dimou, "Progenitors in the adult cerebral cortex: Cell cycle properties and regulation by physiological stimuli and injury," *Glia*, vol. 59, no. 6, pp. 869–881, Jun. 2011, doi: 10.1002/glia.21156.
- [109] P. Zhang, Y. Sun, and L. Ma, "ZEB1: At the crossroads of epithelial-mesenchymal transition, metastasis and therapy resistance," *Cell Cycle*, vol. 14, no. 4. Landes Bioscience, pp. 481–487, Feb. 16, 2015, doi: 10.1080/15384101.2015.1006048.
- [110] E. Sánchez-Tilló, O. de Barrios, L. Siles, M. Cuatrecasas, A. Castells, and A. Postigo, "β-catenin/TCF4 complex induces the epithelial-to-mesenchymal transition (EMT)-activator ZEB1 to regulate tumor invasiveness.," *Proc. Natl. Acad. Sci. U. S. A.*, vol. 108, no. 48, pp. 19204–9, Nov. 2011, doi: 10.1073/pnas.1108977108.
- [111] S. Singh *et al.*, "Zeb1 controls neuron differentiation and germinal zone exit by a mesenchymal-epithelial-like transition," *Elife*, vol. 5, no. MAY2016, pp. 1–31, May 2016, doi: 10.7554/eLife.12717.
- [112] B. Gupta *et al.*, "The transcription factor ZEB1 regulates stem cell self-renewal and cell fate in the adult hippocampus," *Cell Rep.*, vol. 36, no. 8, p. 109588, Aug. 2021, doi: 10.1016/j.celrep.2021.109588.
- [113] W. Lehmann *et al.*, "ZEB1 turns into a transcriptional activator by interacting with YAP1 in aggressive cancer types," *Nat. Commun.*, vol. 7, no. 1, p. 10498, Apr. 2016, doi: 10.1038/ncomms10498.
- [114] N. Feldker *et al.*, "Genome-wide cooperation of EMT transcription factor ZEB 1 with YAP and AP -1 in breast cancer," *EMBO J.*, vol. 39, no. 17, p. e103209, Sep. 2020, doi: 10.15252/embj.2019103209.
- [115] Y. Yang *et al.*, "Determination of a Comprehensive Alternative Splicing Regulatory Network and Combinatorial Regulation by Key Factors during the Epithelial-to-Mesenchymal Transition," *Mol. Cell. Biol.*, vol. 36, no. 11, pp. 1704–1719, Jun. 2016, doi: 10.1128/MCB.00019-16.
- [116] X. Zhang *et al.*, "Cell-Type-Specific Alternative Splicing Governs Cell Fate in the Developing Cerebral Cortex," *Cell*, vol. 166, no. 5, pp. 1147–1162.e15, Aug. 2016, doi: 10.1016/j.cell.2016.07.025.
- [117] S. Choi *et al.*, "RBFox2-regulated TEAD1 alternative splicing plays a pivotal role in Hippo-YAP signaling," *Nucleic Acids Res.*, vol. 50, no. 15, pp. 8658–8673, Aug. 2022, doi: 10.1093/nar/gkac509.
- [118] M. Samardzija *et al.*, "A mouse model for studying cone photoreceptor pathologies," *Investig. Ophthalmol. Vis. Sci.*, vol. 55, no. 8, pp. 5304–5313, 2014, doi: 10.1167/iovs.14-14789.
- [119] J. M. Provis, A. M. Dubis, T. Maddess, and J. Carroll, "Adaptation of the central retina for high acuity vision: Cones, the fovea and the avascular zone," *Prog. Retin. Eye Res.*, vol. 35, pp. 63–81, Jul. 2013, doi: 10.1016/j.preteyeres.2013.01.005.
- [120] M. Ferrara, G. Lugano, M. T. Sandinha, V. R. Kearns, B. Geraghty, and D. H. W. Steel, "Biomechanical properties of retina and choroid: a comprehensive review of techniques and translational relevance," *Eye*, vol. 35, no. 7, pp. 1818–1832, Jul. 2021, doi:

- 10.1038/s41433-021-01437-w.
- [121] P. B. Henrich *et al.*, "Nanoscale Topographic and Biomechanical Studies of the Human Internal Limiting Membrane," *Investig. Ophthalmology Vis. Sci.*, vol. 53, no. 6, p. 2561, Jun. 2012, doi: 10.1167/iovs.11-8502.
- [122] A. Daruich *et al.*, "Mechanisms of macular edema: Beyond the surface," *Prog. Retin. Eye Res.*, vol. 63, no. November, pp. 20–68, Mar. 2018, doi: 10.1016/j.preteyeres.2017.10.006.
- [123] M. Fleckenstein *et al.*, "Age-related macular degeneration," *Nat. Rev. Dis. Prim.*, vol. 7, no. 1, p. 31, Dec. 2021, doi: 10.1038/s41572-021-00265-2.
- [124] T. F. C. Heeren *et al.*, "Macular Telangiectasia Type 2: Visual Acuity, Disease End Stage, and the MacTel Area," *Ophthalmology*, vol. 127, no. 11, pp. 1539–1548, Nov. 2020, doi: 10.1016/j.ophtha.2020.03.040.
- [125] J. M. Escola, M. J. Kleijmeer, W. Stoorvogel, J. M. Griffith, O. Yoshie, and H. J. Geuze, "Selective enrichment of tetraspan proteins on the internal vesicles of multivesicular endosomes and on exosomes secreted by human B-lymphocytes," *J. Biol. Chem.*, vol. 273, no. 32, pp. 20121–20127, Aug. 1998, doi: 10.1074/jbc.273.32.20121.
- [126] C. Théry *et al.*, "Molecular characterization of dendritic cell-derived exosomes: Selective accumulation of the heat shock protein hsc73," *J. Cell Biol.*, vol. 147, no. 3, pp. 599–610, Nov. 1999, doi: 10.1083/jcb.147.3.599.
- [127] C. Théry *et al.*, "Minimal information for studies of extracellular vesicles 2018 (MISEV2018): a position statement of the International Society for Extracellular Vesicles and update of the MISEV2014 guidelines.," *J. Extracell. vesicles*, vol. 7, no. 1, p. 1535750, 2018, doi: 10.1080/20013078.2018.1535750.
- [128] C. S. Cowan *et al.*, "Cell Types of the Human Retina and Its Organoids at Single-Cell Resolution," *Cell*, vol. 182, no. 6, pp. 1623-1640.e34, Sep. 2020, doi: 10.1016/j.cell.2020.08.013.
- [129] A. P. Voigt *et al.*, "Molecular characterization of foveal versus peripheral human retina by single-cell RNA sequencing," *Exp. Eye Res.*, vol. 184, no. May, pp. 234–242, Jul. 2019, doi: 10.1016/j.exer.2019.05.001.

VI. APPENDIX

ACKNOWLEDGMENTS

Science is far from a one-man show, which means there are so many people without whom this piece would not have been possible. First, I would like to thank Antje Grosche, not only for giving me the opportunity to be part of this fantastic group but also for sparking my love for Müller cells, the most beautiful of them all. She encouraged me, against my inner motivation at first, to dive into basic bioinformatic analyses after which I developed Stockholm syndrome and now would not miss programming for the world. She was always supportive, open for my ideas and prudently applied just the right amount of pressure. I felt that she trusted in my judgment and my skills but was never shy to offer advice where needed.

I would also like to state my appreciation for Magdalena Götz, who, with her seemingly infinite knowledge of papers, people, pathways, and proteins offered a constant stream of ideas for new experiments and angles. Without her critical but honest discussions of my project it would not have reached its current form.

A major part of my work was actually based on data and measurements of Stefanie Hauck, who processed a sheer endless amount of my oftentimes difficult samples. Due to our mutual passion towards Müller cells she was able and happy to offer valuable feedback and advice on most of my work.

One of the best parts about my time as a PhD student was being able to share the lab with my dear, dear colleagues. Anna Pfaller, who was seemingly the only person to know in which shelf or drawer everything can be found, was a great mentor for me especially in the beginning of my project, as we shared many late hours processing donor samples. With her and fellow PhD students Josef Biber and Jacqueline Kajtna but also postdocs Oliver Bludau, Nundehui Diaz-Lezama, Susanne Koch and Kirsten Wunderlich we struggled through the daily chaos that is science and enjoyed many a wonderful night out. Gabi Jäger, our experienced technical assistant, was not only

sharing my pain in seemingly never ending immunostaining attempts but also spared many comforting words.

While above people mostly had to deal with me during working hours, many people had to endure me in their free time. I would like to start with a person whom I actually met in the lab but with whom I quickly became friends due to our shared interest in video games, retro tech and beer: Tobias Herbinger, thank you for making my days at work fun and for the many hearty debates that we could never agree about.

There are no words to express my gratitude towards my parents Nelya and Ilya and my sister Katharina, who after leaving everything behind and choosing a life's turning point in the form of emigration, managed to resist all difficulties and offer a level of love and support that made me who I am today. *Большое спасибо!*

I cannot end without expressing my gratefulness to my girlfriend Constanze Weber who has accompanied me for a big part of my life. I don't know how I would have managed my daily life without you. Thank you for enduring my boring but passionate babble about unnecessarily specific science problems, computers, anime and video games. Thank you for taking my mind off struggles. Thank you for dragging me to fun activities I am too phlegmatic to do on my own. Thank you for understanding my quirks. Thank you for always telling me I could do it.

LIST OF PUBLICATIONS

Published:

- 2022 **Kaplan L (GSN)**, Drexler C, Pfaller AM (GSN), Brenna S, Wunderlich KA, Dimitracopoulos A, Merl-Pham J, Perez M, Schlötzer-Schrehardt U, Enzmann V, ... Hauck SM (GSN), Grosche A (GSN), et al (2022) Retinal regions shape human and murine Müller cell proteome profile and functionality. *Glia*
- 2022 Demais V, Pohl A, Wunderlich KA, Pfaller AM (GSN), **Kaplan L (GSN)**, Barthélémy A, Dittrich R, Puig B, Giebel B, Hauck SM (GSN), Pfrieger FW, Grosche A (GSN) (2022) Release of VAMP5-positive extracellular vesicles by retinal Müller glia in vivo. *J Extracell Vesicles* 11: e12254
- 2022 Nagel-Wolfrum K, Fadl BR, Becker MM, Wunderlich KA, Schäfer J, Sturm D, Fritze J, Gür B, **Kaplan L (GSN)**, Andreani T, ... Grosche A (GSN) et al (2022) Expression and subcellular localization of USH1C /harmonin in human retina provides insights into pathomechanisms and therapy. *Hum Mol Genet*
- 2022 Zauhar R, Biber J (GSN), Jabri Y, Kim M, Hu J, **Kaplan L (GSN)**, Pfaller AM (GSN), Schäfer N, Enzmann V, Schlötzer-Schrehardt U, ... Hauck SM (GSN), Grosche A (GSN) et al (2022) As in Real Estate, Location Matters: Cellular Expression of Complement Varies Between Macular and Peripheral Regions of the Retina and Supporting Tissues. *Front Immunol* 13: 1–19
- 2021 Ghaseminejad F, **Kaplan L (GSN)**, Pfaller AM (GSN), Hauck SM (GSN) & Grosche A (GSN) (2020) The role of Müller cell glucocorticoid signaling in diabetic retinopathy. *Graefe's Arch Clin Exp Ophthalmol* 258: 221–230

VII. EIDESSTATTLICHE VERSICHERUNG/*AFFIDAVIT*

Hiermit versichere ich an Eides statt, dass ich die vorliegende Dissertation PROTEOMIC HETEROGENEITY OF GLIAL CELLS OF THE CENTRAL NERVOUS SYSTEM selbstständig angefertigt habe, mich außer der angegebenen keiner weiteren Hilfsmittel bedient und alle Erkenntnisse, die aus dem Schrifttum ganz oder annähernd übernommen sind, als solche kenntlich gemacht und nach ihrer Herkunft unter Bezeichnung der Fundstelle einzeln nachgewiesen habe.

I hereby confirm that the dissertation PROTEOMIC HETEROGENEITY OF GLIAL CELLS OF THE CENTRAL NERVOUS SYSTEM is the result of my own work and that I have only used sources or materials listed and specified in the dissertation.

München/Munich

12.12.2022 _____

(Datum/Date)

Lew Kaplan _____

(Unterschrift/Signature Lew Kaplan)

VIII. DECLARATION OF AUTHOR CONTRIBUTIONS

Manuscript 1: Heterogeneity of glial cells of the central nervous system – a proteomic study

Authors:

Kaplan L, Natarajan P, Ohlig S, Neueder A, Smialowski P, Fischer-Sternjak J, Hauck SM, Götz M, Grosche A

Author contributions:

LK: designed experiments, sorted retinal fractions, performed bioinformatic analyses and immunofluorescence stainings with corresponding microscopy and image analysis. Prepared figures and wrote the manuscript. **PN**: performed immunofluorescence stainings with corresponding microscopy and image analysis. Generated ZEB1 KO and validated the used primary antibody. **SO**: sorted brain fractions for RNAseq and performed RNAseq data acquisition. **AN**: Helped with the establishment of WGCNA analysis and edited the manuscript. **SP**: Primary bioinformatic analysis of brain RNAseq data. **JF**: sorted cells from brain regions, edited the manuscript. **SMH**: designed experiments, performed tandem mass spectrometry of retinal and brain samples and the primary analysis of the resulting data. Edited the manuscript. **MG**: designed experiments, conceptualized and edited the manuscript. **AG**: designed experiments, analyzed data, prepared figures, conceptualized and edited the manuscript.

Manuscript 2: Retinal regions shape human and murine Müller cell proteome profile and functionality

Authors:

Kaplan L, Drexler C, Pfaller AM, Brenna S, Wunderlich KA, Dimitracopoulos A, Merl-Pham J, Perez M, Schlötzer-Schrehardt U, Enzmann V, Samardzija M, Puig B, Fuchs P, Franze K, Hauck SM, Grosche A

Author contributions:

Conceptualization: LK, PF, BP, KF, SMH, AG. *Methodology:* LK, CD, AMP, SB, KAW, AD, MP, US, VE, KF, SMH, AG. *Investigation:* LK, CD, AMP, SMH, AG. *Visualization:* LK, AG. *Supervision:* PF, BP, KF, SMH, AG. *Writing—original draft:* LK, AG. *Writing—review & editing:* LK, VE, MS, PF, BP, KF, SMH, AG.

Manuscript 3: Release of VAMP5-positive extracellular vesicles by retinal Müller glia in vivo

Authors:

Demais V, Pohl A, Wunderlich KA, Pfaller AM, **Kaplan L**, Barthélémy A, Dittrich R, Puig B, Giebel B, Hauck SM, Pfrieger FW, Grosche A

Author contributions:

VD: performed electron microscopy-related work, acquired and analyzed electron micrographs. AP: performed immunofluorescence microscopy-related work, qPCR experiments and analyses, immunoblots for VAMP expression in the healthy and ischemic retina, established protocols for primary Müller cell cultures, performed EV purification, and edited the manuscript. KAW: performed EV purification from primary Müller cell cultures and immunoblot analyses, analyzed EV marker localization via STED microscopy, and edited the manuscript. AMP: generated purified EVs for mass spectrometric analysis, and edited the manuscript. **LK**: performed EV isolation and bioinformatic analysis of proteomic data, and edited the manuscript. AB: performed immunohistochemical staining with selected anti- bodies to prepare immunogold staining. RD: performed NTA. BP: set up the EV isolation protocol, analyzed results, edited the manuscript. BG: analysed NTA results and edited the manuscript. SMH: performed mass spectrometric analysis of retinal cell types and purified EVs, analyzed protein expression levels, and edited the manuscript. AG: designed experiments, analyzed results, prepared figures, and edited the manuscript. FWP: designed experiments, analyzed results, prepared figures, and wrote the manuscript.

Valerie Demais and Anne Pohl were equally contributing first authors of this study:

Valerie Demais: _____
Datum/Date Unterschrift/Signature

Anne Pohl: _____
Datum/Date Unterschrift/Signature

Antje Grosche and Frank W. Pfrieder were the supervising senior scientists:

Antje Grosche: _____
Datum/Date Unterschrift/Signature

Frank W. Pfrieder: _____
Datum/Date Unterschrift/Signature